Chemical and isotopic studies of the Wateranga layered mafic intrusion, southeast Queensland, Australia: magma sources and petrogenesis

Reddy V. R. Talusani

A thesis submitted for the degree of Doctor of Philosophy of the University of New England, Armidale NSW, Australia

March 2003

"We must be the change we wish to see"

M. K. Gandhi

Declaration

I certify that the substance of this thesis has not already been submitted for any degree and is not currently being submitted for any other degree or qualification.

I certify that any help received in preparing this thesis, and all sources used, have been acknowledged in this thesis.

Reddy V. R. Talusani

Contents

List of Figures

Chapter 4 66

List of Plates

List of Tables

Preface

Layered intrusions are the most widespread mafic plutons occurring in several tectonic environments and are known from all ages invading the continental crust. They are the exposed examples of solidified magma chambers, which provide an excellent opportunity for studying the insides of magma chambers.

The present study has been undertaken in order to thoroughly investigate the geochemistry of the Wateranga layered intrusion in southeast Queensland. In addition, detailed geological mapping and extensive petrographic studies have also been carried out. The relatively small size, excellent exposure, availability of drill core, and uncomplicated structure of the Wateranga intrusion make it well suited for a study of its geochemical evolution.

A large body of good quality chemical data is presented in this thesis. Geochemical and Sr, Nd and O isotopic data are obtained for the Wateranga intrusion and a thorough investigation of magma sources, magma compositions and physical and chemical processes that modify magmas during their ascent from the mantle has been completed. Electron microprobe mineral analyses were carried out in order to determine mineral compositional variations within and between the rocks of the subunits and to estimate possible P-T conditions of crystallization of the Wateranga magma. Furthermore, the origin of platinum group elements is discussed.

Systematic isotopic and geochemical studies of the Wateranga layered intrusion in southeast Queensland, Australia, will contribute to the existing knowledge on the layered intrusions and Permo-Triassic post-subduction extensional basic magmatism in the northern New England Fold Belt. The excellent writing style, structure and presentation style of this thesis make it interesting to read and easy to follow and understand. I have done my best to produce a good quality thesis.

Reddy V. R. Talusani

Acknowledgements

This study has been undertaken by the author at the University of New England, Australia, while in receipt of an Australian Postgraduate Research Award.

I am grateful to my supervisors Dr. Warwick J. Sivell and A/Professor Paul M. Ashley for their continued interest, useful discussions, encouragement and helpful review of the manuscript. I am indebted to A/Professor Paul M. Ashley who suggested the project, introduced me to the Wateranga intrusion, guided field work and sampling and provided important geological information on the Wateranga intrusion. I am also grateful to Dr Nick Stephenson for very useful discussions on several occasions. Professor Peter G. Flood is thanked for providing necessary facilities and help with photomicrographs.

Financial support for field work and chemical analyses was provided by the Division of Earth Sciences, University of New England, Australia, which is gratefully acknowledged. Electron microprobe and whole-rock XRF analyses were done at the University of New England with the assistance of Peter Garlick and John Bedford respectively. David Keith made excellent thin and polished sections. Isotope analyses were carried out at the Centre for Isotope Studies, CSIRO, Sydney, and REE and PGE analyses were carried out at Australian Laboratory Services, Brisbane. The Department of Natural Resources and Mines (NRM), Queensland is acknowledged for providing access to drill core.

Thanks are due to Raelene Moloney and David Morgan for general support and help with computers. I also thank my fellow researcher Nancy Vickery for useful discussions.

Finally, I would like to thank my wife Swapna for her patience, support and help with data entry.

Abstract

This research was undertaken in order to thoroughly investigate the geochemistry of the Wateranga mafic layered intrusion in southeast Queensland, Australia. Nd-Sr-O isotopic, whole-rock major and trace element and mineral chemical studies of the Wateranga intrusion were used to understand the nature of mantle sources and mafic magma genesis during a post-compressional extensional regime.

The Wateranga layered mafic intrusion (28 km^2) (>500 m thick) is a tholeiitic, undeformed, unmetamorphosed, Permo-Triassic layered gabbroic pluton intruded into the Late Carboniferous Goodnight beds of the Goodnight Block in southeast Queensland. The intrusion mainly consists of gabbro and norite, associated with subordinate amounts of troctolite, anorthosite and orthopyroxenite, and rare picrite. Olivine gabbro is the dominant rock type of the intrusion. The whole-rock Sm-Nd isochron yields an age of 261±21 Ma. Petrographic, mineral chemical, whole-rock geochemical and Nd-Sr-O isotopic data have been used to divide the intrusion into Lower, Middle and Upper Zones, which are interpreted as reflecting magma chamber replenishment. Although the general crystallization order of minerals is olivine, plagioclase, clinopyroxene, orthopyroxene, Fe-Ti oxides, hornblende and biotite, considerable differences exist between the Zones. The observed changes in the crystallization order between the Zones reveal that a single parental magma was inadequate to explain the data. The common differentiation indices, such as An content of plagioclase, Mg#s of olivine, clinopyroxene, orthopyroxene and whole-rocks, and the whole-rock concentrations of various incompatible trace elements (Zr, Y, Nb, La, Ba, Rb, Sr, and Nd) and Nd-Sr-O isotopic compositions, all vary widely with stratigraphic depth and display abrupt shifts at the Zone boundaries, indicating open-system addition of new mafic magma. Litho- and chemo- stratigraphic analyses of the Wateranga intrusion show that it is the product of at least three major magma pulses.

Mineral chemical and whole-rock geochemical data indicate that fractional crystallization played an important role in the magmatic processes. However, sharp discontinuities and contrasting fractionation trends between the individual

stratigraphic Zones of the intrusion suggest polycyclic fractionation of three major batches of magma. Fractionation followed tholeiitic trends with iron enrichment in the liquids. Rare earth element distributions indicate more than 5% partial melting of the mantle source with limited amounts of residual garnet. Finely disseminated sulphides occur throughout the intrusion. Textural and compositional evidence indicate that the disseminated Fe-Ni-Cu sulphides and platinum group elements are of magmatic origin.

Microprobe analyses of coexisting clinopyroxene and orthopyroxene in different rocks of the intrusion provide consistent P-T data defining the magmatic crystallization condition as 1057 - 927 °C. During the course of crystallization pressure probably was greater than 2 and less than 4 kbar. Whole-rock initial ε_{Nd} (3.26 - 6.44) and initial $^{87}Sr/^{86}Sr$ (0.7026 - 0.7049) compositions, chondrite-normalized REE patterns and the variation trend of anorthite content of plagioclase versus the forsterite content of olivine precludes an arc-related magma source. The composition and geological setting of the intrusion are consistent with emplacement in a post-subduction extensional tectonic environment.

The parental magmas to the Wateranga intrusion are olivine tholeiitic, derived from an asthenospheric mantle source in response to lithospheric extension during the Permo-Triassic (245±8Ma). Olivine tholeiitic magma, already contaminated by lower continental crust, was initially pooled in late Carboniferous sediments where the magma chamber evolved by fractional crystallization and periodic replenishment. Crustal assimilation was limited (2 to 8%).

CHAPTER 1

Introduction

Introduction

1.1 Introduction

Layered igneous intrusions are a feature of several tectonic environments and are known from all ages from Archaean to Tertiary invading the continental crust. They are the most widespread mafic plutons with the overall chemical composition of tholeiitic basalt. Classic examples are provided by immense Proterozoic South African Bushveld Complex and the Stillwater Complex of Montana, and the smaller but intensively investigated Eocene Skaergaard intrusion of eastern Greenland. Although the parental composition in every case was mafic (tholeiitic), the solidified end products cover a wide range of silica content: ultrabasic, basic and even acidic.

Some layered intrusions are of great economic significance as they host virtually all of the world's resources of the platinum-group elements and chromite, as well as important deposits of V, Cu and Ni. Consequently, many of these intrusions have been studied in great detail. Most of these investigations, however, have focussed on magma chamber crystallization processes and volatiles in magmas, in order to explain igneous layering and associated mineralization. Recently, interest has shifted somewhat to questions concerning the tectonic setting of layered intrusions and the source regions of their parental magmas.

Layered mafic intrusions have played an important role in the development of petrology, particularly in the formulation of concepts of fractional crystallization (Wager and Brown, 1968; McBirney, 1975, 1995). They are the natural

laboratories for studying the insides of magma chambers. In addition to fractional crystallization, a number of other magma chamber processes that may affect magma compositions have been proposed in recent years, including magma mixing, liquid stratification (double-diffusion convection), sidewall crystallization, selective contamination and Soret diffusion (Campbell, 1978; McBirney, 1980; Turner, 1980; Walker and DeLong, 1982; Irvine et al., 1983; Spera et al., 1984; McBirney et al., 1985; Campbell and Turner, 1987; Marsh, 1989; Caroff, 1995; Amelin et al., 1996; Tegner et al., 1999). Many of the recent models are based on tank experiments using saltwater and other fluids, numerical experiments and volcanic successions.

Magma chamber processes play an important role in determining chemical, spatial and temporal trends of layered intrusions. Recent attention has also been focused on the role of mafic intrusions in melting and mobilizing the lower crust and in the generation of granitic magmas (Huppert and Sparks, 1988). In the past several years, the number of models for magma chamber processes has increased dramatically, in part due to the application of data from convection experiments in simple crystal-liquid systems, and to computer modelling of fluid dynamical processes (Spera et al., 1982, 1984, 1986; Marsh and Maxey, 1985; Huppert et al., 1986; Boudreau and McBirney, 1997).

The present study of the Wateranga intrusion has been undertaken to investigate magma chamber processes and the evolution of basaltic magmas in such chambers. Detailed geochemical and isotopic analyses of rocks from the Wateranga layered intrusion in southeast Queensland, have been obtained in order to investigate magma sources, magma compositions and physical and chemical processes that modify magmas during their ascent from mantle source(s).

1.2 Significance of layered intrusions

Layered mafic intrusions are important for a number of reasons. They are particularly relevant for the study of processes in magma chambers. Firstly, they are the exposed examples of solidified magma chambers. Under suitable circumstances the floor, walls and roof are available for study. Secondly, the

presence of layering allows "stratigraphic" consideration of thickness, lateral correlation and direction of younging. Thirdly, they commonly show evidence of repeated magma replenishment, allowing study of the mechanisms of magma influx.

Layered intrusions are also important for economic reasons with reserves of platinum-group elements (PGE), chromium, vanadium, nickel, copper, iron, titanium and gold. Studies of processes in magma chambers lead to a better understanding of the formation of these magmatic ore deposits (Barnes et al., 1985; Hamlyn and Keays, 1986; Naldrett and Gruenewaldt, 1989; Boudreau and McCallum, 1992; Nielsen and Brookes, 1995; Ripley et al., 1999; Theriault et al., 2000). Naldrett et al. (1990) provide models for igneous processes that lead to mineralization, involving the collection of the PGE by sulphide. The Merensky Reef and UG-2 reef of the Bushveld Intrusion, the Main Sulphide zones of the Great Dyke (Zimbabwe) and the Robie Zone of the Lac des Iles Intrusion (Ontario) are well known for their extensive PGE mineralization (Wilson et al., 1989; Viljoen, 1994).

1.3 General characteristics of layered intrusions

A brief review of the general characteristic features of layered intrusions as have been observed and recorded by earlier researchers is provided in the following sections.

1.3.1 Age of layered intrusions

Layered intrusions in continental settings have ages ranging from Archaean to Early Tertiary. The oldest intrusions are of special importance because they created the first opportunity for high-level fractional crystallization. These early magma chambers, which include the Bell River Complex in Quebec, the Kam-Kotia Sill in Ontario and the Stillwater Complex of Montana date from about 2.75 Ga (Lambert et al., 1985; Mortensen, 1993). Some layered anorthosites, occurring in Labrador and West Greenland, are thought to have formed at ~3.8 Ga (Morse, 1983; Ashwal et al., 1989; Ashwal, 1993). The Manfred Complex of Western

Australia is the oldest (~3.7 Ga) and first recorded occurrence of Archaean layered anorthosite in Australia (Myers, 1988). The absence of layered intrusions prior to this time (3.8 Ga) suggests that the crust was not rigid and/or thick enough to support large magma chambers.

1.3.2 Tectonic setting of layered intrusions

Although the tectonic setting of most layered intrusions is not well studied, rifting within a continental environment is considered by many authors to be the dominant tectonic setting. Many have formed in zones of crustal extension, perhaps the most favourable settings being failed and successful rift systems. The Duluth Complex of northern USA and Norilsk gabbro-dolerites of northern Russia are believed to be examples of magma chambers which have formed in failed rift environments (Naldrett and MacDonald, 1980; Paces and Miller, 1993). Many layered intrusions near continental margins, such as the Skaergaard and Rhum (UK) intrusions, probably formed during the development of a successful rift (Brooks and Nielsen, 1982; Upton, 1988). Some layered intrusions are believed to be associated with impact structures, e.g., Sudbury (Grieve, 1994). Some other layered intrusions may be associated with hot spots or plumes (Amelin and Semenov, 1996). Numerous lines of evidence have been cited in favour of an extra-terrestrial origin for 1850 Ma old Sudbury structure. Several papers in Pye et al. (1984) give a detailed discussion on this topic. Results of recent isotopic studies (Walker et al., 1991) and thermal modelling (Grieve, 1994) strongly suggest that the entire Sudbury intrusion may be a sheet of impact-generated melt.

1.3.3 Shape and size of layered intrusions

Layered intrusions were originally classified as lopoliths (Grout, 1918), which were defined as large centrally sunken sills with a semi-horizontal roof and with internal layering parallel to the floor. However, detailed observations of the margins of intrusions by Wager and others (e.g., Wager and Brown, 1968; Weiblen and Morey, 1980) showed that they dip inwards at a greater angle than the internal layering of the rocks, indicating that the form of the intrusion is

funnel-shaped rather than lopolithic. The angles at the bases of layered intrusions are variable and influence the shape of the layering. Wide angle intrusions, such as the Muskox intrusion in north western Canada and the Stillwater Complex, have low angle layering, whereas the layering in acute angled intrusions, such as Jimberlana intrusion of western Australia, and the Great Dyke of Zimbabwe is "U" shaped and dips steeply at the margin (Campbell et al., 1970). Although most layered intrusions occur as sills, they are also found as dykes and plugs.

Many layered intrusions are large. They vary widely in size – from complexes larger than 60,000 km^2 such as Precambrian Bushveld Complex in South Africa (with an exposed area of 65,000 km^2 and a thickness of up to 7 km) to occurrences as small as few km^2.

1.3.4 Types of layering

There are numerous types of layering but the three most important types are as follows.

Phase layering is a major stratigraphic layering resulting from the appearance or disappearance of a cumulus phase. Layered intrusions are mapped and subdivided on the basis of phase layering.

Rhythmic layering (small-scale layering) is present in the larger stratiform intrusions (Wager and Brown, 1968). There is a segregation of mineral phases into monomineralic or discrete assemblages (e.g., anorthosite, chromitite, troctolite) on a scale varying from a few centimetres to several meters, forming a stratification whose pattern is repeated through the thickness of an intrusion. The recognition of rhythmic layering remains one of the principal criteria for identifying layered intrusions with the designation of different types of rhythmic layering based on mineralogical and textural contrasts between layers (Jackson, 1970; Irving and Dungan, 1980). Rhythmic layering may be quite regular over great distances within the intrusion, or there may be irregularities of composition, thickness, or mineralogy within one layer as traced through an intrusion.

Cryptic layering is more subtle, and consists of a continuous or discontinuous change in mineral or whole rock chemistry expressed petrographically by changes

in modal distribution of members of mineral solid solution series, e.g., olivines, spinels, pyroxenes and plagioclase feldspars. Some layered intrusions display a cryptic variation within a rhythmically layered sequence that includes virtually a complete variation through the range of mineral solid solutions, e.g., Skaergaard intrusion (McBirney and Noyes, 1979). Such a layering is often regular enough to serve as a stratigraphy. Chemical characteristics such as these can be interpreted either as gravity settling from an evolving magma, or by crystal accumulation in a density stratified magma chamber (Irvine et al., 1983).

1.3.5 Cumulate textures

A cumulate rock is made up of two parts, a liquidus or cumulus component and the trapped intercumulus liquid. This is the most important property of cumulates for it is this property which makes fractional crystallization possible. If the fractionation process is efficient, most of the trapped liquid is expelled from the crystal pile at the liquidus temperature and the rock is said to have an adcumulate texture. If it is inefficient, much of the liquid is trapped between the cumulus grains and an orthocumulate texture results.

In adcumulate sequences the Rayleigh equation (Hart and Allegre, 1980) can be used to model the effects of fractionation, which is as follows.

$$C_L / C_0 = F^{(D-1)}$$

C_L is defined as the concentration of a trace element in the liquid, C_0 is the initial concentration of a trace element in the original liquid (primary magma), F is the fraction of melt remaining and D is the bulk partition coefficient of the fractionating assemblage.

In the case of orthocumulate sequences, the above equation should be replaced by (Albarede, 1976, 1996)

$$C_L / C_0 = F^{(D-1)(1-P)}$$

where P is the fraction of trapped intercumulus liquid.

1.3.6 Magma composition and evolution

The composition of parental magmas of layered intrusions is largely dictated by the nature of the crust-mantle transition beneath the intrusion, and long-term processes that have modified the upper mantle prior to generation of these magmas. Virtually all types of basaltic magmas can give rise to layered intrusions within shallow crustal environments. Layering can be enhanced by processes such as periodic influxes of undifferentiated magma and magma mixing, particularly between influxes of parental magmas of contrasting composition. Under such situations, density stratification of liquids within the magma chamber can develop, which further enhances the development of layering in the intrusions (Irvine et al., 1983; Sharpe, 1985; Naslund and McBirney, 1996).

Chemical studies of naturally occurring mafic magma chambers can be undertaken by essentially two approaches: (1) study of past and present liquids that have been vented from magma chambers (basaltic and andesitic lava flows), or (2) study of the crystallized remnants of mafic magma chambers (layered intrusions). The approaches are complementary to each other, and each has advantages and disadvantages. However, it is rarely possible to study a given magma chamber using both approaches. If lava flows are exposed, the intrusion from which they were vented generally lies at an inaccessibly deep level, whereas if an intrusion is exposed, its eruption products have probably been eroded away.

The idea behind studying lava flows is that each flow represents a sample of the liquid residing in the magma chamber at the time of eruption. Thus, by investigating a succession of lava flows, magma chamber liquid evolutionary history can be developed. The main advantage of this approach is that the magma chamber liquid can be studied directly, without the necessity of making inferences based on theoretical or experimental phase equilibria studies. The disadvantages of studying lavas are (1) samples are only available when the magma chamber vents to the surface, which may result in incomplete or skewed results, and (2) the

magma chamber size and geometry is generally not known (with the exception of active systems, which may be studied geophysically).

As already alluded, layered intrusions represent the crystallized remains of active magma chambers. In most cases, the layering within these chambers is thought to follow the law of superposition, i.e., the layers were deposited from the bottom up. Crystals that are deposited in this way are called *cumulates*. Since cumulate crystals are separated from their parent liquid and sorted by various processes, the bulk composition of a cumulate pile will not in general be the same as the liquid from which it crystallized. Compaction is never 100% effective, and sometimes intercumulus liquid is invariably trapped between the cumulate crystals. Intercumulus liquid often crystallizes to an assemblage very different from, or even out of equilibrium with its coexisting cumulates. A well-exposed intrusion should provide a complete chemical record of the liquid from which it crystallized, regardless of whether and how often magma was vented from the chamber. In addition, many or all aspects of an intrusion's size and geometry can be observed when it is exposed by erosion, and the chemical, physical and temporal relationships among the different parts of the intrusion can be reconstructed. The primary disadvantage of studying magma chamber processes through investigation of layered intrusions is that the preserved crystallization products (cumulates) have very different compositions than the liquids from which they crystallized, thus necessitating inferences about the magma physical and chemical processes based on laboratory or theoretical studies. However, isotopic studies provide a means of bypassing this problem. Isotopes used in this investigation are Nd and Sr.

1.4 A brief introduction to the area of research

The Wateranga intrusion, a mafic layered intrusion situated on the eastern side of the northern New England Fold Belt, forms one of a number of such layered intrusions that were intruded in the evolution of the belt (Fig. 2.5, Chapter 2) (Mathison, 1967; Wilson and Mathison, 1968; Mathison, 1987; Reeves and Keays, 1995). These mafic, unmetamorphosed gabbroic intrusions have similar

composition, age and tectonic setting. In the present work, a detailed study has been carried out on the Wateranga layered intrusion, which is located 80 km southwest of Bundaberg in southeast Queensland (Fig. 2.1, Chapter 2). The ovoid intrusion of 28 km^2, is a tholeiitic, Permo-Triassic, undeformed, layered pluton that has been emplaced into the Late Carboniferous Goodnight beds of the Goodnight Block (Ambler and Ashley, 1977; Day et al., 1983; Cranfield, 1989; Talusani et al., 2000). The chief rock types are gabbro, norite, troctolite and anorthosite, which occur as well developed layers, presenting a varying petrography.

The relatively small size, excellent exposure with remarkably fresh samples, availability of drill core and uncomplicated structure of the Wateranga intrusion make it well suited for a study of its differentiation history and for quantitative modelling of the compositional changes that occurred in the Wateranga magma during crystallization. This study investigates the geochemical evolution of the Wateranga intrusion, which includes fractional crystallization, magma mixing, crustal contamination and inhomogeneities in the mantle source.

1.5 Previous studies on the Wateranga intrusion

The Wateranga intrusion was first mapped by Ellis (1968), which provided information on the areal extent of the intrusion and its regional relationship to the country rocks. Remapping of the intrusion and reinterpretation of the regional relationships have been done by Cranfield (1986, 1989), in association with the Queensland Geological Survey. To facilitate Queensland Geological Survey departmental studies, Robertson (1971) worked on the intrusion for possible economic mineral deposits. During this investigation (1967-70) six diamond drill holes were completed in total. Drill holes NS-1 to 3 were completed to a total depth of ~1050 m and drill holes NS-4 to 6 were completed to a total depth of ~450 m. These studies proved that there is no significant economic potential in the Wateranga intrusion. A magnetite body was discovered, and this proved to be very rich in phosphorus and titanium.

In addition to these investigations carried out by the Queensland Geological Survey, Ambler and Ashley (1977) published data on vermicular orthopyroxene-magnetite symplectites and Evans et al. (1993) and Evans (1992) discussed some petrological variations. Until now there has been no systematic geochemical study of the Wateranga intrusion.

1.6 Objectives of the project

This study was undertaken in order to present the first rigorous and systematic geochemistry of the Wateranga intrusion. Geochemical and Sr, Nd and O isotopic data were obtained to investigate the magma sources and the processes operated during magma generation, ascent, emplacement and crystallization of the Wateranga intrusion. The specific objectives of this study can be summarized as follows.

1. Are all the rocks in the Wateranga intrusion related to a single parental magma and if so what is the composition of this magma?
2. Is the Wateranga intrusion an example of an open magmatic system or a closed magmatic system?
3. What mechanism caused mineralogical and chemical variation in the rocks of the Wateranga intrusion (e.g., crystal fractionation, magma recharge, assimilation and relative contribution of mantle and crustal material)?
4. What are the possible P-T conditions of crystallization of the Wateranga magma?
5. What is the possible tectonic setting of the Wateranga intrusion? Is it a subduction related intrusion or a rift related intrusion?
6. Do the trace amounts of platinum-group elements and gold owe their origin to magma chamber processes (e.g., assimilation), to characteristics inherited at the time of magma generation, or to a combination of both the above? Is there any post-magmatic hydrothermal effect on the intrusion?

1.7 Methods of study

Detailed field work was carried out on the Wateranga intrusion to prepare the geological map as presented in this thesis (Fig. 2.1, Chapter 2). Aerial photographs and Magellan Global Positioning System receivers were used as an aid to location. Different lithological units were carefully examined for their field characters and necessary inferences were drawn regarding the geological setting of the intrusion (see Chapter 2).

More than 150 fresh representative surface rock samples were collected from the intrusion. In addition, extensive drill core (~850 m) examination and sampling (~200 rock samples) have been carried out. Approximately 250 samples were investigated petrographically to fully understand the mineralogical changes within the rocks of the intrusion.

Whole-rock chemical analyses of 72 representative samples for major and trace elements were carried out by X-ray fluorescence (XRF) technique at the University of New England. These analyses were done to document the bulk chemical variations within the rocks of the Wateranga intrusion. Analyses are given in Table 1 (Appendix 1). In addition, 22 unpublished XRF analyses from Ashley and 22 unpublished analyses from Evans (1992) were used in this study [Tables 2 and 3 (Appendix 1)]. Rare earth element (REE) concentrations of 20 samples and Pt, Pd and Au concentrations of 10 samples were measured by ICP-MS technique at Australian Laboratory Services, Brisbane. Analyses are presented in Tables 4.5 and 4.6 (Chapter 4).

More than 400 mineral analyses were carried out by electron microprobe analysis at the University of New England. These data are used to determine patterns of differentiation in the rocks, for testing of model magma compositions and to estimate P-T conditions. Analyses are given in Appendix 2. Sr and O isotopic analyses of 10 samples and Nd isotopic analyses of eight samples were performed at the Centre for Isotope Studies, CSIRO, Sydney. Details regarding the various laboratory procedures are given in Appendices 1 to 4.

1.8 Outline of the study

This study is divided into seven chapters. Chapter 1 provides a general introduction on layered intrusions and to the Wateranga intrusion. Field observations, drill core examination results, regional geology and petrography are presented in Chapter 2. Chapter 3 includes mineral chemistry. In Chapter 4 major and trace element geochemistry is presented. Chapter 5 presents isotope geochemistry. Chapter 6 provides a discussion and interpretation of the results and a model for the development of the Wateranga intrusion. Conclusions are presented in Chapter 7.

CHAPTER 2

Geologic Setting and Petrography

Part A (Geologic Setting)

Part B (Petrography)

Geologic Setting and Petrography

2.1 Introduction

The purpose of this chapter is to provide detailed geology of the Wateranga intrusion and a regional geological framework and tectonic setting of the northern New England Fold Belt. Furthermore, a detailed petrographic description of rocks of the intrusion and characteristics of the important mineral constituents are presented. This chapter is divided into two parts. Part A addresses the geologic setting and part B presents petrographic features of the Wateranga intrusion.

PART-A: GEOLOGIC SETTING

2.2 Geology of the Wateranga Intrusion

As outlined in Chapter 1, the Wateranga intrusion is a layered, tholeiitic, mafic intrusion, located 80 km southwest of Bundaberg, in southeast Queensland. It is a funnel or saucer-shaped lopolith intruded into the Late Carboniferous Goodnight beds (siltstone, chert, metabasalt and quartzite) of the Goodnight Block. The Goodnight Block (Cranfield, 1989), which represents the easternmost and youngest part of the Devonian to Carboniferous accretionary wedge, is an elongated block of Late Carboniferous beds which extends for about 60 km along the eastern side of the northern New England Fold Belt in southeast Queensland (Fig. 2.3). Detailed mapping of the Wateranga intrusion carried out during the

present investigation, coupled with that of Robertson (1971), is presented in Figure 2.1. The exposure of the intrusion is oval shaped, elongated in NE-SW direction and covers an area of about 28 km^2. Olivine gabbro is the dominant rock type. Layering commonly dips towards the centre of the intrusion at angles ranging from 10 to 45 degrees (Talusani et al., 2000). Based on K/Ar dating (241, 242 and 245 ± 8 Ma) Permo-Triassic age, an age close to the Permian-Triassic boundary has been suggested by Day et al. (1983). The intrusion is unmetamorphosed and largely undeformed. Within the intrusion there is no evidence of folding and largely it is free from faulting, but faulting synchronous with the emplacement of the Late Permian-Early Triassic granites has disrupted the layering (Robertson, 1971).

The magmas forming the Wateranga intrusion were intruded into the synclinal structure developed due to folding movements within the Goodnight beds during the Late Permian time. A metamorphic aureole of pyroxene hornfels facies has been developed due to the emplacement of the Wateranga intrusion. Ashley et al. (1979) reported the ultramafic hornfelses containing the assemblages hornblende + olivine + spinel + magnetite, and clinopyroxene + olivine + spinel + magnetite in the Goodnight beds.

In this study, detailed field investigations of the Wateranga intrusion have led to the identification of four main rock types. These include norite, troctolite and anorthosite which occur as small elongated bodies enclosed by the more dominant gabbroic rocks. In the northern part of the intrusion, a chilled gabbro phase has been identified in two locations (samples WG-44 and WG-124). The stratigraphic thickness of the exposed sequence is approximately 140 m, with well exposed outcrops which consists of remarkably fresh samples (Fig. 2.2). Triassic granitoid intrusions have invaded the northern and western margins of the Wateranga intrusion. During the Pleistocene, the Barambah Basalt (alkali basalt) was extruded and flowed along the Burnett River drainage system (Wellman, 1978; Talusani, 2002). This basalt can be easily recognised because of its well preserved flow structures and its localization along present day drainage channels.

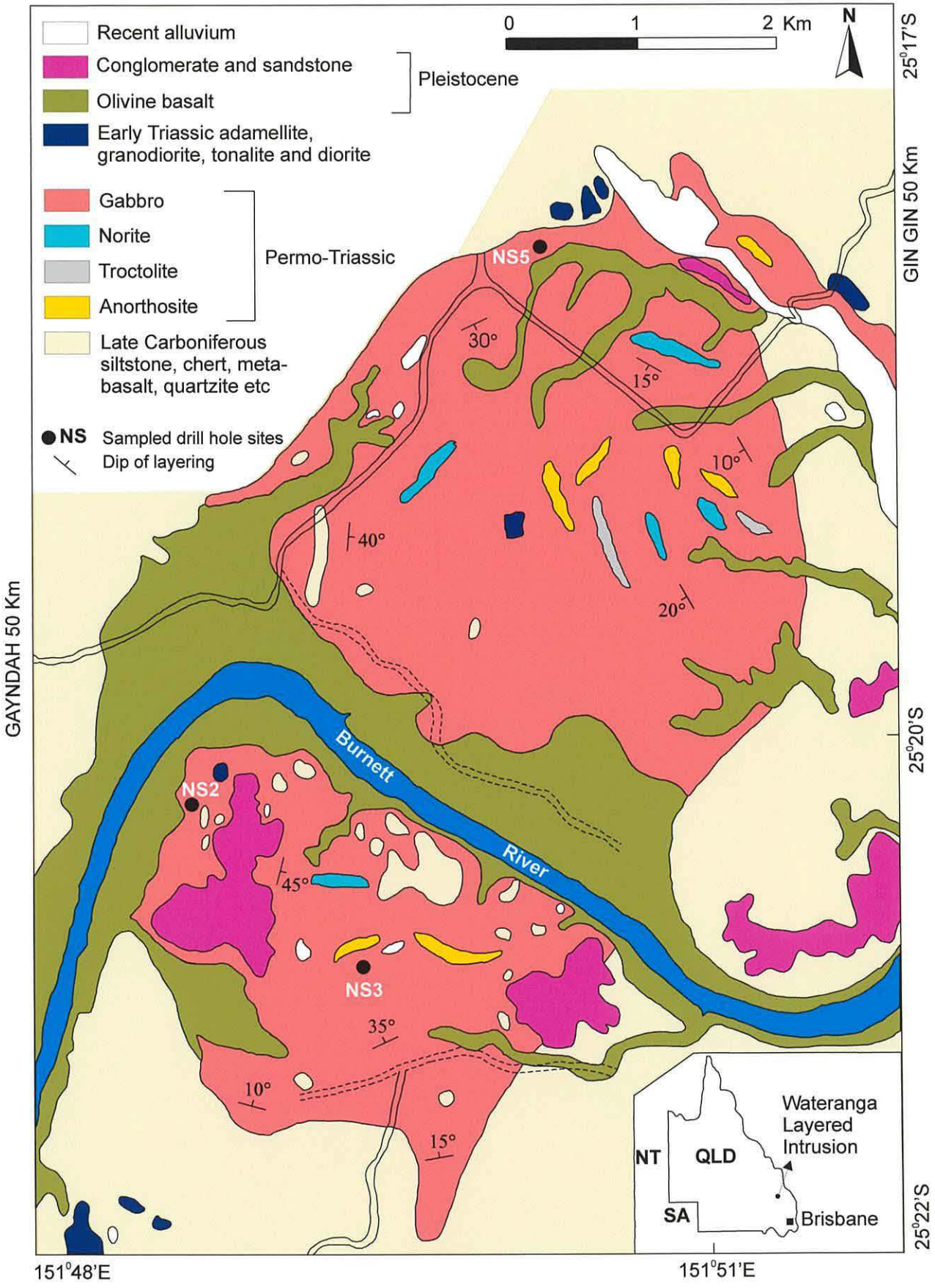

Figure 2.1. Geological map of the Wateranga Layered Intrusion, southeast Queensland - compiled from mapping done for this study and data taken from Robertson (1971).

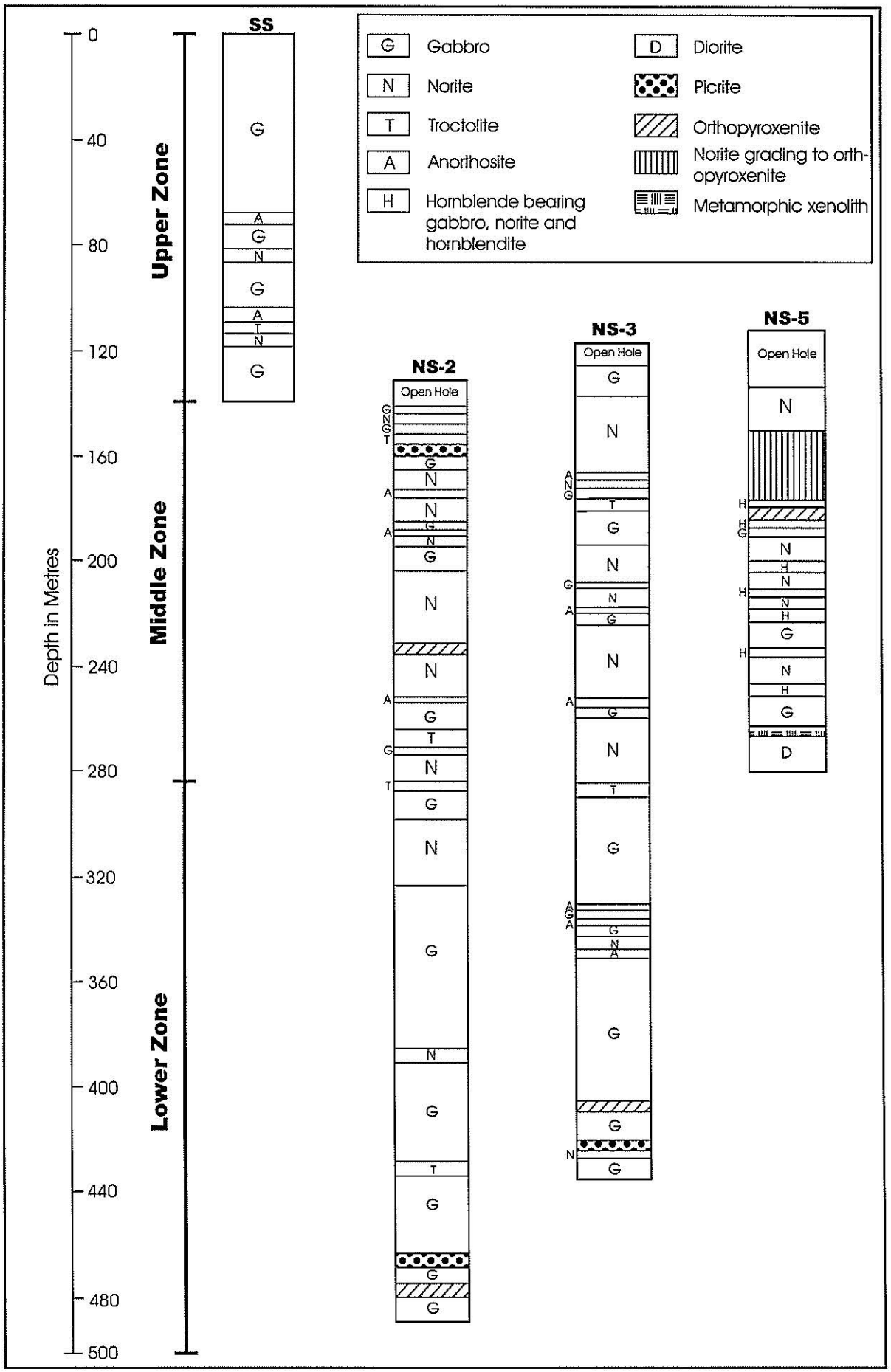

Figure 2.2 Sequence stratigraphy and correlation of columnar surface section (SS) and drill core sections (NS-2, NS-3 and NS-5) of the Wateranga Intrusion.

2.3 Drill core rock types and stratigraphy

Extensive drill core (~850 m) examination and sampling has been carried out to fully characterize the mineralogical and chemical changes within the rocks of the intrusion. The location of the three drill holes studied (NS-2, NS-3 and NS-5) is shown in Figure 2.1. Drill core stratigraphy and surface mapping stratigraphy are presented in Figure 2.2. In the drill core, rock types change abruptly with stratigraphic depth and include olivine gabbro, norite, troctolite, anorthosite, orthopyroxenite and picrite. Most of the body consists of gabbro and norite, with troctolite, anorthosite, orthopyroxenite in parts and rare picrite. Small bodies of granitic rock occur within the Wateranga intrusion as veins and small dykes (not shown in Fig. 2.2). Layering is well developed both on microscopic and mesoscopic scales and is the result of repetition of various rock types, which appear to have been formed by crystal accumulation. Layers vary from 2 to 55 m in thickness. Although sharp contacts between rock types are known, many of the boundaries are transitional from one rock type to another. The stratigraphic thickness of the deepest drill hole (NS-2) is ~350 m and the total cumulative thickness of the three drill holes studied (NS-2, NS-3 and NS-5) is ~850 m. The correlation is mainly based on cryptic variation of the minerals in rocks from the drill core. A list of drill core and surface samples studied and their stratigraphic depths is provided in Appendix 5.

2.4 Regional geology of the northern New England Fold Belt

The New England Fold Belt is a geologically complex region and forms the easternmost and youngest part of the Australian continent, extending from Newcastle to Townsville covering a length of almost 1500 km. It is flanked on its western side by the sedimentary rocks of the Sydney-Bowen Basin, which separates this belt from the Lachlan Fold Belt and its northerly extension. The New England Fold Belt is divided into three regional provinces, the Yarrol Province in the north, the New England Province in the south, and the Gympie Province in the east (Murray, 1987, 1997). The Yarrol and New England Provinces are separated by Mesozoic cover of the Surat and Clarence-Moreton Basins, which

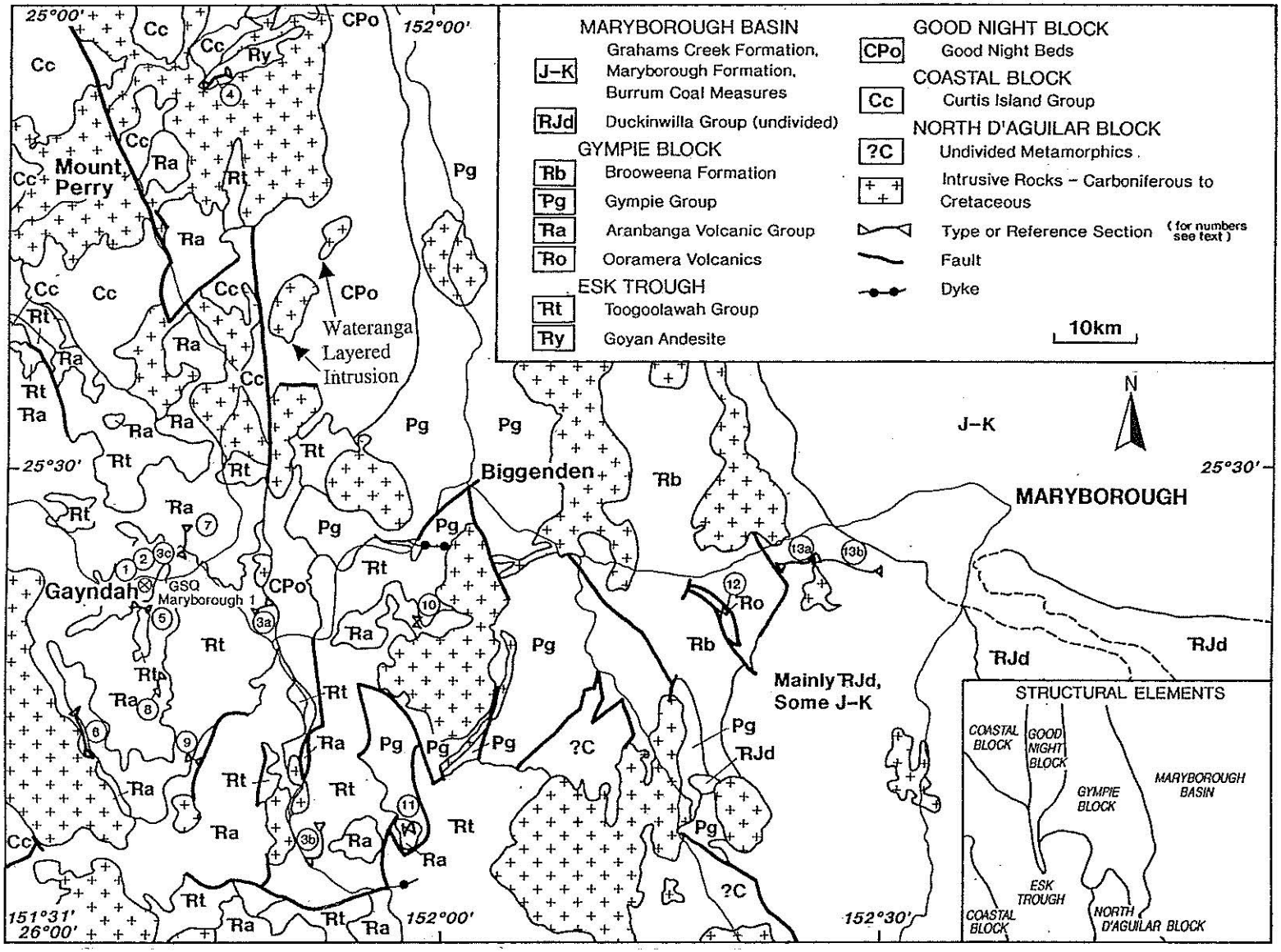

Figure 2.3. Stratigraphic units – Maryborough Sheet Area (Cainozoic omitted). Also shown is the Wateranga layered intrusion towards the northern part of the map, which has been emplaced into the Goodnight beds (CPo). After Cranfield (1989).

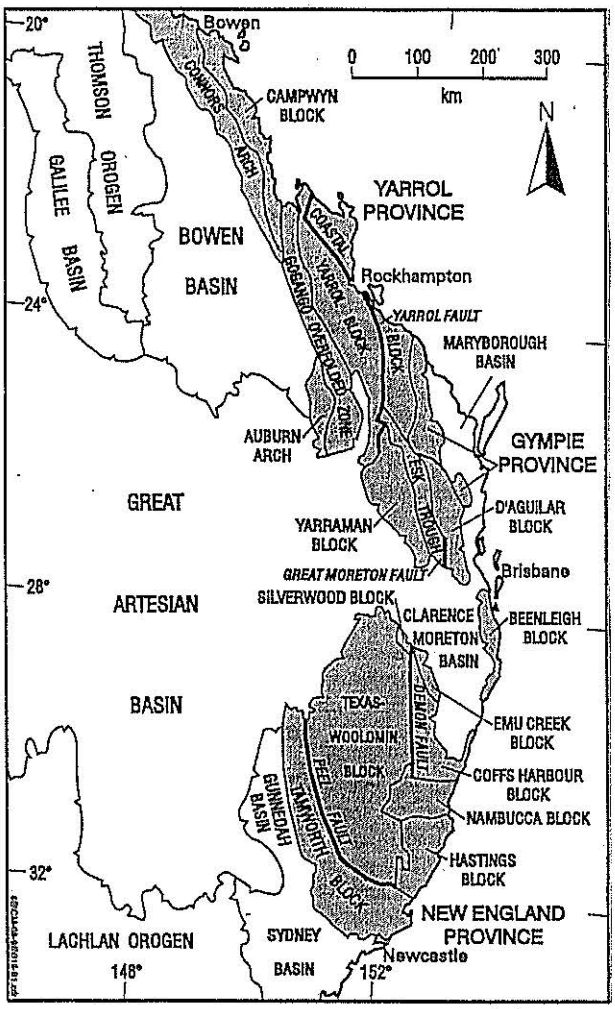

Figure 2.4. Structural units of eastern Australia showing subdivisions of the New England Fold Belt (shaded). After Murray (1997). (Top Figure).

Figure 2.5. Location of major terranes of the northern New England Fold Belt. After Holcombe et al. (1997b). Also shown are the locations of layered intrusions in southeast Queensland (Wilson and Mathison 1968; Nesbitt 1970; Murray 1975; Clifford 1987) (Bottom Figure).

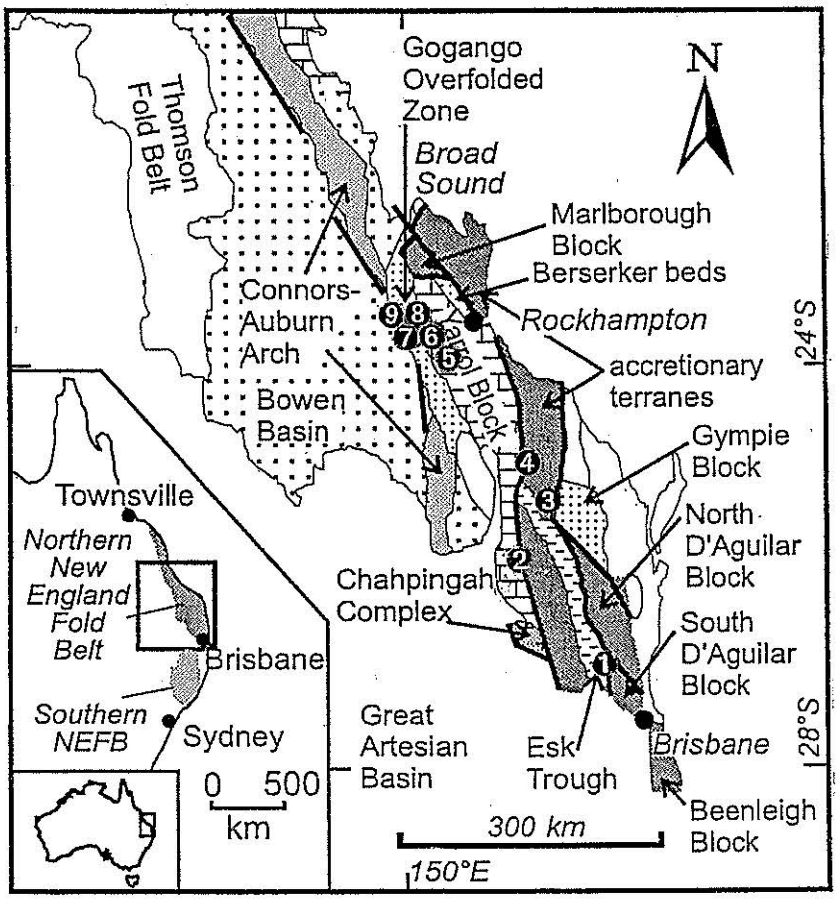

Location of layered intrusions (1-9)

1. Somerset Dam
2. Wigton
3. Wateranga (present study)
4. Goondicum
5. Eulogie Park
6. Boogargan
7. Windah
8. Bucknalla
9. Fred Creek

makes direct correlation of their structures and tectonic elements difficult. Structural units of the New England Fold Belt are shown in Figure 2.4 (Murray, 1997). In more recent work, Holcombe et al. (1997a) divided the New England Fold Belt into the northern New England Fold Belt (NNFB) and the southern New England Fold Belt (SNFB). Present structural units of the northern New England Fold Belt are shown in Figure 2.5. This section presents a brief account of the regional geology of the northern New England Fold Belt.

During the Late Devonian and Carboniferous, eastern Australia was located at an Andean-type convergent margin, with westerly dipping subduction zone responsible for the development of a magmatic arc in the west, flanked by a forearc basin and a subduction complex in the east (Leitch, 1974, 1975; Cawood, 1982; Murray et al., 1987). The similarities of tectonic setting, rock types and fauna in the southern and northern New England Fold Belt make it very probable that the three stratotectonic elements (volcanic arc, forearc basin, continental slope and ocean basin now represented by a subduction complex) were continuous between the two provinces in the Late Devonian-Early Carboniferous (Roberts and Engel, 1980).

Cranfield (1989) remapped the rocks of southeast Queensland (Maryborough 1:250 000 Sheet area) to resolve major inconsistencies in previous interpretation. Based on age and style of deformation the area has been divided into several structural subdivisions called Blocks (Fig. 2.3). They are as follows.

1. Carboniferous Coastal Block and North D'Aguilar Block.
2. Carboniferous to Permian Goodnight Block.
3. Permian and Triassic Gympie Block.
4. Early to Middle Triassic Esk Trough.
5. Latest Triassic to Cretaceous Maryborough Basin.
6. Tertiary to Quaternary deposits (including volcanics).
7. Granitoids, which range in age from Carboniferous to Jurassic-Cretaceous, which have intruded the structural Blocks.

The Coastal, North D'Aguilar and Goodnight Blocks form part of the extensive Carboniferous accretionary wedge assemblage that is developed along almost the entire length of the New England Fold Belt (Murray, 1987; Fergusson

et al., 1993). The Esk Trough is a narrow, north-northwest-trending belt of Early Triassic rocks (Holcombe et al., 1997a). The structure of the belt is generally considered as a graben, with its present margins approximating original rift margins. The north D'Aguilar Block is a deeply subducted, composite terrain consisting of polymetamorphic assemblages (Cranfield, 1994). This block is characterized by units that are dissimilar in both composition and metamorphic grade to adjacent rocks thought to be of the same age. It has been suggested that the North D'Aguilar Block, with its dominantly mafic metavolcanic units and large serpentine bodies, was an accretionary wedge (Holcombe and Little, 1994). The intrusive rocks in the Maryborough 1:250 000 sheet area range from ultramafic to granitic in composition. Radiometric age dates show ages of emplacement from the Carboniferous to the Jurassic-Cretaceous boundary; most intrusions are Middle to Late Jurassic.

The Wateranga intrusion was emplaced into the Late Carboniferous Goodnight beds of the Goodnight Block, which is bordered to the west by the Coastal Block, to the south and southwest by the Esk Trough, and to the east by the Gympie Block (Fig. 2.3). The Goodnight beds form an outcrop area of about 650 km^2 in the northwestern part of the sheet dominantly in the vicinity of the Burnett River west of Gin Gin to the south of Mingo Crossing. The Goodnight beds consist of slate, phyllite, argillite, chert, arenite, limestone, basic metavolcanics, and localized manganiferous chert deposits. Fine-grained rocks such as slate, phyllite and argillite dominate the sequence. The thickness of the Goodnight beds probably exceeds 2 000 m. It is complexly folded and sheared.

In the northern New England Fold Belt widespread deposition began in Silurian-Middle Devonian time. In the Yarrol Province, Late Silurian to Middle Devonian calc-alkaline volcanics, volcaniclastic sediments and limestones are preserved in isolated fault blocks along the western side of the Yarrol Fault (Fig. 2.4). These have been interpreted as remnants of a volcanic island arc, the Calliope Island Arc (Day et al., 1978), which was separated from the Australian continent by a marginal sea in the region of the Bowen Basin or by a much wider ocean basin.

As mentioned previously, in Late Devonian-Carboniferous time, the northern New England Fold Belt was an active Andean-type continental margin. The volcanic arc is only exposed in the north, where Late Carboniferous I-type granitoids were emplaced. Studies of the Connors-Auburn Volcanic Arc in the north show that volcanism changed from dominantly andesitic in the Late Devonian to dominantly dacitic in the Carboniferous (Korsch, 1984).

The Permo-Triassic Gympie Block, comprising mafic volcanics, volcaniclastic sediments and limestone, is unique in eastern Australia and does not fit into the overall palaeogeographic pattern of the New England Fold Belt. Various origins have been suggested for the Gympie Block ranging from an accreted arc (Sivell and Waterhouse, 1987) to an exotic displaced terrain derived perhaps from northern New England Orogen (Holcombe et al., 1997a). In the northern part of the Yarrol Block (Fig. 2.4), the Permian ultramafic components have generally been regarded as ophiolitic in origin (Leitch et al., 1994).

No deposition or magmatic activity of Late Permian-Late Triassic age is recorded from the northern part of the New England Fold Belt north of Rockhampton. In contrast, the reminder of the fold belt was an extremely active region. Widespread continental volcanics, mainly of silicic to intermediate composition were erupted and numerous granite plutons of Late Permian-Late Triassic age were emplaced. In its regional context, the Late Permian-Late Triassic magmatism of the New England Fold Belt is clearly post-orogenic, as it post-dates the main folding events (Day et al., 1978). Some writers (e.g., Holcombe et al., 1997a) have argued that the magmatism was not related to subduction, whereas others have postulated an origin above a west-dipping subduction zone. A great variety of lode deposits ranging in age from Middle Palaeozoic to Early Cretaceous is present in the New England Fold Belt. Most of these are related to emplacement of extensive granite plutons and eruption of continental silicic volcanics in Late Permian-Late Triassic time (Murray, 1986).

Following a period of cratonic stability in Jurassic time, calc-alkaline volcanism and plutonism recommenced in the northern part of the New England Fold Belt in the Early Cretaceous. The volcanics comprise silicic to intermediate flows and pyroclastics, and were probably entirely continental (Murray, 1986).

2.5 Tectonic evolution of the northern New England Fold Belt

The New England Fold Belt is the easternmost and youngest tectonic unit of eastern Australia. It was an active zone of terrain accretion during the Palaeozoic to Early Mesozoic (Flood, 1988; Coney et al., 1990). As already mentioned, traditionally the New England Fold Belt is divided into three regional provinces: Yarrol, Gympie and New England (Fig. 2.4). Recently, Holcombe et al. (1997b) divided the New England Fold Belt into northern and southern New England Fold Belt (Fig. 2.5). This section presents a synthesis of our current understanding of tectonic evolution of the northern New England Fold Belt.

Within a broad convergent continental margin setting, the New England Fold Belt of eastern Australia consists of several variably deformed and metamorphosed terrains each reflecting a different tectonic element or orogenic episode. These terrains range in age from Early Palaeozoic to Late Triassic (Henderson et al., 1993). The main tectonic elements of the northern New England Fold Belt had been recognised by the mid 1970s (a simple convergent margin tectonic model) (Leitch, 1975). During the 1980s and early 1990s several significant advances occurred in understanding the development of the northern New England Fold Belt (simple convergent margin tectonic model was replaced by a complex tectonic collage). During the past decade detailed geological and tectonic studies (State Geological Surveys), extensive geochemical studies (independent groups), regional airborne magnetics and radiometrics (exploration companies) and detailed deep seismic surveys (AGSO) have been carried out in different parts of the northern New England Fold Belt. Although these studies have necessitated a revision of the conceptual framework for the better understanding of the northern New England Fold Belt, its tectonic development is yet to be solved.

The rocks of the northern New England Fold Belt have experienced a long and complicated tectonic history including multiple tectonic episodes. The west-dipping subduction system produced, from west to east, a magmatic arc, a forearc basin and an accretionary wedge. The system had Andean-type continental margin affinities (Leitch, 1975; Murray et al., 1987; Holcombe et al., 1997b). This pattern continued until the Late Carboniferous, when subduction ceased temporarily and

subsequently jumped eastwards, establishing a new convergent system that was to dominate the Permian to Cretaceous tectonics.

In the Late Carboniferous to Early Permian, the northern New England Fold Belt appeared to be dominated by an extensional tectonic setting. The extension may have been related to a change from subduction to strike-slip along the Gondwana margin, and was expressed in a variety of forms, including: (1) major Late Carboniferous extensional structures in the North D'Aguilar Block, including a major low-angle detachment fault, and associated emplacement of S-type granites (Little et al., 1992; Holcombe et al., 1997b), and (2) the Early Permian Gympie Island Arc (Sivell and McCulloch, 1997, 2001; Cranfield et al., 1997), with implications that a backarc basin developed between the Gympie terrain and continental eastern Australia.

The late Early to early Late Permian saw the renewed onset of subduction. The Late Permian-Early Triassic granitic rocks of the New England Batholith are interpreted as the products of a continental margin magmatic arc associated with subduction at an active plate motion (Chappell, 1994). These plutons form a major arcuate belt along almost entire length of the New England Fold Belt (Harrington and Korsch, 1985). During the Late Permian a major thrust-dominant contractional deformation (Hunter-Bowen Orogeny) affected the region (Holcombe et al., 1997a) as well as intrusion of significant volumes of Late Permian to Triassic magma. It is also likely that extensional movements that formed the Esk Trough (Fig 2.5) commenced in the Late Permian or earlier. As a result of the Hunter-Bowen Orogeny, sedimentation in the Esk Trough ceased in the Middle Triassic (~230 Ma) with the onset of significant contractional deformation. At the same time the volume of magma was gradually increasing. The peak of magmatic activity is associated with the Early to Middle Triassic at ~230 Ma, the age of which seems to correspond with early post-orogenic regime of extension and granite emplacement post-dating the Hunter- Bowen Orogeny (Crouch et al., 1995).

From the latest Triassic to Early Cretaceous basin development was the dominant feature affecting southeast Queensland. This period was reflected in the development of the Great Australian Basin. Local examples of this basin in

southeast Queensland are the Surat, Clarence-Moreton, Nambour and Maryborough basins (Fig 2.4). Regional uplift apparently occurred at the end of the early Middle Jurassic, and Late Jurassic to Cretaceous sediments and volcanics were laid unconformably on the Late Triassic to Jurassic sequences (Cranfield, 1994).

PART-B: PETROGRAPHY

2.6 Introduction

About 250 samples were examined petrographically to document their cumulus and intercumulus mineralogy, textures and crystallization sequences. This information is important in determining the affinities of the magma from which the rocks crystallized. Also, these data are useful in modelling differentiation processes. Terminology used in rock type classification is that of Streckeisen (1976) and Irvine (1987).

2.7 Nomenclature of cumulates and textures

Wager and his co-workers (1960) proposed that the two major components of layered mafic intrusions are cumulus and intercumulus minerals. Cumulus minerals are transported through the magma by fluid mechanical processes, whereas intercumulus minerals crystallize from the trapped liquid. There is a continued debate about crystal settling processes in the literature and alternative ideas were proposed, especially after the late 1970s but the terms "cumulate" and "intercumulate" have not been changed (Irvine, 1982). These terms are generally used in the literature to indicate the crystallization order of minerals, rather than the process involved in the formation of igneous layering or in crystal settling. Modern petrographic descriptions retained cumulus, strictly as a textural term, to describe euhedral to subhedral crystals that form a touching matrix of early-formed crystals. Crystals that are texturally cumulus, however, do not necessarily have to have settled under the influence of gravity.

Textures of layered intrusions were classified by Wager et al. (1960) as adcumulate, mesocumulate and orthocumulate on the basis of the amount of intercumulus minerals and relationships among grains. Although there is no general agreement among others (see McBirney and Noyes, 1979), adcumulate, mesocumulate, and orthocumulate are characterized by volume percents of 0-7, 7-25 and 25-50 intercumulus minerals, respectively (Hess, 1989). Most textures of layered intrusions can be described by these terms and the term heteradcumulate.

In cumulates, the name of any particular rock is dependent upon the modal composition of the major cumulus phases, e.g., a rock consisting of plagioclase and orthopyroxene as the sole cumulus minerals is called a norite, but in the case where only one major cumulus phase is present, this rock would be named anorthosite or orthopyroxenite. Cumulus minerals exhibit three main habits: (a) as euhedral to subhedral grains defining the cumulate framework, (b) as inclusions in later cumulus and postcumulus phases, and (c) as discrete grains between cumulus minerals, but not enclosed in postcumulus material. The space between cumulus minerals is filled by postcumulus material, which occurs commonly in two habits: (a) as filling of interstices between cumulus phases, or (b) as large oikocrysts poikilitically enclosing cumulus and/or earlier crystallized postcumulus phases. Later subsolidus reactions, e.g., exsolution of clinopyroxene blebs and lamellae in orthopyroxene, yield additional habits not listed above. Late-stage magmatic processes (e.g., postcumulus metasomatism, hydrothermal alteration) may cause an overprint, which could result in complete transformation (Irvine, 1982).

Table 2.1 Rock types and cumulus mineralogy

Rock type	Cumulus mineral(s)
Gabbro	Plagioclase + clinopyroxene
Norite	Plagioclase + orthopyroxene
Olivine gabbro	Plagioclase + clinopyroxene + olivine
Gabbronorite	Plagioclase + orthopyroxene + clinopyroxene
Olivine gabbronorite	Plagioclase + orthopyroxene + clinopyroxene + olivine
Troctolite	Plagioclase + olivine
Anorthosite	Plagioclase
Orthopyroxenite	Orthopyroxene

The nomenclature for cumulus rocks has been a source of confusion and controversy (Irvine, 1982). A system for naming cumulates on the basis of their cumulus mineralogy is inherently a genetic classification but provides valuable information about the rock modes and texture. In this study the classification of Irvine (1987) is followed and named cumulates based on their cumulus mineralogy (Table 2.1).

2.8 Rock types of the Wateranga intrusion

In the Wateranga intrusion, gabbro and norite are the most common rock types observed, with lesser troctolite, anorthosite, orthopyroxenite and rare picrite (Ambler and Ashley, 1977; Evans, 1992; Evans et al., 1993; Talusani et al., 2000). Broadly, on the basis of the petrographic studies of the surface samples and drill core, the Wateranga intrusion can be subdivided into three stratigraphic zones: a lower gabbroic sequence (Lower Zone), a middle noritic sequence (Middle Zone) and an upper gabbroic sequence (Upper Zone) (Fig. 2.2). Lower and upper gabbroic sequences are mainly composed of gabbro, with lesser norite, troctolite, anorthosite, orthopyroxenite and rare picrite. The middle noritic sequence is composed largely of norite, with lesser gabbro, troctolite, anorthosite, orthopyroxenite and rare picrite. The criteria used to delineate zones are explained in Section 3.4, Chapter 3.

2.8.1 Gabbro

Gabbro is the most abundant rock type of the Wateranga intrusion (~ 55%). Cumulus minerals are plagioclase and clinopyroxene, and ilmenite and magnetite are intercumulus minerals. Generally, the amount of plagioclase is higher than that of clinopyroxene. Average grain size varies from 0.5 to 5 mm. Accessory phases include apatite, hornblende, biotite and sulphides.

Olivine gabbro is the most common rock type of the gabbro group. Olivine gabbro consists of plagioclase, clinopyroxene and olivine as cumulus phases, whereas ferrogabbro comprises plagioclase, clinopyroxene, ilmenite and magnetite as cumulus phases. Both olivine gabbro and ferrogabbro contain the same

accessory phases as the gabbro. Ferrogabbros are not common in the Wateranga intrusion but are quite distinctive where they occur (e.g., samples NS-2/5 and A-WG-24 from the Middle and Upper Zones respectively).

2.8.2 Norite

Norite is the second most abundant rock type of the intrusion. Plagioclase and orthopyroxene in variable ratios constitute the norites. Accessory minerals are clinopyroxene, ilmenite, magnetite, apatite, hornblende, biotite and sulphides. The most abundant postcumulus phase is clinopyroxene. Exsolution blebs and lamellae of clinopyroxene in orthopyroxene are observed in some samples of norite. The orthopyroxene is usually hypersthene and is of euhedral to subhedral prismatic shape, whereas plagioclase commonly displays a lath-like form.

2.8.3 Troctolite

A typical troctolite consists of 77% plagioclase, 20% olivine, 1% clinopyroxene and 2% ilmenite and magnetite. Plagioclase is medium to coarse grained (0.5-3 mm), elongate and euhedral, and occurs typically as a cumulus phase. Olivine is anhedral and commonly occurs as an intercumulus mineral, but locally as cumulus mineral. Clinopyroxene, ilmenite and magnetite occur as intercumulus minerals. Accessory minerals include orthopyroxene, hornblende, biotite and sulphides. Troctolites are not common throughout the Wateranga intrusion and do not occur in drill hole NS-5.

2.8.4 Anorthosite

The modal composition of the anorthosites is generally 90-95% plagioclase, 5-10% clinopyroxene and rare oxide phases. In anorthosite, plagioclase is the only cumulus phase. Clinopyroxene is interpreted, in terms of texture, as a postcumulus phase. Anorthosite adcumulates with well developed triple point junctions and texturally equilibrated geometry are common. Anorthosites, like troctolites, are only a minor rock type in the Wateranga intrusion, and are generally coarse grained.

2.8.5 Orthopyroxenite

In orthopyroxenite, orthopyroxene is the only cumulus mineral. Orthopyroxene forms subhedral to euhedral cumulus crystals, 2-3 mm in size. Plagioclase occurs as anhedral intercumulus grains, occupying the interstices between cumulus orthopyroxenes. Ilmenite and magnetite occur as 0.2 mm euhedral crystals within orthopyroxene and intercumulus plagioclase.

2.8.6 Hornblende-bearing rocks

The abundance of hornblende-bearing rocks in the intrusion is very low and confined to drill hole NS-5. Typical rock types are hornblende gabbro, hornblende norite and hornblendite. Hornblende gabbro and hornblende norite contain approximately equal proportions of hornblende and plagioclase, whereas hornblendite is composed essentially of hornblende and minor plagioclase.

2.8.7 Picrite

Picrite is a rare rock type found in drill holes NS-2 and NS-3. Picrite is composed essentially of olivine and clinopyroxene with minor plagioclase.

2.8.8 Granitic rocks

In the Wateranga intrusion, granitic rocks occur as veins. Over the larger part of the intrusion, the granitic rocks are homogeneous, coarse-grained and pink to grey rocks. They consist essentially of quartz, alkali feldspar and muscovite. Accessory minerals include apatite, zircon and magnetite. The presence of granitic rocks at different depths of the intrusion is incompatible with the stratigraphy of the intrusion, which suggests that these granitic rocks may be later intrusions.

2.8.9 Miscellaneous rocks

Diorite and metamorphic xenolith are the two rare rock types restricted to drill hole NS-5.

2.9 Mineralogy and textures

Textures are the indices of geological processes. The textures of layered intrusions closely reflect the crystallization history of the magma. The rocks of the Wateranga intrusion are predominantly cumulates, with only a few areas where fine-grained gabbro (Plate 2D) represents the chilled margin. The rocks of the intrusion range from adcumulates to mesocumulates. The cumulus phases are plagioclase, olivine, clinopyroxene and orthopyroxene. Ilmenite, magnetite, hornblende, biotite, apatite and zircon are present as intercumulus minerals. The sulphides occur as intercumulus minerals throughout the intrusion.

Plagioclase is the dominant cumulus phase. It is tabular (up to 12 mm long) and commonly shows a well developed preferred orientation (Plate 1A). Optical zoning is common in plagioclase (Plate 1B).

Clinopyroxene is the dominant mafic mineral in these rocks and occurs mainly as a cumulus mineral (Plate 1G). It is also present as 0.5-8 mm poikilitic grains that include plagioclase and olivine, and inclusion-free interstitial grains (Plate 1C). Some of the clinopyroxene grains show sector zoning (Plate 1F). Exsolution of clinopyroxene blebs and lamellae in orthopyroxene are present in many samples (Plate 1D). Although orthopyroxene crystallizes largely as a cumulus phase, it can also occur as oikocrysts that enclose plagioclase and olivine. Also, orthopyroxene occurs as complex intergrowths with magnetite (Plate 2E). Ambler and Ashley (1977) reported symplectitic intergrowths of magnetite and orthopyroxene.

Olivine is less abundant than pyroxenes in the rocks of the Wateranga intrusion. It occurs as cumulus grains (Plate 1H) and locally as phenocrysts. It varies in size from 0.25 to 4 mm. The grains are subhedral and commonly have peritectic reaction rims of orthopyroxene ± magnetite (Plate 2B). Olivines are inclusion free, except for minor plagioclase (Plate 2A). Most olivines are unaltered, with only minor alteration to serpentine and iddingsite along fractures. Olivine and orthopyroxene occur as co-existing phases (Plate 1E). Some of the olivine grains show sector zoning (Plate 2C).

Brown hornblende is a common minor intercumulus mineral in many rocks, forming up to 5 modal %. A late-stage actinolite occurs as an alteration product of clinopyroxene in some samples.

Biotite commonly occurs as isolated grains and as rims on opaque phases, mostly ilmenite and magnetite. Biotite, and occasionally hornblende, occurs as overgrowths on cumulus clinopyroxene grains.

Apatite is a trace, fine-grained phase in these rocks. It is an accessory phase, which exists as clusters of needles, and as minute rods. In some samples, minor zircon has been noted as euhedral grains.

The oxide phases in the rocks of the Wateranga intrusion are ilmenite, magnetite and rare spinel. They are dominantly interstitial although in some finely layered sections, they occur as a cumulus phase with olivine and plagioclase. The relative proportions of ilmenite to magnetite are variable, but ilmenite is always dominant. Both ilmenite and magnetite contain exsolved ulvospinel phase. Magnetite-ilmenite oxidation exsolution intergrowth textures formed by the oxidation process were observed in some samples (Plate 2F).

Sulphide minerals occur as interstitial blebs and lenses with a maximum diameter of 1 mm. Pyrrhotite is the dominant sulphide mineral with exsolved chalcopyrite and pentlandite (Plate 2H).

Despite a thorough examination, platinum-group minerals were identified in only one sample using a scanning electron microscope (SEM) equipped with an EDS system. The platinum-group mineral found was a Rh-Ru phase occurring as inclusions in orthopyroxene of norite (Plate 2G).

2.10 Modal composition

The modal composition of the rocks was determined using an electric point counter, counting 400 points in each thin section. The average percentage modal composition of major rock types is presented in Table 2.2. The variations in modal composition of olivine, plagioclase, clinopyroxene and orthopyroxene vary widely with stratigraphic depth (Fig. 2.6), as would be expected in a layered mafic

PLATE - 1

Plate 1

A *Adcumulate anorthosite with well developed triple point junctions. Texturally equilibrated geometry. (XPL, field width = 1 mm, sample number: R80585).*

B *Oscillatory zoning in plagioclase, olivine gabbro. (XPL, field width = 0.5 mm, sample number: R80620).*

C *Mesocumulate anorthosite with cumulus plagioclase and intercumulus clinopyroxene. Texturally partly equilibrated geometry. (XPL, field width = 2 mm, sample number: R80585).*

D *Exsolution lamellae of clinopyroxene in orthopyroxene, noritic gabbro. (XPL, field width = 0.25 mm, sample number: R80593).*

E *Coexisting olivine and orthopyroxene in olivine norite. (XPL, field width = 0.5 mm, sample number: R80607).*

F *Sector zoning in clinopyroxene from olivine gabbro. 1 and 2 on the photograph are sectors. (XPL, field width = 1 mm, sample number: R80575).*

G *Cumulus clinopyroxene in olivine gabbro. Also seen are plagioclase inclusions in CPX. (XPL, field width = 2 mm, sample number: R80576).*

H *Olivine gabbronorite showing adcumulate texture (olivine) with well developed triple point junctions. (XPL, field width = 0.5 mm, sample number: R80581).*

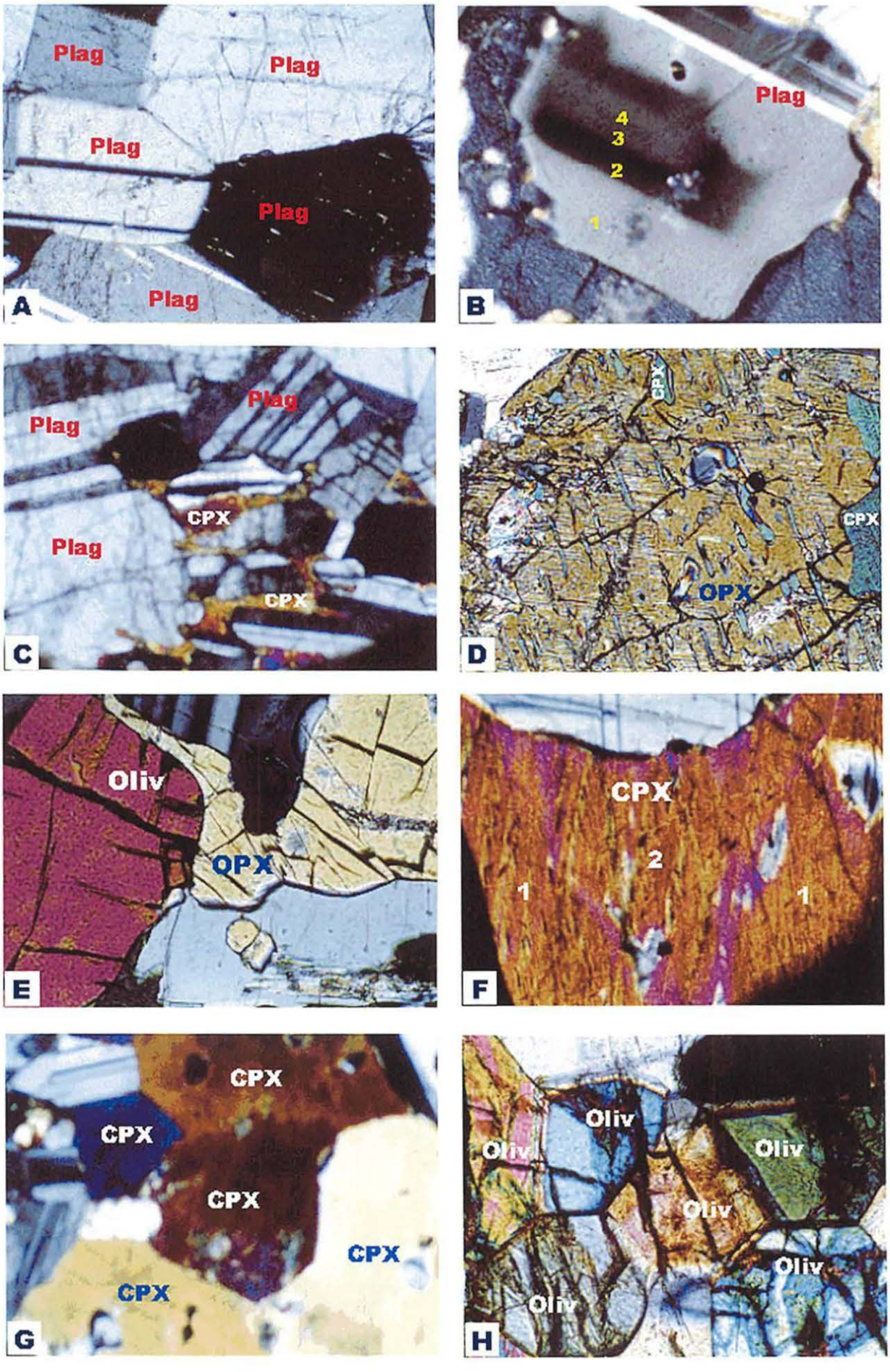

Plate 1 Photomicrographs of different rock units, Wateranga Intrusion.

Plate 2

A *Poikilitic texture in troctolite – large olivine enclosing a number of plagioclase laths. (XPL, field width = 2 mm, sample number: R80588).*

B *This photograph illustrates the unique textural feature, the peritectic reaction (olivine + liquid → enstatite) in olivine norite. (XPL, field width = 1 mm, sample number: R80616).*

C *Sector-zoned olivine in troctolite – olivine grain occupying most of this photograph is sector-zoned. Also seen is plagioclase inclusion in olivine. (XPL, field width = 2 mm, sample number: R80588).*

D *Fine grained olivine gabbronorite from chilled margin of the Wateranga intrusion. This rock contains plagioclase, clinopyroxene, orthopyroxene, olivine and magnetite. Although the rock is fine grained, it is called a 'gabbro' because it is from a large intrusion. The fine grain size results from quick cooling at the intrusion margin. (XPL, field width = 2 mm, sample number: R80579).*

E *Symplectite of magnetite and orthopyroxene in olivine gabbro – magnetite (white) and orthopyroxene (grey) are intimately intergrown in a vermicular fashion. (PPL – reflected light, field width = 0.25 mm, sample number: R80576).*

F *Magnetite-ilmenite oxidation exsolution intergrowth formed by oxidation in olivine norite. (XPL – reflected light, field width = 0.5 mm, sample number: R80619).*

G *Platinum-group mineral (Rh-Ru phase) in orthopyroxene from norite. (SEM – back scattered image. Length of the scale on the photograph is 10 μm, sample number: R80640).*

H *Pyrrhotite host with inclusions of chalcopyrite in norite. (PPL – reflected light, field width = 0.25 mm,* sample number: R80635*).*

PLATE - 2

Plate 2

A *Poikilitic texture in troctolite – large olivine enclosing a number of plagioclase laths. (XPL, field width = 2 mm, sample number: R80588).*

B *This photograph illustrates the unique textural feature, the peritectic reaction (olivine + liquid → enstatite) in olivine norite. (XPL, field width = 1 mm, sample number: R80616).*

C *Sector-zoned olivine in troctolite – olivine grain occupying most of this photograph is sector-zoned. Also seen is plagioclase inclusion in olivine. (XPL, field width = 2 mm, sample number: R80588).*

D *Fine grained olivine gabbronorite from chilled margin of the Wateranga intrusion. This rock contains plagioclase, clinopyroxene, orthopyroxene, olivine and magnetite. Although the rock is fine grained, it is called a 'gabbro' because it is from a large intrusion. The fine grain size results from quick cooling at the intrusion margin. (XPL, field width = 2 mm, sample number: R80579).*

E *Symplectite of magnetite and orthopyroxene in olivine gabbro – magnetite (white) and orthopyroxene (grey) are intimately intergrown in a vermicular fashion. (PPL – reflected light, field width = 0.25 mm, sample number: R80576).*

F *Magnetite-ilmenite oxidation exsolution intergrowth formed by oxidation in olivine norite. (XPL – reflected light, field width = 0.5 mm, sample number: R80619).*

G *Platinum-group mineral (Rh-Ru phase) in orthopyroxene from norite. (SEM – back scattered image. Length of the scale on the photograph is 10 μm, sample number: R80640).*

H *Pyrrhotite host with inclusions of chalcopyrite in norite. (PPL – reflected light, field width = 0.25 mm,* sample number: R80635*).*

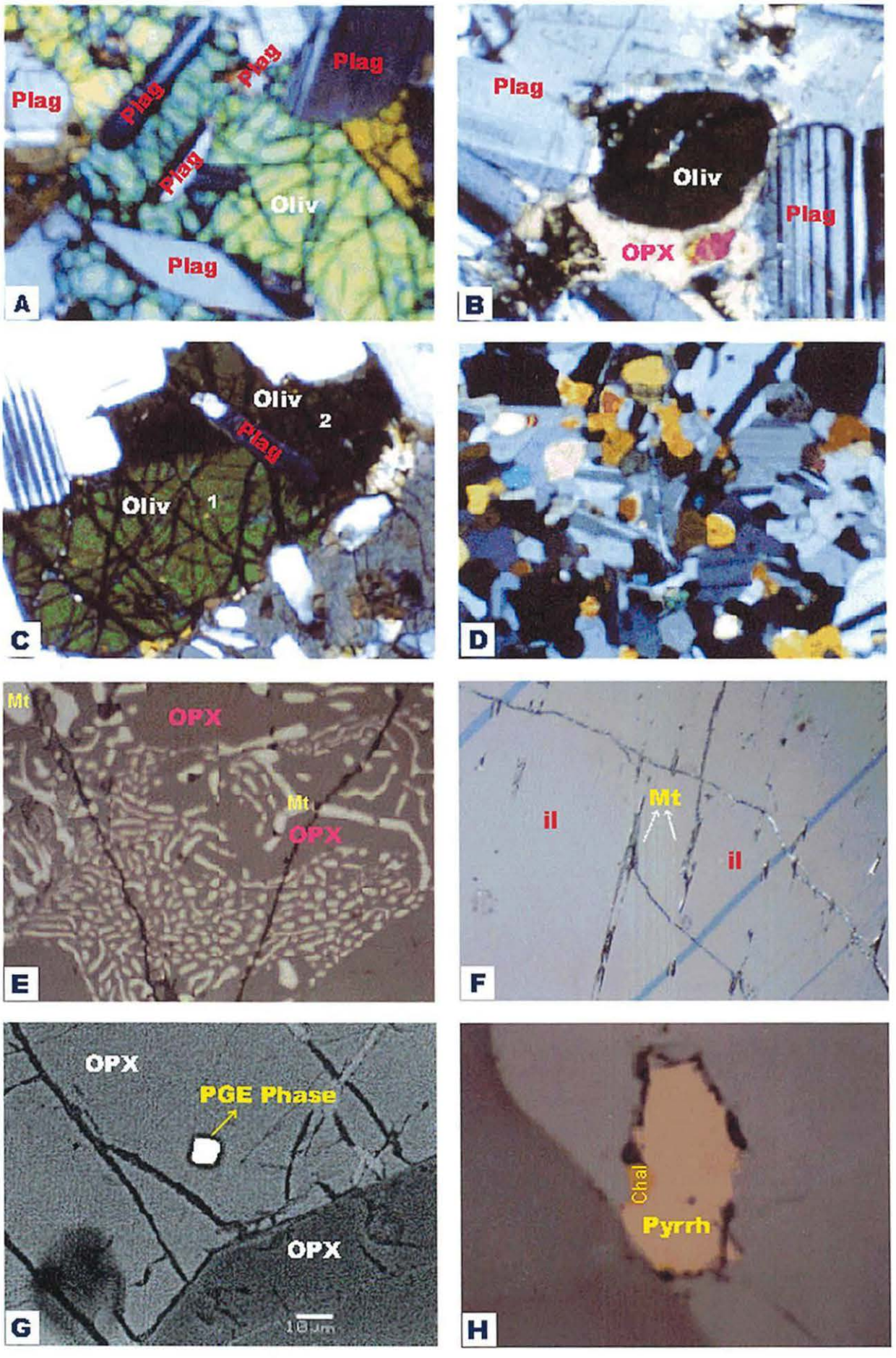

Plate 2 Photomicrographs of different rock units, Wateranga Intrusion.

intrusion. Open system behaviour of the magma chamber would produce oscillatory trends in modal composition as observed in the Wateranga magma chamber.

Classification and nomenclature (IUGS, Streckeisen, 1976) of the Wateranga rocks based on proportions (vol.%) of plagioclase, pyroxene, olivine, orthopyroxene and clinopyroxene is shown in Figure 2.7.

Table 2.2 Average percentage modal composition of major rock types

Rock Type	Plagi-oclase	Olivine	Clinopy-roxene	Orthopy-roxene	Oxides	Horn-blende	Others*
Gabbro	58.5	-	38.2	0.5	1.6	0.4	0.8
Olivine gabbro	57.2	15.3	23.1	0.9	2.1	0.5	0.9
Ferrogabbro	53.1	-	26.8	0.8	18.2	Tr	1.1
Gabbronorite	59.6	-	27.3	11.2	1.1	0.2	0.6
Olivine gabbronorite	59.3	12.3	19.4	6.6	1.3	0.3	0.8
Norite	62.2	-	1.0	35.0	0.9	0.3	0.6
Troctolite	77.4	18.1	0.8	0.3	3.0	Tr	0.4
Anorthosite	94.0	-	5.5	-	Tr	-	0.5
Orthopyrox-enite	8.0	5.9	0.8	75.2	8.4	0.5	1.2

Tr - Trace quantity. * biotite, apatite and sulphides.

2.11 Crystallization sequences

For each rock type, crystallization sequences were determined based on petrographic observations. The order of crystallization was determined by cumulus-intercumulus relationships among minerals. A general crystallization

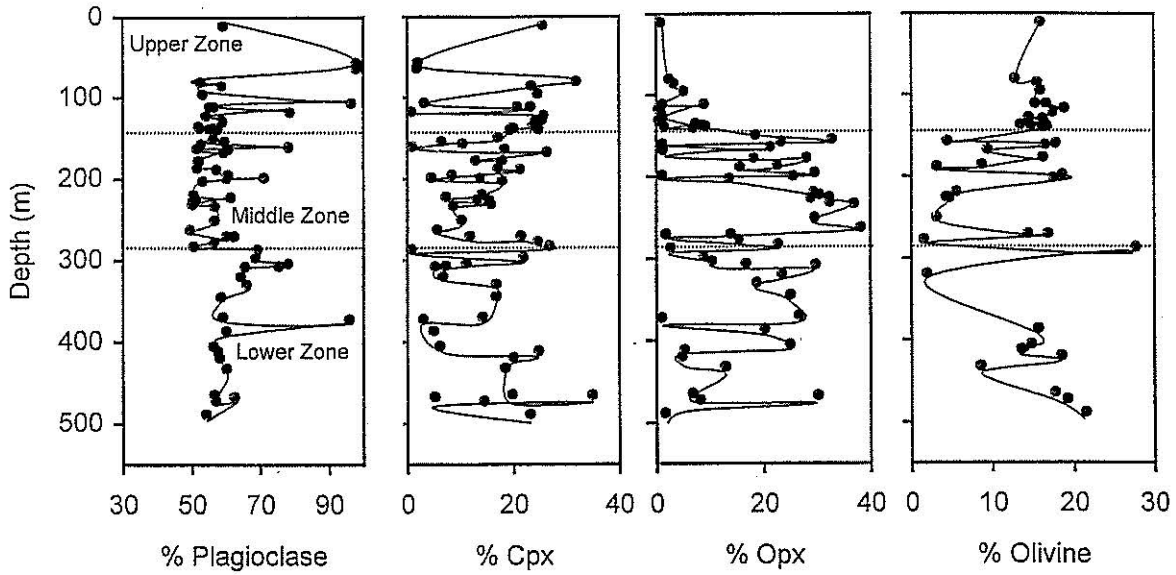

Figure 2.6 Variation of modal abundances (vol%) with stratigraphic depth in the Wateranga intrusion.

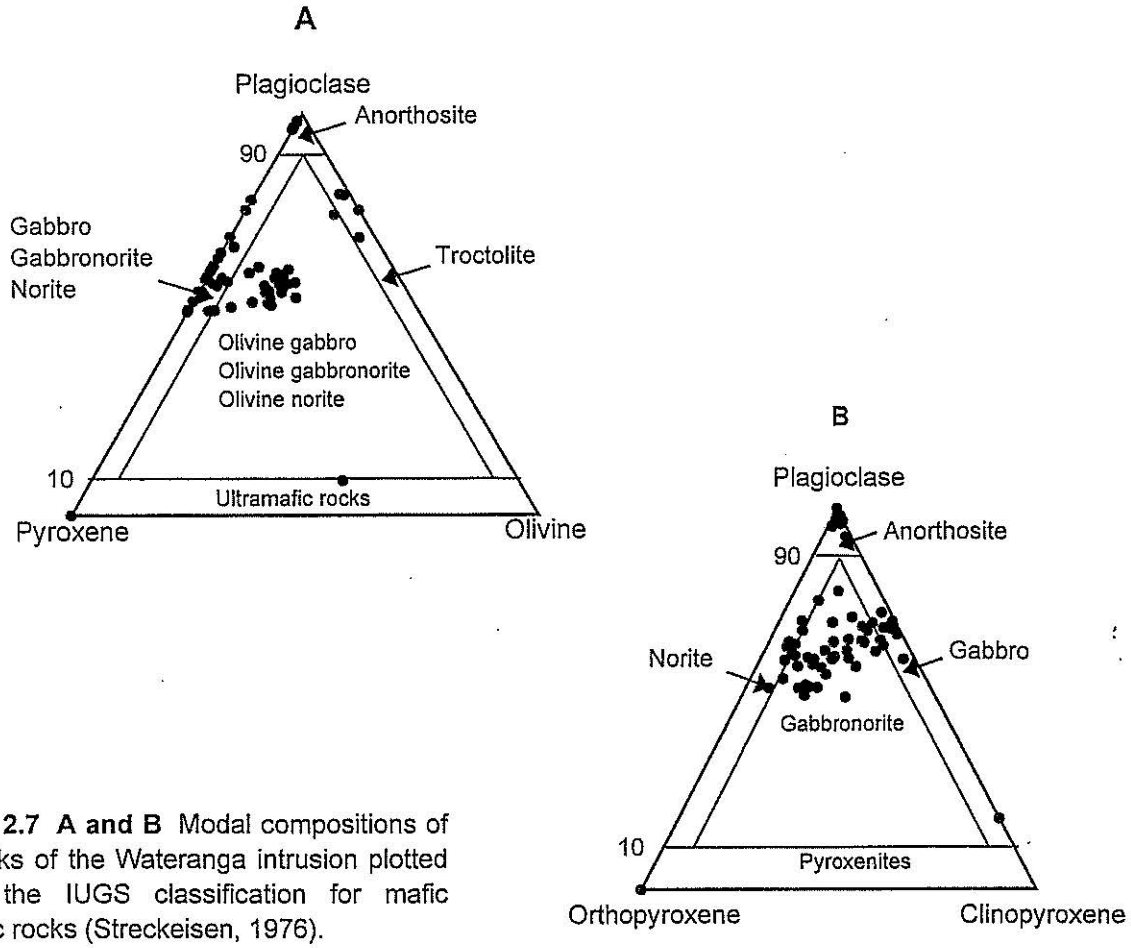

Figure 2.7 A and B Modal compositions of the rocks of the Wateranga intrusion plotted within the IUGS classification for mafic plutonic rocks (Streckeisen, 1976).

order of minerals in the Wateranga intrusion is olivine → plagioclase → clinopyroxene → orthopyroxene → Fe-Ti oxides → hornblende → biotite.

Irvine (1970) showed that olivine, clinopyroxene, orthopyroxene and plagioclase could yield as many as 30 different crystallization sequences. The actual order of crystallization depends on the composition of the initial magma. The crystallization order of minerals was different in samples from the Lower, Middle and Upper Zones of the intrusion (Table 2.3). These differences may be caused by an influx of fresh magma. Irvine and Smith (1967) and Irvine (1979) noted that the change in crystallization order implies a change in magma composition that cannot have been caused by fractional crystallization within the intrusion.

Table 2.3 Crystallization sequences in each zone of the Wateranga intrusion

Zone	Crystallization sequence
Upper Zone	Olivine → Plagioclase → Clinopyroxene → Orthopyroxene → Fe-Ti oxides → Hornblende → Biotite
Middle Zone	Plagioclase → Olivine → Orthopyroxene → Clinopyroxene → Fe-Ti oxides → Hornblende → Biotite
Lower Zone	Olivine → Plagioclase → Clinopyroxene → Orthopyroxene → Fe-Ti oxides → Hornblende → Biotite

2.12 Summary

The Wateranga intrusion is a small, Permo-Triassic, layered mafic intrusion. Most of the body consists of gabbro and norite, with troctolite, anorthosite, orthopyroxenite in parts and rare picrite. In the drill core, rock types change abruptly with stratigraphic depth. The most abundant minerals are plagioclase and clinopyroxene. Orthopyroxene and olivine are locally abundant. Hornblende is minor except in few rare layers. Olivine appears to have been the first mineral to crystallize in the Lower and Upper Zones of the intrusion, except in orthopyroxenites, where orthopyroxene crystallizes first and plagioclase is an intercumulus phase, and in the Middle Zone, plagioclase is the first mineral to crystallize.

CHAPTER 3

Mineral Chemistry

Mineral Chemistry

3.1 Introduction

Minerals from fresh rocks collected at fairly regular intervals through the intrusion were analyzed (more than 400 analyses) using a JEOL JSM-5800LV Scanning Electron Microscope fitted with an Oxford Link ISIS EDS system at The University of New England. These analyses were carried out in order to determine the compositional variations of cumulus, post-cumulus and other minerals in the Wateranga rocks, as well as patterns of differentiation, P-T conditions of crystallization, and to test model magma compositions.

Mineral compositions are compared to those of other rift-related gabbroic intrusions e.g. Skaergaard, East Greenland (Wager and Brown, 1968; Hoover, 1989; McBirney, 1989, 1996) and gabbro intrusions from the Oslo rift, Norway (Neumann et al., 1985). Analytical procedures are outlined in Appendix 2 and data for each mineral are presented in Tables 1-8 of Appendix 2. Also, representative analyses of each mineral are presented in this Chapter in Tables 3.1-3.5.

3.2 Crystallization phenomena

The minerals which belong to solid solution series play an important role in petrology because their compositions depend on intensive variables of magmas. Such minerals in layered intrusions are used frequently for determination of intensive variables either as absolute or relative values (Irvine, 1980; Robins et al., 1987; McBirney, 1993). The effects of intensive variables on crystallization

phenomena are described by thermodynamic equations. For example, the composition of a solid solution which consists of end members *A* and *B* is calculated by the following equations (Ragland, 1989).

$$\ln\left(\frac{a^L}{a^S}\right)=\left(\frac{\Delta H_A}{R}\right)\left(\frac{1}{T_A}-\frac{1}{T}\right) \qquad \Lambda\ 3.1$$

$$\ln\left[\frac{\left(1-a^L\right)}{\left(1-a^S\right)}\right]=\left(\frac{\Delta H_B}{R}\right)\left(\frac{1}{T_B}-\frac{1}{T}\right) \qquad \Lambda\ 3.2$$

where R is the gas constant, T is temperature in degrees Kelvin, a is activity, ΔH is enthalpy of fusion, and T_A and T_A are melting points of A and B. Superscripts L and S stand for liquid and solid. The equation can be modified for a specific mineral by including activities of elements in different crystallographic sites (Wood and Fraser, 1976; Philpotts, 1990). Solving equations 3.1 and 3.2 simultaneously results in equations for the liquidus and solidus of the system (Fig. 3.1).

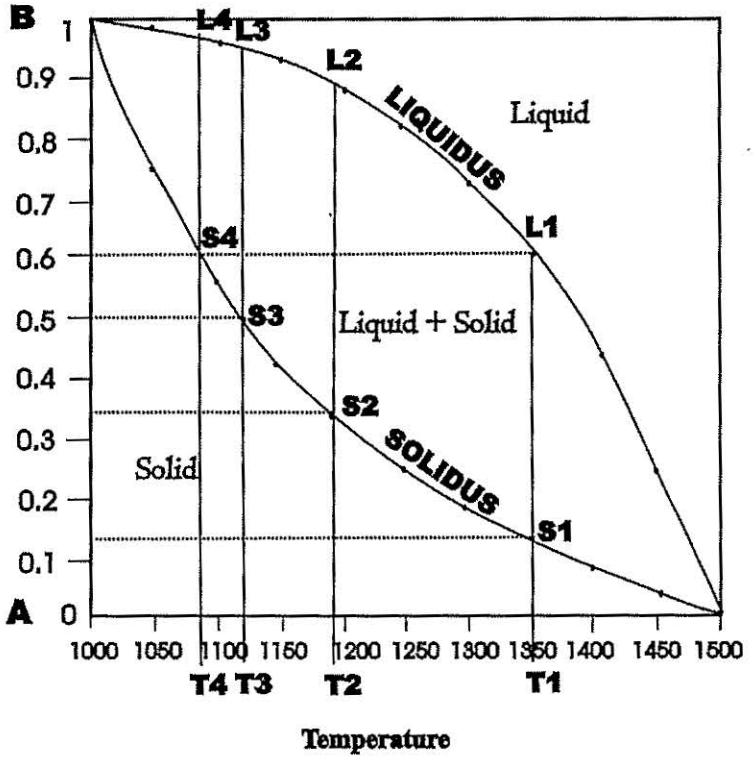

Figure 3.1. A schematic binary system for which ΔH_A = 90 kj, ΔH_B = 50 kj, T_A = 1500 k, T_B = 1000 k.

Any point on the solidus curve represents the amount of *A* and *B* in the crystal removed from the liquid at the specified temperature. For perfect equilibrium crystallization, the composition of all crystals at temperature *T3* will be *S3*; for fractional crystallization mineral compositions vary with temperature. In a basaltic magma, fractional crystallization is predominant so that the composition of minerals in a layered intrusion should change as a function of stratigraphic height and presumed decrease in temperature.

Mg and Fe are the end member cations for mafic minerals and Ca and Na are the end member cations for plagioclase. The shape of the solidus and liquidus curves will change for a particular mineral melt diagram, but the mineral composition will be a function of *T*. Among the mafic minerals, clinopyroxene, orthopyroxene, olivine and amphibole were analyzed by the electron microprobe and their Mg#s were determined, where Mg# = 100Mg/(Mg+Fe).

3.3 Open and closed system

In a simple intrusion that behaves as a closed system, upward decrease of Mg#s of minerals indicates fractionation of the magma (Naslund, 1989). The slope of the decrease in Mg#s is a function of the rate at which the minerals are separated from magma. An increase in the Mg#s of minerals may indicate an increase in temperature. However, temperature increase in a closed system is unlikely. Open system addition of new mafic magma into a magma chamber can result in both an increase in temperature and in Mg# (Irvine, 1980; Wiebe, 1988; Klewin, 1990; Chalokwu and Seney, 1995).

If an intrusion did not form by a single pulse of magma, then the intervals whose rocks formed between two magmatic pulses are called cyclic units. Cyclic units of the Stillwater complex were explained as a result of convective flow (Jackson, 1961), and Spera et al. (1982) showed that the velocity of convection is many times faster than solidification.

Reversals in the trend of Mg#s of minerals can occur at discrete intervals. The reversal may be either continuous or discontinuous. Continuous reversals may be caused by the reaction of primary cumulus minerals with an upward-increasing

amount of intercumulus liquid (Irvine, 1980; Cawthorn et al., 1992) as the cumulus pile thickens (Irvine, 1980). This idea is supported by lower Mg#s of natural cumulus minerals compared to Mg#s of mafic minerals grown experimentally (Cawthorn et al., 1992). They may also be caused by the slow and continuous emplacement of compositionally zoned magma followed by crystallization on an inclined floor (Wilson et al., 1987). If the reversal is discontinuous, it may be caused by the crystallization of repeated injections of increasingly magnesium-rich magmas.

3.4 Mineral compositions of the Wateranga intrusion

Variations in mineral composition record subtle changes in magma composition far more effectively than the presence or absence of specific phases. Compositions of plagioclase, pyroxenes, olivine and Fe-Ti oxides in the rocks of the Wateranga intrusion vary widely with stratigraphic depth. The mineral compositions provide perhaps the best indication of how fractional crystallization proceeded in different parts of the intrusion. On a smaller scale, the compositions of minerals from individual rocks also provide information on crystallization and reequilibration processes. Mineral compositional variations in the Wateranga intrusion are consistent with a fractionating tholeiitic magma. Compositional reversals and irregularities are important indicators of magmatic processes. Representative analyses of each mineral are presented in Tables 3.1-3.5. Trivalent iron contents and haematite and ulvospinel contents of ilmenite and magnetite respectively have been calculated using QUILF95 program (Andersen et al., 1993).

On the basis of electron microprobe analyses and petrographic examination the igneous stratigraphy of the Wateranga intrusion can be divided into three zones: (1) the Lower Zone, (2) the Middle Zone and (3) the Upper Zone (Fig. 3.3). These zones and the variations of major element compositions of minerals in each zone are discussed in the following sections. The criteria used to delineate zones include (i) reversals of the Mg#s of mafic minerals and An-contents of plagioclase, (ii) changes in the cumulus mineral assemblage that indicate an increase in

temperature, such as the reappearance of cumulus olivine, (iii) textural evidence such as resorption of minerals and (iv) changes in the crystallization order of minerals.

The common differentiation indices, such as Mg#s of clinopyroxene, orthopyroxene and olivine, and anorthite content of plagioclase all vary widely with stratigraphic depth and show discontinuities and reversals at the zone boundaries (Fig. 3.3). These changes are consistent with a magma chamber that was open to periodic influxes of new magmas, and the mixing of new and fractionated resident magma. The range of Mg#s of minerals in the Wateranga intrusion are 39 to 82 for clinopyroxene, 38 to 87 for orthopyroxene and 10 to 74 for olivine. Anorthite content of plagioclase ranges from 34 to 77. In Figure 3.2 the range of these common differentiation indices are compared to those of other rift-related gabbroic intrusions e.g., Skaergaard intrusion of East Greenland and gabbro intrusions from the Oslo rift, Norway. The ranges of plagioclase, pyroxene and olivine compositions observed in the Wateranga intrusion are similar to (or greater than) the ranges observed in the Skaergaard intrusion (Wager and Brown, 1968; Hoover, 1989; McBirney, 1989, 1996; Tegner, 1997; Jang et al., 2001) and gabbro intrusions from the Oslo rift (Neumann et al., 1985) and, therefore, the Wateranga intrusion represents one of the most extensive differentiation sequences.

3.4.1 Plagioclase

As already mentioned in Chapter 2, plagioclase is the dominant cumulus phase in the rocks of the Wateranga intrusion. It forms up to 95 modal % of some Wateranga samples (anorthosites), but is usually within the range of 53-77% (e.g. gabbro, norite, troctolite) (Table 2.2, Chapter 2). Anorthite contents vary with stratigraphic depth and display abrupt shifts at the Zone boundaries (Fig. 3.3). Plagioclase compositions are less variable than those in the gabbros from the Oslo region (Neumann et al., 1985) but are similar to the rocks of the Skaergaard intrusion (Fig. 3.2).

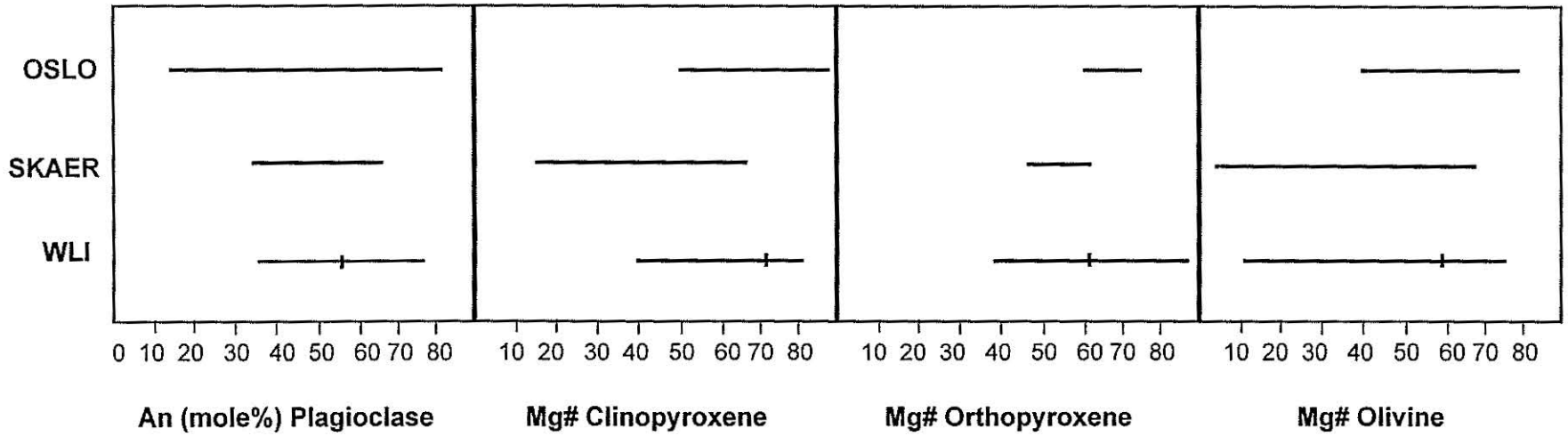

Figure 3.2. Comparison of composition of main cumulus phases in the rocks of the Wateranga intrusion with minerals from gabbroic intrusions in the Oslo region, Norway and the Skaergaard intrusion, East Greenland. Bars indicate maximum and minimum values. Vertical lines show mean composition of each mineral. **WLI** - Wateranga layered intrusion; **SKAER** - Skaergaard intrusion, East Greenland; **OSLO** - Gabbro intrusions from the Oslo region, Norway. Data of Skaergaard intrusion is from Wager and Brown (1968). Data of Oslo gabbro intrusions is from Neumann et al. (1985).

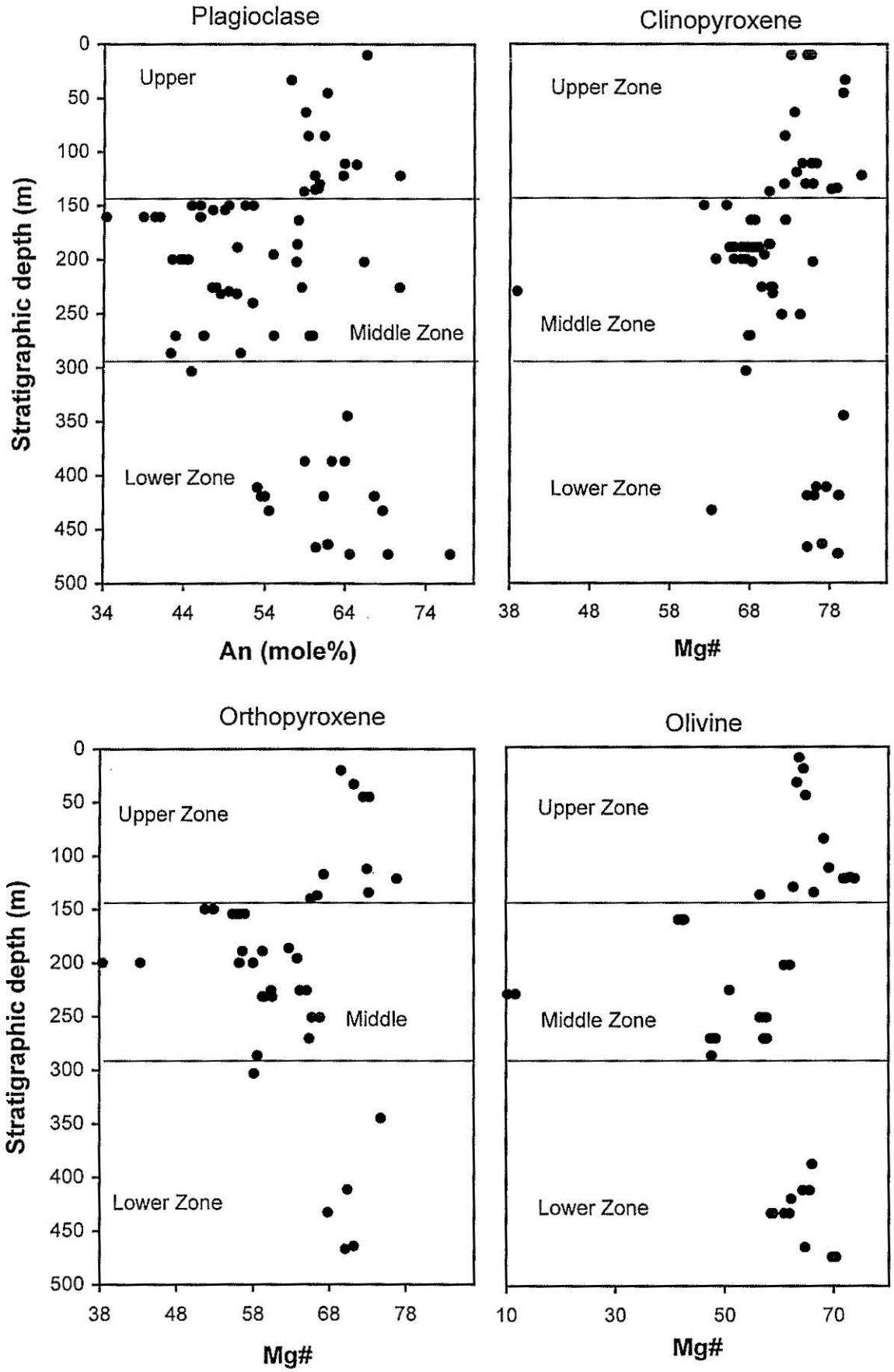

Figure 3.3 Variation of An-content of plagioclase, and Mg#s of clinopyroxene, orthopyroxene and olivine with stratigraphic depth (m) in the Wateranga intrusion.

Plagioclase compositions vary from An_{34} to An_{77} [Appendix 2 (Table 1) and Figs. 3.2 and 3.4]. The plagioclase mostly contains 8-14 wt% CaO, 3-6 wt% Na_2O and very low K_2O (0.05-0.44 wt%). Plagioclase shows significant crystal zoning or extensive compositional variation within individual samples. Plagioclase is either reversely zoned or exhibits simple normal zoning or oscillatory zoning. Anorthite content averages An_{50-60}, with the most calcic cores being An_{70}, and the most sodic rims being An_{39}. The variation in % anorthite within single zoned grains ranges from 2 to 23%.

As seen in Figure 3.3, plagioclase becomes significantly less calcic (anorthitic) in the Middle Zone, a trend that matches the trend of decreasing Mg# of pyroxenes and olivine. Plagioclase has a similar distribution to Mg#s of clinopyroxene, orthopyroxene, olivine and whole rocks, and the whole rock concentrations of various incompatible trace elements for the entire section of the intrusion.

3.4.2 Clinopyroxene

Pyroxene has complex chemical and mineralogical characteristics, and its systematic compositional variation with contemporary evolving magmas has received a great deal of attention. The crystallization trends of Ca-rich and Ca-poor pyroxenes in the Skaergaard (Brown and Vincent, 1963; Wager and Brown, 1968) have been the classic standard example of the compositional changes that occur in pyroxene during the differentiation of basaltic magma. The extended subsolidus trend of compositional variation of pyroxene crystallization was investigated by Nwe (1975). Recent investigations of Skaergaard pyroxenes have been expanded to cover the whole body of the intrusion (Hoover, 1989; McBirney, 1989, 1996).

Clinopyroxene is the major ferromagnesian mineral in the Wateranga intrusion. Compositions of clinopyroxene are presented in Appendix 2 (Table 2) and representative compositions are provided in Table 3.2. In most analyses, the CaO content of clinopyroxene ranges from 18 to 22 wt% and the MgO content varies from 13 to 16 wt%. The Cr_2O_3 (0.05-0.40 wt%) is low and TiO_2 is 0.18-0.68 wt%. In the clinopyroxenes, Mg#s [100Mg/(Mg+Fe)] range from 39 to 82. The highest Mg#s are found in the Lower and Upper Zones (Fig. 3.3). Clinopyroxene is

frequently zoned, and Mg#s and Cr_2O_3 are found both to increase and decrease from core to rim.

Clinopyroxenes from the rocks of the Wateranga intrusion are similar in Mg# to those from Oslo rift gabbros (Neumann et al., 1985). The clinopyroxenes from the Skaergaard intrusion show a greater range in composition (Fig. 3.2). This suggests that the iron-rich rocks of the Skaergaard intrusion are more evolved than those of the Wateranga intrusion.

Compositions of pyroxenes from the rocks of each zone are plotted on the pyroxene quadrilateral (Fig. 3.5). The compositions are augite with minor salite and ferroaugite and plot on the Skaergaard calcium-rich pyroxene trend. The clinopyroxenes from the Wateranga intrusion are slightly more calcic than those from the Skaergaard intrusion (Fig. 3.5) and are concentrated in the augite-rich part of the quadrilateral. The compositions are typical of tholeiitic layered gabbros.

Clinopyroxene can often be used as a guide to the chemical affinities of the magma from which it crystallized (LeBas, 1962; Nisbet and Pearce, 1977). In Figure 3.6 clinopyroxenes from the rocks of the Wateranga intrusion plot in the non-alkaline field (LeBas, 1962). Clinopyroxenes from the rocks of the Wateranga intrusion falls in the same field as pyroxenes from gabbro intrusions in the Oslo rift (not shown in Fig. 3.6).

Discriminant function analysis of clinopyroxenes (Nisbet and Pearce, 1977) from the rocks of the Wateranga intrusion show that they have volcanic arc basalt and ocean floor basalt affinities (Fig. 3.7). Data from the Wateranga intrusion compare well with data from the rift-related gabbros from the Oslo region (Fig. 3.7).

3.4.3 Orthopyroxene

In the Wateranga intrusion orthopyroxene is less abundant than clinopyroxene (Table 2.2, Chapter 2). It occurs as cumulus grains and peritectic reaction rims, which form by reaction of olivine with silica from interstitial melt. Orthopyroxene also occurs as exsolution lamellae in cumulus clinopyroxene.

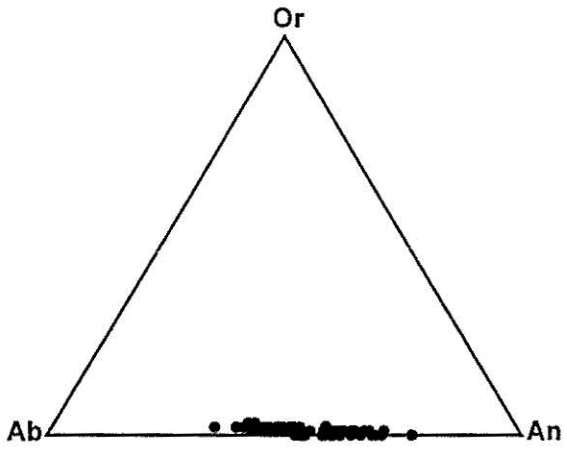

Figure 3.4. Plagioclase compositions in the rocks of the Wateranga intrusion.

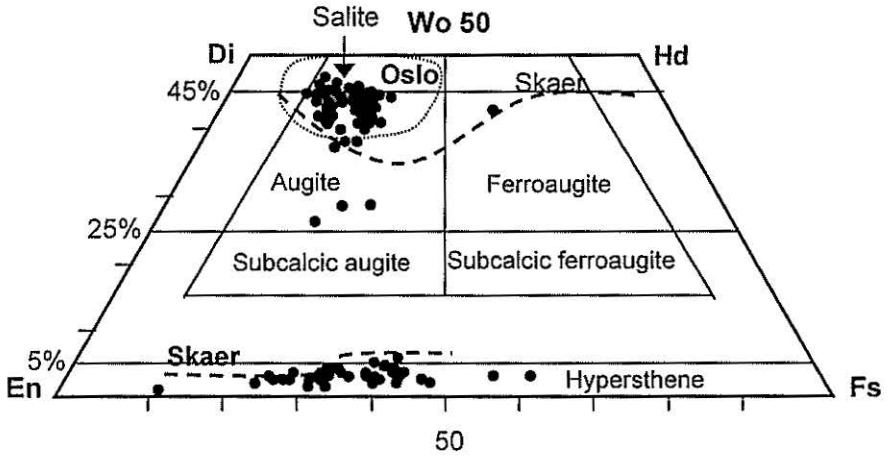

Figure 3.5. Pyroxene compositions for the Wateranga intrusion on a quadrilateral plot. Also shown are the trends of the Skaergaard (Wager and Brown, 1968) and Oslo rift intrusions (Neumann et al., 1985) with thick dashed line and thin dotted line respectively.

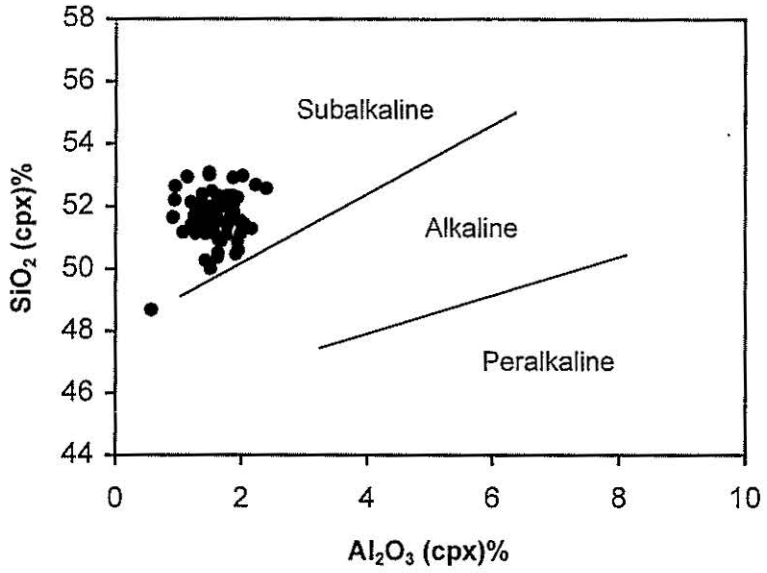

Figure 3.6. SiO_2 - Al_2O_3 covariation in clinopyroxenes from the rocks of the Wateranga intrusion (boundaries are from LeBas, 1962).

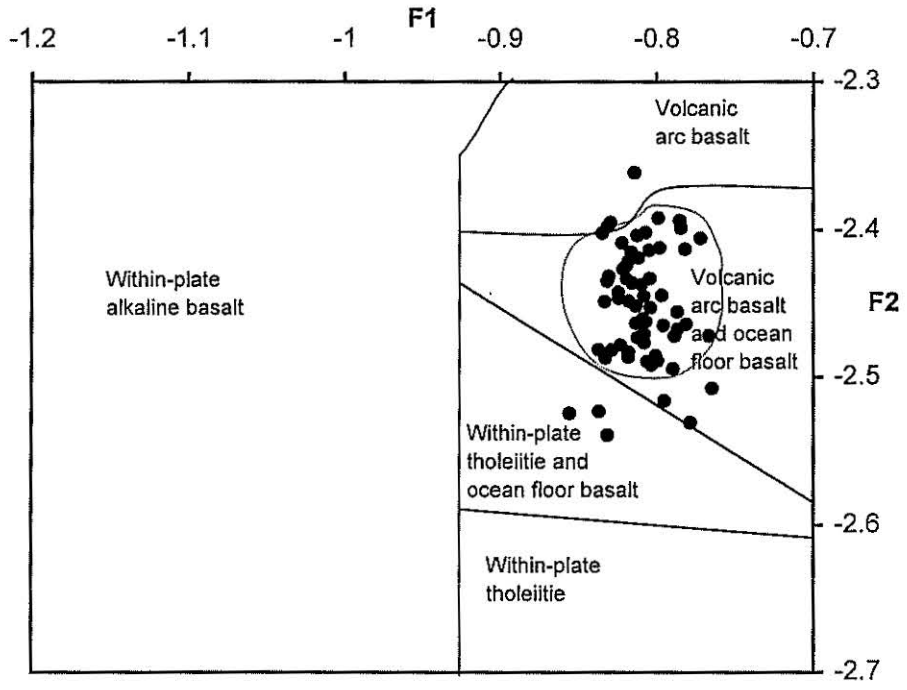

Figure 3.7. Plot of discriminant functions, **F1** against **F2**, (Nisbet and Pearce, 1977) for clinopyroxene analyses from the rocks of the Wateranga intrusion as a function of magma type. Dotted circle represents Oslo rift gabbros data (Neumann, 1985).

F1 = $-0.012*SiO_2-0.0807*TiO_2+0.0026*Al_2O_3-0.0012*FeO-0.0026*MnO+0.0087*MgO - 0.0128*CaO-0.0419*Na_2O$.

F2 = $-0.0469*SiO_2-0.0818*TiO_2-0.0212*Al_2O_3-0.0041*FeO-0.1435*MnO-0.0029*MgO+ 0.0085*CaO +0.0160* Na_2O$.

The presence of cumulus orthopyroxene and peritectic reaction rims suggests that the parent magma had a high activity of silica.

The CaO content of orthopyroxene ranges from 0.88 to 2.70 wt% and the TiO_2 content varies from 0.05 to 0.56 wt%. The total FeO is high (21-28 wt%) as is MgO (18-25 wt%). The Cr_2O_3 is negligible (0.05-0.26 wt%) (Appendix 2, Table 3).

Compositional variation in orthopyroxene [Appendix 2 (Table 3) and Fig. 3.3] is similar to clinopyroxene. The Mg#s [100Mg/(Mg+Fe)] of orthopyroxene range from 38 to 87. The highest Mg#s are found in the Lower and Upper Zones (Fig. 3.3). Single grains show some compositional zonation, and the compositions vary only slightly (<4% En). The compositional variation within a sample is less than 5% En. The orthopyroxene from the rocks of the Wateranga intrusion has a wider range of Mg# than those from the Skaergaard intrusion or the gabbros from the Oslo region (Fig. 3.2). On the pyroxene quadrilateral, orthopyroxene of the Wateranga intrusion plots on the Skaergaard trend for Ca-poor pyroxene (Fig. 3.5).

3.4.4 Olivine

Olivine occurs as cumulus phase, constituting 5-18 modal % of the Wateranga rocks. Olivine ranges in composition from Fo_{10} to Fo_{74} Appendix 2 (Table 4). Individual grains show slight compositional zonation (<2% Fo), and compositions vary only slightly (<4% Fo) within samples.

The olivines mostly contain 17-36 wt% MgO, 23-45 wt% total FeO and 0.16-0.94 wt% MnO. Variations of the Mg# of cumulus olivine with stratigraphic depth are shown in Figure 3.3. Overall, the compositional trends mirror those described for plagioclase, clinopyroxene and orthopyroxene. Olivines in the rocks of the Wateranga intrusion (Fig. 3.2) are within the range of compositions observed in the Skaergaard intrusion and slightly greater than the range observed in rift associated gabbros from the Oslo region.

3.4.5 Fe-Ti-oxides

Fe-Ti oxide phases are ilmenite and magnetite that make up less than 8 modal % in most of the rocks of the Wateranga intrusion. Only ferrogabbros contain 18%

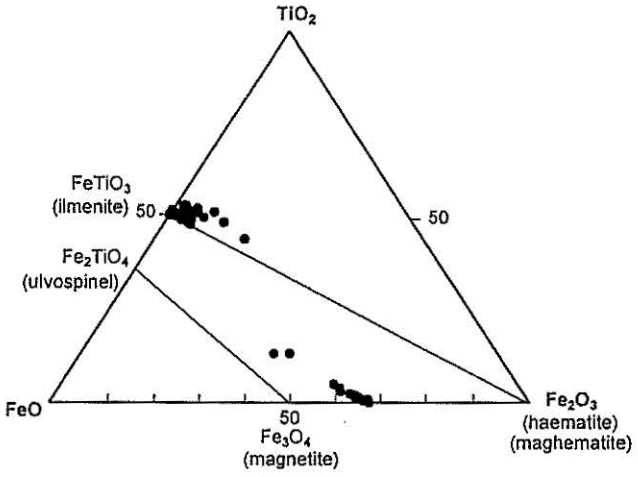

Figure 3.8. Fe-Ti oxide compositions in the Wateranga intrusion.

Fe-Ti oxides (Table 2.2). Fe-Ti oxides occur as postcumulus minerals. Magnetite occurs with orthopyroxene in symplectites associated with olivine in some samples.

The percentages of hematite in ilmenite and of ulvospinel in magnetite have been calculated using QUILF95 program (Andersen et al., 1993). Most of the ilmenites analysed contain a maximum of 5% of hematite representing an almost pure end member. Only three analyses contain % of hematite greater than five (6-24%). Most magnetites range between Mt_{100} to $Mt_{86}Us_{14}$ (except two samples with 35-39 % of ulvospinel) and often vary greatly within a single rock sample. [Appendix 2 (Tables 5 and 6) and Fig. 3.8]. The wide variation in magnetite compositions may be due to oxidation exsolution.

3.4.6 Amphibole

In the Wateranga intrusion, brown hornblende is an accessory phase, forming less than 1% of the mode, and appears in the late stages of the crystallization history. The compositions of amphiboles are listed in Appendix 2 (Table 7). Most

amphiboles are calcic-type and show normal igneous compositions. Individual mineral grains are homogeneous, and hornblende composition does not vary much throughout the intrusion. The late crystallization of hornblende is a sign of a noticeable increase of the fugacity of oxygen during the late stages of crystallization (Cawthorn and O'Hara, 1976; Tribuzio et al., 1998).

3.4.7 Biotite

Biotite is present as an accessory phase in the rocks of the Wateranga intrusion. It forms small anhedral, interstitial crystals related to a late stage of the crystallization sequence. The biotites are Ba-enriched (0.4-1.60 wt%) and show normal igneous compositions. The Mg#s [100Mg/(Mg+Fe)] of biotite range from 34 to 71, and TiO_2 varies from 2.33 to 5.93 wt%. The late crystallization of the biotite and its restricted role seems to reflect both the low K content (K activity) of the magma and its relatively low water pressure.

Further discussion on the significance of mineral chemical data of the Wateranga intrusion will be presented in Chapter six (Discussion).

Table 3.1 Selected electron microprobe analyses of plagioclase

Sample	NS-2/1	NS-2/4	NS-2/19	NS-2/35	NS-2/57	NS-2/63	NS-3/34	NS-5/12	WG-27	WG-84	WG-107
Oxide (wt%)											
SiO_2	54.21	56.40	52.63	53.74	49.69	47.55	51.94	55.38	49.20	52.86	52.45
TiO_2	0.06	0.18	<0.05	0.16	0.05	0.15	0.09	<0.05	0.15	0.15	<0.05
Al_2O_3	29.06	26.60	30.80	28.69	29.70	28.40	29.03	27.45	30.81	28.52	29.11
FeO*	0.22	0.05	0.13	0.05	0.50	0.14	0.39	0.12	<0.05	0.48	0.37
MnO	0.06	0.11	0.06	<0.05	<0.05	<0.05	<0.05	<0.05	0.12	0.12	<0.05
MgO	0.07	<0.05	<0.05	<0.05	0.59	<0.05	0.44	0.14	0.21	<0.05	0.24
CaO	10.65	8.42	11.89	10.68	14.52	20.20	13.47	10.46	15.13	12.63	12.89
Na_2O	5.38	6.57	4.56	5.49	3.69	3.25	4.16	5.82	3.56	4.43	4.44
K_2O	0.31	0.37	0.18	0.27	0.09	0.07	0.05	0.22	0.08	0.24	0.06
BaO	0.06	<0.05	0.11	<0.05	0.25	<0.05	<0.05	0.14	<0.05	<0.05	0.40
Sum	100.08	98.70	100.36	99.08	99.08	99.76	99.57	99.73	99.26	99.43	99.96
Cations per 8 oxygens											
Si	2.46	2.55	2.37	2.44	2.31	2.30	2.37	2.50	2.32	2.42	2.38
Ti	0.00	0.01	0.00	0.01	0.00	0.01	0.00	0.00	0.01	0.01	0.00
Al	1.54	1.44	1.63	1.54	1.62	1.59	1.61	1.48	1.66	1.53	1.56
Fe	0.01	0.00	0.01	0.00	0.02	0.01	0.01	0.00	0.00	0.03	0.01
Mn	0.00	0.00	0.00	0.00	0.00	0.00	0.00	0.00	0.00	0.00	0.00
Mg	0.00	0.00	0.00	0.00	0.04	0.00	0.03	0.01	0.01	0.00	0.02
Ca	0.51	0.40	0.58	0.52	0.69	0.84	0.63	0.50	0.70	0.62	0.63
Na	0.46	0.57	0.40	0.48	0.32	0.25	0.35	0.50	0.29	0.38	0.39
K	0.02	0.02	0.01	0.02	0.01	0.00	0.00	0.01	0.00	0.01	0.00
Ba	0.00	0.00	0.00	0.00	0.00	0.00	0.00	0.00	0.00	0.00	0.01
Sum	5.00	4.99	5.00	5.01	5.01	5.00	5.00	5.00	4.99	5.00	5.00
End members (mole%)											
An	51.5	40.4	58.6	51.0	67.6	77.1	64.3	49.5	70.7	61.4	61.8
Ab	46.5	57.6	40.4	47.1	31.4	22.9	35.7	49.5	29.3	37.6	38.2
Or	2.0	2.0	1.0	2.0	1.0	0.0	0.0	1.0	0.0	1.0	0.0

* Total iron as FeO. Lower detection limit for all elements is 0.05 wt%.

Table 3.2 Selected electron microprobe analyses of pyroxenes

Sample	NS-2/11 Cpx	NS-2/19 Cpx	NS-2/57 Cpx	NS-3/2 Cpx	NS-5/12 Cpx	WG-7 Cpx	WG-27 Cpx	WG-124 Cpx	NS-2/1 Opx	NS-2/14 Opx	NS-2/19 Opx	NS-2/29 Opx	NS-2/54 Opx	NS-3/12 Opx	NS-3/34 Opx	NS-5/6 Opx
Oxide (wt%)																
SiO_2	50.02	52.00	51.45	50.53	48.69	52.98	52.69	51.52	52.52	51.94	51.34	52.32	53.63	56.80	53.52	48.93
TiO_2	0.31	0.48	0.64	0.43	0.11	0.31	0.39	0.68	0.06	0.18	0.20	0.25	0.14	0.17	0.26	0.13
Al_2O_3	1.51	1.55	2.04	1.63	0.57	2.02	2.23	1.98	1.13	0.67	0.66	0.71	0.64	0.26	0.86	0.66
FeO*	12.34	10.24	8.54	11.79	20.71	8.09	6.01	7.79	28.17	24.23	23.70	20.62	18.42	8.60	16.08	32.13
MnO	0.56	0.28	0.20	0.35	1.34	0.21	0.23	0.23	0.86	0.82	0.91	0.59	0.58	0.23	0.38	1.36
MgO	13.08	13.84	15.58	14.44	7.48	15.09	15.74	15.43	16.34	19.01	20.52	22.56	25.17	32.56	26.88	13.83
CaO	20.94	21.40	21.08	19.34	19.25	20.27	21.26	21.94	0.88	2.24	1.54	1.99	1.39	0.43	0.96	1.49
Na_2O	0.16	0.18	0.16	0.18	0.19	0.15	0.16	0.16	0.13	0.18	0.17	0.16	0.16	0.16	0.15	0.16
K_2O	0.07	0.06	0.07	0.05	<0.05	0.05	0.12	0.05	0.06	0.10	0.06	<0.05	0.07	0.05	0.06	<0.05
Cr_2O_3	0.22	0.13	0.18	0.05	0.06	0.44	0.85	0.11	0.09	0.06	<0.05	<0.05	<0.05	<0.05	0.16	0.09
NiO	0.05	<0.05	0.06	<0.05	0.44	<0.05	0.31	0.13	<0.05	<0.05	<0.05	<0.05	<0.05	0.39	0.42	0.35
Sum	99.22	100.14	100.00	98.79	98.82	99.57	99.99	99.98	100.24	99.41	99.10	99.20	100.20	99.62	99.70	99.13
Cations per 6 oxygens																
Si	1.92	1.95	1.90	1.93	1.97	1.96	1.94	1.89	1.99	1.96	1.94	1.95	1.96	1.99	1.93	1.95
Ti	0.01	0.01	0.02	0.01	0.00	0.01	0.01	0.02	0.00	0.01	0.01	0.01	0.00	0.00	0.01	0.00
Al	0.07	0.07	0.09	0.07	0.03	0.09	0.10	0.09	0.05	0.03	0.03	0.03	0.03	0.01	0.04	0.03
Fe	0.39	0.32	0.27	0.37	0.69	0.26	0.19	0.24	0.91	0.78	0.76	0.65	0.57	0.25	0.49	1.07
Mn	0.02	0.01	0.01	0.01	0.04	0.01	0.01	0.01	0.03	0.03	0.03	0.02	0.02	0.01	0.01	0.05
Mg	0.74	0.77	0.86	0.81	0.44	0.84	0.86	0.86	0.98	1.08	1.16	1.25	1.36	1.70	1.46	0.82
Ca	0.83	0.86	0.83	0.79	0.82	0.81	0.84	0.88	0.04	0.09	0.06	0.08	0.05	0.02	0.04	0.06
Na	0.01	0.01	0.01	0.01	0.01	0.01	0.01	0.01	0.00	0.01	0.01	0.01	0.01	0.01	0.01	0.01
K	0.00	0.00	0.00	0.00	0.00	0.00	0.01	0.00	0.00	0.01	0.00	0.00	0.00	0.00	0.01	0.00
Cr	0.01	0.00	0.01	0.00	0.00	0.01	0.02	0.00	0.00	0.00	0.00	0.00	0.00	0.00	0.00	0.00
Ni	0.00	0.00	0.00	0.00	0.01	0.00	0.01	0.00	0.00	0.00	0.00	0.00	0.00	0.01	0.00	0.01
Sum	4.00	4.00	4.00	4.00	4.01	4.00	4.00	4.00	4.00	4.00	4.00	4.00	4.00	4.00	4.00	4.00
End members (mole%)																
En	37.8	39.5	43.9	41.1	22.6	44.0	45.5	43.4	50.8	55.4	58.6	63.1	68.7	86.3	73.4	42.1
Fs	19.9	16.4	13.8	18.8	35.4	13.6	10.1	12.1	47.2	40.0	38.4	32.8	28.8	12.7	24.6	54.9
Wo	42.3	44.1	42.3	40.1	42.1	42.4	44.4	44.4	2.1	4.6	3.0	4.0	2.5	1.0	2.0	3.1
mg#	65.5	70.6	76.1	68.6	38.9	76.4	81.9	78.2	51.9	58.1	60.4	65.8	70.5	87.2	74.9	43.4

* Total iron as FeO. Cpx = clinopyroxene; Opx = orthopyroxene. Lower detection limit for all elements is 0.05 wt%.

Table 3.3 Selected electron microprobe analyses of olivine

Sample	NS-2/4	NS-2/29	NS-2/31	NS-2/48	NS-2/54	NS-2/57	NS-2/59	NS-2/63	NS-3/25	WG-27	WG-107
Oxide (wt%)											
SiO_2	35.45	35.50	34.57	37.14	36.07	36.05	35.65	36.49	35.54	39.15	36.50
FeO*	44.58	36.77	41.96	29.50	29.82	32.59	34.90	26.40	36.32	23.27	30.76
MnO	0.87	0.75	0.79	0.57	0.25	0.59	0.78	0.33	0.80	0.26	0.53
MgO	18.57	26.74	21.98	32.29	32.18	29.79	28.04	35.99	27.46	36.44	31.98
CaO	<0.05	0.06	<0.05	0.06	<0.05	0.12	<0.05	<0.05	0.15	0.06	<0.05
NiO	0.16	<0.05	0.08	0.05	0.12	0.17	<0.05	<0.05	<0.05	0.06	0.12
Sum	99.63	99.82	99.38	99.61	98.44	99.31	99.37	99.21	100.27	99.24	99.89
Cations per 4 oxygens											
Si	1.05	1.00	1.01	1.01	0.99	1.00	1.00	0.99	0.99	1.03	0.99
Fe	1.10	0.86	1.01	0.67	0.69	0.75	0.82	0.59	0.85	0.51	0.70
Mn	0.02	0.02	0.02	0.01	0.01	0.01	0.02	0.01	0.02	0.01	0.01
Mg	0.82	1.12	0.95	1.31	1.32	1.24	1.16	1.41	1.14	1.44	1.30
Ca	0.00	0.00	0.00	0.00	0.00	0.00	0.00	0.00	0.00	0.00	0.00
Ni	0.00	0.00	0.00	0.00	0.00	0.00	0.00	0.00	0.00	0.00	0.00
Sum	2.99	3.00	2.99	3.00	3.01	3.00	3.00	3.00	3.00	2.99	3.00
End members (mole%)											
Fo	42.7	56.6	48.5	66.2	65.7	62.3	58.6	70.5	57.3	73.8	65.0
Fa	57.3	43.4	51.5	33.8	34.3	37.7	41.4	29.5	42.7	26.2	35.0

* Total iron as FeO. Lower detection limit for all the elements is 0.05 wt%.

Table 3.4 Selected electron microprobe analyses of Fe-Ti oxides

Sample	NS-2/1 Il	NS-2/22 Il	NS-2/59 Il	NS-3/8 Il	NS-5/6 Il	WG-27 Il	NS-2/46 Ma	NS-2/59 Ma	NS-3/7 Ma	NS-5/12 Ma	WG-107 Ma
Oxide (wt%)											
TiO_2	52.46	50.09	52.80	51.96	50.34	50.72	0.10	12.93	1.37	1.33	2.10
Al_2O_3	0.05	0.15	0.19	<0.05	0.34	<0.05	0.30	1.78	1.48	1.24	0.89
FeO(t)	44.95	46.60	44.18	45.82	44.61	45.30	99.11	81.16	95.10	97.18	92.28
MnO	2.31	0.87	0.38	0.68	1.25	0.32	0.10	0.51	0.24	<0.05	0.09
MgO	0.05	1.10	1.47	1.22	0.26	3.78	0.05	2.88	0.21	<0.05	0.23
Cr_2O_3	0.13	0.07	<0.05	0.12	<0.05	<0.05	0.07	0.18	1.12	<0.05	2.89
ZnO	0.09	<0.05	<0.05	0.10	0.54	<0.05	0.28	0.06	<0.05	0.57	0.14
Sum	100.04	98.88	99.02	99.90	97.34	100.12	100.01	99.50	99.52	100.32	98.62
Cations per 3 oxygens											
Ti	1.00	0.95	1.00	0.98	0.98	0.92	0.00	0.35	0.04	0.04	0.06
Al	0.00	0.00	0.01	0.00	0.01	0.00	0.02	0.07	0.06	0.05	0.04
Fe^{3+}	0.01	0.09	0.00	0.04	0.02	0.14	1.97	1.23	1.84	1.86	1.80
Fe^{2+}	0.94	0.90	0.93	0.92	0.94	0.79	1.01	1.18	0.99	1.03	1.00
Mn	0.05	0.02	0.01	0.01	0.03	0.01	0.00	0.02	0.01	0.00	0.00
Mg	0.00	0.04	0.05	0.05	0.01	0.14	0.00	0.15	0.01	0.00	0.02
Cr	0.00	0.00	0.00	0.00	0.00	0.00	0.00	0.01	0.03	0.00	0.08
Zn	0.00	0.00	0.00	0.00	0.01	0.00	0.01	0.00	0.00	0.02	0.00
Sum	2.00	2.00	2.00	2.00	2.00	2.00	3.00	3.00	2.98	3.00	2.99
He %	0.1	4.9	0.0	2.2	1.2	8.1					
Usp %							0.1	35.4	3.5	3.7	5.9

Il = ilmenite; Ma = magnetite; He = hematite % in ilmenite; Usp = ulvospinel % in magnetite. Lower detection limit for all the elements is 0.05 wt%.

Table 3.5 Amphibole mineral compositions of the Wateranga intrusion

Sample	NS-2/1	NS-2/4	NS-2/11	NS-2/22	NS-2/31	NS-2/41	NS-2/59	NS-2/61	NS-5/6	WG-84	WG-107
Oxide (wt%)											
SiO_2	52.03	54.27	46.06	44.72	45.10	45.66	45.50	45.05	45.26	42.55	50.42
TiO_2	0.06	<0.05	2.39	3.26	3.53	3.88	0.61	3.86	2.36	0.11	0.16
Al_2O_3	0.58	1.75	9.85	10.36	10.72	10.08	12.08	11.20	8.94	13.34	5.62
FeO*	11.44	20.89	14.52	14.15	14.44	14.32	12.30	11.31	19.90	15.51	21.32
MnO	0.47	0.95	0.22	0.09	0.24	0.21	0.08	0.15	0.43	0.19	0.35
MgO	11.54	16.18	10.48	10.33	10.40	9.84	12.77	13.09	6.98	14.45	15.62
CaO	20.50	2.34	9.67	9.82	10.16	10.30	10.21	9.50	9.46	8.98	1.16
Na_2O	0.18	0.29	2.05	2.21	2.15	1.71	2.35	2.23	2.04	0.47	0.56
K_2O	0.10	0.08	0.68	0.81	0.77	0.71	0.44	0.64	0.92	0.14	0.76
Cr_2O_3	0.16	0.06	<0.05	0.08	0.08	0.10	0.06	0.09	0.37	0.06	0.05
Sum	97.05	96.81	95.92	95.84	97.59	96.81	96.39	97.11	96.64	95.80	96.02
Cations per 23 oxygens											
Si	7.74	7.98	6.90	6.71	6.66	6.77	6.70	6.57	6.92	6.37	7.49
Ti	0.00	0.00	0.27	0.37	0.39	0.43	0.07	0.42	0.27	0.01	0.02
Al^{iv}	0.26	0.02	1.10	1.29	1.34	1.23	1.30	1.43	1.08	1.63	0.51
Al^{vi}	0.16	0.28	0.64	0.54	0.53	0.53	0.80	0.49	0.53	0.72	0.47
Fe	1.42	2.59	1.82	1.78	1.78	1.78	1.51	1.38	2.55	1.94	2.65
Mn	0.06	0.12	0.03	0.01	0.03	0.03	0.01	0.02	0.05	0.02	0.04
Mg	2.56	3.59	2.34	2.31	2.29	2.18	2.80	2.85	1.59	3.22	3.46
Ca	3.27	0.43	1.55	1.58	1.61	1.64	1.61	1.49	1.55	1.44	0.18
Na	0.05	0.08	0.60	0.65	0.61	0.49	0.67	0.63	0.60	0.14	0.16
K	0.02	0.01	0.13	0.16	0.15	0.13	0.08	0.12	0.18	0.03	0.14
Cr	0.02	0.00	0.00	0.01	0.01	0.01	0.00	0.01	0.04	0.00	0.01
Sum	15.56	15.10	15.38	15.41	15.40	15.22	15.55	15.41	15.36	15.52	15.13
mg#	64.3	58.1	56.3	56.5	56.3	55.1	65.0	67.4	38.4	62.4	56.6

* Total iron as FeO. Lower detection limit for all the elements is 0.05 wt%.

3.5 Geothermometry and oxygen fugacity (fO_2)

Geothermometers and geobarometers are commonly based on mineral assemblage and mineral composition information. The fundamental premise of geothermobarometry is that a rock's mineral assemblage and mineral compositions are sensitive to pressure and temperature conditions of formation and that events subsequent to mineral equilibration have not significantly modified these rock properties.

QUILF95: QUILF95 is a powerful program and it assesses equilibria among Ti-magnetite, ilmenite, augite, pigeonite, orthopyroxene, olivine, and quartz (Andersen et al., 1993). Depending on the assemblage, QUILF95 can provide information on temperature, pressure, oxygen fugacity, and the activities of SiO_2, TiO_2 and FeO at which the phases were last in equilibrium.

Mineral equilibrium temperatures and fO_2 were determined for the Wateranga rocks using QUILF95 program to gain insights into the conditions of magma chamber. Two independent geothermometers were applied: two-pyroxene and magnetite-ilmenite thermometry using solution and equilibria model of Lindsley and Frost (1992) following the method of Andersen et al. (1993).

Two-pyroxene thermometry calculations were carried out on ten mineral pairs. Application of two-pyroxene thermometer gave reasonable results for the rocks of the Wateranga intrusion. This thermometer is variable with pressure. Only analyses from apparently unaltered mineral grains were used. Results of geothermometry are presented in Table 3.6 and shown in Figure 3.9. The temperatures range from 1057 to 927°C at 2 kbar. These estimates deviate by <8°C if pressures of 4 kbar are applied. Furthermore, pressure prevailing during crystallization can be estimated from the mineralogy of the rocks of the intrusion. For example, the presence of primary amphibole throughout the intrusion suggests a pressure greater than 2 kb (Spulber and Rutherford, 1981).

Liquidus temperatures of tholeiitic layered gabbros range from 1300-1150°C (Williams, 1971; Biggar, 1974; McBirney, 1993). The temperatures obtained from the Wateranga rocks are 1057-927°C. Because these estimates were made from

minerals that were not the first phases to crystallize, these temperatures are indicative of crystallization temperatures between the liquidus and solidus.

Table 3.6 Results of two-pyroxene thermometer using QUILF95.

Sample	Temperature^{0}C
NS-2/11	990
NS-2/14	993
NS-2/22	975
NS-2/54	1007
NS-2/61	1002
NS-3/7	980
NS-3/25	1011
NS-3/34	927
WG-44	1057
WG-107	1002

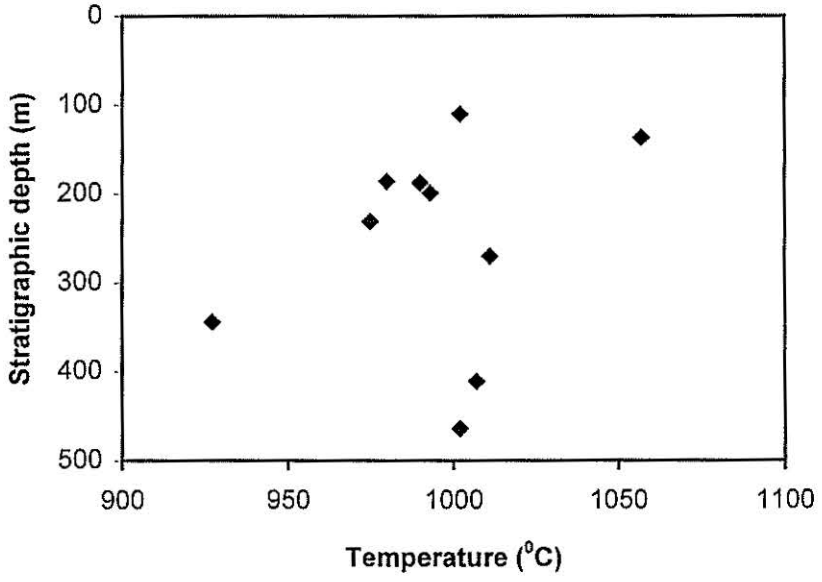

Figure 3.9 Results of two-pyroxene thermometer vs stratigraphic depth.

Temperature estimates using the magnetite-ilmenite geothermometer should be evaluated carefully, owing to the tendency of these minerals to re-equilibrate rapidly during sub-solidus processes (McBirney, 1996). Magnetite-ilmenite thermometry yielded ranges of 876-922°C for the Wateranga rocks. These temperatures are slightly lower than the estimates from the two-pyroxene thermometer. Lower temperatures most likely reflect mineral re-equilibration temperatures and suggest sub-solidus re-equilibration of the Fe-Ti oxide minerals in the rocks of the Wateranga intrusion. Log fO_2 values range from –13.8 to –12.6.

Oxygen fugacity is not well characterized because of extensive magnetite-ilmenite oxidation exsolution and subsolidus oxidation. Cumulus magnetite-ilmenite locally occurs in the Upper (sample A-WG-24) and Middle (sample NS-2/5) Zones suggesting that the melt became more oxidizing with fractionation.

The primary melt was hydrous as indicated by the presence of hornblende. As already mentioned, hornblende is an accessory phase forming less than 1% of the mode. Concentration of water in the course of crystallization of cumulates allowed hornblende to crystallize ultimately from the pore fluid. If the volatile content determined from whole-rock analyses is ascribed solely to water, then none of the rocks analysed could have been saturated with water at the temperatures and pressures of cumulate crystallization.

3.6 Summary

Detailed mineral chemistry divided the intrusion into Lower, Middle and Upper Zones, which are interpreted as reflecting magma chamber replenishment. The common mineral chemical differentiation indices, such as An content of plagioclase, Fo or Mg# in olivine, Mg#s of clinopyroxene and orthopyroxene, all vary widely with stratigraphic depth and display discontinuities and reversals at the Zone boundaries, indicating open system addition of new mafic magma. The Wateranga intrusion was the product of at least three recognizable magma pules, giving rise to the Lower, Middle and Upper Zones.

The mineral compositional variations in the rocks of the Wateranga intrusion provide evidence for extensive fractionation of the parent magma consistent with a

fractionating tholeiitic magma. The ranges of common mineral chemical differentiation indices observed in the Wateranga intrusion are similar to the ranges observed in the Skaergaard intrusion, East Greenland (Wager and Brown, 1968; Hoover, 1989; McBirney, 1996) and gabbro intrusions from the Oslo rift, Norway (Neumann et al. 1985), and, therefore, the Wateranga intrusion represents one of the most extensive differentiation sequences.

Temperatures estimated from two-pyroxene geothermometer varied from 1057-927°C. Pressure during the course of crystallization probably was greater than 2 and less than 4 kbar. Log fO_2 values range from –13.8 to –12.6.

CHAPTER 4

Geochemistry – I Major Oxides and Trace Elements

4 Geochemistry – I Major Oxides and Trace Elements

4.1 Introduction

Whole-rock chemical analyses of the rocks of the Wateranga intrusion were carried out to (i) investigate the geochemical variation, (ii) ascertain the nature of parental magma(s) and (iii) delineate the petrogenetic history of the intrusion. In this Chapter the whole-rock geochemical data are presented and discussed. Further discussion on the petrogenetic significance of the whole-rock major and trace element data and petrogenetic modelling is presented in Chapter 6 (Discussion).

Although much fresh rock was available for petrographic and geochemical study from outcrops and drill core, screening out of altered rock samples was considered particularly important to determine primary geochemical trends in the igneous rock suite studied. The exclusion process avoided veined or weathered rocks in the field and samples that displayed alteration when viewed petrographically.

Seventy-two whole-rock samples were analyzed for major and trace elements by X-ray fluorescence spectrophotometer at the University of New England. Additionally, 22 unpublished XRF analyses were provided by P.M. Ashley (from the study by Ambler and Ashley, 1977) and 22 unpublished XRF analyses were taken from Evans (1992). Analytical procedures and complete analyses are presented in Appendix 1. Also, representative analyses are presented in this

Chapter in Table 4.1. Whole-rock rare earth element (REE) abundances, platinum-group element and Au concentrations were measured by ICP-MS at Australian Laboratory Services, Brisbane. Analytical details are presented in Appendix 3. Analyses are presented in this Chapter in Tables 4.5 and 4.6.

4.2 Cumulus and intercumulus material

As already mentioned in Chapter 2, many layered intrusions consist of two main parts: the cumulus material and the intercumulus material. Cumulate rocks consist of variable proportions of liquidus crystals and interstitial silicate melt, all assumed to be in equilibrium with one another at near liquidus temperatures. The initial proportion of trapped liquid in the rock is referred to as the initial porosity, following Irvine (1982).

The fate of trapped intercumulus liquid in slowly cooled layered intrusions has been examined by many workers (Chalokwu and Grant, 1983, 1990; Barnes, 1986; Cawthorn et al., 1992). The incompatible trace element abundances in a cumulate rock reflect the composition and proportion of trapped liquid (Henderson, 1975; Cawthorn, 1996). As these authors showed, variations in abundances between adjacent samples probably reflect varying proportions of trapped liquid. If a large section of the intrusion is studied, it would be expected that, on average, the concentration of incompatible elements in the liquid would increase with differentiation and hence increase in the cumulates even though the proportion of trapped liquid does not change. However, if there is an addition of magma with different incompatible-element abundances and ratios, this would be reflected by sustained changes in concentration in the ensuing cumulates. Hence, gross trends for incompatible elements in cumulate suites may provide evidence for multiple magmas.

The rocks of the Wateranga intrusion range from mesocumulates to adcumulates with very little and nearly identical amounts of intercumulus liquid in all the three stratigraphic Zones. In addition, there is little geochemical evidence to suggest the presence of a significant amount of late-stage trapped intercumulus liquid (e.g. low P_2O_5, K_2O, Rb and Y in most samples) throughout the analyzed

sequence. Furthermore, mineral chemical trends with stratigraphic depth (Fig. 3.3, Chapter 3) mimic whole-rock chemical trends (Fig. 4.4). This suggests that the original liquids from which the cumulates have been derived did not differ significantly. So, the fractional crystallization products of the parent magma(s) can be related to the bulk rock chemistry of the cumulates and, thus, variation in bulk rock chemistry throughout the cumulate stratigraphy will record changes in magma composition(s) during fractional crystallization.

4.3 Magma type

Several geochemical classifications are available in the literature for the magma types and series (e.g., MacDonald and Katsura, 1964; Kuno, 1968; Irvine and Baragar, 1971; Miyashiro, 1974, 1978; Middlemost, 1975; Miyashiro and Shido, 1975; Sakuyama, 1981; Le Bas et al., 1986; Le Maitre, 1989). Because the terms alkaline, calc-alkalic and tholeiitic are well established, it is necessary to find out which term best describes the Wateranga intrusion. The tholeiitic and calc-alkalic series are the two major rock series in the non-alkalic (subalkalic) igneous rocks. In each series, the composition of rock (or magma) should vary with advancing fractional crystallization. So, the major and trace element compositions of igneous rocks could be understood in relation to the rocks and the stage of fractional crystallization.

4.3.1 Alkalic - subalkalic discrimination

Middlemost (1975) used a plot of SiO_2 versus K_2O to distinguish between alkalic and subalkalic magmas. On the diagram, most of the analyzed Wateranga samples lie in the field of low potassic, subalkalic series (Fig. 4.1A). This diagram suggests that the Wateranga intrusion is subalkalic and probably tholeiitic in nature. This is consistent with the general petrography (abundance of orthopyroxene) and low concentrations of alkali element in clinopyroxenes and amphiboles (Tables 2 and 7 of Appendix 2). Mafic alkalic magmas lack orthopyroxene.

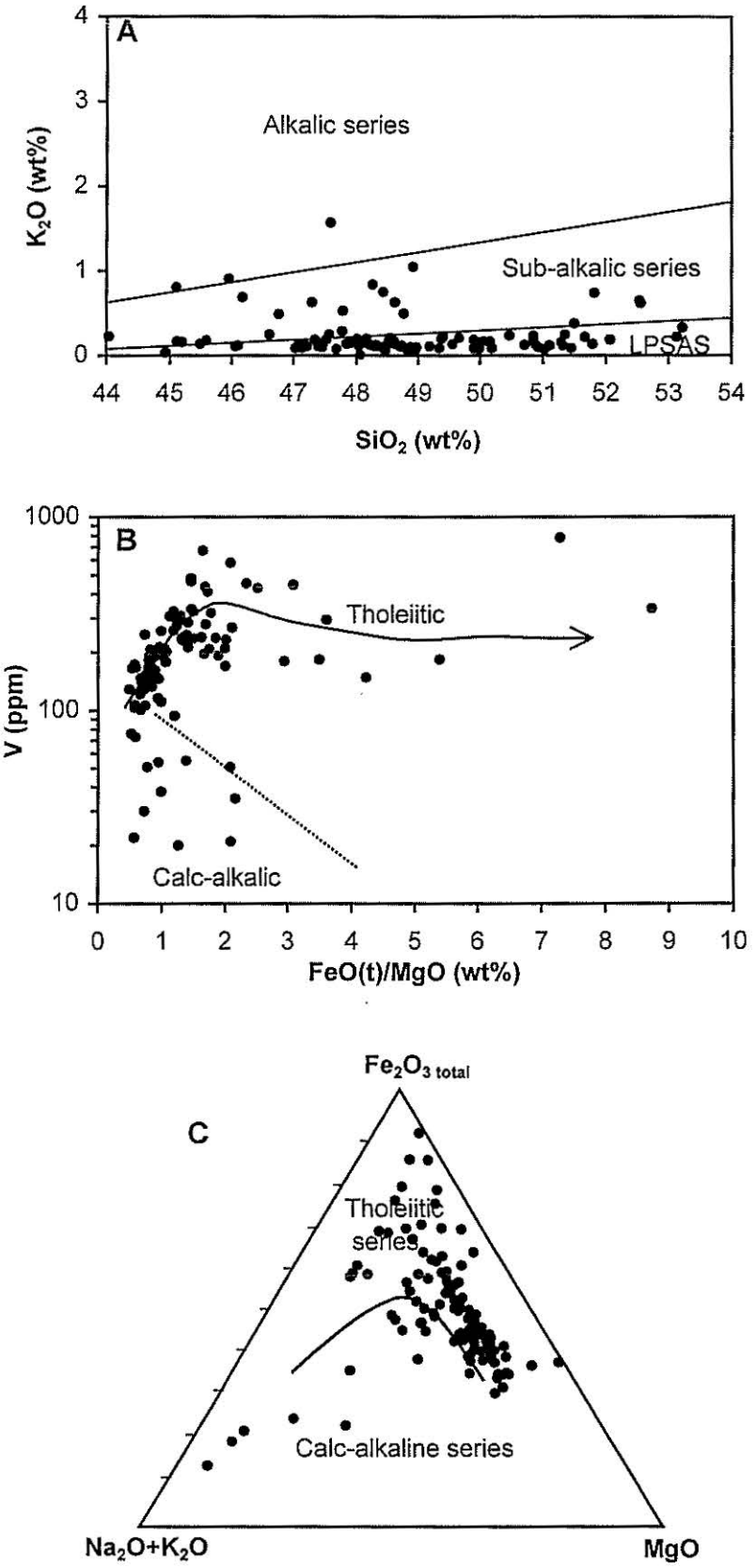

Figure 4.1 Classification diagrams for the Wateranga intrusion. **(A)** SiO2 versus K2O (Middlemost, 1975) LPSAS - Low potassic, sub-alkalic series, **(B)** FeO(t)/MgO versus V (Miyashiro and Shido, 1975), **(C)** AFM diagram (dividing line is from Irvine and Baragar, 1971).

Table 4.1. Selected whole-rock major oxide (wt%) and trace element (ppm) analyses and calculated CIPW norms of the Wateranga intrusion

Rock type	OG	OGN	A	T	N	OG	OGN	N	T	N	P	AOOR
Sample	WG16	WG44	WG96	NS2/4	NS2/14	NS2/35	NS2/54	NS3/8	NS3/32	NS3/38	NS3/51	NS5/4
SiO_2	47.04	47.10	51.50	44.04	50.85	45.59	48.62	49.56	50.88	51.45	43.64	20.77
TiO_2	0.98	1.61	0.28	2.91	1.01	1.05	0.80	2.09	0.25	0.35	0.15	10.78
Al_2O_3	15.86	15.92	27.94	17.11	18.32	16.93	17.78	16.72	20.64	17.96	15.97	3.36
Fe_2O_3	1.77	1.47	0.35	3.42	1.53	5.51	2.43	2.40	1.57	1.86	2.07	9.22
FeO	6.87	9.71	0.94	11.69	7.82	6.43	5.43	7.12	3.48	2.93	7.60	25.22
MnO	0.16	0.21	0.02	0.27	0.21	0.21	0.14	0.19	0.12	0.12	0.14	0.63
MgO	11.49	8.53	0.58	5.01	5.54	5.69	8.39	7.53	7.35	9.21	16.56	4.60
CaO	12.18	11.15	10.96	7.68	8.10	8.88	10.83	9.72	11.35	11.81	7.23	12.04
Na_2O	2.07	2.65	4.92	3.47	3.97	3.82	3.19	2.91	2.90	2.75	1.71	2.25
K_2O	0.09	0.12	0.38	0.23	0.24	0.18	0.17	0.14	0.14	0.09	0.10	0.46
P_2O_5	0.02	0.03	0.03	1.32	0.34	0.65	0.05	0.02	0.01	0.02	0.02	8.57
S	0.04	0.16	0.06	0.15	0.12	0.44	0.18	0.13	0.06	0.05	0.12	0.70
LOI	1.40	0.80	1.66	2.36	1.66	4.26	1.73	1.00	0.95	1.04	4.91	1.38
Total	**99.97**	**99.45**	**99.63**	**99.66**	**99.71**	**99.64**	**99.73**	**99.53**	**99.67**	**99.63**	**100.22**	**99.99**
Mg#[a]	76.67	66.01	56.39	47.71	59.01	54.04	72.47	69.33	76.99	82.06	79.14	30.07
CIPW normative minerals[b]												
Q												
Or	0.53	0.71	2.25	1.36	1.42	1.06	1.00	0.83	0.83	0.53	0.59	2.72
Ab	17.52	22.42	35.92	29.36	33.59	29.83	26.66	24.62	24.54	23.27	14.47	2.27
An	33.72	31.19	53.03	29.48	31.46	28.52	33.69	32.15	42.89	36.40	35.60	
Ne			3.09			1.35	0.18					6.74
Di	21.39	19.55	0.95		5.37	9.38	15.96	12.96	10.74	17.62	0.11	3.21
Hy	1.11	1.37		9.40	15.64			18.14	12.57	13.68	8.16	
Ol	20.67	18.02	1.80	15.64	5.96	18.72	17.10	3.79	5.59	5.33	34.03	33.83
Mt	1.62	2.11	0.24	2.83	1.76	2.18	1.46	1.78	0.94	0.88	1.81	4.52
Ilm	1.86	3.06	0.53	5.53	1.92	1.99	1.52	3.97	0.47	0.66	0.28	20.47
Ap	0.05	0.07	0.07	3.11	0.80	1.53	0.12	0.05	0.02	0.05	0.05	20.22
Trace elements (ppm)												
Nb	<1	<1	<1	6	3	1	2	3	<1	<1	<1	29
Zr	22	30	7	137	106	47	108	22	5	9	8	219
Y	12	14	<1	24	13	16	20	9	5	6	2	177
Sr	248	268	446	331	338	304	184	306	288	277	144	104
Rb	<1	<1	6	2	3	2	2	<1	<1	1	2	14
Th	4	4	<2	5	4	7	<2	4	2	5	3	9
Pb	<2	4	<2	6	4	4	<2	<2	<2	<2	4	6
As	<1	<1	14	<1	<1	<1	<1	<1	<1	<1	<1	<1
U	<1	<1	<1	<1	<1	<1	<1	<1	<1	<1	<1	4
Ga	15	14	19	21	17	15	15	17	14	13	11	14
Zn	55	72	8	91	79	73	65	66	36	30	71	214
Cu	10	63	76	31	35	36	74	50	18	30	115	184
Ni	172	84	42	13	39	41	115	31	51	43	203	46
Cr	649	219	11	23	130	119	280	131	178	267	33	146
Ce	<5	<5	<5	49	27	29	26	16	10	7	14	174
Nd	14	15	5	43	20	24	8	12	5	8	8	153
Ba	43	100	141	407	392	312	134	104	98	33	14	92
V	247	309	35	180	196	210	151	274	121	129	22	784
La	15	12	5	29	18	19	12	9	<3	<3	13	75
Sc	41	27	5	14	22	17	32	34	29	38	6	51

[a] Mg# = 100Mg/(Mg + Fe^{2+}), calculated assuming Fe_2O_3/FeO = 0.15. [b] Norms calculated on an anhydrous basis with iron ratio normalized to 0.15, as above. **Note:** See appendix 1 for the abbreviations of rock types.

Table 4.2 Minimum, maximum and average major (wt%) and trace element (ppm) compositions of the Wateranga intrusion

Element	Min	Max	Avg
SiO_2	20.77	53.22	47.53
TiO_2	0.15	10.78	1.59
Al_2O_3	3.36	28.39	16.76
Fe_2O_3	0.16	22.34	2.36
FeO	0.61	25.22	7.61
MnO	0.01	0.66	0.20
MgO	0.36	22.12	7.56
CaO	3.83	14.74	10.24
Na_2O	0.23	5.15	2.94
K_2O	0.01	1.57	0.24
P_2O_5	0.01	8.57	0.38
S	0.02	1.10	0.14
LOI	0.04	4.94	1.60
Trace elements (ppm)			
Nb	1	35	5
Zr	4	2422	121
Y	1	219	25
Sr	22	479	261
Rb	1	169	7
Th	1	27	4
Pb	2	23	4
As	1	28	2
U	1	10	2
Ga	8	27	16
Zn	1	276	83
Cu	2	184	57
Ni	1	249	83
Cr	3	649	221
Ce	5	174	26
Nd	3	153	22
Ba	14	740	180
V	2	784	223
La	3	75	15
Sc	2	169	35
Selected element ratios			
Al_2O_3/TiO_2	22.40	2.63	10.56
Ba/Rb	14.00	4.38	25.31
Ba/Zr	3.50	0.31	1.49
K/Rb	100	111	393
K/Zr	25	8	23
Zr/Nb	4	69	25
Zr/Y	4.00	11.06	4.82
Ti/Zr	250	32	93
Ti/Y	1000	350	450
Ti/V	500	98	51
Nb/Th	1.00	1.30	1.24

For major oxides, except FeO and Fe_2O_3, (N = 114)

For FeO and Fe_2O_3 (N = 99); S (N = 92)

For trace elements (N = 92)

Note: Lower detection limits: Nb 1, Y 1, Rb 1, Th 2, Pb 2, As 1, U 1, Zn 1, Cu 2, Ni 1, Cr 3, Ce 5, Nd 3, V 2, La 3, Sc 2 ppm.

Table 4.3 Chemical composition of fine-grained samples (chilled margin), Wateranga intrusion

Sample	WG-44	WG-124
Wt%		
SiO_2	47.10	48.76
TiO_2	1.61	0.37
Al_2O_3	15.92	17.19
Fe_2O_3	1.47	0.93
FeO	9.71	6.62
MnO	0.21	0.15
MgO	8.53	10.50
CaO	11.15	11.47
Na_2O	2.65	2.71
K_2O	0.12	0.10
P_2O_5	0.03	0.02
S	0.16	0.08
LOI	0.80	0.80
Total	**99.45**	**99.69**
Trace elements (ppm)		
Nb	1	1
Zr	30	15
Y	14	7
Sr	268	239
Rb	1	1
Th	4	2
Pb	4	2
As	1	1
U	1	1
Ga	14	13
Zn	72	40
Cu	63	129
Ni	84	158
Cr	219	561
Ce	5	14
Nd	15	12
Ba	100	143
V	309	135
La	12	9
Sc	27	29
Selected element ratios		
Al_2O_3/TiO_2	9.89	46.46
Ba/Rb	100	143
Ba/Zr	3.33	9.53
K/Rb	1400	1200
K/Zr	47	80
Zr/Nb	30	15
Zr/Y	2.14	2.14
Ti/Zr	380	173
Ti/Y	814	371
Ti/V	37	19
Nb/Th	0.25	0.50

Note: Lower detection limits: Nb 1, Y 1, Rb 1, Th 2, Pb 2, As 1, U 1, Zn 1, Cu 2, Ni 1, Cr 3, Ce 5, Nd 3, V 2, La 3, Sc 2 ppm. For WG-44 and WG-124, Norms and Mg#s are presented in Appendix 1 (Table 1).

Table 4.4 Average major oxide (wt%) and trace element (ppm) compositions of the Upper, Middle and Lower Zones, Wateranga intrusion

Element	Upper Zone	Middle Zone	Lower Zone
SiO_2	48.45	45.96	49.20
TiO_2	1.00	2.38	0.98
Al_2O_3	18.45	14.66	18.17
Fe_2O_3	1.87	3.21	2.13
FeO	6.46	10.66	5.47
MnO	0.14	0.27	0.16
MgO	8.16	6.96	7.74
CaO	11.19	9.57	9.88
Na_2O	2.88	2.84	3.26
K_2O	0.14	0.35	0.20
P_2O_5	0.12	0.73	0.12
S	0.08	0.18	0.12
LOI	1.10	1.86	1.99
Trace elements (ppm)			
Nb	1	7	3
Zr	20	182	86
Y	7	37	16
Sr	299	249	271
Rb	1	7	3
Th	3	3	4
Pb	2	4	3
As	1	3	1
U	1	2	1
Ga	15	17	16
Zn	42	111	67
Cu	53	64	48
Ni	98	80	84
Cr	279	208	216
Ce	9	36	19
Nd	10	31	14
Ba	92	222	180
V	150	292	159
La	8	18	12
Sc	23	45	28
Selected element ratios			
Al_2O_3/TiO_2	18.38	6.17	18.56
Ba/Rb	83.87	30.39	63.81
Ba/Zr	4.65	1.22	2.10
K/Rb	0.16	0.06	0.09
K/Zr	0.01	0.002	0.003
Zr/Nb	28	25	29
Zr/Y	2.86	4.89	5.29
Ti/Zr	0.04	0.01	0.01
Ti/Y	0.10	0.05	0.04
Ti/V	0.005	0.006	0.004
Nb/Th	0.24	2.16	0.84

For major oxides, except FeO and Fe_2O_3, (total N = 114); (U. Zone, N = 43); (M. Zone, N = 49); (L. Zone, N = 22)

For FeO and Fe_2O_3 (total N = 99); (U. Zone, N = 43); (M. Zone, N = 36); (L. Zone, N = 20)

For S (total N = 92); (U. Zone, N = 21); (M. Zone, N = 49); (L. Zone, N = 22)

For trace elements (total N = 92); (U. Zone, N = 21); (M. Zone, N = 49); (L. Zone, N = 22)

4.3.2 Establishment of tholeiitic character

Whole-rock major and trace element analyses, together with calculated C.I.P.W norms, are presented in Appendix 1 (Tables 1-3). The normative minerals were calculated with the Fe_2O_3/FeO ratio normalized to 0.15. This process was adopted in an attempt to offset the effects of variable oxidation on the calculated norm. Without this correction a slightly more saturated norm would have resulted.

Most of the analyses show normative hypersthene. Most analyses are olivine-normative and a few samples are quartz-normative. In most of the samples, normative feldspar is calcic-labradorite (An/An + Ab = 48 - 71, mean 61) and on this basis the intrusion may be regarded as the intrusive equivalent of tholeiitic basalts. Furthermore, the $Na_2O + K_2O$ content of most samples varies from 0.63 - 3.98 weight percent. This is in the range of typical tholeiitic basalts (Le Maitre, 1976).

After Wager and Deer's (1939) study of the Skaergaard intrusion, most petrologists agreed that fractionation of tholeiitic magma produces iron-rich melts and the late-stage felsic rocks in tholeiitic systems are the result of liquid immiscibility (McBirney and Nakamura, 1973; Naslund, 1983). This idea was followed by Miyashiro and Shido (1975), who divided tholeiitic and calc-alkalic suites on the basis of relative iron enrichment.

Figure 4.1B shows variation of V with FeO(t)/MgO (Miyashiro and Shido, 1975). A tholeiitic trend is marked by a positive correlation. A boundary between the fields of the two series is shown with a broken line.

The AFM variation diagram, Figure 4.1C, demonstrates moderate to high iron enrichment and a close approximation to trends recorded from other tholeiitic suites (cf. Wager and Brown, 1968; McBirney and Naslund, 1990; Morse, 1990; McBirney, 1995). Thus, in agreement with normative mineralogy and chemical variation, the rocks of the Wateranga intrusion may be justifiably classified as tholeiitic.

4.4 Use of correlation coefficients

It is a common practice to calculate the correlation coefficient (r) for each pair of variables and present the data as a matrix. The calculation of a correlation matrix will be the initial step in the examination of a geochemical data-set to identify the level of correlation for each element pair. Correlation coefficients allow the examination of overall compositional relationships. Correlations range from +1 to -1. A correlation of +1 indicates a perfect direct relationship, while a -1 indicates a perfect inverse relationship. Values between +1 and -1 indicate a less than perfect relationship, while zero indicates lack of any relationship at all.

The correlation matrix of major and trace elements from the rocks of the Wateranga intrusion is presented in Table 4 (Appendix 1). Correlation matrix is calculated from the log values of the major and trace elements as the concentrations show a wide range. In Table 4 (Appendix 1), correlation coefficients (r) that are statistically significant are presented in italics. For about 100 samples, r values >0.25 (+ or -) are statistically significant (Rollinson, 1993).

Elements with similar ionic radii and ionic charge substitute for each other in a crystal structure. Many major and minor element correlations can be explained either by similar charge or similar size. This, in turn, reflects the change in the bulk composition of the liquid either in enrichment or depletion of a few elements.

When a mineral is added to or removed from a basaltic liquid, there will be a net change in the bulk composition of the liquid. For example, olivine has least effect on the enrichment of the light/heavy REE, while the plagioclase crystallization is likely to produce a distinct Eu anomaly (Haskin, 1984).

In general, fractionation of plagioclase depletes the liquid in CaO, Sr and Al_2O_3, while most of the other elements are enriched. Sr enters Ca sites in plagioclase while Eu is less enriched or depleted in the liquid when compared to other REE. MgO, FeO, Fe_2O_3, Ni and Cu are depleted during olivine fractionation whereas Na_2O, Al_2O_3, CaO and REE are enriched.

Clinopyroxene fractionation may deplete CaO and MgO along with Cr and Sc. Sm, Eu and Lu enter Ca^{++} sites while La is enriched in the liquid. With increasing

fractionation, La/Sm ratio will increase along with the incompatible elements such as Zr, Ti, P, Y, Nb and REE.

The correlation coefficients for all the major and trace elements of the rocks of the Wateranga intrusion (Appendix 1, Table 4) indicate distinct chemical characteristics. Olivine and clinopyroxene removal from the liquid is represented by the positive correlation of Ni and Cr with MgO, where these two elements enter the olivine and clinopyroxene structure. MgO showing a positive correlation with FeO indicates olivine fractionation. Many incompatible elements TiO_2, P_2O_5, K_2O, Ba, Rb, Zr, Y and Nb show moderate to high positive correlation to each other and a few elements show a negative correlation with MgO suggesting the role of fractionation in the enrichment of these elements. Opaque mineral phases are represented by the positive correlations amongst FeO, MnO, TiO_2, V, Sc and Zn.

4.5 Major element variations

Most samples of the Wateranga intrusion are low in TiO_2, K_2O and P_2O_5 and high in Al_2O_3 and MgO. Most samples are enriched in Sr, Ba, V, Ni and Cr and poorer in Rb, Th, Pb and Nb. Major and trace element analyses and correlation matrix are presented in Appendix 1 (Tables 1-4). The representative analyses, and the range in composition and average chemical analyses are presented in Tables 4.1 and 4.2 respectively. Average compositions of each stratigraphic Zone are presented in Table 4.4. The different rock types of the intrusion show wide Mg# [Mg# = 100 x Mg/(Mg + Fe^{2+})] variations, consistent with a tholeiitic differentiation process controlled by fractional crystallization. The spread of Mg#s (82-23) indicate the extent of differentiation. Hence, plots of various major and trace elements against the Mg# fractionation index will be used to illustrate the geochemical variations within the Wateranga intrusion (Figs. 4.2 and 4.3).

Selected major elements plotted against Mg# are shown in Figure 4.2. The rocks of the Wateranga intrusion show wide variations in major elements. In general, Mg#s negatively correlate with P_2O_5 (0.01-8.57 wt%), K_2O (0.01-1.57 wt%), TiO_2 (0.15-10.78 wt%), Na_2O (0.23-5.15 wt%) and total iron (as Fe_2O_3) (0.86-48.58 wt%) and positively correlate with MgO (0.36-22.12 wt%), CaO

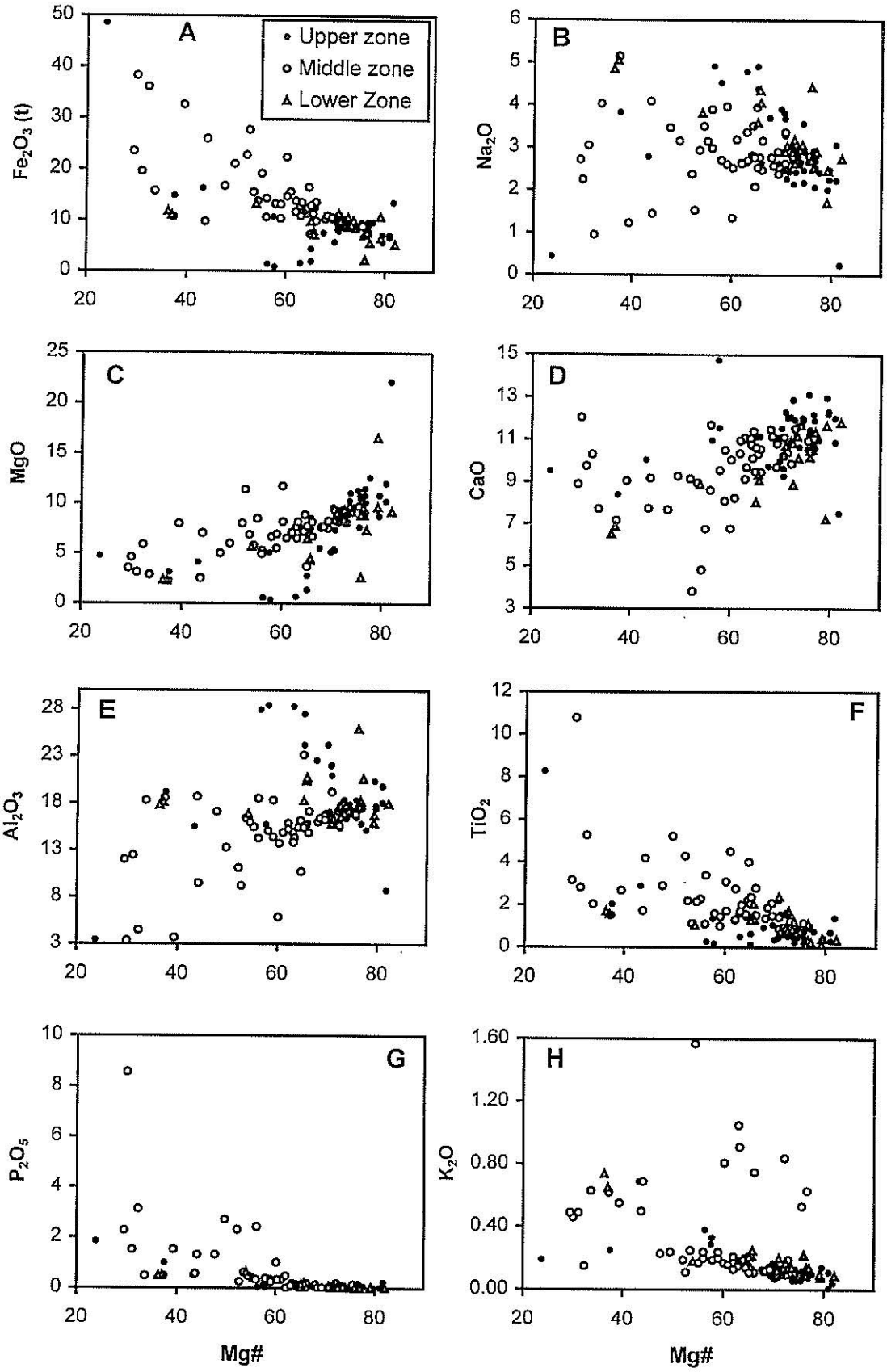

Figure 4.2 Variation diagrams showing selected major element oxides (wt%) plotted against the differentiation index (Mg#) in the Wateranga intrusion [where Mg# = 100*Mg/ (Mg + Fe^{2+})].

(3.83-14.74 wt%) and Al_2O_3 (3.36-28.39 wt%). The systematic trends of the Wateranga rocks in Figure 4.2 are attributed to progressive differentiation by fractional crystallization.

Plagioclase is the dominant cumulus phase and preferentially fractionates Al_2O_3. This explains the higher concentrations of Al_2O_3 (up to 28 wt%), which is 13 wt% higher than normal tholeiitic basalts (Le Maitre, 1976; Wilson, 1989). The decrease of Al_2O_3 and CaO with differentiation would be expected if plagioclase fractionation was important, as the earlier crystallizing calcic plagioclases have more Al_2O_3 than the sodic plagioclases. K_2O is low in most samples analyzed, reflecting the K-poor nature of the parent magma or the incompatible nature of potassium in the minerals present.

4.6 Trace element variations

In Figure 4.3 selected trace elements are plotted against Mg#. Discontinuous and contrasting fractionation trends between individual stratigraphic zones indicate involvement of more than one batch of magma.

4.6.1 Compatible trace elements

As the compatible trace element concentrations change dramatically in an igneous liquid during fractional crystallization, bivariate plots of compatible elements plotted against an index of fractionation (e.g. Mg#) can be used to test for fractional crystallization. Nickel contents of the rocks of the Wateranga intrusion show a well defined positive correlation with Mg#, varying from 1102 ppm for the primitive samples to 8 ppm for the evolved samples (Fig 4.3a). The Cr contents also decrease with decreasing Mg# from 3179 to 5 ppm (Fig 4.3c).

Contents of V and Sc vary randomly within the ranges 20-784 ppm and 3-169 ppm respectively (Figs. 4.3 f and j). There are contrasting correlations between Mg# and V between individual stratigraphic zones: e.g. broad positive correlations are observed for the Middle Zone samples, while negative correlations are evident for the Lower Zone samples (Fig. 4.3j).

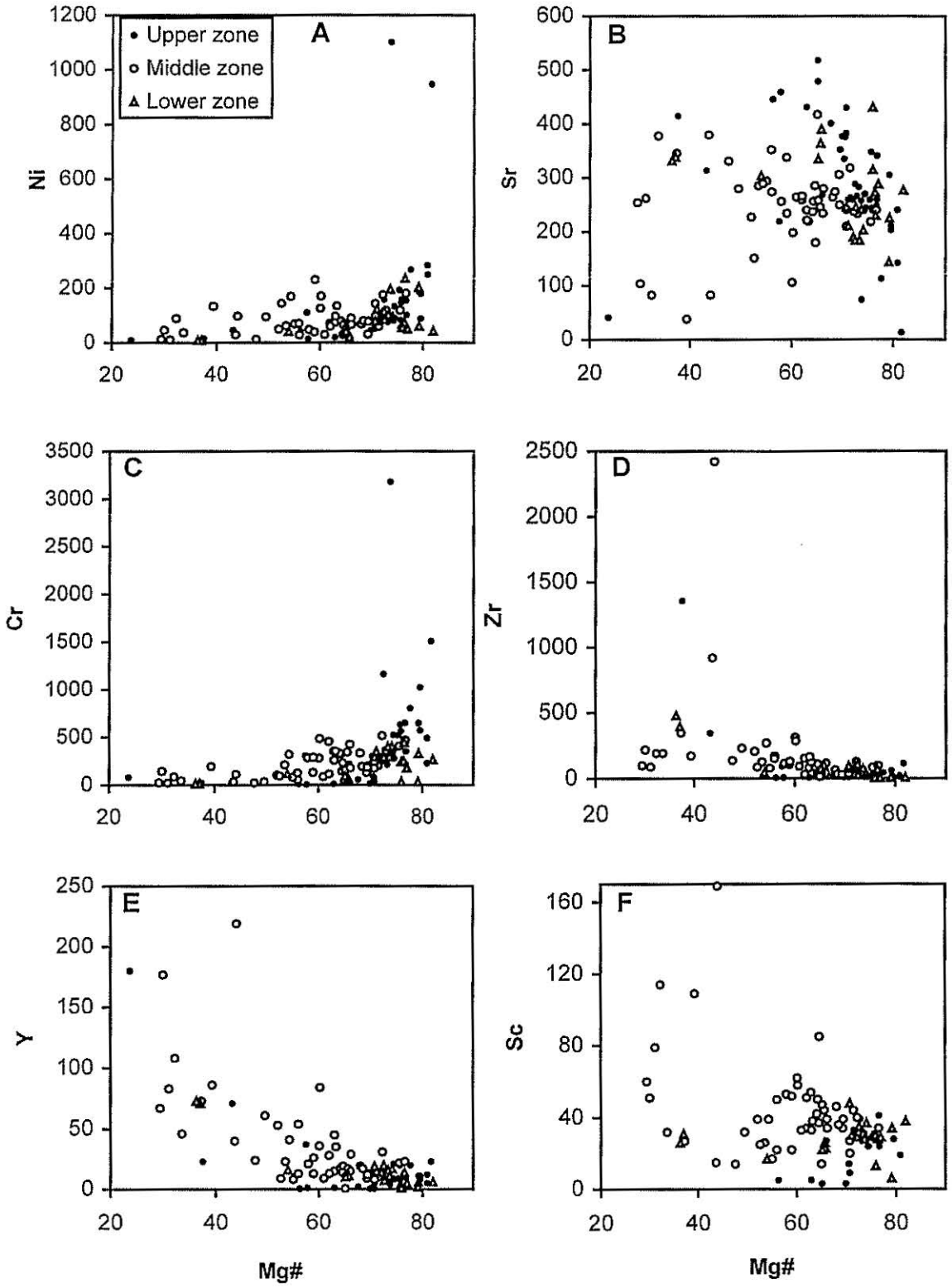

Figure 4.3 (l)

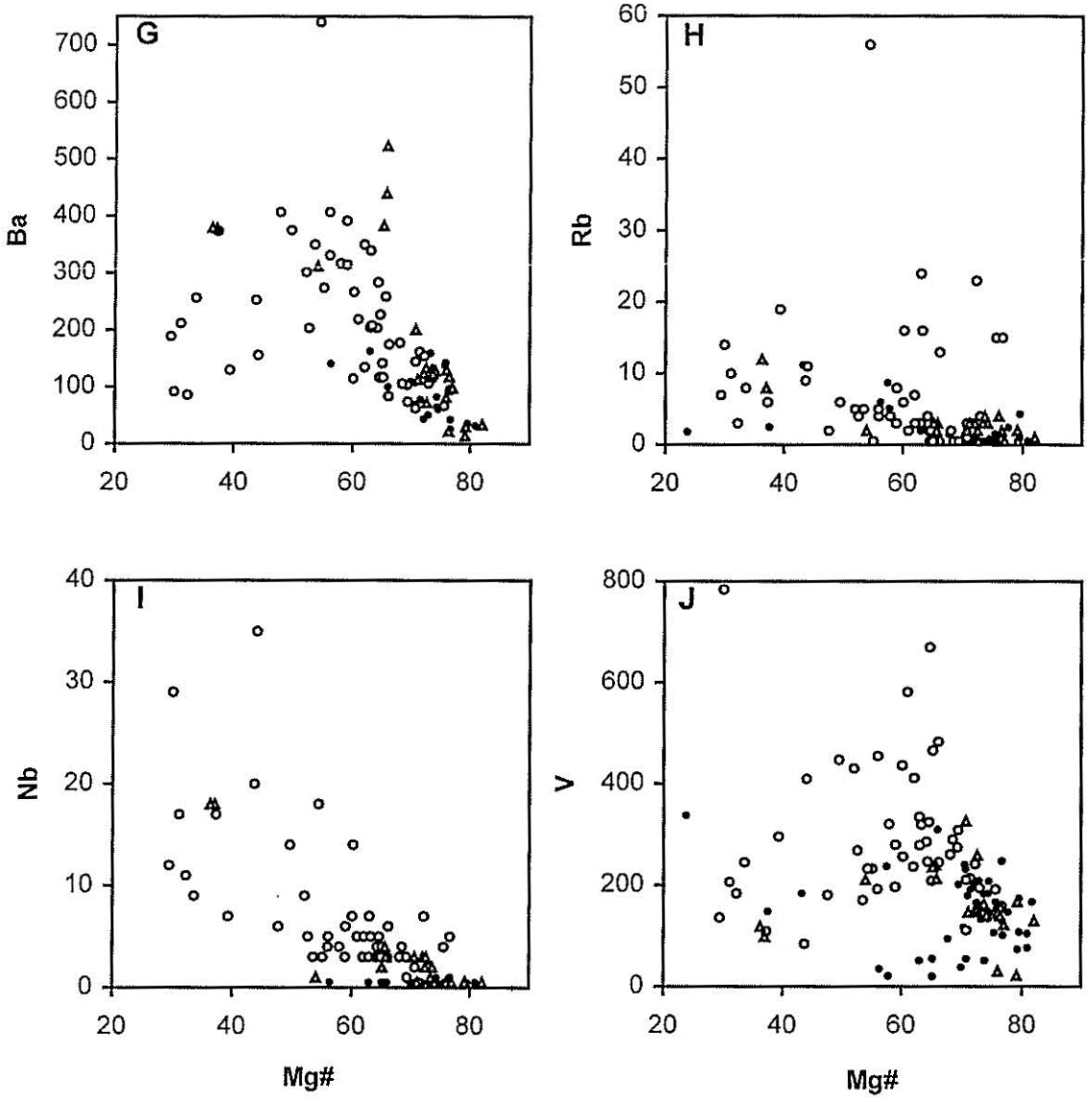

Figure 4.3 (II)

Figure 4.3 Variation diagrams showing selected trace elements (ppm) plotted against the differentiation index (Mg#) in the Wateranga intrusion [where Mg# = 100* Mg/(Mg + Fe^{2+})].

4.6.2 Incompatible trace elements

Incompatible trace element contents (Fig. 4.3) of the rocks of the Wateranga intrusion are highly variable (e.g. Zr, 4-7668 ppm; Ba, 14-740 ppm; Nb, 1-35 ppm; Y, 1-219 ppm). Figure 4.3 shows with decreasing Mg#: Zr, Y and Nb increases; Ba and Rb increases with some scatter; and Sr shows much scatter but generally increases. The scatter in Ba, Rb and Sr probably reflects crustal contamination. Zr concentrations show a range from 4 ppm upto 7668 ppm. One sample, with very high abundance of Zr (A-WG24 - 7668 ppm), is omitted in the Mg# versus Zr plot for better correlation. Although the incompatible trace element graphs show overall trends of increase with decreasing Mg#, there are some regressions of the trend, suggesting that more than one batch of magma is represented.

4.7 Fine grained samples of the intrusion

Two fine grained samples (WG-44 and WG-124) collected from chilled margins of the intrusion were analyzed for major, trace and rare earth elements (Tables 4.3 and 4.5) to determine a possible parental magma composition for the rocks of the Wateranga intrusion. Samples WG-44 and WG-124 are MgO and CaO rich, and P_2O_5 and K_2O poor compared to the average composition of the Wateranga intrusion (Tables 4.2 and 4.3). They are enriched in Ni, Cr and Cu, and poorer in all other trace elements compared to the average composition of the Wateranga intrusion.

4.8 Chemical variations with stratigraphic depth

Figure 4.4 shows the variation in whole-rock Mg#, TiO_2, Fe_2O_3 (total), P_2O_5 and selected trace elements (Zn, V, Zr, Y, Nb, La, Ba, Rb, Sr and Nd) with stratigraphic depth of the intrusion. All the elements plotted have similar distribution pattern through the vertical section. Significant variations in chemical composition with stratigraphic depth are present, and the variations reveal a three fold stratigraphic subdivision, which are named as the Upper, Middle and Lower Zones. Each zone represents a major magma batch. Data show geochemical breaks

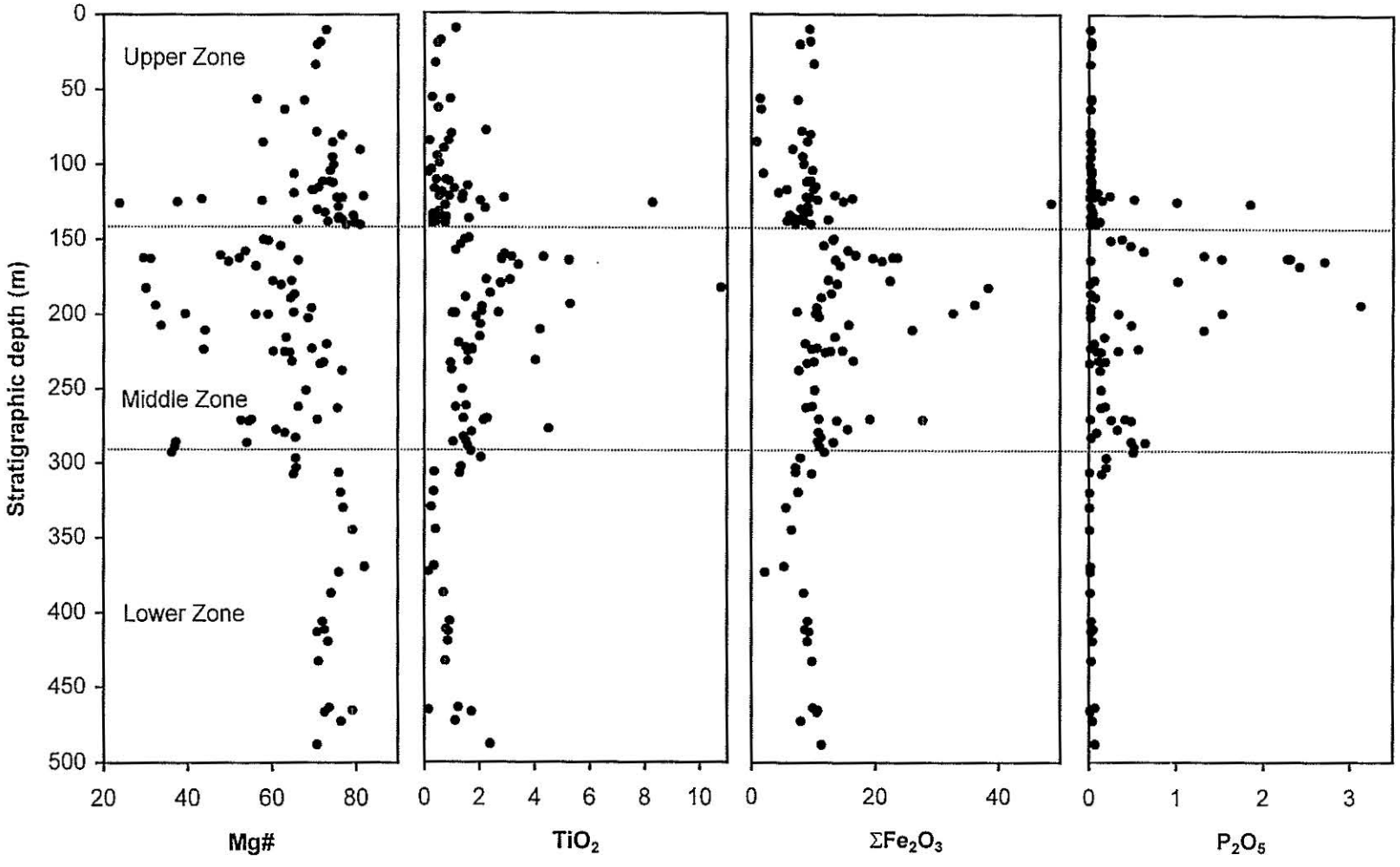
Stratigraphic depth (m)
0
50
100
150
200
250
300
350
400
450
500
Upper Zone
Middle Zone
Lower Zone
20
40
60
80
Mg#
0
2
4
6
8
10
TiO2
0
20
40
ΣFe2O3
0
1
2
3
P2O5

Figure 4.4 (l)

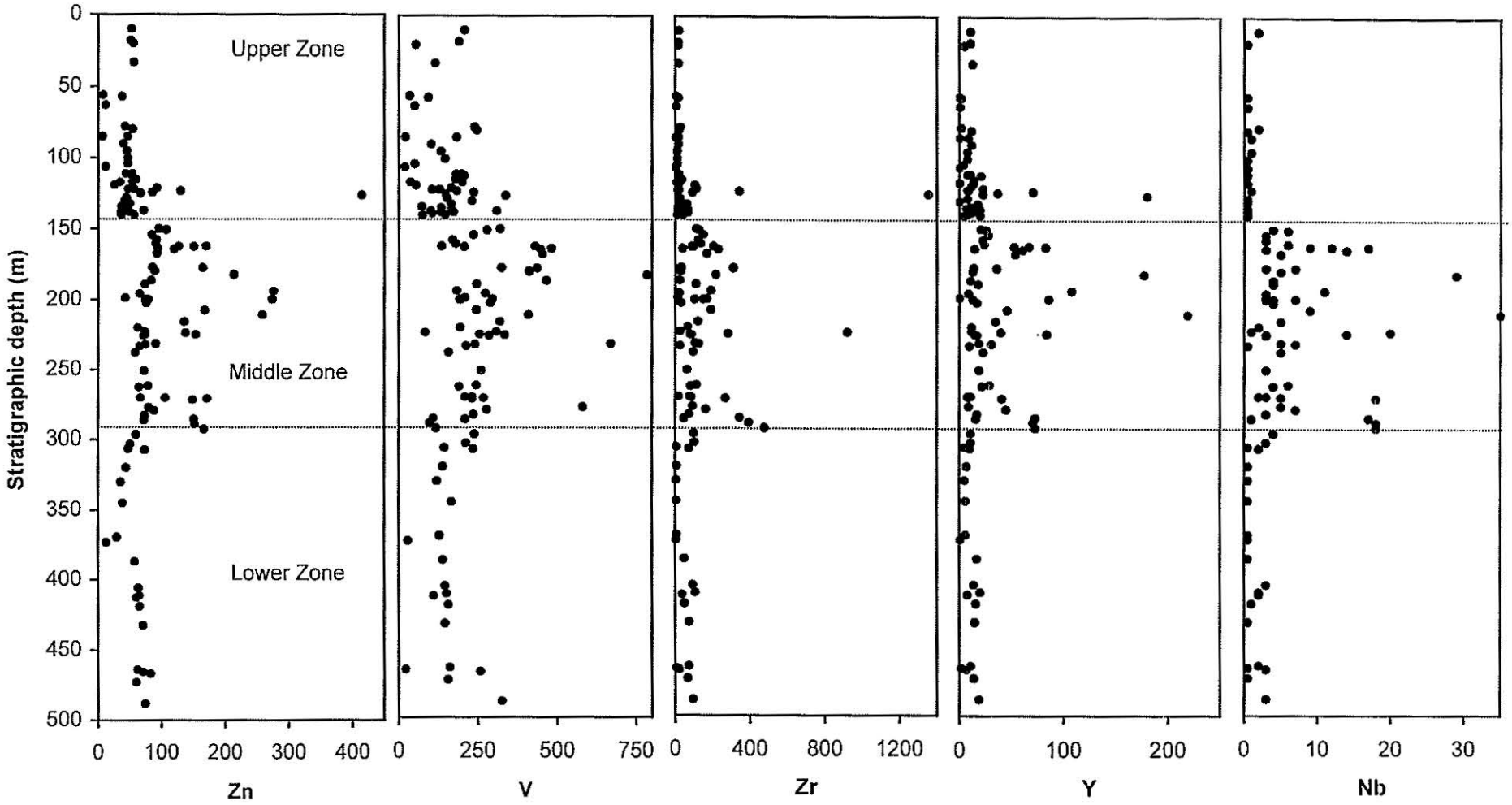
Stratigraphic depth (m)
0
50
100
150
200
250
300
350
400
450
500
Upper Zone
Middle Zone
Lower Zone
0
100
200
300
400
Zn
0
250
500
750
V
0
400
800
1200
Zr
0
100
200
Y
0
10
20
30
Nb

Figure 4.4 (II)

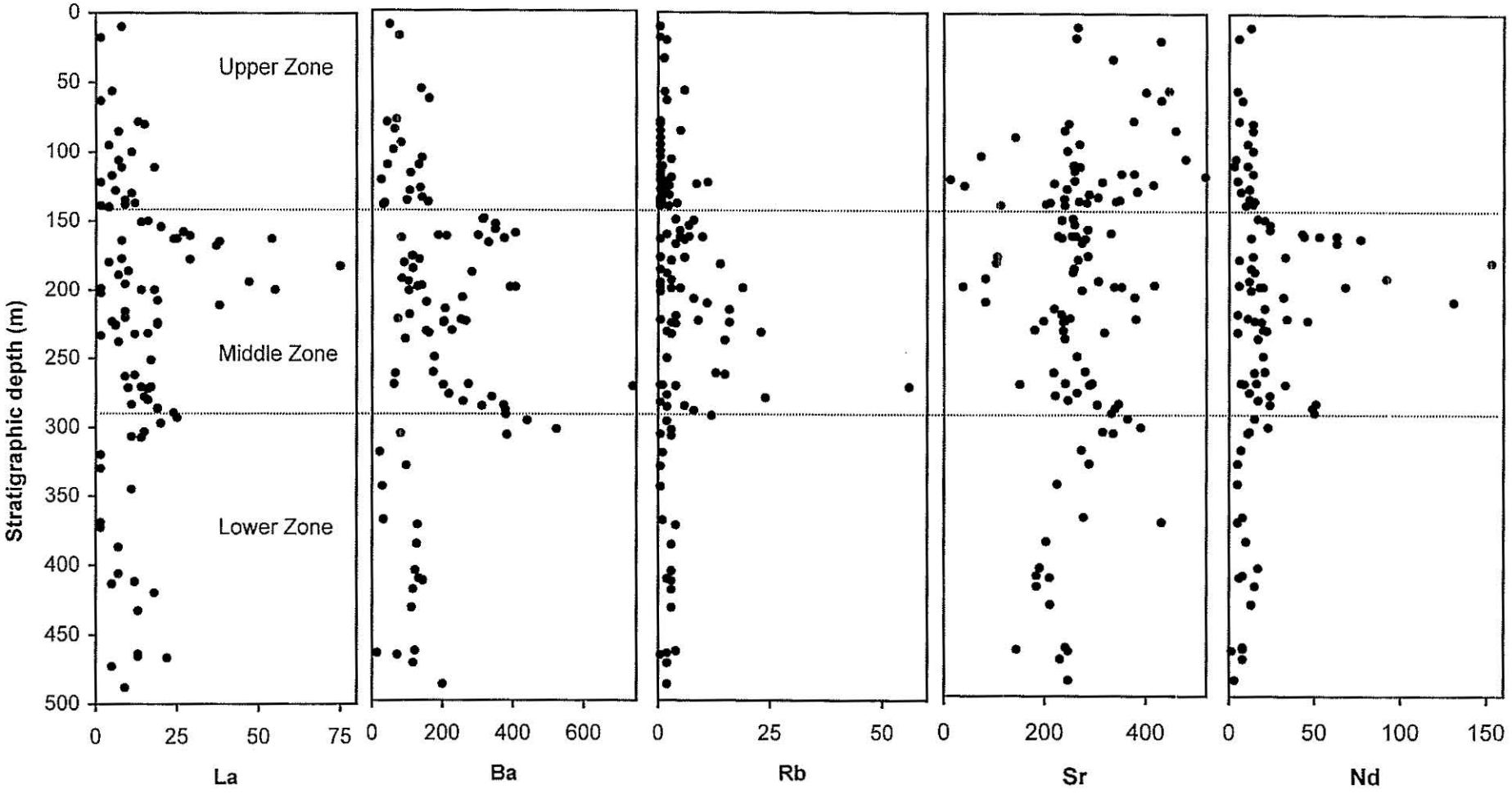

Figure 4.4 (III)

Figure 4.4 Plots of selected major element oxides (wt%) and trace elements (ppm) versus stratigraphic depth (m) in the Wateranga intrusion. **Note:** Two samples, with very high contents of Zr (A-WG 24 - 7668 ppm and E-NS5/5 - 2422 ppm), are omitted in the Zr versus stratigraphic depth plot. Also, sample NS-5/4 with very high P_2O_5 (8.57 ppm) is omitted in the P_2O_5 plot.

at 140 m and 285 m. The Middle zone, between about 140 and 285 m, consists of distinctly higher concentrations of incompatible elements compared with the Lower and Upper Zones. The sudden and sustained changes at the zone boundaries are consistent with a magma chamber that was open to periodic influxes of new magmas (e.g., Cawthorn, 1983; Wiebe, 1988; Klewin, 1990; Cawthorn et al., 1991). This explanation is entirely consistent with the mineral chemical variations (Chapter 3) and isotopic data (Chapter 5).

4.9 Normalized multi-element diagrams (spider diagrams)

In order to understand the pattern of trace element abundances in basalts it is useful to have a reference frame to which the elemental abundances in a particular rock can be compared. The concept of spider diagrams (Sun, 1980; Thompson, 1982) has been developed from this idea, in which the abundances of a range of incompatible trace elements are normalized to estimates of their abundances in the Primordial earth.

Figure 4.5a presents primitive mantle normalized incompatible element diagrams (spider diagrams) that characterize and summarize the average incompatible element distribution for each of the major stratigraphic subdivisions. The patterns are subparallel and have the similar shape for all the stratigraphic zones (Upper, Middle and Lower Zones) of the Wateranga intrusion with higher incompatible element abundance in the Middle Zone samples compared to Lower and Upper Zones. This difference in abundance could be influenced by variable degrees of partial melting of a similar source and by fractionation. The spider diagram highlights depletions in Nb, P, and Ti relative to LILE and REE (Nb depletion in all the three stratigraphic zones, P depletion in the Upper Zone samples and Ti depletion in the Lower Zone samples). Furthermore, the spider diagram patterns of the two fine grained chilled margin samples (Fig 4.5b) show strong similarities with the average composition of the Upper Zone samples (Fig. 4.5a). Distinct features of these fine grained samples are negative Nb and P anomalies. The depletions in Nb, P and Ti in the rocks of the intrusion imply the effect of either lower crustal contamination during the magma evolution or

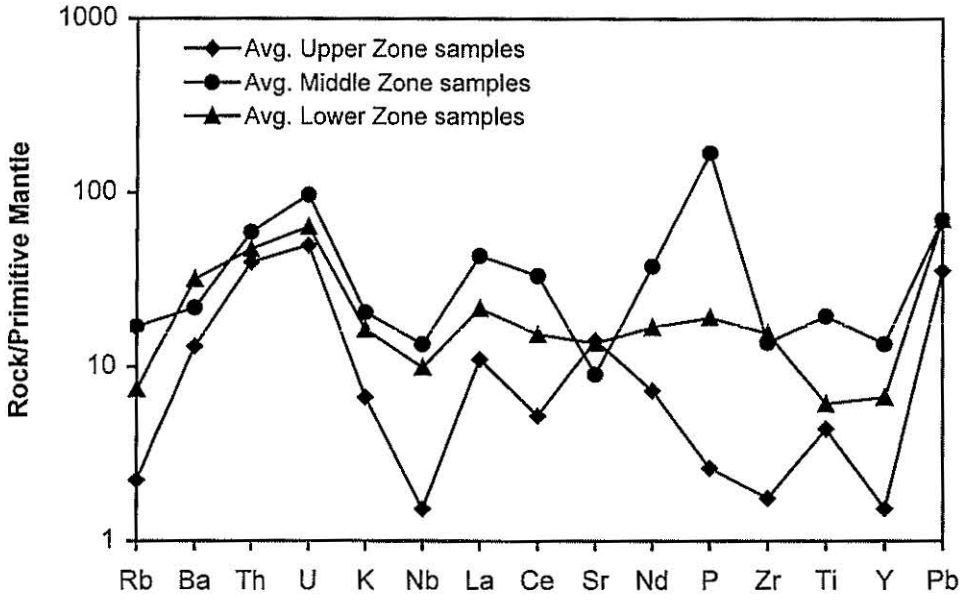

Figure 4.5 A Primitive mantle-normalised (McDonough et al., 1992) incompatible element diagram for the average Upper, Middle and Lower Zone samples of the Wateranga intrusion.

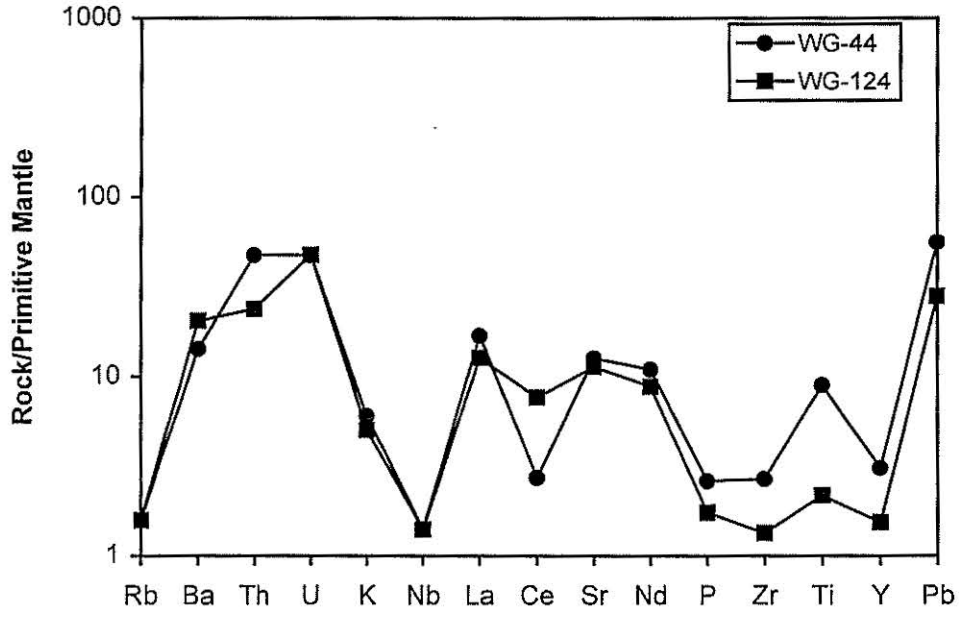

Figure 4.5 B Primitive mantle-normalised (McDonough et al., 1992) incompatible element diagram for the two fine grained (chilled margin) samples of the Wateranga intrusion. WG-44 and WG-124 are sample numbers.

recycling of continental crust in the mantle source (Thompson et al., 1983; Saunders et al., 1992). These data are relevant to the petrogenetic evolution of the Wateranga intrusion, and are considered later in Chapter 6. Pronounced positive P anomalies in the Middle Zone samples, correlate with high apatite abundances.

4.10 Rare earth elements

The rare earth elements La to Lu with atomic numbers ranging from 57 (La) to 71 (Lu) are members of Group III A in the periodic table. They are particularly useful in petrogenetic studies of igneous rocks because all the REE are geochemically similar. They are grouped in the periodic table because of their similar chemical properties, however they do not necessarily behave as a chemically coherent group due to their distribution being controlled by magmatic processes (e.g., crystal fractionation) and hydrothermal alteration (Bowden et al., 1977; Rollinson, 1993). For example, the crystallization of plagioclase results in europium depletion in the fractionating liquid. Fractionation of the mafic minerals results in a concentration of the light rare earth elements (La to Sm) in the remaining liquid due to the fact that partition coefficients (crystal/liquid) for the light rare earth elements are considerably higher than for the heavy rare earth elements (Gd to Lu) for mafic minerals (Haskin, 1977, 1984). Rare earth element ratios and patterns are, therefore, characteristic of particular magmatic processes and stages of fractional crystallization. For example, the chondrite normalized La/Lu ratios for basanites are 13.7-34, continental tholeiites 0.5-7.6, K-rich mafic rocks 19.5-262 and tholeiitic intrusive complexes 0.3-19.3 (Cullers and Graf, 1984).

The rare earth element data for 20 selected rocks of the Wateranga intrusion have been obtained using ICP-MS technique (Appendix 3) in order to gain further insights into the geochemistry of the intrusion. The data are presented in Table 4.5.

Figure 4.6 presents average chondrite normalized REE patterns for the Upper, Middle and Lower Zone samples, to compare their compositional characteristics and determine their compositional relationships between them. Marked similarities exist between the Lower and Upper Zones. Furthermore, the REE pattern of

Table 4.5 Rare earth element abundances (ppm) of whole-rock samples, Wateranga intrusion

Sample	Stratigra-phic Zone	La	Ce	Pr	Nd	Sm	Eu	Gd	Tb	Dy	Ho	Er	Tm	Yb	Lu	*Eu/Eu*[b]
WG-44[a]	**UZ**	2	5	0.9	4.7	1.6	1.6	2	0.4	2.4	0.5	1.4	0.2	1.2	0.2	*2.73*
WG-75	**UZ**	1.2	3	0.5	2.7	1	1	1.3	0.2	1.6	0.3	1	0.1	0.7	0.1	*2.68*
WG-103	**UZ**	1.9	3.6	0.5	2	0.5	1.1	0.5	0.1	0.5	0.1	0.3	0.1	0.3	0.1	*6.73*
WG-124[a]	**UZ**	1.4	3.4	0.5	3	1	1.5	1.2	0.2	1.4	0.3	0.8	0.1	0.6	0.1	*4.19*
NS-2/2	**MZ**	13.2	31.6	4.7	23.2	5.1	3.8	5.3	0.9	5	1	3.1	0.4	2.5	0.4	*2.23*
NS-2/5	**MZ**	35.6	86.7	13.6	65.5	13.5	5.9	13.6	1.9	9.8	1.9	5.2	0.6	3.5	0.6	*1.33*
NS-2/8	**MZ**	36.3	89	13.7	66.2	13.7	6.5	13.6	1.9	10.2	2	5.2	0.6	3.7	0.6	*1.46*
NS-2/14	**MZ**	9.8	21	2.9	13	2.6	4.4	2.7	0.4	2.4	0.5	1.5	0.2	1.3	0.2	*5.08*
NS-2/33	**MZ**	5.8	12.7	1.9	9.2	2.1	3	2.3	0.3	2.1	0.4	1.2	0.2	1	0.2	*4.17*
NS-2/41	**LZ**	10.1	20.5	2.7	11.9	2.3	4.5	2.3	0.3	1.9	0.4	1.2	0.2	1.1	0.2	*5.98*
NS-2/42	**LZ**	8.2	16.5	2.2	9.3	1.9	4	2	0.3	1.8	0.4	1.2	0.2	1.1	0.2	*6.27*
NS-2/48	**LZ**	3.8	9.3	1.5	7.2	2.2	1.5	2.5	0.5	3.1	0.6	1.8	0.2	1.6	0.3	*1.96*
NS-2/54	**LZ**	5.6	13.2	2.1	9.9	2.7	1.4	3	0.6	3.4	0.8	2.2	0.3	2	0.3	*1.50*
NS-2/65	**LZ**	4.7	11.6	1.9	9.6	2.7	2.1	3.2	0.6	3.4	0.7	2.1	0.3	1.8	0.3	*2.18*
NS-3/4	**MZ**	2.3	5.8	1	5.6	1.8	2	2.2	0.4	2.6	0.6	1.5	0.2	1.4	0.2	*3.07*
NS-3/8	**MZ**	1.9	4.1	0.7	3.5	1.1	1.8	1.4	0.3	1.8	0.4	1.2	0.2	1.1	0.2	*4.43*
NS-3/28	**LZ**	1.5	3	0.5	2.3	0.7	1	0.9	0.2	1.1	0.3	0.8	0.1	0.7	0.1	*3.85*
NS-3/53	**LZ**	2.5	5.2	0.8	3.5	1	1	1.2	0.2	1.5	0.3	1	0.2	1	0.2	*2.79*
NS-5/4	**MZ**	59	155	26.6	136	36.6	8.3	39.3	6	31.9	6.2	16.1	1.9	10.4	1.6	*0.67*
NS-5/6	**MZ**	34.3	86.7	12.9	58	15.7	3	16.3	2.7	15.6	3.1	8.9	1.1	7	1.1	*0.57*

Note: Lower detection limit for all elements is 0.1ppm.

Eu/Eu^b is chondrite normalized; $Eu/Eu^b = Eu_{CN}/\sqrt{(Sm_{CN} \times Gd_{CN})}$. [a] chilled margin samples. UZ - Upper Zone; MZ - Middle Zone; LZ - Lower Zone

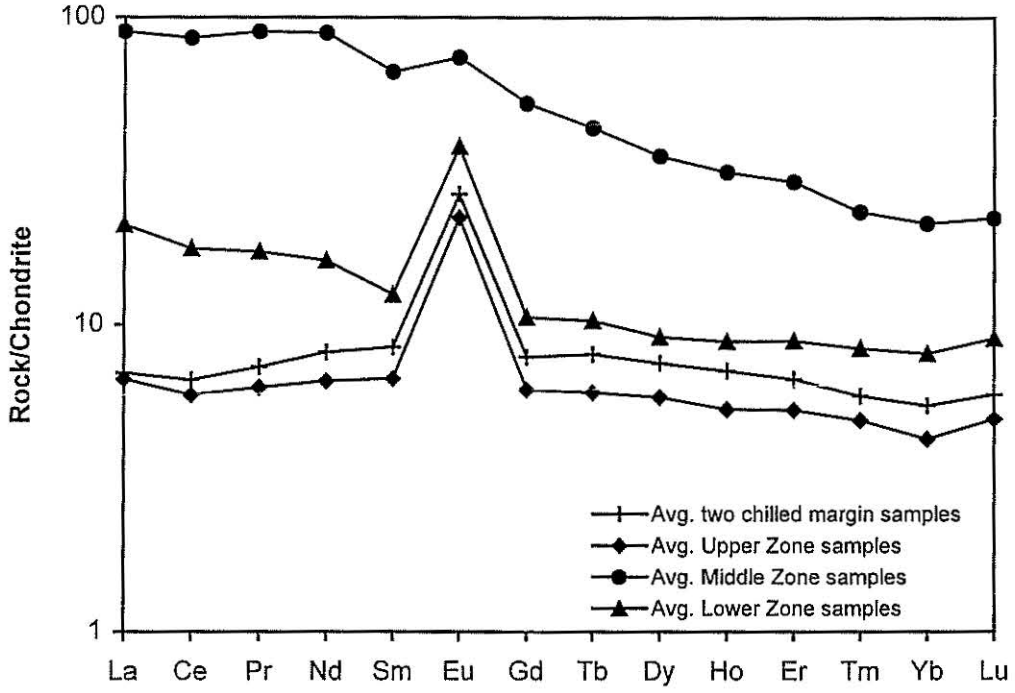

Figure 4.6 Chondrite-normalized (Evensen et al., 1978) REE variation diagram for the average two fine grained chilled margin, Upper, Middle and Lower Zone samples of the Wateranga intrusion.

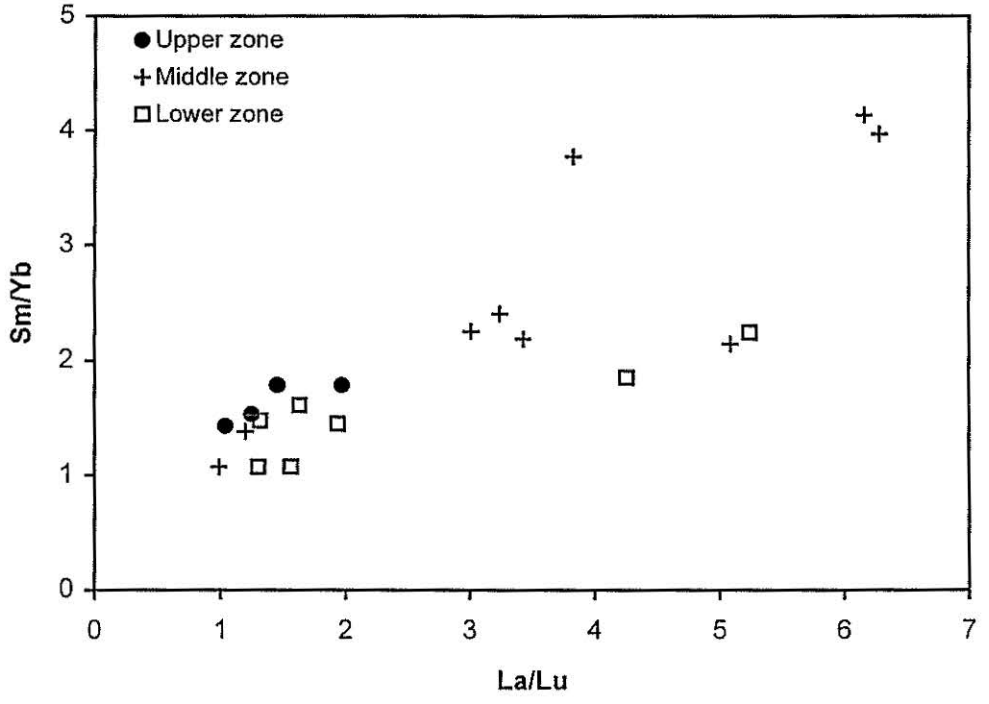

Figure 4.7 La/Lu versus Sm/Yb for selected rocks from the Wateranga intrusion

average fine grained chilled margin samples show strong similarity with the average Upper Zone samples. The Middle Zone contains significantly higher REE abundances and higher LREE enrichment than the Lower and Upper Zones, which may be due to difference in degree of partial melting (Jaques and Green, 1980), source heterogeneity and/or fractionation.

The REE patterns show negative slopes with moderate to large positive Eu anomalies (Fig. 4.6), which indicate plagioclase accumulation. The Middle Zone displays evidence for the least plagioclase accumulation. In general, the REE patterns of the Wateranga intrusion are similar to that of enriched mid-ocean-ridge basalt (E-MORB), continental flood basalts (e.g., Columbia River Basalts), and Proterozoic rift-related basalt (Keweenawan suite), but is unlike patterns typical of N-MORB or of arc-tholeiite (Basaltic Volcanism Study Project, 1981).

In Table 4.5, the ratio Eu/Eu* [$Eu/Eu^* = Eu_{CN}/\sqrt{(Sm_{CN} \times Gd_{CN})}$] is a measure of the europium anomaly and a value of greater than 1.0 indicates a positive anomaly while a value of less than 1.0 is a negative anomaly. A strong positive Eu/Eu* result indicates the presence of Eu-bearing plagioclase and a strong negative anomaly indicates that plagioclase fractionation has left the residual liquid depleted in Eu.

Perhaps the best discriminant plot to exploit the REE data is La/Lu versus Sm/Yb (Fig. 4.7) as the ratio La/Lu will increase strongly with fractional crystallization involving mafic minerals while the ratio Sm/Yb will increase less strongly. This plot serves to spread the data out so that trends or clusters are better established for the various igneous rock suites. The plot is remarkable for the linearity displayed between the three stratigraphic zones of the intrusion. The broadest spread in data for the Middle Zone indicates fractionation. The generally low La/Lu ratios (< 6.28) suggest that the classification of tholeiitic intrusive complex is relevant (Cullers and Graf, 1984). The Middle Zone samples would appear more evolved than the Lower and Upper Zones (high La/Lu and Sm/Yb). This is supported by whole rock geochemistry.

4.11 Platinum group elements

4.11.1 PGE and magmatic processes

As already discussed in Chapter 1, layered mafic intrusions are significant sources of the platinum group elements (PGEs). The platinum group elements are valuable tools in providing information about magmatic processes, in particular S-saturation, as well as crystal fractionation trends. Barnes et al. (1985) showed that the PGEs, when chondrite-normalized, are fractionated in order of decreasing melting point, which decreases in the order Os, Ir, Ru, Rh, Pt, Pd and Au. Using chondrite-normalized PGE patterns it is possible, to a certain extent, to distinguish between sulphides that segregated from primitive magmas such as komatiites and sulphides which segregated from more fractionated magmas such as tholeiites (Barnes et al., 1988).

Barnes et al. (1988), have constructed diagrams which plot mantle-normalized data in the order Ni, Os, Ir, Ru, Rh, Pt, Pd, Au and Cu. Placing Ni to the left of the plot and Cu to the right allows the effect of sulphide segregation as well as chromite crystallization to be discerned. Since Ni and Cu are partitioned less strongly than the noble metals into sulphides relative to melt (e.g. Peach et al., 1990), sulphide segregation will result in a trough-shaped plot in magma which relinquishes this residue. Any rocks containing these sulphides (i.e second-stage melts such as boninites) will inherit an arched pattern (Barnes et al., 1988). Chromite-rich rocks are commonly enriched in Os, Ir and Ru and therefore if chromite is lost to crystallization a positive slope will result and a negative slope will result from rocks enriched in early crystallized chromite.

4.11.2 Distribution of PGE and Au in the Wateranga intrusion

Ten samples were analyzed for PGEs (Pt and Pd) and Au using ICP-MS technique (Appendix 3). The data are presented in Table 4.6. Because of the sample spacing, the variation relative to stratigraphic depth cannot be assessed quantitatively. In each sample the sum of PGE (Pt and Pd) + Au (ΣPGE) is very low (<28 ppb) compared to the abundance of PGEs in C1-chondrites (1730 ppb)

(Sun, 1982). The average ΣPGE is 5 ppb and average values of Pt, Pd and Au are 1, 3 and 11 ppb respectively.

Elemental correlations between Pt, Pd, Au, S, Ni, Cu and Cr are presented in Table 4.7. Pd correlates strongly with Pt, Au, S and Cu indicating that these elements behaved similarly during magmatic crystallization. Pt exhibits moderate correlations with Au, S and Cu. Pd correlates moderately negatively with Ni and weakly negatively with Cr.

The association between Pt, Pd, Au and Cu is illustrated in Figure 4.8. A good positive correlation exists between Pd and Pt (r=0.81) indicating that these elements behaved sympathetically during magmatic crystallization. Au and Cu shows no obvious systematic covariation. Pd – Pd/Pt, Pd+Pt – Au, Pd – Cu and Pt – Cu are moderately positively correlated. Thus it would appear that the chalcophile characters of Pt, Pd and Au are controlling their distribution.

Selected bivariate plots of chalcophile elements are presented in Figure 4.9 in order to assess the behaviour of the PGE and Au with fractionation. A good negative correlation exists between Mg# and Pd (r = -0.91), and Mg# and S (r = -0.85). Mg# - Pt, Mg# - Au and Mg# - Cu are moderately negatively correlated. A well defined positive correlation exists between Mg# and Ni.

Cu and Ni are potential pathfinders for the PGE (Buchanan, 1988). If the PGE are concentrated by magmatic sulphide, then they are likely to be associated with base metal sulphides, and hence with anomalous levels of Ni and Cu. Cr also has been described as a pathfinder for the PGE (Buchanan, 1988). But the concentrations of Ni and Cr do not show no overall association of anomalous levels with Pt and Pd (Fig. 4.10). Cu, to some extent shows anomalous levels with Pt and Pd.

The mantle-normalized metal contents of the Wateranga intrusion are presented in Figure 4.11. All the rock types of the intrusion exhibit similar mantle normalized metal patterns, reflecting crystallization from a fairly homogeneous source. All the rock types possess a positive slope pattern and Ni is depleted relative to Cu. Thus the pattern would appear to reflect a simple fractionation pattern, early olivine crystallization having depleted the magma in Ni.

Table 4.6 Whole-rock platinum-group element and Au data, Wateranga intrusion. Also presented are S, Ni, Cu, Cr, Mg# data

Sample	Mg#	S (wt%)	Ni (ppm)	Cu (ppm)	Cr (ppm)	Pt (ppb)	Pd (ppb)	Au (ppb)
WG-44	66.01	0.16	84	63	219	1	2	8
NS-2/5	52.15	0.30	50	95	104	1	4	13
NS-2/9	60.17	0.55	126	178	282	1	2	8
NS-2/22	64.70	0.24	65	74	231	1	1	7
NS-2/59	71.09	0.14	124	80	350	1	2	9
NS-2/63	76.46	0.13	237	80	446	2	2	12
NS-2/65	70.70	0.31	80	41	296	1	2	17
NS-3/51	79.14	0.12	203	115	33	1	1	9
NS-3/53	72.59	0.19	84	54	292	1	1	8
NS-5/4	30.07	0.70	46	184	146	3	8	17

Note: Lower detection limit for Pt, Pd and Au is 1.00 ppb.

Table 4.7 Correlation matrix (r values) for whole-rock platinum group elements and selected trace elements, Wateranga intrusion (N=10)

	Ni	Cu	Cr	S	Pt	Pd	Au
Ni	1.00						
Cu	-0.01	1.00					
Cr	0.30	-0.34	1.00				
S	-0.47	***0.78***	-0.21	1.00			
Pt	0.00	0.53	0.02	0.57	1.00		
Pd	-0.43	0.61	-0.29	***0.76***	***0.81***	1.00	
Au	-0.22	0.15	-0.07	0.48	0.59	***0.70***	1.00

Note: Statistically significant correlation coefficients (>0.63) are in italic-bold (Rollinson, 1993).

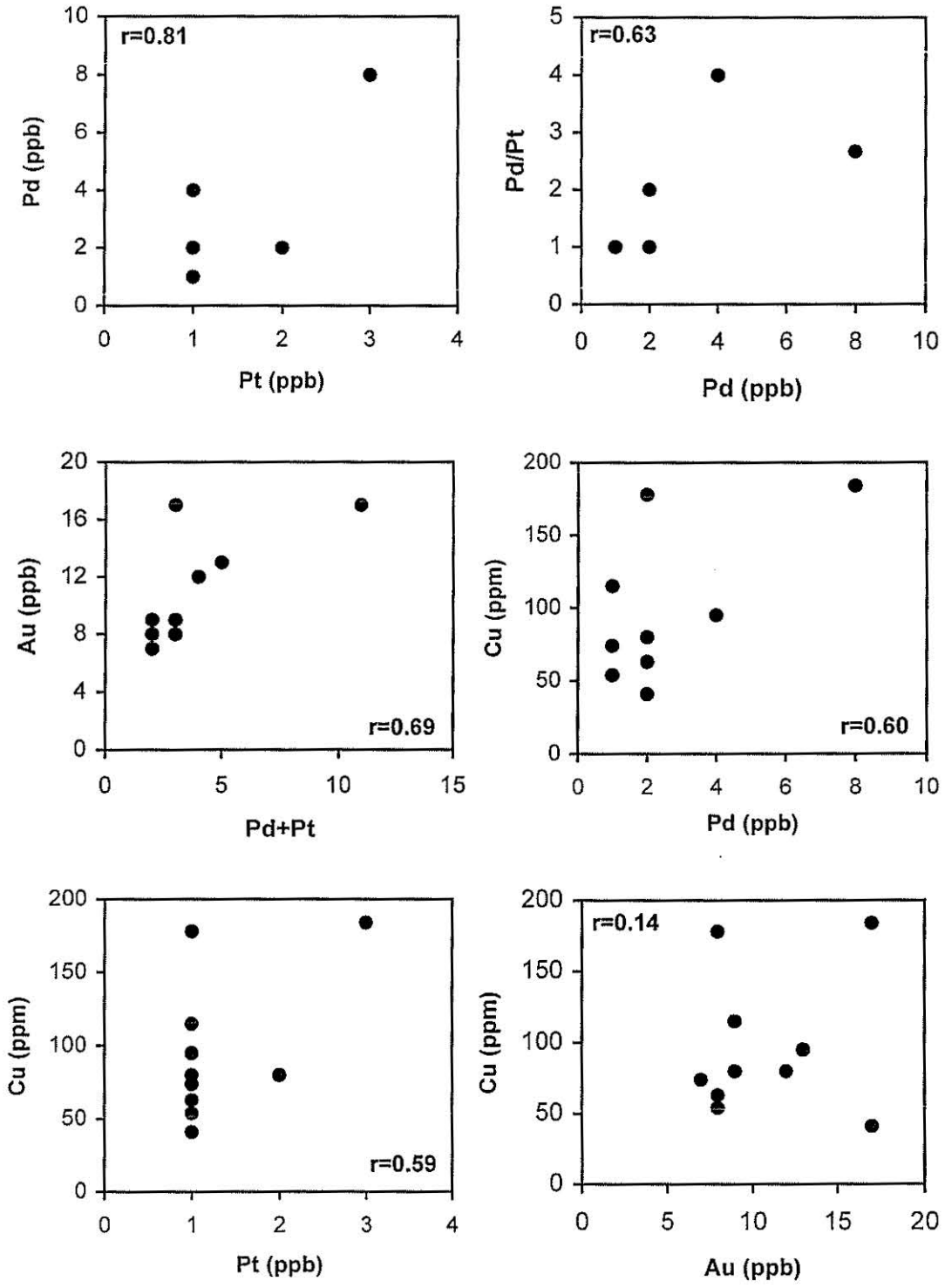

Figure 4.8 Selected binary plots of whole-rock data for precious metals and Cu for the Wateranga intrusion.

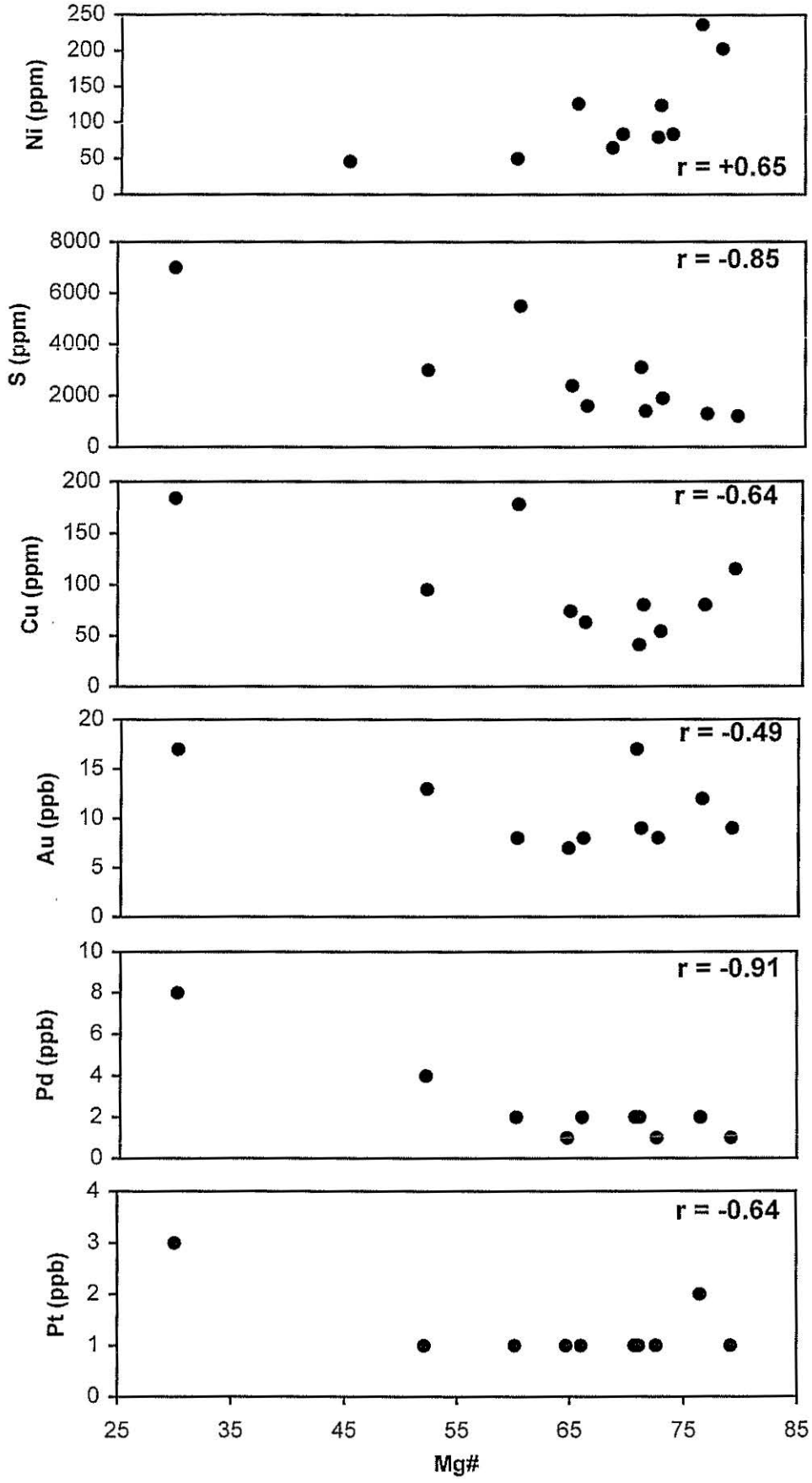

Figure 4.9 Whole-rock Mg# versus Pt, Pd, Au, Cu and S, Wateranga intrusion

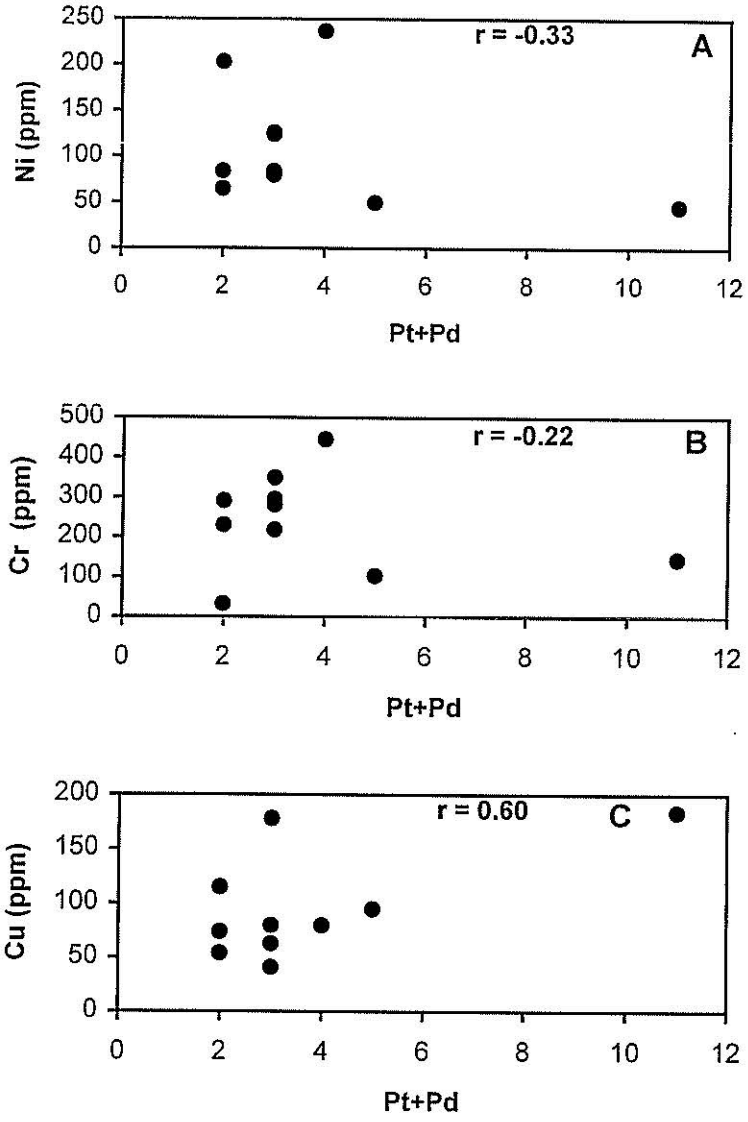

Figure 4.10 Graphical comparison of PGE content, expressed as the sum of the Pt and Pd concentrations of the rocks from the Wateranga intrusion with concentrations of pathfinder elements Ni (A), Cr (B) and Cu (C).

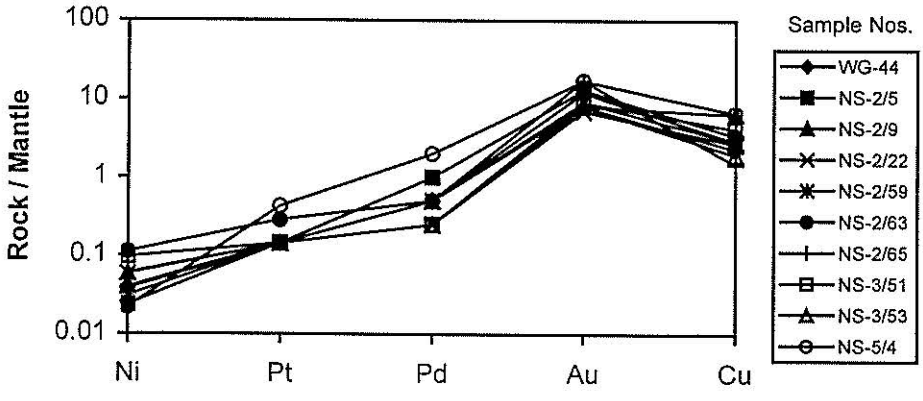

Figure 4.11 Average mantle-normalized multi-chalcophile element diagram for the Wateranga intrusion. Normalization values are after Brugmann et al.(1987).

Petrogenetic significance of the whole rock major and trace elements, REE and PGE is further discussed in Chapter 6 (Discussion). Also, tectonic setting of the Wateranga intrusion is discussed in Chapter 6.

4.12 Granitic rocks

As already mentioned in Chapter 2, the Wateranga intrusion is crosscut by granitic rocks that occur as veins and small dykes. The compositions of selected specimens (WG-39 and NS-2/10) from granitic rocks of the intrusion are given in Appendix 1 (Table 1). The presence of granitic rocks as veins at different depths of the intrusion is incompatible with the stratigraphy of the intrusion. Furthermore, they are petrochemically distinct from mafic rocks. Intermediate compositions are absent, so that the granitic rocks appear to be bimodal and later intrusions.

4.13 Summary

The whole-rock geochemistry and compositional trends displayed by the Wateranga intrusion indicate that it crystallized from tholeiitic magma. These rocks show a wide range of chemical composition. The systematic trends of the major and trace elements are attributed to progressive differentiation by fractional crystallization. The intrusion is subdivided into three evolutionary stages (Upper, Middle and Lower Zones) on the basis of whole-rock geochemical variations. Whole-rock Mg#, TiO_2, Fe_2O_3 (total), P_2O_5 and incompatible trace elements vary with depth and display abrupt shifts at the zone boundaries, which indicate open system addition of new mafic magma. This conclusion is entirely consistent with the mineral chemical variations (Chapter 3).

In the rocks of the Wateranga intrusion, the sum of PGE (Pt + Pd) + Au is very low (<28 ppb) compared to the abundance of PGEs in C1 – chondrites (1730 ppb). The association between Pt, Pd, Au and Cu with a positive correlation suggests that the chalcophile characters of Pt, Pd and Au are controlling their distribution.

CHAPTER 5

Geochemistry – II
Nd-Sr-O Isotopes

Geochemistry – II Nd-Sr-O Isotopes

5.1 Introduction

Whole-rock isotopic analyses were carried out to explore four different aspects of the magmas of the Wateranga intrusion: (1) periodic recharge of fresh magma during magma chamber crystallization; (2) the role of crustal assimilation; (3) identification of possible source constraints for the three Zones (Lower, Middle and Upper) of the intrusion; (4) the possibility of post-magmatic fluid interaction (O isotopes) with the intrusion. In this Chapter, the whole-rock isotopic data are presented and discussed. Further discussion is presented in Chapter 6.

In this study, ten whole-rock samples were analyzed for Sr and O isotopes, and eight for Nd isotopes at the Centre for Isotope Studies, CSIRO, Sydney, Australia. Sr and Nd isotopic analyses were carried out using a VG Sector 354 thermal ionization mass spectrometer and O isotopic analyses using a Finnigan 252 mass spectrometer. Analytical procedures are presented in Appendix 4. Isotopic analyses are presented in this Chapter in Tables 5.1 - 5.2.

5. 2 Nd-Sr-O isotopes in magmatic rocks

5.2.1 Radiogenic isotopes (Nd and Sr)

The isotopic compositions of Sr and Nd have shed new light on the complex problems of the origin of magma and the formation of igneous rocks. Radiogenic

isotopic variations can be used to determine the origin of magmas and the chemical evolution of the Earth. An increasingly important application of radiogenic isotopes is in their use as tracers of otherwise undetectable contributors to composite, complex, and heterogeneous environments. Radiogenic isotope tracer applications using Nd and Sr, among others, rely on the fact that these are heavy isotopes. Thus, in contrast to lighter isotopes such as O, H and S, they remain unaffected by (i) changes in temperature and pressure during transport and accumulation, (ii) different rates of chemical reactions and (iii) the presence of different chemical species available in the environment.

Considerable geochemical and isotopic evidence has accumulated, supporting the concept that many parts of the mantle have experienced a complex history of partial melting, intrusion, crystallization, recrystallization, deformation and metasomatism. A result of this complex history is that the mantle is chemically and isotopically heterogeneous. Heterogeneities in radiogenic isotopes are relatively easy to detect because the processes which produce basaltic melts and a refractory residue do not fractionate radiogenic isotopes. Many excellent papers on the origin of basalt based on geochemical and isotopic data were published (Morris and Hart, 1983; Zindler et al., 1984; Allegre et al., 1984). This information is being used to refine our understanding of the geochemical differentiation of the mantle with subsequent contributions by Halliday et al. (1988) and Cousens (1996).

The asthenospheric upper mantle has undergone long-term incompatible element depletion. Any magma derived from it will therefore have low $^{87}Sr/^{86}Sr$ and high $^{143}Nd/^{144}Nd$ relative to bulk Earth at the time. The continental crust (and lithospheric upper mantle?) has been enriched in the same elements over geological time. Any magma derived from these will therefore have high $^{87}Sr/^{86}Sr$ and low $^{143}Nd/^{144}Nd$ (Attendorn and Bowen, 1997).

The $^{87}Sr/^{86}Sr$ ratio of the mantle is generally in the range between 0.702 - 0.705. Thus, rocks derived from melting of the mantle should have $^{87}Sr/^{86}Sr$ ratios in this range. $^{87}Sr/^{86}Sr$ of crustal rocks will depend on their age and concentration of Rb. Older crustal rocks will have high values of $^{87}Sr/^{86}Sr$ in the range 0.705 - 0.720, younger crustal rocks having been recently derived from the mantle will

have $^{87}Sr/^{86}Sr$ ratios more similar to mantle (Dickin, 1995; Attendorn and Bowen, 1997). If mantle derived magmas assimilate or are contaminated by older crustal rocks, then we would expect to find ratios of $^{87}Sr/^{86}Sr$ in these contaminated rocks that are higher than those found in the mantle and extend up to values found in older crustal rocks.

5.2.2 Stable isotopes (O)

Ratios of stable, low mass isotopes, like those of O, S, C and H can be used as tracers, as well as geothermometers, since fractionation of light isotopes can take place as a result of chemical process. We can thus use these ratios of light isotopes to shed light on processes and temperatures of past events.

Stable isotope ratios are affected by various partial melting-crystal fractionation processes because they are governed by the temperature-dependent fractionation factors between residual crystals and partial melt and between cumulate crystals and residual liquid, but the magnitude of such effects is small at high temperature. Unlike radiogenic isotopes, stable isotopes are also fractionated by low temperature surface processes. Therefore, they offer a potentially important means by which recycled crustal material can be distinguished from intra-mantle fractionation processes (Hoefs, 1987).

In nature oxygen occurs as three isotopes: ^{16}O, ^{17}O and ^{18}O which can fractionate from each other by mineral reactions, crystallization of minerals from a liquid and isotope exchange reactions between minerals and fluids. The degree of fractionation mainly depends on the oxygen isotope composition of the involved phases and temperature. Because of the higher fractionation between ^{18}O and ^{16}O and low abundance of ^{17}O, the $^{18}O/^{16}O$ ratio is commonly used in oxygen isotope studies. The high abundance of oxygen in nature facilitates the use of oxygen isotopes as a tool to investigate geological and petrological processes.

Generally $^{18}O/^{16}O$ ratios are measured relative to a reference standard. For igneous systems this standard is Standard Mean Ocean Water (SMOW). Thus the notation for oxygen isotopes is

$$\delta^{18}O = \left[\frac{\left(\frac{^{18}O}{^{16}O}\right)_{sample} - \left(\frac{^{18}O}{^{16}O}\right)_{standard}}{\left(\frac{^{18}O}{^{16}O}\right)_{standard}} \right] \times 1000 \quad [‰]$$

Large areas of the upper mantle are homogeneous with respect to the oxygen isotope composition. For example, mid ocean ridge basalts show a narrow range of $\delta^{18}O$ values (5.2 – 6.4 ‰) (Harmon and Hoefs, 1995; Hoefs, 1997). For the upper mantle a composition of about 5.4±0.2 ‰ for olivines, 5.9±0.1 ‰ for orthopyroxenes and 5.7±0.2 ‰ for clinopyroxenes is assumed (Hoefs, 1997).

The primary oxygen isotopic composition of mantle melts can be modified by contamination processes either of the source itself or during the uprise of the magma through the crust or due to subsequent fluid interaction on cooling (Ohmoto, 1986; Taylor, 1986). Contamination within the crust is caused by assimilation of crustal material or by alteration with fluids. Fractional crystallization changes the oxygen isotopic composition only slightly resulting in a shift to higher values with a maximum shift of about + 1.2 ‰ for a rock suite from basic to acidic rocks (Holm and Munksgaard, 1982).

5.3 Nd and Sr isotopic studies of layered intrusions

The primary tools used in this investigation are the isotopic compositions of Nd and Sr. Neodymium (atomic number 60) has seven naturally occurring isotopes (mass numbers 142, 143, 144, 145, 146, 148 and 150), while strontium (atomic number 38) has four (mass numbers 84, 86, 87 and 88). Nd and Sr each have one isotope that is produced by the decay of another element. ^{147}Sm undergoes alpha decay (with a half-life, $t_{½}$, of 106 b.y.) to produce ^{143}Nd, and ^{87}Rb decays by emission of a beta particle ($t_{½}$ = 48.8 b.y.) to produce ^{87}Sr. The "excess" of ^{143}Nd and ^{87}Sr is the basis for the Nd and Sr isotope system. The degree to which a rock or mineral is enriched in ^{143}Nd and ^{87}Sr depends on its Sm/Nd and Rb/Sr ratio. In general, the mantle and mantle-derived magmas (basalts) have relatively high Sm/Nd and low Rb/Sr ratios, while continental crust has low Sm/Nd and high Rb/Sr ratios (Faure, 1986). Thus, over time, the crust develops a low $^{143}Nd/^{144}Nd$

and high $^{87}Sr/^{86}Sr$ (^{144}Nd and ^{86}Sr being stable isotopes which do not change abundance over time), while the opposite is true for the mantle. This fact makes Nd and Sr isotopes ideal tools for the study of mixing between mantle-derived magmas and continental crust; the large difference in the isotopic ratios of the two end member components makes these systems sensitive tracers for interaction.

The strategy in the investigation of the Wateranga intrusion has been to measure the isotopic ratios from samples spanning the entire available stratigraphy of the intrusion, thus developing a complete record of liquid from which the intrusion crystallized. Nd and Sr isotopes are particularly sensitive to assimilation of crustal wallrock and to the injection of liquids with different isotopic compositions (which may be derived from separate sources). No corrections or fractionation factors need to be employed in using Nd and Sr isotopes in this way, because (1) the high atomic mass of the elements minimizes the amount of mass fractionation that occurs, especially at magmatic temperatures, and (2) any mass fractionation that occurs is corrected for during the mass spectrometer measurement procedures. In fact, the greatest amount of mass fractionation occurs in the mass spectrometer itself, but this is corrected for by normalizing to a stable isotope pair ($^{146}Nd/^{144}Nd$ or $^{86}Sr/^{88}Sr$) and applying an appropriate fractionation law to the remaining isotopes. The result is that only the "excess" ^{143}Nd and ^{87}Sr are measured.

By integrating the Nd and Sr isotopic ratios measured over the available stratigraphy of the intrusion, the total amount of assimilant added to the magma chamber can be calculated, given some knowledge of the isotopic characteristics of the assimilant. The combined effects of fractional crystallization, assimilation and recharge of fresh magma can be modelled (using, for example, the equations of Taylor, 1980 and DePaolo, 1981, 1985) to determine the rates at which these various processes were occurring during the life of the magma chamber. The Nd and Sr isotopes used together on the problem of magma chamber evolution has the potential to identify and quantify numerous physical and chemical processes that have defied traditional approaches; thus they are a natural and necessary compliment to field, petrographic and geochemical studies of layered mafic intrusions.

All isotopic ratios discussed in the text that follows are corrected for in situ ^{87}Rb and ^{147}Sm decay using an age of 245 Ma. The $^{143}Nd/^{144}Nd$ ratio is reported in the usual ε notation (DePaolo and Wasserburg, 1976).

$$\varepsilon_{Nd}(T) = \left[\frac{^{143}Nd/^{144}Nd_{SAMP}(T)}{^{143}Nd/^{144}Nd_{CHUR}(T)} - 1 \right] 10^4$$

where T is the crystallization age and SAMP and CHUR refer to sample and chondrite Nd isotopic ratios, respectively. The chondrite ratio is given by

$$^{143}Nd/^{144}Nd_{CHUR}(T) = 0.51265 - 0.1967\ (e^{\lambda T} - 1)$$

Decay constants (λ) used are 0.00654 b.y.$^{-1}$ for λ_{Sm} and 0.0142 b.y.$^{-1}$ for λ_{Rb}.

5.4 Sm-Nd whole-rock isochron of the Wateranga intrusion

To calculate initial isotopic ratios it is necessary to know the age of the intrusion with some certainty. As already mentioned in Chapter 2, the Wateranga intrusion was dated by K-Ar method to 245±8 Ma (Day et al., 1983). In this study, the age was determined by a whole-rock isochron using the Sm-Nd method (Table 5.1 and Fig 5.1). Sample NS-2/54 displays scatter. It is therefore not used for the age calculation. The whole-rock Sm-Nd data (seven samples) of the Wateranga intrusion yield an age of 261±21 Ma. The age and uncertainties were calculated using ISOPLOT program (Ludwig, 1994). The scatter in the data may reflect isotopic heterogeneity of source materials, mixing processes and contamination of the magma during ascent and emplacement. The calculated 261±21 Ma age is in agreement with the 245±8 Ma K-Ar age of Day et al. (1983). In this study, the crystallization age of 245 Ma is used to calculate initial ratios.

Table 5.1 Rb, Sr, Sm and Nd elemental abundances, and Sr and Nd isotopic ratios for the Wateranga intrusion

Sample	Rock[a] Type	Rb (ppm)	Sr (ppm)	$^{87}Rb/^{86}Sr$ calculated	$^{87}Sr/^{86}Sr$ measured	$^{87}Sr/^{86}Sr$ initial	Sm (ppm)	Nd (ppm)	$^{147}Sm/^{144}Nd$ calculated	$^{143}Nd/^{144}Nd$ measured	$^{143}Nd/^{144}Nd$ initial	ε_{Nd} (T)
WG-44[b]	OGN	1	268	0.010735	0.703688±16	0.703651	1.5	4.3	0.210341	0.512897±16	0.512560	4.391
WG-124[b]	ONG	1	239	0.012037	0.703314±16	0.703272	–	–	–	–	–	–
NS-2/5	FG	5	227	0.063370	0.704833±13	0.704612	12	58.3	0.124159	0.512701±16	0.512502	3.259
NS-2/8	OG	4	274	0.042000	0.704659±16	0.704513	12.2	59.2	0.124657	0.512706±11	0.512506	3.337
NS-2/33	T	2	264	0.021795	0.704995±16	0.704919	1.7	7.8	0.135349	0.51274±16	0.512523	3.669
NS-2/48	ON	3	203	0.042517	0.702774±17	0.702626	–	–	–	–	–	–
NS-2/54	OGN	2	184	0.031271	0.702901±11	0.702792	2.6	9.2	0.168849	0.512936±15	0.512665	6.441
NS-3/4	ON	1	285	0.010094	0.703708±12	0.703673	1.6	4.6	0.204260	0.512846±14	0.512519	3.591
NS-3/28	AN	1	315	0.009133	0.703909±13	0.703877	0.6	1.8	0.196808	0.512875±14	0.512560	4.391
NS-5/4	PY	14	104	0.387288	0.705473±15	0.704123	34.4	123.8	0.167870	0.512824±13	0.512555	4.290

[a] Rock type abbreviations as follows: OGN = olivine gabbronorite; ONG = olivine noritegabbro; FG = ferro gabbro; OG = olivine gabbro; T = troctolite; ON = olivine norite; AN = anorthositic norite; PY = pyroxenite. [b] Fine grained chilled margin samples.

$^{87}Sr/^{86}Sr$ (initial), $^{143}Nd/^{144}Nd$ (initial) and ε_{Nd} (T) were calculated using the K-Ar age of 245 Ma (Day et al., 1983).

Rb and Sr concentrations were obtained by XRF, whereas Sm and Nd were determined by isotope dilution.

$^{87}Sr/^{86}Sr$ normalized to $^{86}Sr/^{88}Sr = 0.1194$, $^{143}Nd/^{144}Nd$ normalized to $^{146}Nd/^{144}Nd = 0.7219$ for mass fractionation correction.

Measurements of the NBS 987 Sr standard yielded an average value of $^{87}Sr/^{86}Sr = 0.710247\pm17$ (2σ; n=11). O'Nions Nd standard gave an average value of $^{143}Nd/^{144}Nd = 0.511114\pm12$ (2σ; n=15).

Measurement of precision for individual runs of $^{87}Sr/^{86}Sr$ and $^{143}Nd/^{144}Nd$ were better than ± 0.000017 and ± 0.000016 respectively.

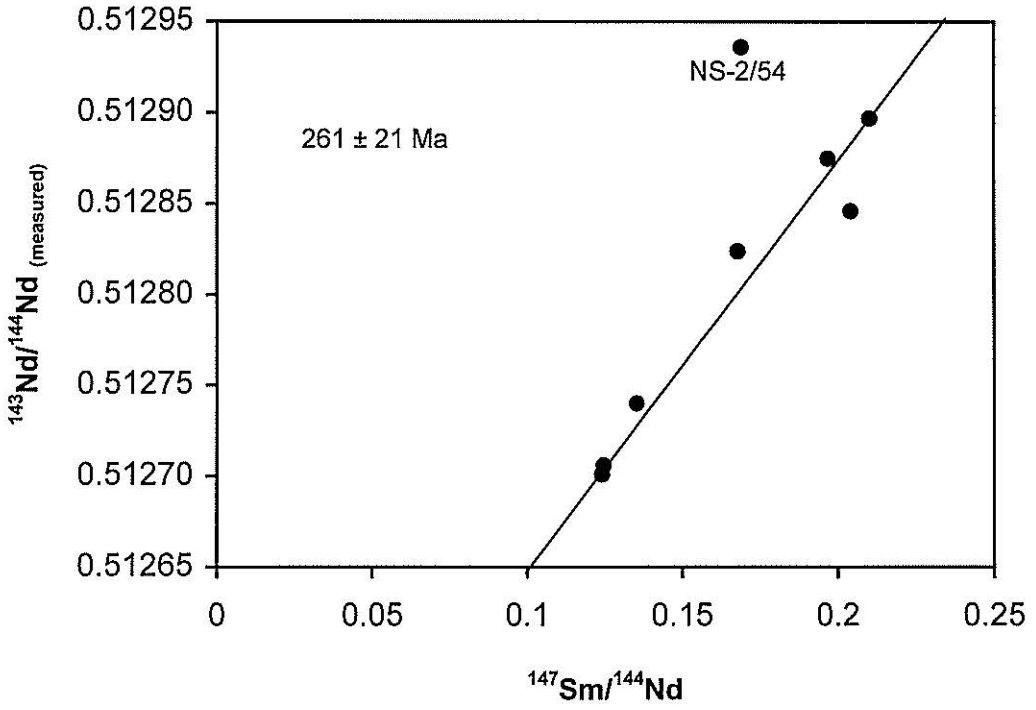

Figure 5.1 Sm-Nd isochron plot for whole-rock isotopic data, Wateranga intrusion.

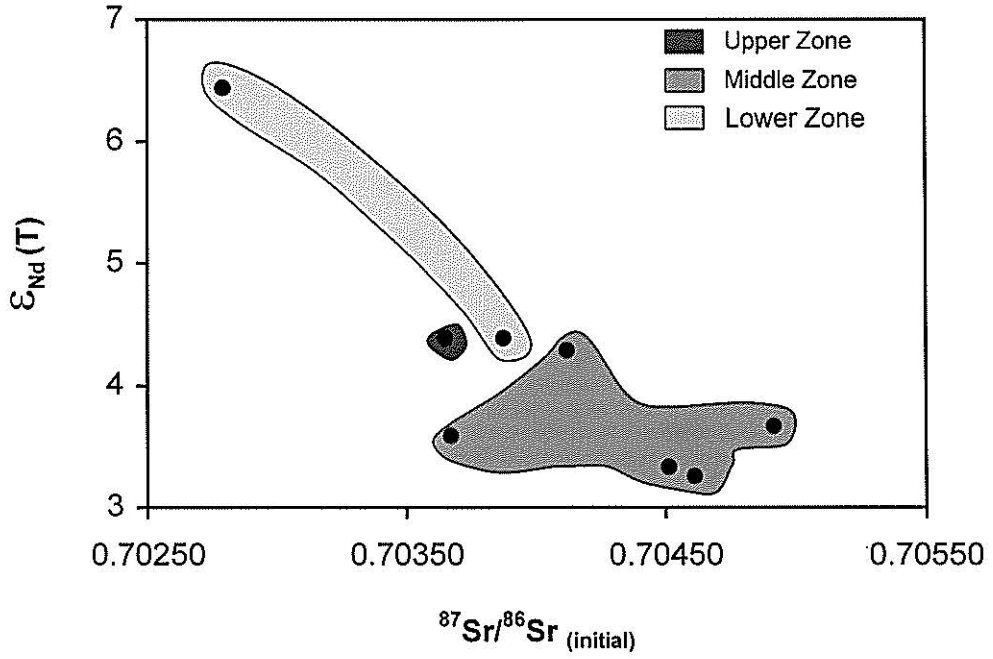

Figure 5.2 Whole-rock initial $^{87}Sr/^{86}Sr$ and $\varepsilon_{Nd\,(T)}$ results for the Wateranga intrusion. Initial ratios and ε_{Nd} calculated at 245 Ma

5.5 Nd and Sr isotopic variations in the Wateranga intrusion

Nd and Sr isotopic data from the Wateranga intrusion are presented in Table 5.1 and plotted in Figures 5.2 – 5.6. The initial Nd and Sr isotope ratios of the intrusion, calculated using an age of 245 Ma, are plotted in Figures 5.3 and 5.4 against the stratigraphic depth of the intrusion. The range of initial $^{87}Sr/^{86}Sr$ and ε_{Nd} within the Wateranga intrusion is small. $^{87}Sr/^{86}Sr$ values range from 0.7026 to 0.7049 (Table 5.1) with a total variation of 0.0023. In comparison, the total range in $^{87}Sr/^{86}Sr$ within the Skaergaard intrusion is 0.0008 (chilled margin is excluded because of its obvious contamination from the numerous gneiss xenoliths) (Stewart and DePaolo, 1990). In the Kiglapait intrusion, the total range in $^{87}Sr/^{86}Sr$ is 0.0025 (DePaolo, 1985), in spite of the smaller difference between Kiglapait cumulate isotope ratio and those of the likely contaminant.

The ε_{Nd} values within the Wateranga intrusion range from + 3.26 to + 6.44 with a total variation of 3.12 ε units. Again, this variation is greater than the Skaergaard intrusion (total variation = 2.2 ε units) and less than the Kiglapait intrusion (total variation = 4 ε units). These data suggest that assimilation occurred at a higher rate in the Kiglapait intrusion relative to the Wateranga (discussed in Chapter 6) and Skaergaard intrusions. Both the Kiglapait (DePaolo, 1985) and the Skaergaard (Stewart and DePaolo, 1990) intrusions were interpreted being formed as a consequence of assimilation-fractional crystallization-recharge processes.

The patterns of variation in $^{87}Sr/^{86}Sr$ with stratigraphic depth correlates well with that of ε_{Nd} in all the three Zones of the Wateranga intrusion (Figs. 5.3 and 5.4). This remarkable correlation is the strong evidence that the measured variations are real, i.e. due to competing sources with different isotopic compositions contributing to each Zone. Good correlation in the variations of $^{87}Sr/^{86}Sr$ and ε_{Nd} with stratigraphic depth of the Sokndal layered intrusion, Norway has been interpreted as reflecting magma chamber replenishment (Barling et al., 1993).

In a diagram ε_{Nd} versus $^{87}Sr/^{86}Sr_{(initial)}$ there is a general trend of decreasing ε_{Nd} with increasing $^{87}Sr/^{86}Sr_{(initial)}$ (Fig. 5.2). The ranges in isotopic compositions are ε_{Nd} 3.26 – 6.44 and $^{87}Sr/^{86}Sr_{(initial)}$ 0.7026 - 0.7049. Even though the variation is

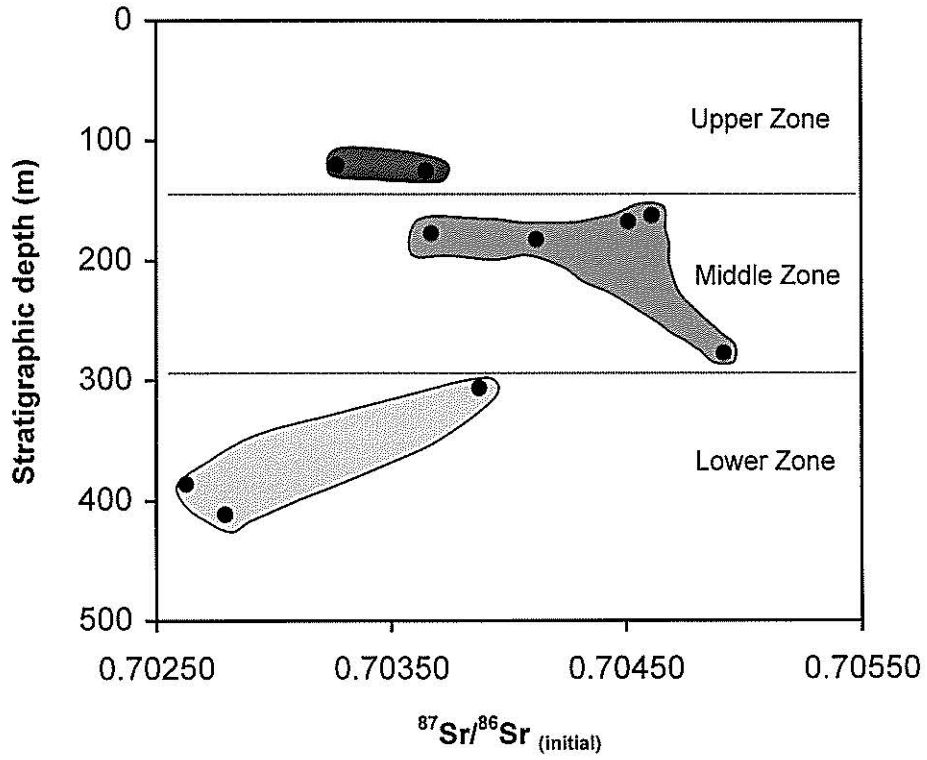

Figure 5.3 Whole-rock Sr isotope compositions are plotted against stratigraphic depth of the Wateranga intrusion. Initial ratios calculated at 245 Ma. The samples shown plotted in the Upper Zone are from the chilled margin.

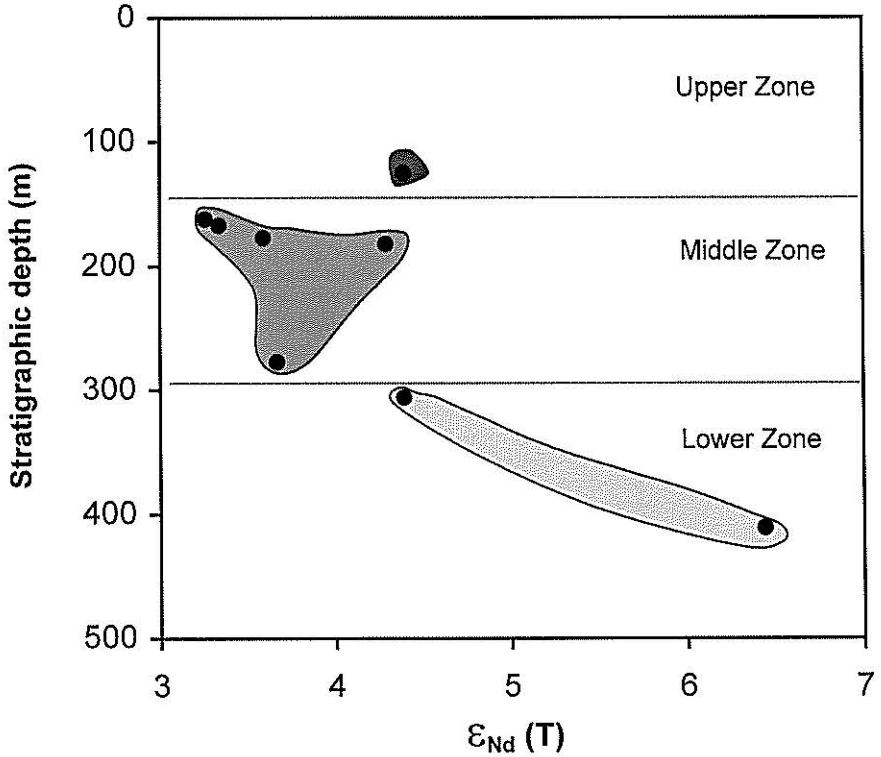

Figure 5.4 Nd isotope compositions vs stratigraphic depth of the Wateranga intrusion. The neodymium data are reported in the usual ε notation. ε_{Nd} calculated at 245 Ma. The sample shown plotted in the Upper Zone is from a chilled margin.

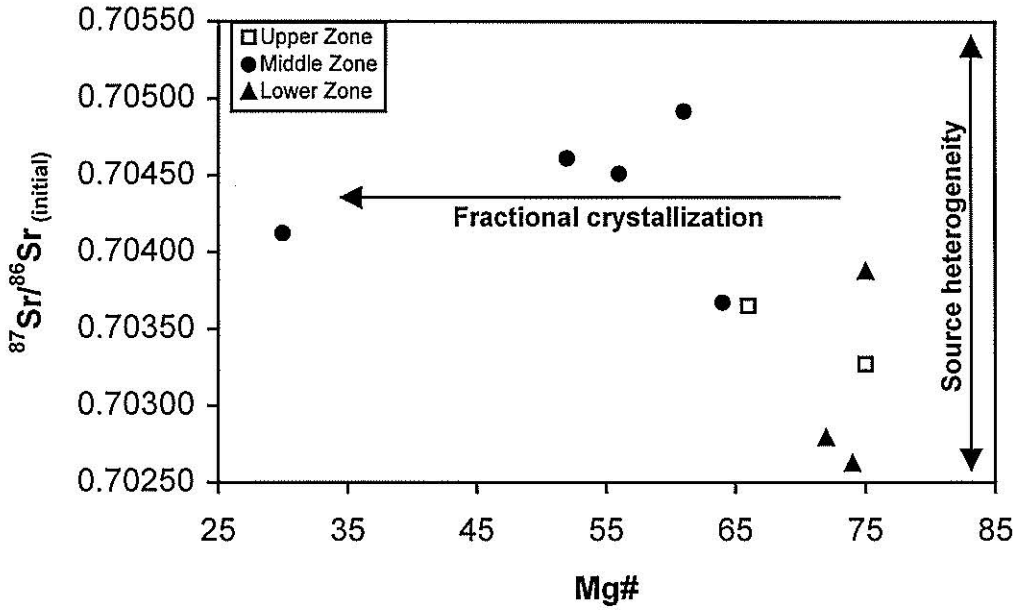

Figure 5.5 Plot of whole-rock initial $^{87}Sr/^{86}Sr$ vs Mg#, Wateranga intrusion.

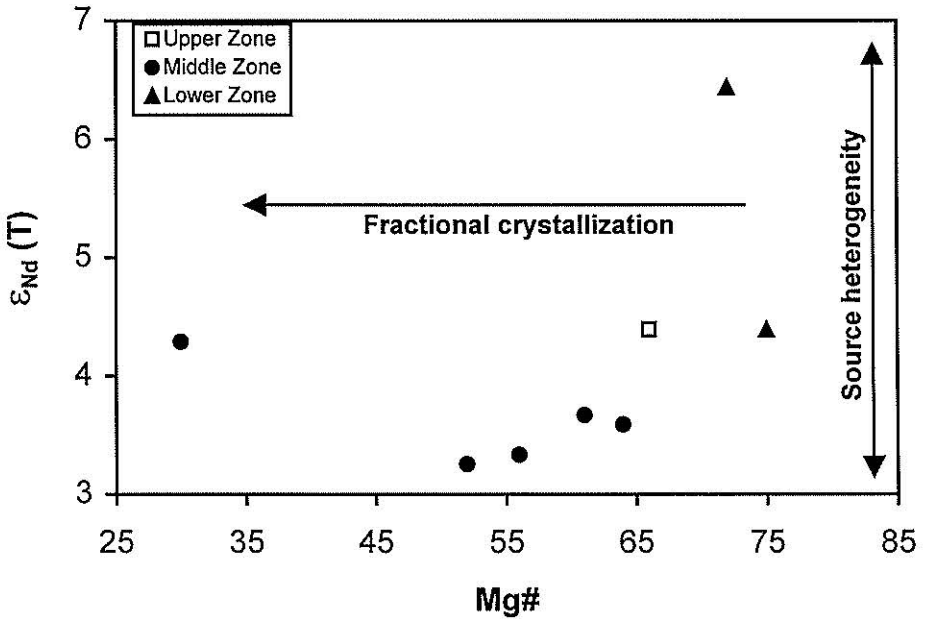

Figure 5.6 Plot of whole-rock ε_{Nd} (T) vs Mg#, Wateranga intrusion.

limited, the anti-correlation suggests mixing between two relatively well-constrained end members. In diagrams whole-rock Mg# versus $^{87}Sr/^{86}Sr_{(initial)}$ and ε_{Nd} there is a general correlation, with more evolved samples having higher $^{87}Sr/^{86}Sr_{(initial)}$ and lower ε_{Nd} (Figs. 5.5 and 5.6). Furthermore, good correlation between mineral compositions (Fig. 3.3, Chapter 3) and isotopic compositions (Figs. 5.3 and 5.4) suggests either mixing between two magmas with different bulk and isotopic composition or assimilation of crustal rocks of contrasting isotopic composition coupled with fractional crystallization. The first process has been inferred to cause correlation between Mg# of OPX and $^{87}Sr/^{86}Sr_{(initial)}$ in the Bushveld Complex (Eales et al., 1990), whereas the latter corresponds to an assimilation-fractional crystallization (AFC) process (DePaolo, 1981). In Chapter 6, an interpretation on the Nd-Sr isotopic variations in the Wateranga intrusion is presented.

5.6 Oxygen isotopic variations in the Wateranga intrusion

Oxygen isotopes are an efficient monitor of crustal interaction with mantle-derived basic magmas because the oxygen isotope ratio of the mantle varies little and that of the continental crust varies considerably (e.g., Kyser, 1986; Mattey et al., 1994). Oxygen isotopic data from the Wateranga intrusion are presented in Table 5.2 and plotted in Figures 5.7 and 5.8. In Table 5.3, oxygen isotopic composition of various magmatic materials (Hoefs, 1987) and the Wateranga intrusion are presented. The range of $\delta^{18}O$ (6.16 - 9.90 ‰) from the Wateranga intrusion is comparable to continental tholeiitic basalts (6.4 - 9.0 ‰).

Whole-rock $\delta^{18}O$ values of the Wateranga intrusion are uniform in the Upper and Lower Zones with an average of 6.99 ‰ and 6.97 ‰ but vary widely in the Middle Zone with an average of 8.1 ‰ (excluding WG-16, an altered sample in the Upper Zone) (Fig 5.7 and Table 5.2). Variations in $\delta^{18}O$ with stratigraphic depth correlate well (with the exception of WG-16, an altered sample) with initial $^{87}Sr/^{86}Sr$ and ε_{Nd}.

Whole-rock $\delta^{18}O$ values of the Wateranga intrusion (6.16 - 9.90‰) are too high for a melt derived from a primary unmodified mantle (Taylor and Sheppard,

Table 5.2 Whole-rock oxygen isotope analyses of the Wateranga intrusion

Sample	Rock Type	$\delta^{18}O‰$ SMOW
WG-16	Olivine gabbro	9.90
WG-44*	Olivine gabbronorite	7.29
WG-124*	Olivine noritegabbro	6.69
NS-2/8	Olivine gabbro	8.09
NS-2/17	Olivine norite	6.16
NS-2/65	Olivine gabbro	7.03
NS-3/20	Norite	8.77
NS-3/51	Picrite	6.90
NS-3/52	Norite	6.99
NS-5/6	Orthopyroxenite	9.38

* Fine grained samples

Table 5.3 Oxygen isotopic composition of various magmatic materials (data from Hoefs, 1987) and the Wateranga intrusion

Origin	$\delta^{18}O‰_{SMOW}$ range
Wateranga intrusion	6.16 - 9.90
Tholeiitic basalts from mid-ocean ridge	5.4 - 6.6
Tholeiitic basalts from oceanic islands	5.0 - 5.8
Continental tholeiitic basalts	6.4 - 9.0
Alkali basalts from oceanic islands	5.5 - 8.2
Alkaline basalts from the continent	5.9 - 8.2
Oceanic island arcs	5.0 - 9.7
Continental margin arcs	5.2 - 8.8

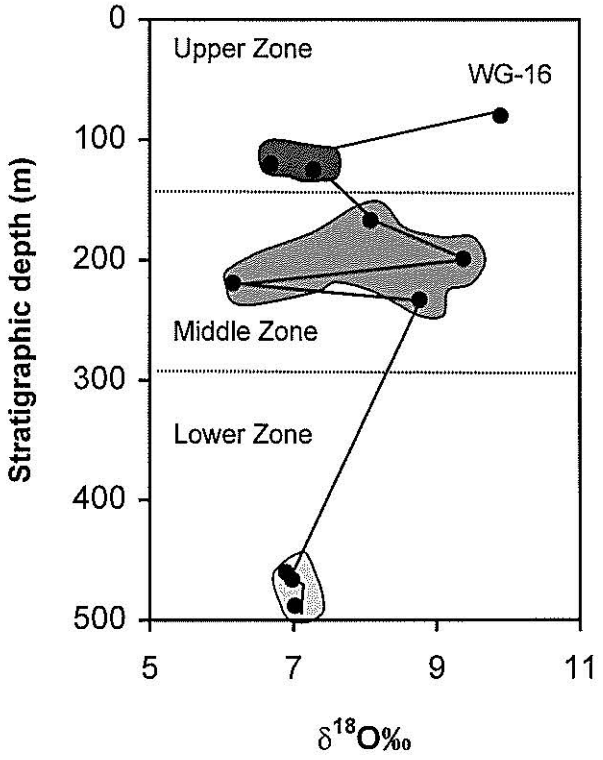

Figure 5.7 Plot of whole-rock $\delta^{18}O$ vs stratigraphic depth, Wateranga intrusion. WG-16 is an altered sample.

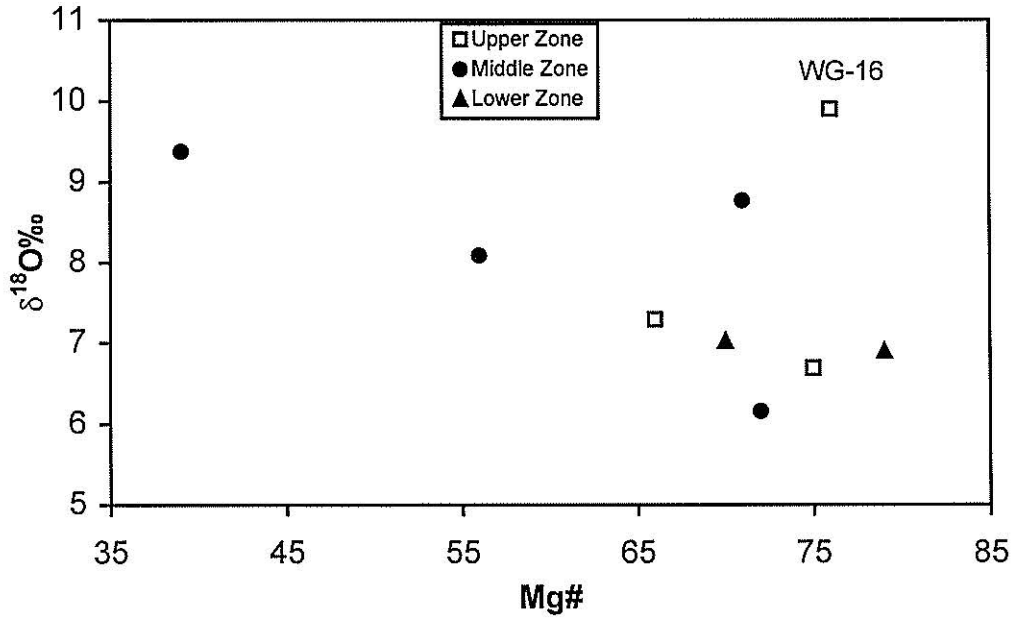

Figure 5.8 Whole-rock $\delta^{18}O$ values vs Mg#, Wateranga intrusion. WG-16 is an altered sample.

1986; Mattey et al., 1994; Harmon and Hoefs, 1995; Hoefs, 1997). The $\delta^{18}O$ values for a primary unmodified mantle melt are about 5.2 ‰ (Mattey et al., 1994). Figure 5.8 shows variations of $\delta^{18}O$ with whole-rock Mg#. A strong negative correlation exists (r = -0.75) between $\delta^{18}O$ and whole-rock Mg# (with the exception of an altered sample, WG-16). An increase of the $\delta^{18}O$ values with decreasing Mg# of the bulk rock can be explained by fractional crystallization and crustal assimilation. Fractional crystallization in combination with crustal assimilation and differences in $\delta^{18}O$ values of input magmas can explain the observed oxygen isotope variations in the Wateranga intrusion. In addition, secondary alteration may have contributed for the higher $\delta^{18}O$ values in slightly altered samples WG-16 (9.90 ‰), NS-3/20 (8.77 ‰) and NS-5/6 (9.38‰).

The susceptibility of some minerals to alter to ^{18}O-rich secondary minerals during low-temperature weathering often results in higher whole-rock $\delta^{18}O$ values than those estimated from analyses of unaltered samples (e.g., Johnson and O'Neil, 1984; Taylor et al., 1984). Some researchers have attempted to account for the effects of weathering on the $\delta^{18}O$ values of mafic lavas using factors such as water contents or Fe_2O_3/FeO ratios which change concurrently with the isotopic compositions. For example, Staudigel et al. (1981) report substantial increases in the $^{18}O/^{16}O$ ratios of some submarine basalts that correlate directly with water contents and Fe_2O_3/FeO ratios despite the young ages of the samples (<3 Ma). In the Wateranga intrusion, increase in the $\delta^{18}O$ values of a few slightly altered samples may be due to low-temperature weathering.

Further discussion on the significance of oxygen isotope variations will be presented in Chapter 6.

5.7 Summary

The whole-rock Sm-Nd data of the Wateranga intrusion yield an age of 261±21 Ma which is in agreement with the 245±8 Ma K-Ar age of Day et al. (1983). The whole-rock $^{87}Sr/^{86}Sr$ initial ratios range from 0.702626 to 0.704919 and are matched by similar systematic changes in $^{143}Nd/^{144}Nd$ initial ratios from 0.512502 (ε_{Nd} = +3.26) to 0.512665 (ε_{Nd} = +6.44). The differences in Sr and Nd isotopic

compositions between the stratigraphic Zones of the intrusion, suggest source heterogeneity and/or crustal contamination. Furthermore, there is a general correlation, with more evolved samples having lower ε_{Nd} and higher $^{87}Sr/^{86}Sr_{(initial)}$.

The whole-rock $\delta^{18}O$ values of the Wateranga intrusion range from 6.16 to 9.90 ‰ with an average of 7.72 ‰ that is comparable with the continental tholeiitic basalt (Hoefs, 1987). In the Wateranga intrusion, good negative correlation between $\delta^{18}O$ and whole-rock Mg# can be explained by fractional crystallization and crustal assimilation.

Variations in whole-rock $\delta^{18}O$ with stratigraphic depth correlate well with initial $^{87}Sr/^{86}Sr$ and ε_{Nd}. Furthermore, variations in Nd, Sr and O isotopic data with stratigraphic depth correlate well with the mineral chemical (Chapter 3) and the whole-rock incompatible element (Chapter 4) variations. Overall, Nd-Sr-O isotopic compositions suggest that the Wateranga intrusion may have formed by assimilation-fractional crystallization-recharge processes.

CHAPTER 6

Discussion

Discussion

6.1 Introduction

Origin of layered intrusions is a key problem in petrology. They are the exposed examples of solidified magma chambers and have long served as a testing ground for a wide range of petrologic concepts. Layered mafic intrusions, in which the cumulates record a history of complex magma chamber processes such as fractional crystallization, replenishment, venting, convection, stratification and contamination, provide important constraints on the degree and physical processes of crustal assimilation, the crystallization sequence and the liquid line of descent of mantle-derived magmas. Enigmatic questions include the nature of the assimilated material, where and when in the magma chamber assimilation took place, the amount of assimilation, the amount of heat available, and the relation to fractional crystallization. Other questions include the extent of fractional crystallization, what were the fractionating phases, magma replenishment and the composition(s) of the parental magma(s). This chapter provides answers to some of these questions on the basis of the data presented in the earlier chapters and the information available in published literature. A petrogenetic model is suggested for the origin of the Wateranga intrusion.

6.2 Subdivisions of the Wateranga intrusion into Zones

The igneous stratigraphy of the Wateranga intrusion is divided into three Zones (Lower, Middle and Upper) based on detailed petrographic, mineral chemical, whole-rock geochemical and Nd-Sr-O isotopic data (Chapters 2 to 5). Zones are interpreted as reflecting magma chamber replenishment with discontinuities and reversal in the compositional trends at the Zone boundaries. The Wateranga samples show a wide range of compositions both in terms of mineral chemical and whole-rock major and trace element abundances. Both the source characteristics and magmatic processes would have played important roles in determining the geochemical and Nd-Sr-O isotopic variations of the intrusion.

6.3 Crystallization sequences

Distinct crystallization sequences of minerals in different rock units (see Section 2.11, Chapter 2) indicate that the cumulates were probably not derived from a common magma. The most obviously different crystallization sequences are those of the Middle Zone, and the Lower and Upper Zones. The crystallization sequence of mafic minerals in the Middle Zone is olivine, orthopyroxene, clinopyroxene. This sequence is typical of tholeiitic intrusions in continental crust, whereas the sequence olivine, clinopyroxene, orthopyroxene of the Lower and Upper Zones is more typical of mantle-derived oceanic magmas (Campbell, 1985). Campbell (1985) interpreted the former sequence as having occurred at higher SiO_2 activity, possibly reflecting greater crustal contamination. The presence of cumulus plagioclase coexisting with olivine of Mg# 54 in the Middle Zone indicates that Middle Zone liquid was much higher in aluminium than liquid of the Lower and Upper Zones at comparable Mg#. Sparks (1986) suggested that this type of high-Al basalt magma was derived from primitive magmas by crustal contamination, possibly through underplating mechanisms.

6.4 Mineral chemical compositions

Distinguishing geochemical effects associated with primary cumulus stage events, such as fractional crystallization, magma mixing or magma recharge, from those related to post-cumulus processes is one of the major problems in efforts to understand cumulate rock sequences. As already mentioned in chapter 4, the textural data indicate that the rocks of the Wateranga intrusion range from adcumulates to mesocumulates with very little trapped liquid. The low abundances of trapped liquid is in agreement with low incompatible element abundances. The small volume of trapped liquid probably reflects the mode of mineral accumulation or later expulsion of intercumulus liquids. The absence of such liquids in these rocks explains the lack of important post-cumulus re-equilibrium, such as was reported by Chalokwu and Grant (1987) for the Duluth layered intrusion. Furthermore, the amounts of trapped liquid are nearly identical in all the three stratigraphic Zones of the Wateranga intrusion. This indicates the offset of cumulate mineral compositions was negligible because of post-cumulus re-equilibration. Thus, we can assume that these mineral compositions reflect near equilibrium trends, complementary to a tholeiitic liquid line of descent.

The mineral compositions of the Wateranga rocks span a wide range, from very magnesian olivine gabbronorites to very fractionated Fe-Ti oxide gabbros. Comparison of the An content of plagioclase and the Mg#s of cumulus mafic minerals shows a good correlation (Fig. 6.1) suggesting significant fractionation during the crystallization of the Wateranga intrusion. The variation trend is nearly parallel to that of the layered series of the Skaergaard intrusion (Wager and Brown, 1968; Naslund, 1976; Hoover, 1978, 1989). Despite the generally coherent trend for all the three stratigraphic Zones of the Wateranga intrusion, there are contrasting trends between the Zones suggesting differences in fractionation (Fig. 6.1).

Changes in mineral compositions with stratigraphic depth in cumulate rock sequences are known as cryptic variations, and have generally been attributed to changes in magma compositions with time, brought about by processes such as fractional crystallization, magma recharge and magma mixing. In large layered

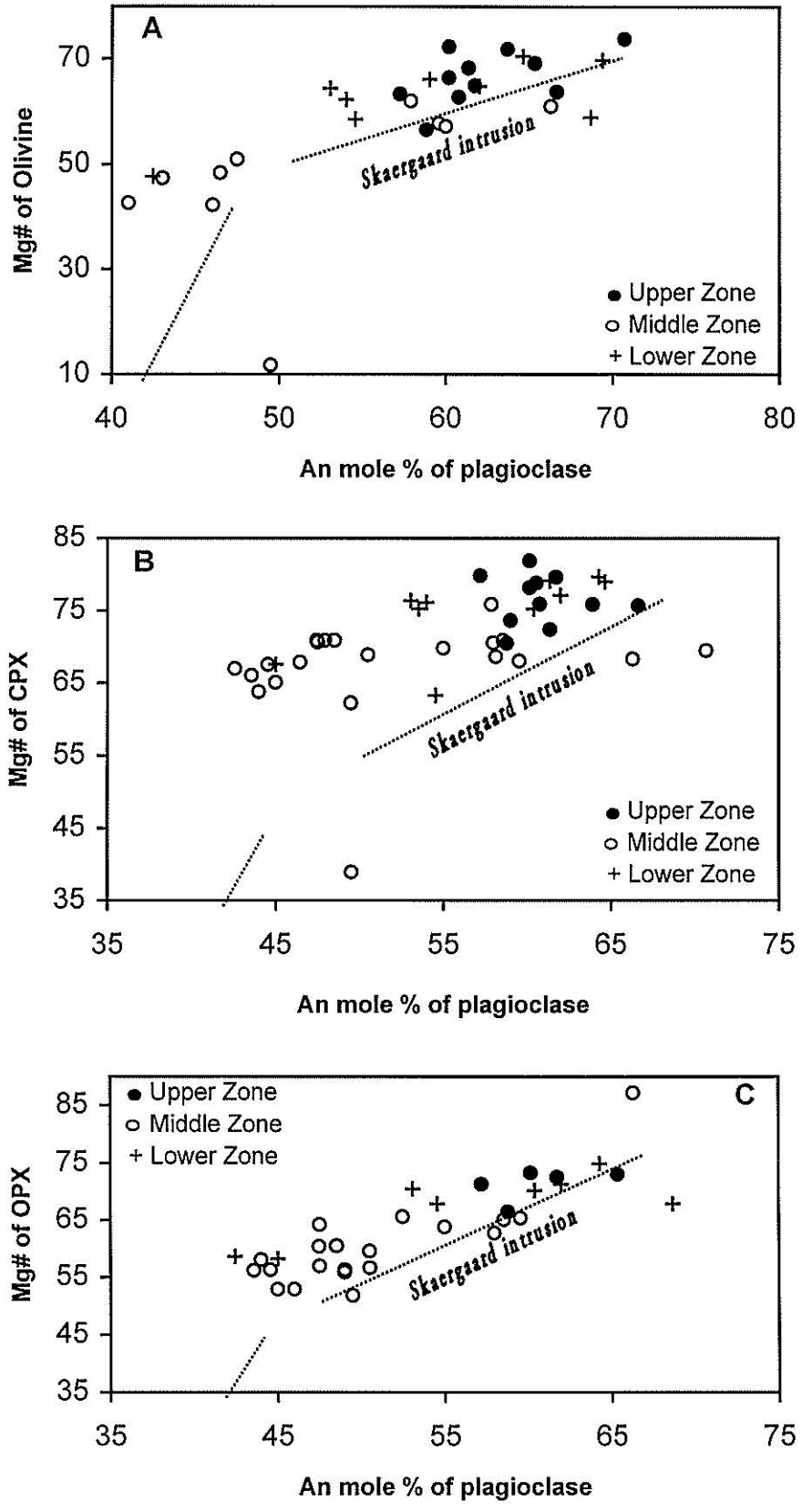

Figure 6.1 An content in plagioclase vs Mg# of mafic minerals (A, Olivine. B, Clinopyroxene. C, Orthopyroxene) in the Wateranga intrusion. Data for Skaergaard intrusion (dotted line) are from Wager and Brown (1968).

intrusions such as the Stillwater Complex, observation of these cryptic variations has often been accomplished by sampling the layered sequence at an interval of tens of meters per sample. Such studies have revealed how mineral compositions vary over the complex as a whole (McCallum et al., 1980; Raedeke and McCallum, 1984; McCallum, 1996). Cumulus mineral compositions in the Wateranga intrusion vary widely with stratigraphic depth. Mg# in pyroxenes and olivine, and An content of plagioclase do not vary monotonically with depth, but rather sharp discontinuities and reversals in compositions are seen at 140m and 285m (Fig. 3.3, Chapter 3). Such discontinuities and reversals in mineral compositions are generally believed to indicate the introduction of new mafic magma into the magma chamber (Irvine, 1980; Wiebe, 1988; Klewin, 1990). Thus, the variability of mineral compositions can be explained by episodic influx and mixing of fresh mafic magma into the Wateranga magma chamber.

The fine grained chilled margin samples of the Wateranga intrusion have the following average Mg#s: 60 in olivine, 74 in clinopyroxene and 64 in orthopyroxene. Primary mantle derived basaltic magmas are expected to be in equilibrium with olivines having Mg#s between 86 and 69 (Basaltic Volcanism Study Project, 1981). Olivines of chilled margin samples are thus less magnesian than those expected to be in equilibrium with primitive basaltic melts. This implies that the magma may have experienced some fractionation prior to emplacement in the Wateranga magma chamber.

6.5 Whole-rock major and trace element compositions

Most efforts to study igneous differentiation have centered on volcanic systems because of the availability of liquid compositions. There have also been many studies of fractionation in plutonic systems, even though liquid compositions are not directly available and processes such as open-system behaviour of magma chambers, magma convection and crystal sorting and subsolidus re-equilibration complicate the picture. In rare cases, however, intrusive systems are simple enough that the efforts of relatively straight-forward fractional crystallization can be discerned. The Wateranga intrusion appears to be such a system. The wide

range in compositional variation in the Wateranga intrusion can be attributed to fractionation of plagioclase, olivine, clinopyroxene, orthopyroxene and Fe-Ti oxides. Although fractional crystallization played an important role in the evolution of the magma, there is also evidence for open system addition of new mafic magma and crustal contamination.

6.5.1 Fractional crystallization

Fractional crystallization generally plays an important role in magma processes, especially in early stages and at depth (Hawkesworth et al., 2000). Coherent major and trace element trends on bivariate plots (Figs. 4.2 and 4.3, Chapter 4) suggest that fractional crystallization played an important role in controlling the wide range of compositional variation in the Wateranga magma evolution. Fractionation of clinopyroxene and olivine is evident from positive correlation of Ni and Cr with Mg#. Plagioclase fractionation is reflected in Mg# vs CaO plot. In addition, the linear array on the plot of incompatible elements Zr and Ba (Fig. 6.3) are consistent with the fractionation hypothesis (e.g., Hanson, 1989). Enrichment of TiO_2 and Fe_2O_3 with decreasing Mg# suggests Fe-Ti oxide fractionation.

The major element variations of the Wateranga intrusion may be explained by variations in the proportion of plagioclase, olivine, clinopyroxene, orthopyroxene and Fe-Ti oxide (Fig. 6.2). The Middle Zone appears to be compositionally distinct with slightly higher abundances of Fe-Ti oxide phase.

Fractional crystallization model

The hypothesis that some of the major element and compatible trace element variation among the Wateranga rocks is consistent with fractional crystallization can be tested quantitatively by trace element modelling. Fractional crystallization has been modelled using the computer program FC-Modeler (Keskin, 2002). This program models Rayleigh fractionation vectors and produces high-quality graphic output in the form of log-log bivariate diagrams (Fig. 6.4). The behaviour of trace elements during fractionation can be studied more quantitatively by comparing observed and theoretical fractionation trends on log-log variation diagrams (Pearce

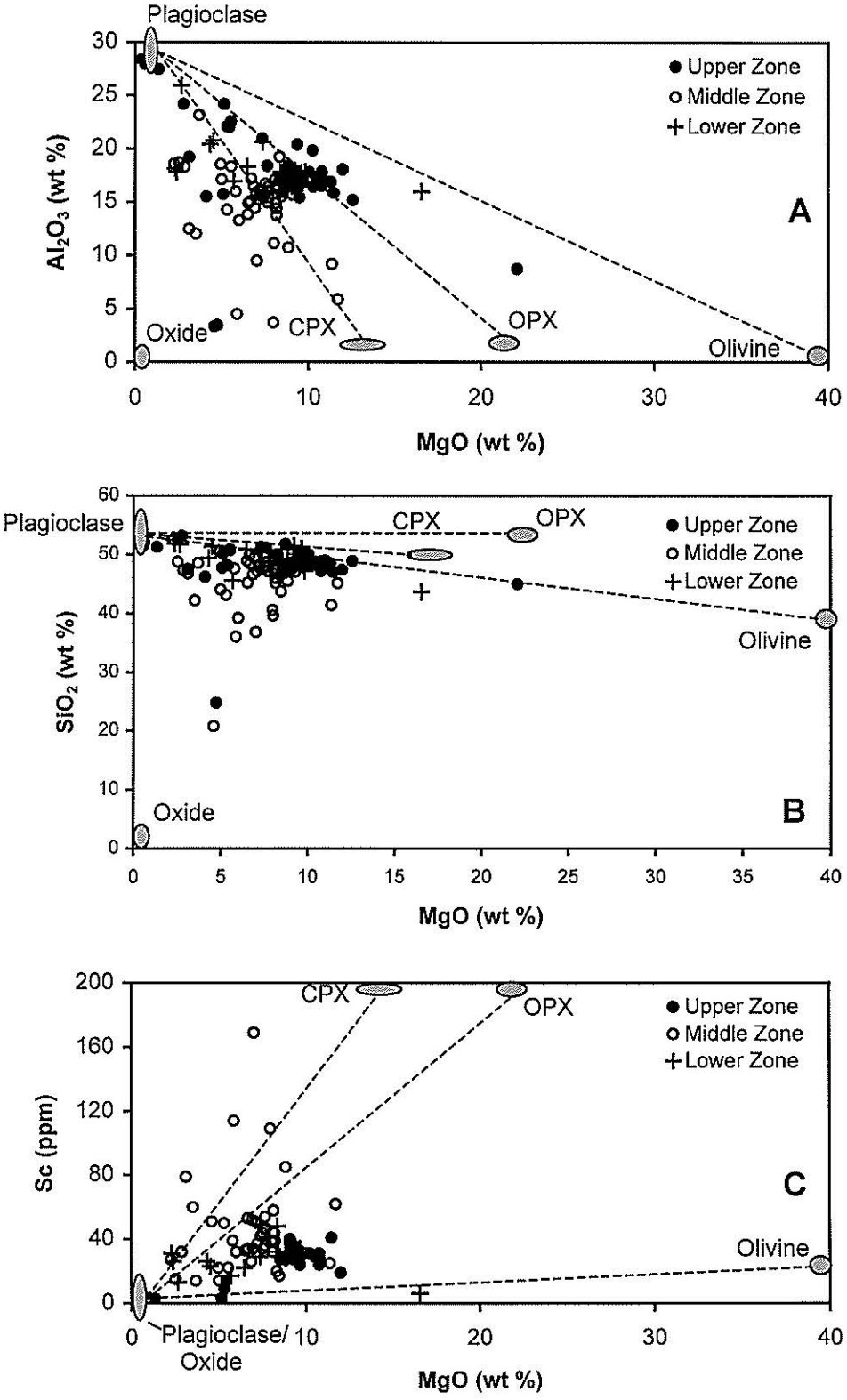

Figure 6.2 Whole-rock data from the Wateranga intrusion plotted onto diagrams of (A) Al_2O_3 vs MgO, (B) SiO_2 vs MgO and (C) Sc vs MgO. The data define mixing lines between plagioclase, olivine, clinopyroxene, orthopyroxene and Fe-Ti oxide.

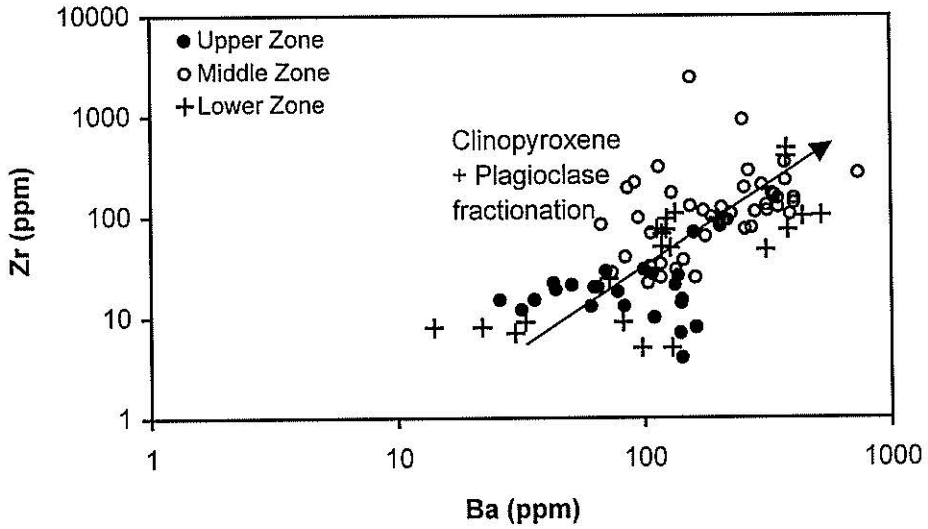

Figure 6.3 Plot of whole-rock Ba vs Zr showing clinopyroxene and plagioclase fractionation trend in the Wateranga intrusion.

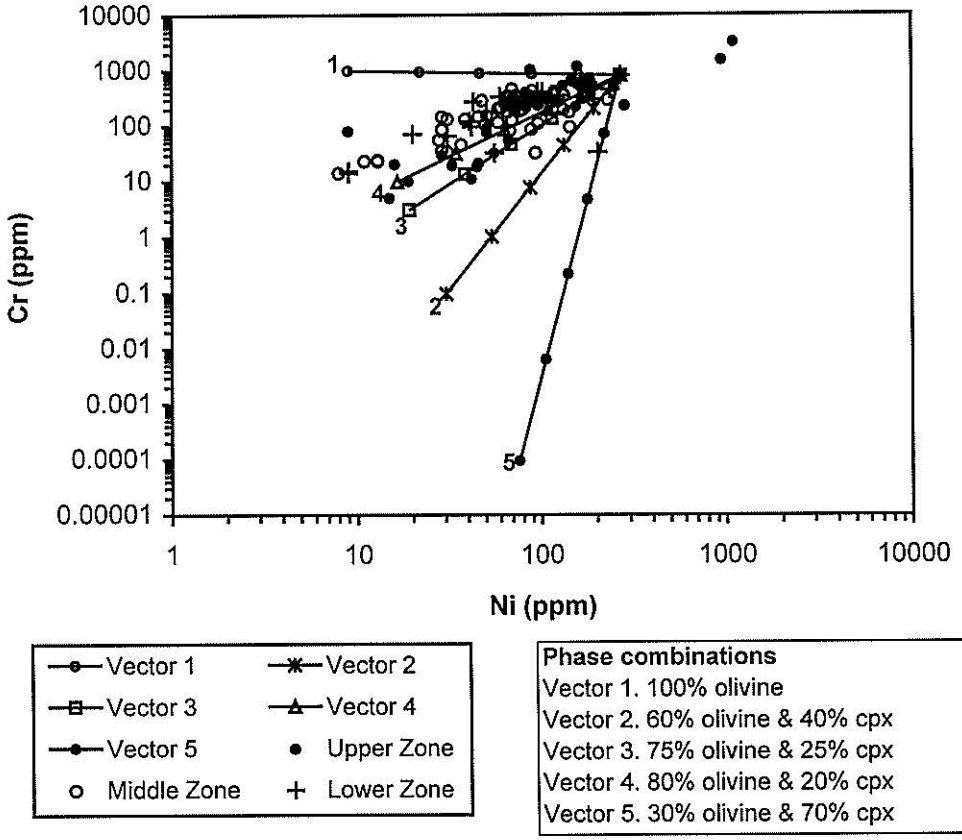

Figure 6.4 Compatible trace element variation diagram of whole-rock Cr vs Ni. The diagram shows theoretical Rayleigh fractionation vectors for 50% crystallization of the phase combinations indicated below the figure. The marks on each vector correspond to 10% crystallization intervals.

Table 6.1 The input data and the results of the fractional crystallization modelling

Partition coefficients (Kd)*					
Mineral	Plagioclase	Clinopyroxene	Orthopyroxene	Olivine	
Ni	0.01	1.50	5.00	5.90	
Cr	0.01	34.00	10.00	0.70	
Starting compositions					
Ni	268 ppm				
Cr	802 ppm				
Calculated compositions					
% of fractional crystallization	*10%*	*20%*	*30%*	*40%*	*50%*
Vector 1					
Ni	159.9	89.8	46.7	21.9	9.0
Cr	827.8	857.5	892.6	934.8	987.4
Vector 2					
Ni	192.5	133.0	87.5	53.9	30.4
Cr	203.4	43.9	7.7	1.0	0.1
Vector 3					
Ni	179.6	114.8	69.1	38.5	19.2
Cr	344.3	133.8	45.8	13.3	3.1
Vector 4					
Ni	175.5	109.3	63.9	34.4	16.5
Cr	410.4	194.0	83.0	31.1	9.8
Vector 5					
Ni	221.2	178.6	140.0	105.8	75.9
Cr	71.0	4.7	0.2	0.0	0.0

*The partition coefficients are from FC-Modeler computer software (Keskin, 2002)

et al., 1990). The diagram Ni-Cr, in Figure 6.4 highlights the variation. Also plotted in this diagram are the theoretical Rayleigh fractionation vectors showing the effects of 50% fractional crystallization of individual phases and relevant phase combinations. The input data and modelling results are shown in Table 6.1.

The model considered involves fractional crystallization of various proportions of olivine and clinopyroxene to explain the chemical variation on the Ni versus Cr diagram. Fractional crystallization models vary from olivine only (Vector 1, Fig. 6.4) to 30% olivine–70% clinopyroxene (Vector 5, Fig. 6.4). Starting compositions are selected on the basis of the highest Cr and Ni (excluding two scattered samples). The diagram suggests that the data can be explained by about 50% fractional crystallization (excluding two scattered samples). The large amount of fractional crystallization is consistent with wide mineral chemical and whole-rock major and trace element variations suggesting dominant role of fractional crystallization.

Although the fractional crystallization models explain the major element and compatible trace element variations well, they fail to explain some incompatible trace element and isotopic variations. As explained in Chapter 4 and 5, several factors contribute to this problem, including source heterogeneity and crustal contamination. Thus, although the modelling results indicate that fractional crystallization could play an important role in controlling compositional variation among the rock units from each Zone, other processes are important. In the following sections other processes such as source heterogeneity, magma recharge and crustal contamination are discussed.

6.5.2 Trace element variations

Incompatible elements are those most likely to be transported by melts and other fluids passing through the mantle. They are, therefore, the elements most likely to preserve evidence of mantle enrichment and depletion (Hart et al., 1989; Arndt et al., 1998). Incompatible trace elements include Zr, Y, Nb, La, Rb and Nd (Fig. 4.4, Chapter 4). Their relative abundances are primarily governed by the mantle enrichment and depletion processes and relative degree of differentiation.

Concentration profiles through the stratigraphic sequence of the intrusion are asymptotic with very low incompatible trace element abundances in the Upper and Lower Zones, and higher abundances in the Middle Zone. In detail, there is a recognizable discontinuity at the Lower Zone–Middle Zone boundary and the Middle Zone–Upper Zone boundary, manifested by a sudden decrease in incompatible trace element abundances from the Middle Zone to the overlying Upper Zone and the underlying Lower Zone. This sudden shift reflects the influx of a new magma pulse.

Selected bivariate plots for the samples of the Wateranga intrusion are illustrated in Figures 6.5 to 6.7. The plot of Zr versus Y (Fig. 6.5a) shows the contrast in the compositional trends of different Zones in the Wateranga intrusion. The differences in trends between the Zones and lack of very good linear correlation between Y and Zr suggests heterogeneity in the source, magma mixing and/or crustal contamination. Figure 6.5b illustrates variation between Y and Mg# with contrasting variation trends between the Zones supporting an open-system process. In addition, most Middle Zone samples plot at lower Mg# and higher Y.

During fractional crystallization of common silicate phases (e.g. olivine, pyroxene) the ratios between highly incompatible elements such as Zr, Y and Nb should not vary dramatically. Figure 6.6 shows wide variation in incompatible element ratios. This implies that the source region of the Wateranga magmas may have been relatively heterogeneous. Furthermore, high Y/Nb ratios (average = 5.31) suggest crustal contamination, which would have influenced these element ratios (Wilson, 1989).

The chondrite-normalized REE patterns in the Wateranga intrusion change from slightly LREE enriched with positive Eu anomalies in the Lower and Upper Zone to strongly LREE enriched patterns with slight positive Eu anomaly in the Middle Zone (Fig. 4.6, Chapter 4). In detail, compared to the Lower and Upper Zones, the Middle Zone is characterized by stronger LREE enrichment (average Ce/Yb_{CN} = 3.61), stronger HREE fractionation (average Gd/Yb_{CN} = 2.07) and higher REE abundances, probably related to a more important role of garnet and a deeper source in its origin (Ellam, 1992; Stein et al., 1997).

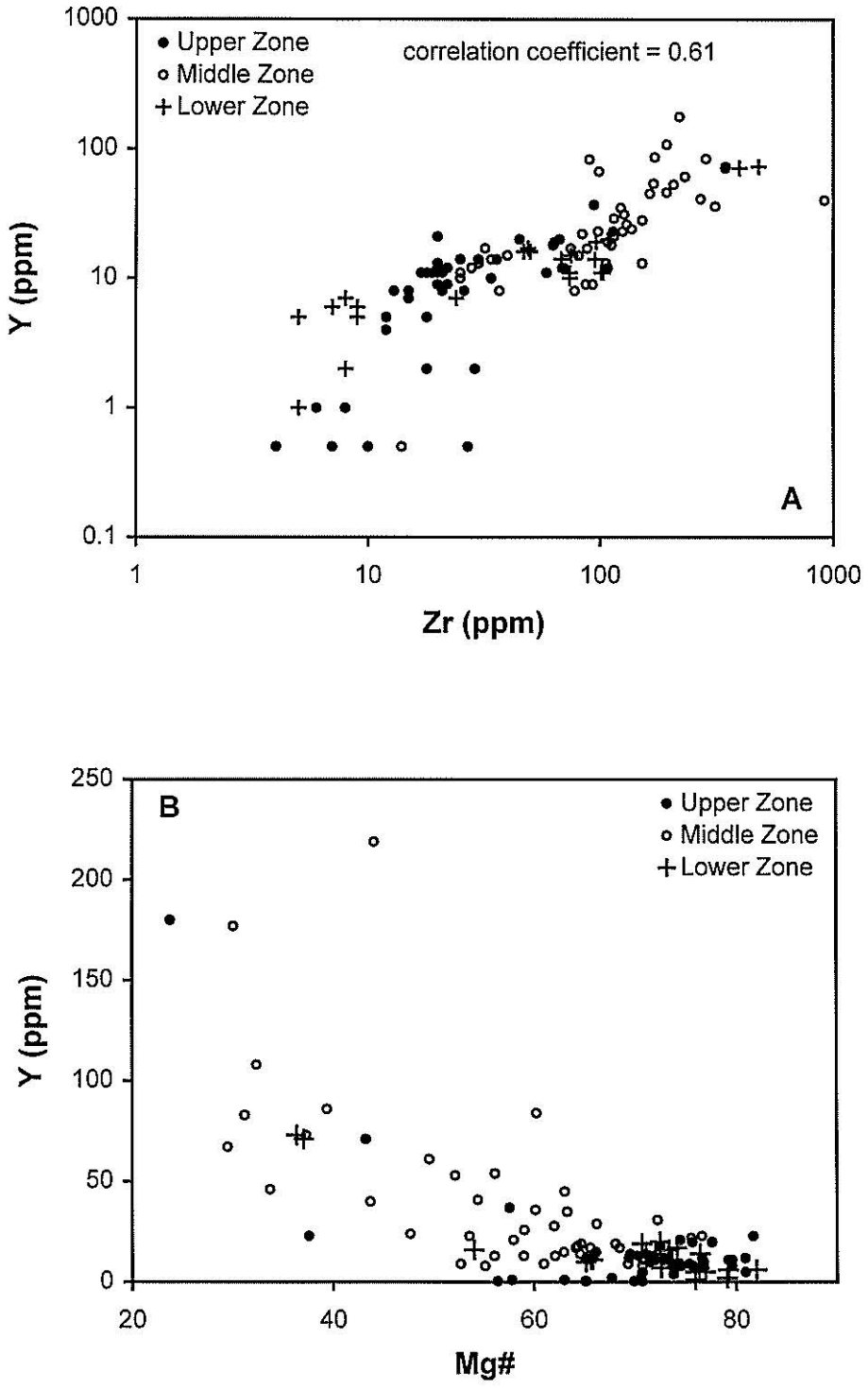

Figure 6.5 Selected bivariate plots of whole-rock (A) Y vs Zr and (B) Y vs Mg# for the Wateranga intrusion. **Note:** Three samples, with very high contents of Zr (A-WG-24 - 7668 ppm, E-NS5/5 - 2422 ppm and A-WG-13 - 1356 ppm), are omitted in the Zr vs Y plot.

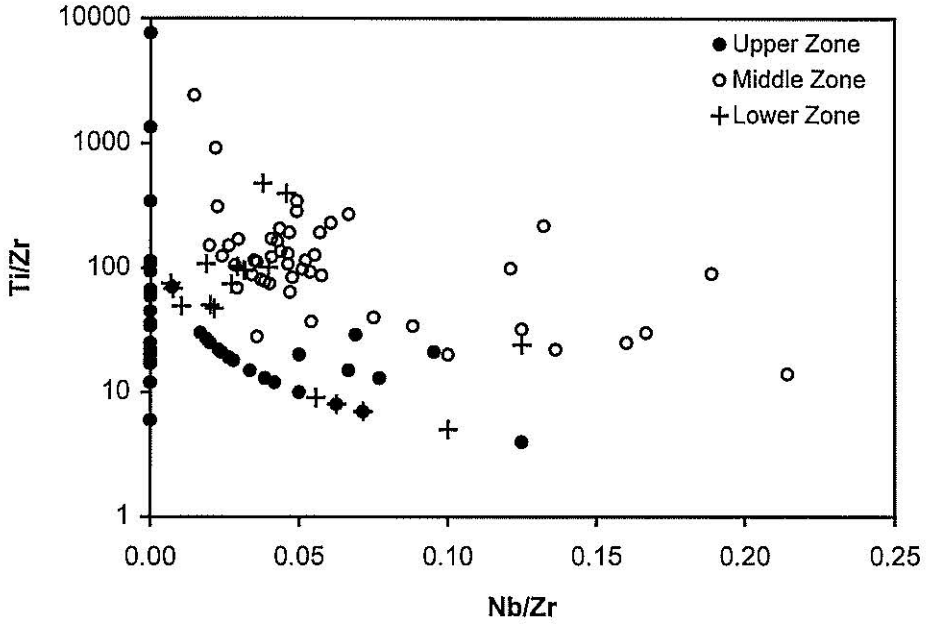

Figure 6.6 Nb/Zr versus Ti/Zr for the Wateranga samples

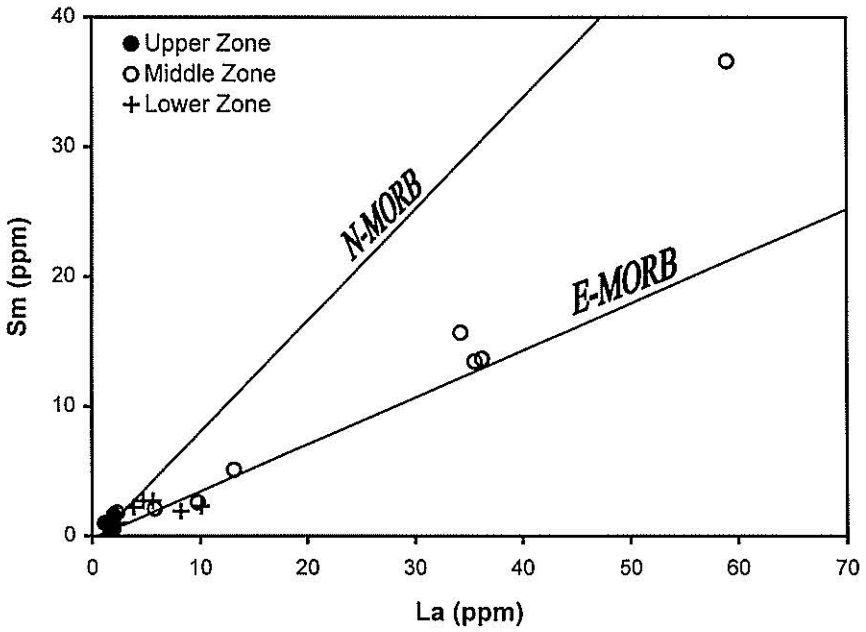

Figure 6.7 La versus Sm for the Wateranga intrusion. The values of E- and N-MORB are from Sun and McDonough (1989)

The positive Eu anomaly exhibited by the chilled margin samples suggests that plagioclase crystallization had already commenced at depth, prior to emplacement, perhaps in deeper magma chambers.

It is evident from Figure 6.7 that the trace element contents of the Wateranga rocks possess values similar to E-MORB. Furthermore, the REE patterns of the intrusion with $(La/Ce)_{CN} > 1$ and $(Ce/Yb)_{CN} > 1$, fit the characteristics of E-MORB well (Sun and McDonough, 1989). Such compositional trends are common in lavas from rifted continental margins (Petrini et al., 1988).

6.5.3 Melting processes

The ratios of the LREE to the MREE and to the HREE can be used as a rough measure of the melting percentage of a mantle source (e.g., Nakamura et al., 1989; Ramos and Kay, 1992). The LREE are relatively incompatible with residual mantle minerals. The concentration of the HREE, as represented by Yb, is sensitive to the presence of residual garnet in the source (e.g., Henderson, 1984). Thus decreasing La/Yb, La/Sm and Ce/Sm ratios are diagnostic for an increasing melt production in garnet bearing sources. The analyzed Wateranga rocks have chondrite- normalized $(La/Yb)_{CN}$ ratios of 1.11 to 6.87, $(La/Sm)_{CN}$ ratios of 0.76 to 2.72 and $(Ce/Sm)_{CN}$ ratios of 0.72 to 2.15. Figure 6.8 shows the change in normalized (Ce/Sm) vs (La/Yb) during partial melting of a primitive mantle source with the mineralogy: olivine 55%, orthopyroxene 25%, clinopyroxene 11% and garnet 9%. The melting model is based on melting a primitive mantle with initial normalized REE concentrations at about two-times chondritic level. The mineralogy and chemical composition are taken from the "primordial mantle" of McDonough et al. (1992). Chondrite normalization is based on the data of Nakamura (1974) and bulk partition coefficients are taken from Rollinson (1993). The vectors for modal batch melting and modal fractional melting are calculated according to the basic equations of Wood and Fraser (1976) and DePaolo (1981). The low $(La/Yb)_{CN}$ and $(Ce/Sm)_{CN}$ ratios of the Wateranga samples indicate melting percentages higher than c. 5% (Fig. 6.8). Additionally, the $(La/Yb)_{CN}$ ratio of the Wateranga samples indicates a small amount of residual garnet in the mantle

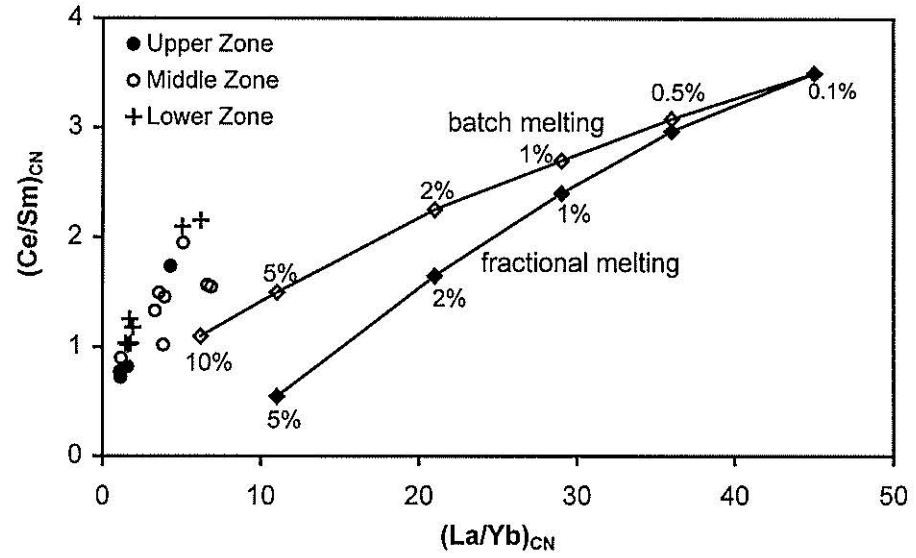

Figure 6.8 Vector diagram showing the change in chondrite-normalised (Ce/Sm) vs (La/Yb) during the partial melting of a primitive mantle source. Melting percentages are given for modal batch melting (open squares) and modal fractional melting (closed squares). Plotted data represent the samples of the Wateranga intrusion. The melting model is based on melting of a primitive mantle with REE concentrations at c. two-fold chondritic concentrations.

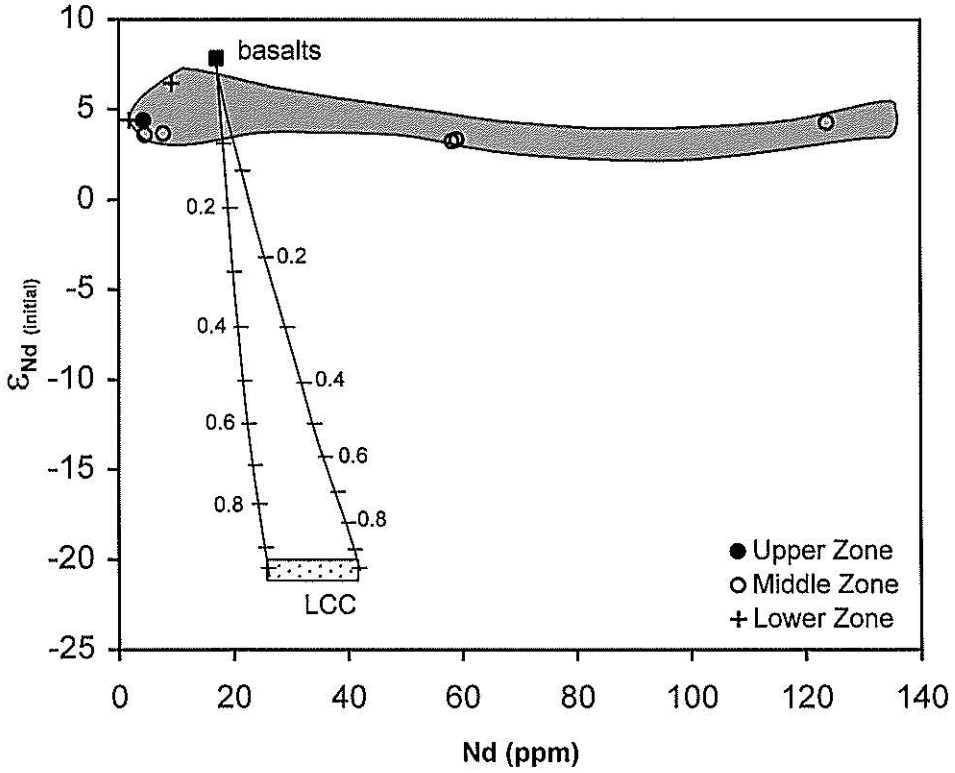

Figure 6.9 Isotopic modelling for mixing between a depleted mantle-derived mafic magma and a lower continental crust (LCC), using the mixing equation proposed by Langmuir et al. (1978). Parameters used: mafic magma, Nd 15 ppm, ε_{Nd} +8 (Taylor & McLennan, 1985); LCC, Nd 24-40 ppm, ε_{Nd} -20 (Jahn et al., 1988; Chen & Jahn, 1998).

source.

6.6 Nd-Sr-O isotopic variations

6.6.1 Neodymium and strontium isotopes

Replenishment of fresh magma has been recognized in the Stillwater (Raedeke and McCallum, 1984; McCallum, 1996; Horan et al., 2001), Rhum (Palacz, 1984; Emeleus et al., 1996) and Bushveld intrusions (Sharpe, 1985; Cawthorn et al., 1991), and may in fact have played an important role in the evolution of the Kiglapait, Skaergaard and Fongen-Hyllingen intrusions (DePaolo, 1985; Stewart and DePaolo, 1990; Sorensen and Wilson, 1995). The work on these intrusions has emphasized the potential of isotopes in identifying episodes of magma replenishment and assimilation processes. The Wateranga intrusion provides an excellent example of periodic recharge of fresh magma during magma chamber crystallization (Talusani and Sivell, 2002).

The isotopic variations within the Wateranga intrusion, although small with respect to the endmember components in the magmatic system, are substantial in relation to the variations resulting from complete crystallization of the intrusion (Figs. 5.3 and 5.4, Chapter 5). In the Wateranga intrusion ε_{Nd} varies by ~3 ε units, from +3.26 to +6.44, and the initial $^{87}Sr/^{86}Sr$ ratio by ~0.0023, from 0.7026 to 0.7049. These ranges are grossly similar to those observed in the Kiglapait intrusion (DePaolo, 1985). In detail, there appear to be at least three cycles in the Nd and Sr isotopic data. The first cycle is from the top of the intrusion to ~140m (Upper Zone); the second is from ~140m to ~285 m (Middle Zone), and the third cycle from 285-500m (Lower Zone) at the base of the intrusion. If there is any systematic in situ contamination, the samples measured should be the most contaminated samples from each zone. Therefore, the differences in ε_{Nd} and $^{87}Sr/^{86}Sr$ probably reflect either contamination during emplacement of each new pulse or shifts in the chemical characteristics of the magma feeding the chamber. In the former case, roof rock would melt and remain isolated from the mafic magma during periods of essentially quiescent crystallization within the magma

chamber. Then, during turbulent injection of a replenishing liquid, molten roof rock could be forced down to mix with the flowing magma. The degree to which an influx of fresh magma may become contaminated depends on (1) the amount of melting that occurred at the roof during crystallization of the pre-existing cyclic unit (2) the turbulence of the magma injection and (3) the amount of new magma entering the chamber.

If the isotopic shifts reflect changes in the magmas feeding the chamber, the trend of increasing ε_{Nd} and decreasing $^{87}Sr/^{86}Sr$ is opposite the expectation for gradual contamination of these source liquids. Nonetheless, such a trend could be produced by magma inputs from a deeper-level system in which recharge greatly exceeds crustal contamination, thus pushing ε_{Nd} and $^{87}Sr/^{86}Sr$ values toward the recharging endmember, or from a recharging system which gradually becomes insulated from crystal accumulation. An alternative explanation is that the shifts represent interaction of mantle melts with lower continental crust. The role of lower continental crust beneath continents has been increasingly recognized and may contribute to the geochemical signature of continental basalts (Johnson, 1991; Perry et al., 1993). Whether the shifts are from crustal contamination or source heterogeneities, the highest ε_{Nd} and lowest $^{87}Sr/^{86}Sr$ of the magmas feeding the chamber is most likely to represent "pristine" mantle melt. In the Wateranga intrusion, the highest ε_{Nd} and lowest $^{87}Sr/^{86}Sr$ are 6.44 and 0.7026 respectively, similar to the uncontaminated source for the Deccan Flood Basalt Province (Peng et al., 1998). This suggests an asthenospheric mantle source for Wateranga magmatism.

Isotopic signatures of the Wateranga intrusion indicate time-integrated enrichment of their sources that may not be explained by within chamber assimilation. Therefore, we have to consider preemplacement contamination or the origin of the magmas from enriched mantle sources as possible causes of the enriched isotopic signatures. Because the magmas were derived from mantle sources (whether enriched or depleted) and ascended through continental crust, the magma-crust interaction was a likely process (e.g., Huppert and Sparks, 1985; Arndt and Jenner, 1986; Arndt et al., 1993), and is considered as a first possibility.

In an attempt to quantify contamination, a simple mixing model has been used (Fig. 6.9). The amount of crustal contamination required is between 2 and 8 percent. The amount of crustal component, required to reproduce the isotopic compositions of the Middle Zone (ε_{Nd} = 3.26 – 4.26 and $^{87}Sr/^{86}Sr_{(initial)}$ = 0.7036 – 0.7049) is higher than the Lower and Upper Zones (ε_{Nd} = 4.39 – 6.44 and $^{87}Sr/^{86}Sr_{(initial)}$ = 0.7026 – 0.7038).

6.6.2 Oxygen isotopes

Variations in $\delta^{18}O$ values within Zones of the Wateranga intrusion may result from: (1) differences in $\delta^{18}O$ values of input magmas, (2) processes that occur within the magma chamber such as temperature changes, fractional crystallization and mineral accumulation, (3) assimilation of country rocks and magma contamination and (4) low-temperature secondary alteration (weathering). The whole-rock $\delta^{18}O$ values of the Upper and Lower Zones (6.69 to 7.29‰; with the exception of WG-16, an altered sample) are not unusual in comparison to those considered typical for a melt derived from a primary unmodified mantle [(5.2‰) Mattey et al., 1994; Hoefs, 1997)]. Unlike the samples from Lower and Upper Zones the Middle Zone samples show a wide variation and shifts to higher $\delta^{18}O$ values (6.16 to 9.38‰) (Fig. 5.7, Chapter 5).

In the Wateranga intrusion, the $\delta^{18}O$ values fall into two groups: one for samples from the Upper and Lower Zones, and one for the Middle Zone samples. The $\delta^{18}O$ values of the Upper (with the exception of an altered sample, WG-16) and Lower Zone samples are uniform at 6.69 to 7.29‰. Similar to the Upper Zone rocks, the Lower Zone rocks are only slightly crustally contaminated (as evidenced by Nd and Sr isotopic variations), so their measured $\delta^{18}O$ values are probably only slightly shifted from primary values. Nd and Sr isotopic variations suggest that the Middle Zone magmas may have interacted with crust more than the Lower and Upper Zone magmas (Fig. 6.9). Nd and Sr isotopic compositions of the intrusion can be used to place constraints on the kind of processes that might be responsible for stable isotope signatures. For example, $\delta^{18}O$ value which is the product of assimilation of continental crust may be paralleled by Nd and Sr isotopic effects

(Halliday et al., 1983; Halliday, 1984). Overall, the observed Nd-Sr isotopic variations in the three stratigraphic Zones of the Wateranga intrusion are mirrored in the oxygen isotope compositions.

The small variation in $\delta^{18}O$ values observed in the Lower and Upper Zone samples (excluding WG-16) of Wateranga intrusion can be explained by processes (1) to (3) mentioned above. The higher $\delta^{18}O$ values in WG-16 may be due to secondary alteration. Taken together with the higher level of crustal assimilation and the petrographic evidence for slight secondary alteration (samples NS-3/20 and NS-5/6) which would lead to elevated $\delta^{18}O$ values of the Middle Zone samples, variations in $\delta^{18}O$ values are thought to result from processes (1) to (4).

6.7 Two magma series

Two distinct magma series are required to explain the different crystallization orders, trace element compositions and range of radiogenic isotope compositions observed in the rocks of the Wateranga intrusion. One magma, which was the dominant melt forming the Middle Zone is characterized by the crystallization order plagioclase → olivine → orthopyroxene → clinopyroxene → Fe-Ti oxides. This magma type is also characterized by strong LREE enrichment (La/Yb_{CN} = 4.20) and higher abundances of REE with approximately 6 times higher La and 3 times higher Lu than the average Lower and Upper Zone magmas (Fig. 4.6, Chapter 4). The ranges in isotopic compositions of the Middle Zone magma type are ε_{Nd} 3.26 – 4.29 and $^{87}Sr/^{86}Sr_{(initial)}$ 0.7036 – 0.7049 (Figs. 5.3 and 5.4, Chapter 5).

The second magma type, derived from a relatively depleted mantle source, is likely to be parental to the Lower and Upper Zones. Crystallization order of minerals in this magma type is olivine → plagioclase → clinopyroxene → orthopyroxene → Fe-Ti oxides. This magma type is characterized by less LREE enrichment and low REE abundances relative to the Middle Zone magmas. The ranges in isotopic compositions of the Lower and Upper Zone magma type are ε_{Nd} 4.39 – 6.44 and $^{87}Sr/^{86}Sr_{(initial)}$ 0.7026 – 0.7038. The difference in isotopic

compositions between the two magma series indicates that different source regions or assimilation is required.

6. 8 PGE, Au, Cu, Ni and S variations in the Wateranga intrusion

Sulphur is a minor component of the Earth's upper mantle (250 ppm, Lorand, 1990). It can be assumed that at the temperatures achieved during partial melting of the upper mantle (> 1100°C), all sulphides present in the affected portion of the mantle would melt. Thus, sulphur concentrations in magmas derived from the mantle would be expected to range from 2.5% (potassic and ultrapotassic magmas, 1% melting) to 0.05% (komatiites, 50% melting). However, most basalts actually contain values in the range 0.01 to 0.2% sulphur. The reason for this is that silicate magmas can only dissolve a limited amount of sulphur. The experimentally determined solubility of sulphur in basaltic magmas lies between 0.05 and 0.26 wt% (Wendlandt, 1982), with the surplus sulphur segregating out as an immiscible sulphide melt upon melting of the mantle, and possibly remaining in the source. Central to the formation of economic sulphide deposits is the principle that the solubility of sulphur in basic and ultrabasic magmas decreases with falling temperature (0.04 wt% sulphur per 100°C, Wendlandt, 1982) and FeO content of the silicate magma.

Finely disseminated and locally coarse grained sulphide mineralization occurs throughout the Wateranga intrusion. Given that the PGE have extremely high sulphide-silicate partition coefficients (e.g. Peach et al., 1990), they are very sensitive indicators of sulphide ore-forming processes. Their abundance and distribution in a given rock provide a measure of the S-saturation status of the magma from which the rock crystallized (Peck and Keays, 1990; Vogel and Keays, 1997). This information is relevant to establishing the general metallogenic potential of the Wateranga intrusion in terms of PGE, Cu and Ni, as well as further characterizing its petrogenesis.

PGE (Pt and Pd) and Au concentrations in ten rocks from different stratigraphic Zones within the Wateranga intrusion show limited variation and are relatively low (Table 4.6, Chapter 4), namely: Pt ranges from 1 to 3 ppb, Pd varies

from 1 to 8 ppb and Au varies between 7 and 17 ppb. For example, these concentrations are generally lower than [or greater than (Au)] those reported for unmineralized mafic rocks from below the J-M Reef in the Stillwater Complex (13 ppb Pt, 7 ppb Pd, 0.4 ppb Au; Peck and Keays, 1990). Whole rock S concentrations in the Wateranga rocks are high and vary from 200 to 11000 ppm (typically >500 ppm in most samples; Appendix 1).

In the Wateranga intrusion, the sulphides have a distinctly intercumulus character, which is interpreted to reflect a primary magmatic origin, and show exsolution textures. The sulphides and silicates exhibit sharp boundaries and there is no petrographic evidence of replacement of silicates by sulphides.

Cu, Au and the PGE show good correlations with S in the rocks of the Wateranga intrusion suggesting control of the abundance of these metals by sulphides (Table 4.7, Chapter 4). A strong positive correlation between Pt and Pd indicates that these elements behaved sympathetically during magmatic crystallization. Ni and Cu show positive and negative correlations with whole-rock Mg#, respectively, suggesting that Ni partitioned into olivine primocrysts during magmatic differentiation, whereas Cu preferentially partitioned into the residual liquid (Fig. 4.9, Chapter 4). A good positive correlation exists between Cu and Pt+Pd (Fig. 4.10, Chapter 4) indicative of magmatic origin. Furthermore, the highest PGE contents are invariably associated with high Cu and S (see Table 4.6, Chapter 4).

Figure 6.10 presents Pd and Cu data. Most samples plot well within the S-saturated field. The analyzed Wateranga samples are depleted in Ni and Pt, and yield positively sloping metal patterns (Fig. 4.11, Chapter 4) that are similar to those of ocean-floor basalts (Barnes et al., 1988). Ocean-floor basalts are believed to be the products of S-saturated magmas from which the metal-bearing sulphides were segregated in the mantle source or *en route* to the surface (Hamlyn et al., 1985).

The S data are plotted on a Poulson-Ohmoto diagram (Fig. 6.11), which discriminates, on the basis of FeO content, between magmas that have S abundances in excess of their S capacity and those that are undersaturated in S

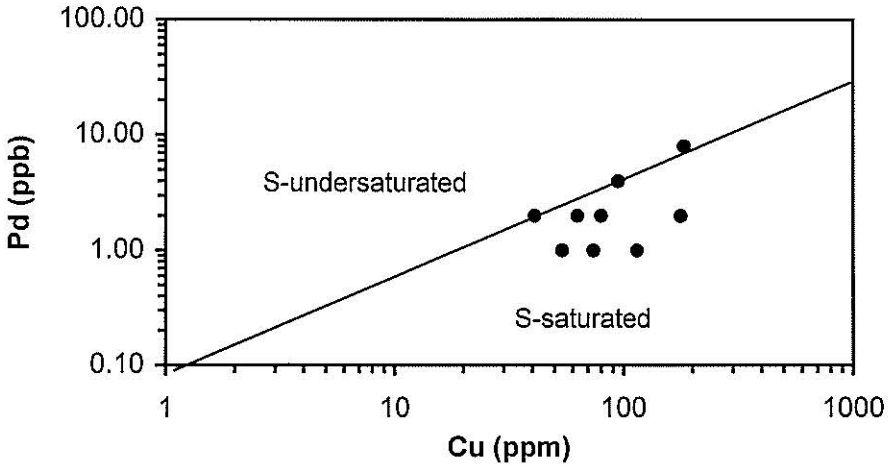

Figure 6.10 Pd versus Cu discrimination diagram showing the S-saturated nature of the Wateranga intrusion (dividing line is from Vogel and Keays, 1997).

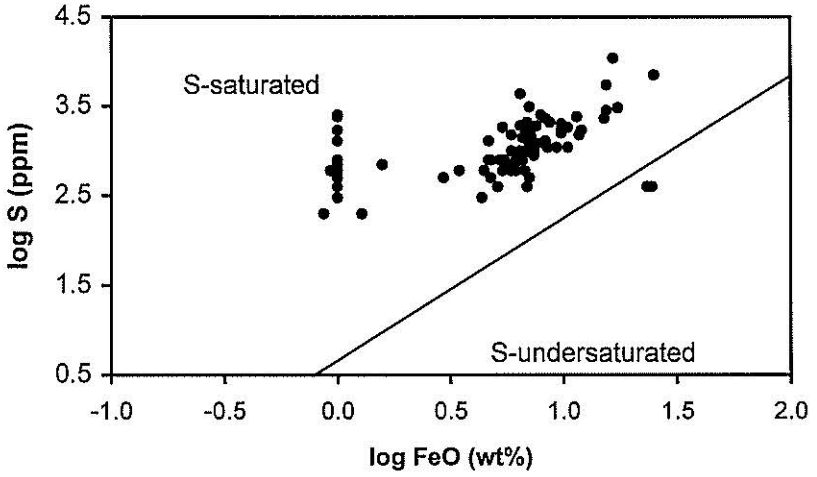

Figure 6.11 Poulson-Ohmoto diagram used to determine the S capacity of a magma based on its FeO content (Poulson and Ohmoto, 1990) for the Wateranga intrusion.

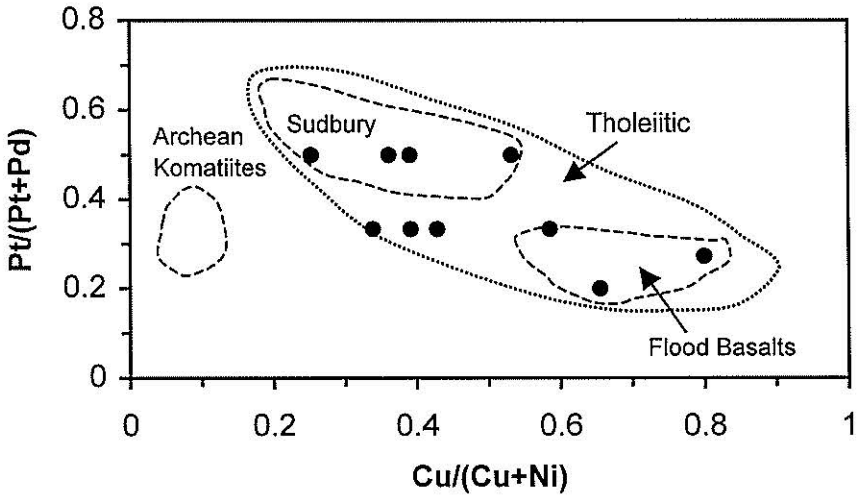

Figure 6.12 Pt/(Pt+Pd) versus Cu/(Cu+Ni) diagram for the Wateranga samples. The fields are from Naldrett (1981).

(Poulson and Ohmoto, 1990). Wateranga samples are clearly the most S saturated and given their low PGE concentrations (e.g., Pt = 1-3 ppb), they were metal-poor magmas.

The similarity of metal content of the Wateranga intrusion to tholeiitic type occurrences is supported by Figure 6.12 (Naldrett, 1981), wherein all the Wateranga samples plot in the tholeiitic field.

In summary, the textural and geochemical evidence demonstrates that the disseminated Fe-Ni-Cu sulphides and platinum group elements in the Wateranga intrusion are of magmatic origin.

6.9 Parental magmas of the Wateranga intrusion compared to other layered intrusions

Two chilled margin samples (WG-44 and WG-124) were analyzed in an effort to identify a possible parental magma composition for the Wateranga intrusion. Table 6.2 presents major element data for proposed parental magmas of the gabbroic portions of some of the best known layered intrusions in the world. All have high-Al basaltic compositions (>16 wt% Al_2O_3) and similar Mg#s. The proposed parental magmas of the Stillwater and Bushveld Complexes are also characterized by very low TiO_2 concentrations, whereas the much younger Skaergaard and Wateranga intrusions were fed by magmas containing approximately two times as much TiO_2. Column 5 in Table 6.2 is a model parent liquid composition (A_0) for the Stillwater and Bushveld Complexes calculated through the addition of 17% plagioclase (An_{70}) to a chilled Bushveld rock composition (Irvine et al., 1983). The major element data indicate that the parental magma proposed for the Skaergaard intrusion has almost identical composition to the Wateranga intrusion.

An average composition for modern boninites is also provided in Table 6.2. Boninites are thought to be analogous in composition to the parental magmas that gave rise to the ultramafic portions of the Stillwater and Bushveld Complexes (e.g. Hamlyn and Keays, 1986). Clearly, such magmas are very different in composition

Table 6.2 Parental magma compositions proposed for gabbroic portions of selected layered intrusions.

Intrusion	1 Wateranga chilled margin	2 Skaergaard marginal gabbro	3 Stillwater basal chilled zone	4 Bushveld chilled norite	5 Bushveld-Stillwater A_0 – model liquid	6 Boninites world-wide
Major oxides (wt%)						
SiO_2	47.93	48.08	50.68	51.50	51.49	55.30
TiO_2	0.99	1.17	0.45	0.34	0.49	0.21
Al_2O_3	16.56	17.22	17.64	18.70	17.87	9.47
Fe_2O_3*	10.30	10.70	11.24	10.33	9.82	9.48
MnO	0.18	0.16	0.15	0.47	-	0.18
MgO	9.52	8.62	7.67	6.84	6.37	14.98
CaO	11.31	11.38	10.47	11.00	11.77	8.09
Na_2O	2.68	2.37	1.87	1.58	2.59	1.75
K_2O	0.11	0.25	0.24	0.14	0.16	0.28
P_2O_5	0.03	0.10	0.09	0.09	-	-
Mg-number	*71*	*65*	*61*	*61*	*60*	*79*

Data sources: 1. see Table 4.3 (Chapter 4); 2. Wager & Brown (1968); 3. Hess (1960); 4. Tilley et al. (1967); 5. Irvine et al. (1983); 6. Hamlyn & Keays (1986; average of 32 samples).

and appear very difficult to relate by fractional crystallization to parental magmas of gabbroic portion of layered intrusions.

6.10 Structure of the Wateranga intrusion

Emplacement of the Wateranga intrusion occurred in the Permo-Triassic times at c. 245±8 (Day et al., 1983) within a synclinal structure developed due to folding movements within the Goodnight beds (Robertson, 1971). Based on detailed field mapping by Robertson (1971) and this study, the intrusion has been described as a funnel or saucer-shaped lopolith and the layering dips towards the centre of the intrusion at angles ranging from 10 to 45 degrees. Approximately 500 meters of section is available which includes surface section and drill core. Figure 6.13 shows a simplified NE-SW cross section of the intrusion with the subdivisions Lower, Middle and Upper Zones defined by petrography, mineral chemistry, whole-rock geochemistry and Nd-Sr-O isotopic variations. The basis of

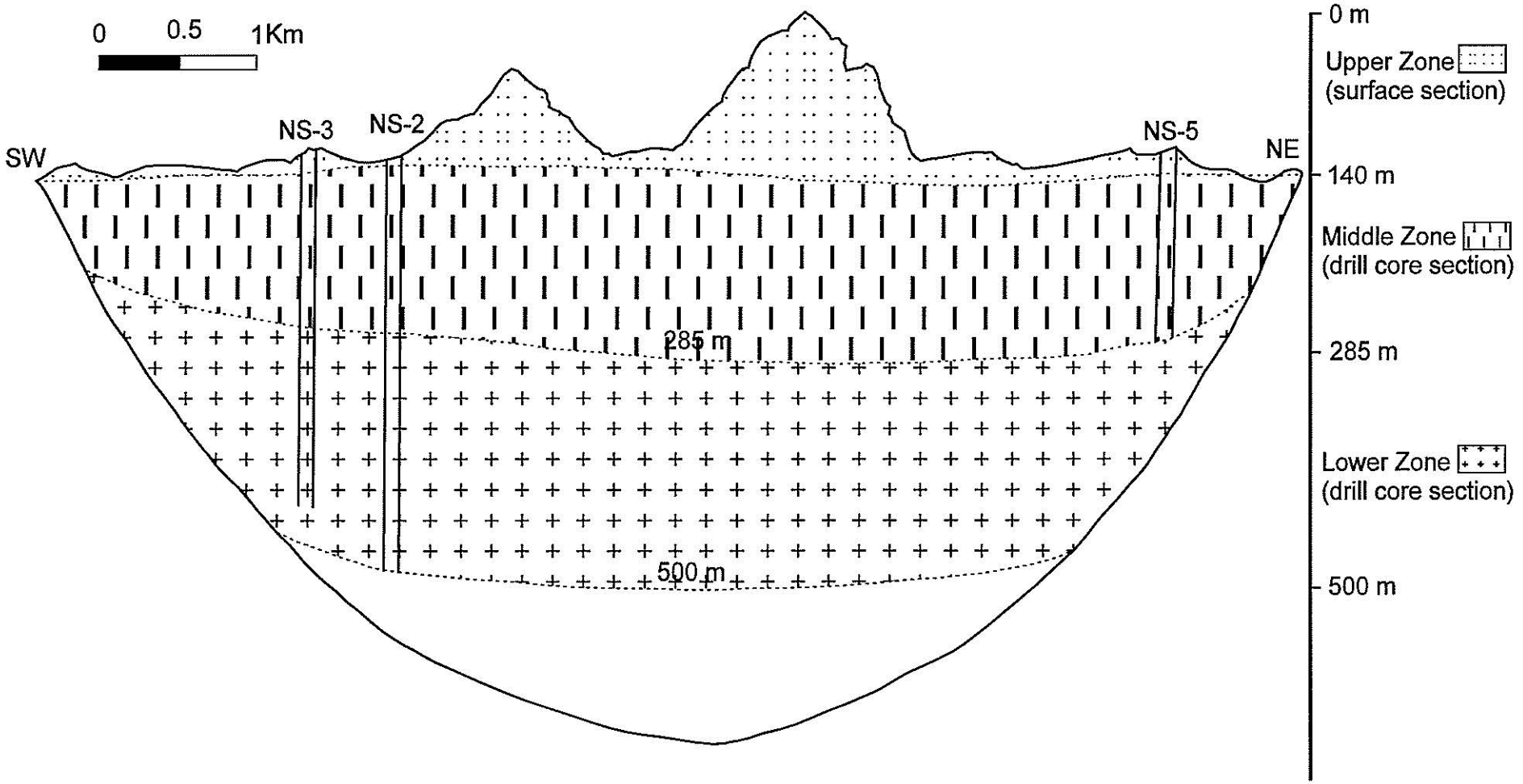

Figure 6.13 Southwest-Northeast cross section of the Wateranga intrusion. NS-2, NS-3 and NS-5 are drill holes.

subdivision into Zones has been discussed at relevant places in the previous Chapters.

6.11 Tectonic setting and regional implications

Arcs, rifts, continental collisions, thrusting and magmatic underplating each occur under different pressure and temperature regimes, and the magmas generated in these various tectonic environments have unique chemical and isotopic signatures. When determining the tectonic setting in which ancient igneous rocks originated, all available evidence must be considered: the lithology, geochemistry, intrusive styles, and significance of adjacent rock units (Pearce, 1987). Because the rocks of the Waternaga intrusion are cumulates, the compositions are plotted on tectonic discrimination diagrams designed to classify cumulate rocks on the basis of their mineral chemistry (Figs. 6.14 and 6.15).

Several workers noted the mineral chemical differences between arc cumulates and tholeiitic layered intrusions (Stern, 1979; Arculus and Wills, 1980; Smith et al., 1983; Loucks, 1990; Elthon et al., 1992). In the gabbroic rocks from arc-settings, high anorthite contents in plagioclase are ubiquitous but are absent in tholeiitic layered intrusions such as the Skaergaard (Wager & Brown, 1968; Hoover, 1989; McBirney, 1989, 1996; Tegner, 1997). This characteristic is useful in defining the tectonic setting of gabbroic plutons (Beard, 1986). The variation trend of anorthite content of plagioclase versus the forsterite content of olivine in the rocks of the Wateranga intrusion is typical of tholeiitic layered intrusions (Fig. 6.15), which clearly differs from that of arc-related cumulates (Beard, 1986). Crystallization of the Wateranga mineral assemblages from basaltic magma emplaced in an extensional setting is also supported by distinctive trend in terms of the variation of Al_z versus TiO_2 in clinopyroxenes. Figure 6.14 shows that the Wateranga intrusion falls on the rift cumulate trend. Furthermore, chondrite-normalized REE patterns of the intrusion show strong similarities with continental tholeiites which is further supported by initial $^{87}Sr/^{86}Sr$ (0.7026 to 0.7049) and ε_{Nd} (+3.26 to +6.44) isotope signatures (Talusani and Sivell, 2002). Depletions in Nb,

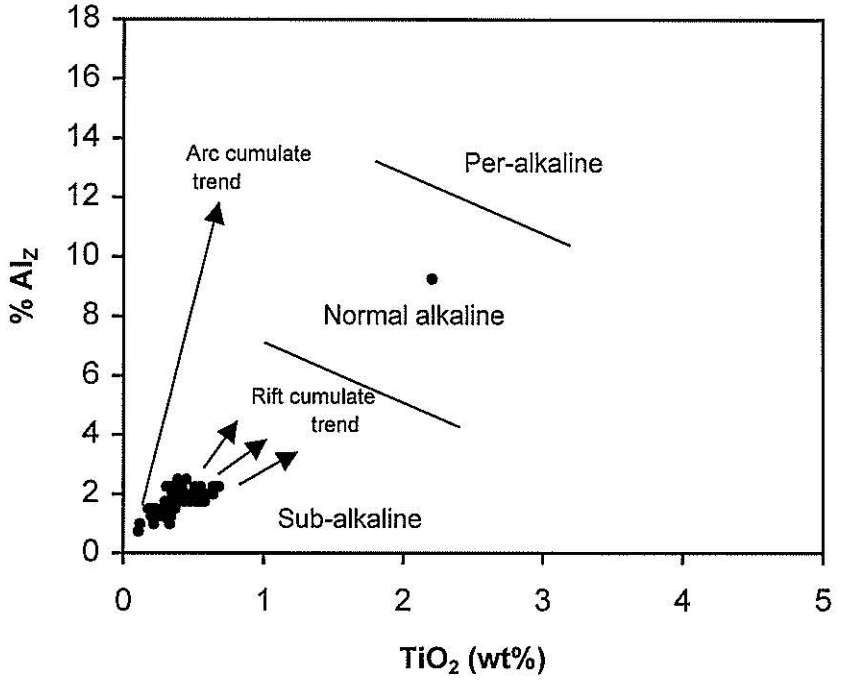

Figure 6.14 Plot of Al_z content expressed as a percentage of total Al, against $Ti0_2$ for clinopyroxene in the Wateranga intrusion. Field boundaries are from LeBas (1962), and trends are from Loucks (1990).

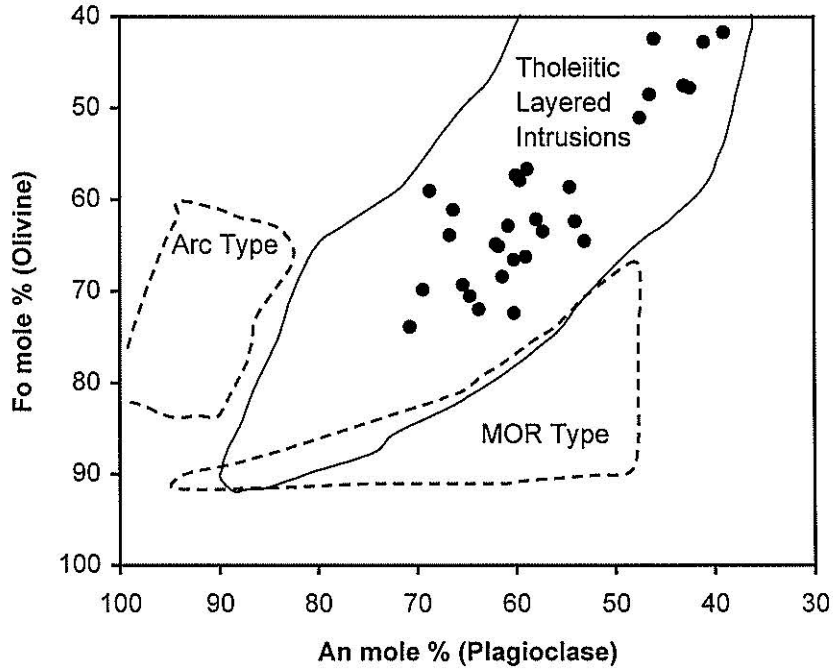

Figure 6.15 Anorthite content of plagioclase versus forsterite content of olivine in the rocks of the Wateranga intrusion. Fields of arc-related, tholeiitic layered intrusions and slow spreading ridge cumulates (MOR type) are from Beard (1986).

P and Ti are characteristic of the rocks of the intrusion. These features are reminiscent of subduction zone magmatism although subduction ceased long before the origin and emplacement of the Wateranga magma. These anomalies do not appear to be the result of HFSE fractionation during melting in the source. This is best explained by the enrichment of the lithospheric mantle by subduction-derived fluids and its subsequent involvement in extensional magmatism, where asthenospheric melts had interacted with the subduction-modified lithospheric mantle during ascent. The tectonic model to account for the Wateranga tholeiitic magmatism involves a post-subduction, Permo-Triassic asthenospheric rise due to a lithospheric thinning associated with extension and this model has important bearing for our understanding of post-collisional basic magmatism in the northern New England Fold Belt. This model provides strong support to the hypothesis of a general post-Permian extensional event postdating regional crustal contraction in the northern New England Fold Belt (Holcombe et al., 1997a). As mentioned in Chapter 1, the Wateranga intrusion is one of several unmetamorphosed mafic intrusions in the northern New England Fold Belt extending from Brisbane to Rockhampton. These mafic intrusions have similar composition, tectonic setting and age, and are generally proximal to major faults. It is reasonable to conclude, therefore, that existing zones of post-collisional crustal weakness controlled the localization of basic magmatism.

CHAPTER 7

Conclusions

Conclusions

The combination of petrological, mineral chemical, whole-rock geochemical and Nd-Sr-O isotopic investigations has allowed to unravel the origin and evolution of the Wateranga intrusion. Several conclusions that emerge from this study are summarized below.

1. The Permo-Triassic (245±8 Ma) Wateranga layered mafic intrusion (28 km^2) is a >500 m thick, undeformed, unmetamorphosed, tholeiitic pluton emplaced into the Late Carboniferous Goodnight beds of the Goodnight Block in southeast Queensland. The intrusion is mainly composed of gabbro and norite, associated with subordinate amounts of troctolite, anorthosite and orthopyroxenite, and rare picrite. In the drill core, rock types change abruptly with stratigraphic depth.

2. The whole-rock Sm-Nd isochron of the Wateranga intrusion define an emplacement age of 261±21 Ma which is slightly higher than the 245±8 Ma K-Ar age of Day et al. (1983).

3. Based on detailed petrographic, mineral chemical, whole-rock geochemical and Nd-Sr-O isotopic data, the igneous stratigraphy of the Wateranga intrusion can be divided into three zones: (1) the Lower Zone, (2) the Middle Zone and (3) the Upper Zone. The Zones represent magma chamber replenishment with discontinuities and reversal in the compositional trends at the Zone boundaries. The cryptic layering pattern

of the Wateranga intrusion is typical for a continuously differentiating layered intrusion that experienced replenishment episodes.

4. The most abundant minerals are plagioclase and clinopyroxene. Orthopyroxene and olivine are locally abundant. Hornblende is minor except in few rare layers. The observed changes in the crystallization order of minerals between the Zones implies a change in magma composition that cannot have been caused by fractional crystallization.

5. Textural data indicate that the rocks are mesocumulates to adcumulates and very low abundance of intercumulus minerals suggest that intercumulus liquid was insignificant. Furthermore, the amounts of intercumulus liquid are nearly identical in all the three stratigraphic Zones of the intrusion. The whole-rock geochemical evidence (e.g. low K_2O, P_2O_5, Rb and Y in most samples) also suggests insignificant amount of late-stage trapped intercumulus liquid.

6. Many rocks of the intrusion contain modal olivine + orthopyroxene, and most of the whole-rock chemical analyses show normative hypersthene and the compositions of all the analyses are olivine-normative. Thus, in agreement with petrography and normative mineralogy, the rocks may be justifiably classified as olivine tholeiitic.

7. The different rock types of the Wateranga intrusion show wide variations in common mineral chemical differentiation indices. The mineral compositional variations are consistent with a tholeiitic differentiation process controlled by fractional crystallization. In addition, sharp inflections in mineral chemical parameters at the Zone boundaries, supported by textural evidence, suggests rejuvenation of the magma chamber by injection of fresh magma.

   The co-variation trend of An content in plagioclase and Mg# of mafic minerals is nearly parallel to that of the layered series of the Skaergaard intrusion (Naslund, 1976; Hoover, 1978, 1989).

8. The parental magmas to the Wateranga intrusion are asthenospheric mantle-derived olivine tholeiitic magmas.

9. The rocks of the Wateranga intrusion show a wide range in compositional variation which can be attributed to fractional crystallization of plagioclase, olivine, clinopyroxene, orthopyroxene and Fe-Ti oxides. Fractionation followed a tholeiitic trend with iron enrichment in the liquid. Variations in major and trace element compositions reflect fractional crystallization, source heterogeneity, magma mixing and/or crustal contamination as the cause of compositional variations in the intrusion. Whole-rock REE compositions suggest that substantial trace element heterogeneity existed between the magmas that crystallized the Upper and Lower Zones, and the Middle Zone of the intrusion. In particular, the Middle Zone crystallized from magmas with approximately 6 times higher La and 3 times higher Lu than the average Lower and Upper Zone magmas. REE modelling indicates more than 5% degree of mantle melting with a low amount of residual garnet in the source.

10. Crystallization of the Wateranga intrusion occurred under open-system conditions. The $\varepsilon_{Nd(i)}$ and $^{87}Sr/^{86}Sr_{(i)}$ values provide evidence for isotopic heterogeneity or multiple magma injections. Petrologic, mineral chemical and geochemical data and oxygen isotopic compositions are also in favour of open-system crystallization.

11. Models of contamination of a primary depleted mantle-derived mafic magma with lower continental crust can explain the trend of isotopic variations in the Wateranga intrusion. The required amount of contaminant is between 2 and 8 percent.

12. The temperatures estimated from two-pyroxene geothermometer varied from 1057 to 927°C. During the course of crystallization, pressure was probably greater than 2 and less than 4 kbar. fO_2 is not well constrained

but was sufficient to allow the formation of local magnetite-cumulates (e.g., in samples NS-2/5 and A-WG-24) late in the crystallization. The primary melt was hydrous as indicated by the presence of hornblende. It is very unlikely that the melt was saturated with water during crystallization of the cumulus phases.

13. Fine grained disseminated Fe-Ni-Cu sulphides occur throughout the intrusion. The sulphide assemblage is dominated by pyrrhotite with minor pentlandite and chalcopyrite. Sulphide textures are attributed to magmatic processes. The highest combined Pt+Pd+Au is 28 ppb. Geochemical evidence indicates that PGE content of the Wateranga intrusion is of magmatic origin and is an original signature of the mantle.

The platinum group elements are not of much significance as major ore mineralization but are of interest as an important igneous process.

14. The Wateranga magma chamber is inferred to have been initiated by pooling of asthenospheric mantle-derived olivine tholeiitic magma (already contaminated by lower continental crust) in late Carboniferous sediments. The magma chamber evolved by fractional crystallization and replenishment by pulses of new magma.

15. This study suggests that two geochemically distinct magmas were delivered to the Wateranga magma chamber; one of which, derived from a homogeneous depleted mantle source (N-MORB type), was parental to the Lower and Upper Zones, and the other, derived from a slightly enriched mantle source, was parental to the Middle Zone. The nature of the parental liquids of igneous rocks from continental settings may not easily be discernible because crustal assimilation commonly obliterates the geochemical signature of primary melts.

16. The Wateranga mafic intrusion is tholeiitic in character, of within plate basalt, similar to many other mafic intrusions of equivalent age in the northern New England Fold Belt. The Wateranga intrusion is free from

metamorphic recrystallization and deformation, revealing a post-collisional character. The variation trend of anorthite content of plagioclase versus the forsterite content of olivine, whole-rock REE patterns and initial ε_{Nd} (3.26-6.44) and initial $^{87}Sr/^{86}Sr$ (0.7026-0.7049) compositions suggest an extension-related magma source. The geodynamic model to account for the Wateranga tholeiitic magmatism involves a post-subduction, Permo-Triassic asthenospheric rise due to lithospheric thinning associated with extension. This model has important bearing for our understanding of post-collisional basic magmatism in the northern New England Fold Belt.

As a whole, the Wateranga intrusion and several other mafic intrusions in the northern New England Fold Belt can be ascribed to the intrusion at different crustal levels of tholeiitic mantle-derived melts during Permo-Triassic time.

17. The Wateranga intrusion is similar to other rift-related gabbro intrusions such as the Skaergaard intrusion (Hoover, 1989; Stewart and DePaolo, 1990) and gabbro intrusions from the Oslo rift, Norway (Neumann et al., 1985).

18. Further isotopic work on the Wateranga intrusion may be required to fully characterize isotopic variations in each stratigraphic Zone and provide additional information on three dimensional geochemistry of the intrusion.

References

Albarede, F. (1976) Some trace element relationships amongst liquid and solid phases in the course of the fractional crystallization of magmas. *Geochimica et Cosmochimica Acta* 40, 667-673.

Albarede, F. (1996) *Introduction to Geochemical Modelling.* Cambridge University Press 541 pp.

Allegre, C. J., Hamelin, B. and Dupre, B. (1984) Statistical analysis of isotope ratios in MORB: the mantle blob cluster model and the convective regime of the mantle. *Earth and Planetary Science Letters* 71, 71-84.

Ambler, E. P. and Ashley, P. M. (1977) Vermicular orthopyroxene-magnetite symplectites from the Wateranga mafic layered intrusion, Queensland, Australia. *Lithos* 10, 163-172.

Amelin, Y. V. and Semenov, V. S. (1996) Nd and Sr isotopic geochemistry of mafic layered intrusions in the eastern Baltic shield: implications for the evolution of Paleoproterozoic continental mafic magmas. *Contributions to Mineralogy and Petrology* 124, 255-272.

Amelin, Yu. V., Neymark, L. A., Ritsk, E. Yu. And Nemchin, A. A. (1996) Enriched Nd-Sr-Pb isotopic signatures in the Dovyren layered intrusion (eastern Siberia, Russia): evidence for source contamination by ancient upper crustal material. *Chemical Geology* 129, 39-69.

Andersen, D. J., Lindsley, D. H. and Davidson, P. M (1993) QUILF: A Pascal program to assess equilibria among Fe-Mg-Mn-Ti oxides, pyroxenes, olivine, and quartz. *Computers and Geosciences* 19, 1333-1350.

Arculus, R. J. and Wills, K. J. A. (1980) The petrology of plutonic blocks and inclusions from the Lesser Antilles island arc. *Journal of Petrology* 21, 743-799.

Arndt, N. T. and Jenner, G. (1986) Crustally contaminated komatiites and basalts from Kambalda, Western Australia. *Chemical Geology* 56, 229-255.

Arndt, N. T., Czamanske, G. K., Wooden, J. L. and Fedorenko, V. A. (1993) Mantle and crustal contributions to continental flood volcanism. *Tectonophysics* 223, 39-52.

Arndt, N., Chauvel, C., Czamanske, G. and Fedorenko, V. (1998) Two mantle sources, two plumbing systems: tholeiitic and alkaline magmatism of the Mayinecha River basin, Siberian flood volcanic province. *Contributions to Mineralogy and Petrology* 133, 297-313.

Ashley, P. M., Ambler, E. P. and Flood, R. H. (1979) Two occurrences of ultramafic hornfels in the Biggenden beds, southeast Queensland. *Journal of the Geological Society of Australia* 26, 29-37.

Ashwal, L. D. (1993) *Anorthosites*. Springer, Berlin Heidelberg New York.

Ashwal, L. D., Jacobsen, S. B., Myers, J. S., Kalsbeek, F. and Goldstein, S. J. (1989) Sm-Nd age of the Fiskenaesset Anorthosite Complex, West Greenland. *Earth and Planetary Science Letters* 91, 261-270.

Attendorn, H. G. and Bowen, R. N. C. (1997) *Radioactive and Stable Isotope Geology*. Chapman and Hall, London. 522 pp.

Barling, J., Weis, D. and Demaiffe, D. (1993) A Sr-, Nd- and Pb- isotopic investigation of the transition between two macrocyclic units of the Bjerkreim-Sokndal layered intrusion, southern Norway. *In* Cawthorn, R. G. (ed) *Layering in Igneous Complexes*. Wager and Brown 25th Anniversary Commemorative Meeting, Johannesburg, South Africa, 8-10 September 1993. Johannesburg, Department of Geology, University of Witwatersrand.

Barnes, S. J. (1986) The effect of trapped liquid crystallization on cumulus mineral compositions in layered intrusions. *Contributions to Mineralogy and Petrology* 93, 524-531.

Barnes, S. J., Boyd, R., Korneliussen, A., Nilsson, L. P., Often, M. and Pedersen, R. B. (1988) The used of mantle normalization and metal ratios in discriminating between the effects of partial melting, crystal fractionation and sulphide segregation on platinum-group elements Gold, Nickel and Copper: examples from Norway. In Prichard, H. M., Potts, P. J., Bowls, J. F. W. and Cribb, S. J. (eds) *Geoplatinum 87 Symposium Volume*. Amsterdam: Elsevier, pp. 113-142.

Barnes, S. J., Naldrett, A. J. and Gorton, M. P. (1985) The origin of the fractionation of platinum group elements in terrestrial magmas. *Chemical Geology* 53, 303-323.

Basaltic Volcanism Study Project (1981) *Basaltic Volcanism on the Terrestrial Planets*. Pergamon Press, New York.

Beard, J. S. (1986) Characteristic mineralogy of arc-related cumulate gabbros: Implications for the tectonic setting of gabbroic plutons and for andesite genesis. *Geology* 14, 848-851.

Biggar, G. M. (1974) Phase equilibrium studies of the chilled margins of some layered intrusions. *Contributions to Mineralogy and Petrology* 46, 159-167.

Boudreau, A. E. and McBirney, A. R. (1997) The Skaergaard layered series. Part III. Non-dynamic layering. *Journal of Petrology* 38, 1003-1020.

Boudreau, A. E. and McCallum, I. S. (1992) Concentration of platinum group elements by magmatic fluids in layered intrusions. *Economic Geology* 87, 1830-1848.

Bowden, P., Bennett, J. N., Whitley, J. E. and Moyes, A. B. (1977) Rare earths in Nigerian Mesozoic granites and related rocks. *In* Ahrens, L. H. (ed) *The Origin and Distribution of the Elements*. Permagon Press.

Brooks, C. K. and Nielsen, T. F. D. (1982) The Phanerozoic development of the Kangerdlugssuaq area, East Greenland. *Meddr. Gronland. Geosci.* 9, 1-30.

Brown, G. M. and Vincent, E. A. (1963) Pyroxenes from late stages of fractionation of the Skaergaard intrusion, East Greenland. *Journal of Petrology* 4, 175-197.

Brugmann, G. E., Arndt, N. T., Hoffmann, A. W. and Tobschall, H. J. (1987) Nobel metal abundances in komatiite suites from Alexo, Ontario and Gorgona Island, Colombia. *Geochimica et Cosmochimica Acta* 51, 2159-2169.

Buchanan, D. L. (1988) Platinum group element exploration. Elsevier, London.

Campbell, I. H. (1978) Some problems with cumulus theory. *Lithos* 11, 311-323.

Campbell, I. H. (1985) The differences between oceanic and continental tholeiites: a fluid dynamic explanation. *Contributions to Mineralogy and Petrology* 91, 37-43.

Campbell, I. H. and Turner, J. S. (1987) A laboratory investigation of assimilation at the top of a basaltic magma chamber. *Journal of Geology* 95, 155-172.

Campbell, I. H., McCall, G. J. H. and Tyrwhitt, D. S. (1970) The Jimberlana Norite, Western Australia – a smaller analogue of the Great Dyke of Rhodesia. *Geological Magazine* 107, 1-11.

Caroff, M. (1995) Open system crystallization and mixing in two-layer magma chambers. *Lithos* 36, 85-102.

Cawood, P. A. (1982) Structural relations in the subduction complex of the Palaeozoic New England Fold Belt, eastern Australia. *Journal of Geology* 90, 381-392.

Cawthorn, R. G. (1983) Magma addition and possible decoupling of major and trace element behaviour in the Bushveld Complex, South Africa, *Chemical Geology* 39, 335-345.

Cawthorn, R. G. (1996) Re-evaluation of magma compositions and processes in the uppermost Critical Zone of The Bushveld Complex. *Mineralogical Magazine* 60, 131-148.

Cawthorn, R. G. and O'Hara, M. J. (1976) Amphibole fractionation in calc-alkaline magma genesis. *American Journal of Science* 276, 309-329.

Cawthorn, R. G., Meyer, P. S. and Kruger, F. J. (1991) Major addition of magma at the Pyroxenite Marker in the Western Bushveld Complex, South Africa. *Journal of Petrology* 32(4), 739-763.

Cawthorn, R. G., Sander, B. K. and Jones, I. M. (1992) Evidence for the trapped liquid shift effect in the Mount Ayliff Intrusion, South Africa. *Contributions to Mineralogy and Petrology* 111, 194-202.

Chalokwu, C. I. And Grant, N. K. (1983) The importance of trapped liquid abundances to the reequilibrium of primary mineral compositions in the Partridge River troctolite, Duluth Complex, Minnesota. *Geological Society of America Abstracts with Program* 15, 541.

Chalokwu, C. I. And Grant, N. K. (1987) Re-equilibration of olivine with trapped liquid in the Duluth complex, Minnesota. *Geology* 15, 71-74.

Chalokwu, C. I. And Grant, N. K. (1990) Petrology of the Partridge River Intrusion, Duluth Complex, Minnesota: 1. Relationships between mineral

compositions density and trapped liquid abundance. *Journal of Petrology* 31, 265-293.

Chalokwu, C. I. And Seney, P. J. (1995) Open-system magma chamber process in Freetown Complex of Sierra Leone: evidence from Zone 3. *Geological Magazine* 132, 261-266.

Chappell, B. W. (1991) Trace element analysis of rocks by X-ray spectrometry. *In* Barrett, C. S. et al., (eds) *Advances in X-ray Analysis* 34, 263-276.

Chappell, B. W. (1994) Lachlan and New England: Fold belts of contrasting magmatic and tectonic development. *Journal and Proceedings of the Royal Society of New South Wales* 127, 47-59.

Chen, J. F. and Jhan, B. M. (1998) Crustal evolution of southeastern China: Nd and Sr isotopic evidence. *Tectonophysics* 284, 101-133.

Clayton, R. N. and Mayeda, T. K. (1963) The use of bromin penta-fluoride in the extraction of oxygen from oxides and silicates for isotopic analysis. *Geochimica et Cosmochimica Acta* 27, 45-52.

Clifford, M. J. (1987) Geology of the Westwood layered gabbro and associated copper, palladium and platinum mineralization. Unpublished Hons thesis, James Cook University of North Queensland.

Coney, P. J., Edwards, A., Hine, R., Morrison, F. and Windrim, D. (1990) The regional tectonics of the Tasman orogenic system, eastern Australia. *Journal of Structural Geology* 12, 519-543.

Cousens, B. L. (1996) Depleted and enriched upper mantle sources for basaltic rocks from diverse tectonic environments in the northern pacific ocean: The generation of oceanic alkaline vs. tholeiitic basalts. *In* Basu, A. and Hart, S. (eds) *Earth Processes: Reading the Isotopic Code*. American Geophysical Union, Geophysical Monograph 95, 207-232.

Cranfield, L. C. (1986) The geology of the south Burnett district. *In* Willmott, W. F. (ed) *1986 Field Conference The South Burnett District*. Geological Society of Australia, Queensland Division, Brisbane. 1-12.

Cranfield, L. C. (1989) New Palaeozoic stratigraphic units in the Maryborough 1:250000 sheet area, south Queensland. *Queensland Government Mining Journal* 90, 115-120.

Cranfield, L. C. (1994) Maryborough, Queensland. Sheet SG56-6. 1:250000 Geological Series – Explanatory Notes. *Geological Survey of Queensland*, Department of Minerals and Energy.

Cranfield, L. C., Shorten, G., Scott, M. and Baker, R. M. (1997) Geology and mineralization of the Gympie Province. *In* Ashely, P. M. and Flood, P. G. (eds) *Tectonics and Metallogenesis of the New England Orogen*. Geological Society of Australia, Special Publication 19, 128-147.

Crouch, S. B. S., Donchak, P. J. T., Tenison-Woods, K., Scott, M., Kwiecen, W. and Grayson (1995) Plutonic rocks of the North D' Aguilar Block. *Queensland Geological Record* 1995/8.

Cullers, R. L. and Graf, J. L. (1984) Rare earth elements in igneous rocks of the continental crust: predominantly basic and ultrabasic rocks. *In* Henderson, P. (ed). *Rare Earth Element Geochemistry*. Elsevier. 237-274.

Day, R. W., Murray, C. G. and Whitaker, W. G. (1978) The eastern part of the Tasman orogenic zone. *Tectonophysics* 48, 327-364.

Day, R. W., Whitaker, W. G., Murray, C. G., Wilson, I. H. and Grimes, K. G. (1983) Queensland Geology, a companion volume to the 1:250 000 scale geological map (1975). *Geological Survey of Queensland Publication* 383.

DePaolo, D. J. (1981) Trace element and isotopic effects of combined wallrock assimilation and fractional crystallization. *Earth and Planetary Science Letters* 53, 189-202.

DePaolo, D. J. (1985) Isotopic studies of processes in mafic magma chambers: I. The Kiglapait intrusion, Labrador. *Journal of Petrology* 26, 925-951.

DePaolo, D. J. and Wasserburg, G. J. (1976) Nd isotopic variations and petrogenetic models. *Geophysical Research Letters* 3, 249-252.

Dickin, A. P. (1995) *Radiogenic Isotope Geology*. Cambridge University Press, Cambridge. 490 pp.

Eales, H. V., DeKlerk, W. J. and Teigler, B. (1990) Evidence for magma mixing processes within the Critical and Lower Zones of the northwestern Bushveld Complex, South Africa. *Chemical Geology* 88, 261-278.

Ellam, R. M. (1992) Lithospheric thickness as a control on basalt geochemistry. *Geology* 20, 153-156.

Ellis, P. L. (1968) Geology of the Maryborough 1:250 000 sheet area. *Geological Survey of Queensland*, Report 26.

Elthon, D., Stewart, M. and Ross, K. M. (1992) Compositional trends of minerals in oceanic cumulates. *Journal of Geophysical Research* 97, 15189-15199.

Emeleus, C. H., Cheadle, M. J., Hunter, R. H., Upton, B. G. J. and Wadsworth, W. J. (1996) The Rhum Layered Suite. *In* Cawthorn, R. G. (ed) *Layered Intrusions*. Developments in Petrology 15, Elsevier, 403-439.

Evans, W. J. (1992) Petrological investigation of the Wateranga layered intrusion, southeast Queensland. Unpublished BSc (Hons) Thesis. 92 pp.

Evans, W. J., Arculus, R. J. and Ashley, P. M. (1993) Petrological variation within the Wateranga layered intrusion, southeast Queensland. *In* Flood, P. G. (ed) *New England Orogen Conference Proceedings*. Department of Geology and Geophysics, University of New England, Armidale, Australia, 629-635.

Evensen, N. M., Hamilton, J. P. and O'Nions, R. K. (1978) Rare earth abundances in chondritic meteorites. *Geochimica et Cosomochimica Acta* 42, 1199-1212.

Faure, G. (1986) *Principles of Isotope Geochemistry, Second edition*. John Wiley and Sons, New York 589 pp.

Fergusson, C. L., Henderson, R. A., Leitch, E. C. and Ishiga, H. (1993) Lithology and structure of the Wandilla terrain, Gladstone-Yeppoon district, central Queensland and an overview of the Palaeozoic subduction complex of the New England Fold Belt. *Australian Journal of Earth Sciences* 40, 403-414.

Flood, P. G. (1988) New England Orogen: Geosyncline, Mobile Belt and Terrains. *In* Kleeman, J. D. (ed) *New England Orogen: Tectonics and Metallogenesis*. Department of Geology and Geophysis, University of New England, Armidale, Australia, 1-16.

Grieve, R. A. F. (1994) An impact model of the Sudbury structure. *In* Proceedings of the Sudbury-Noril'sk Symposium (P. C. Lightfoot and A. J. Naldrett eds). *Ontario Geological Survey Special Volume* 5, 119-132.

Grout, F. F. (1918) The lopolith; an igneous form exemplified by the Duluth Gabbro. *American Journal of Science* 46, 516-522.

Halliday, A. N. (1984) Coupled Sm-Nd and U-Pb systematics in late Caledonian granites and basement under northern Britain. *Nature* 307, 229-233.

Halliday, A. N., Dickin, A. P., Fallick, A. E. and Fitton, J. G. (1988) Mantle dynamics: a Nd, Sr, Pb and O isotopic study of the Cameroon line volcanic chain. *Journal of Petrology* 29, 181-211.

Halliday, A. N., Fallick, A. E., Dickin, A. P., MacKenzie, W. E., Stephens, A. B. and Hildreth, W. (1983) The isotopic and chemical evolution of Mount St. Helens (USA). *Earth and Planetary Science Letters* 63, 241-256.

Hamlyn, P. R. and Keays, R. R. (1986) Sulphur saturation and second-stage melts: application to the Bushveld platinum metal deposits. *Economic Geology* 81, 1431-1445.

Hamlyn, P. R., Keays, R. R., Cammeron, W. E., Crawford, A. J. and Waldron, H. M. (1985) Precious metals in magnesian low-Ti lavas: implications for metallogenesis and sulphur saturation in primary magmas. *Geochimica et Cosmochimica Acta* 9, 1791-1811.

Hanson, G. N. (1989) An approach to trace element modelling using a simple igneous system. *Reviews in Mineralogy* 21, 79-97.

Harmon, R. S. and Hoefs, J. (1995) Oxygen isotope heterogeneity of the mantle deduced from global ^{18}O systematics of basalts from different geotectonic settings. *Contributions to Mineralogy and Petrology* 120, 95-114.

Harrington, H. J. (1983) Correlation of the Permian and Triassic Gympie terrain of Queensland with the Brook Street and Maitai terrains of New Zealand. In *Permian Geology of Queensland.* Geological Society of Australia, Queensland Division, 431-436.

Harrington, H. J. and Korsch, R. J. (1985) Late Permian to Cainozoic tectonics of the New England Orogen. *Australian Journal of Earth Sciences* 32, 181-203.

Hart, S. R. and Allegre, C. J. (1980) Trace element constraints on magma genesis. *In* Hargraves, R. B. (ed) *Physics of Magmatic Processes*. Princeton, New Jersey, Princeton Press 121-159.

Hart, W. K., Gabriel, G. W., Walter, R. C. and Mertzman, S. A. (1989) Basaltic volcanism in Ethiopia: constraints on continental rifting and mantle interactions. *Journal of Geophysical Research* 94, 7731-7748.

Haskin, L. A. (1977) On the rare earth element behaviour in igneous rocks. *In* Ahrens, L. H. (ed). *The Origin and Distribution of the Elements*. Pergamon Press.

Haskin, L. A. (1984) Petrogenetic modelling – use of rare earth elements. *In* Henderson, P. (ed). *Rare Earth Element Geochemistry*. Elsevier. 115-152.

Hawkesworth, C. J., Blake, S., Evans, P., Hughes, R., Macdonald, R., Thomas, L. E., Turner, S. P. and Zellmer, G. (2000) Time scales of crystal fractionation in magma chambers – Integrating physical, isotopic and geochemical prospectives. *Journal of Petrology* 41, 991-1006.

Henderson, P. (1975) Geochemical indicator of the efficiency of fractionation of the Skaergaard intrusion, east Greenland. *Mineralogical Magazine* 40, 285-291.

Henderson, P. (1984) General geochemical properties and abundances of the rare earth elements. *In* Henderson, P. (ed). *Rare Earth Element Geochemistry*. Elsevier, Amsterdam Oxford, pp 10-55.

Henderson, R. A., Fergusson, C. L., Leitch, E. C., Morand, V. J., Reinhard, J. J. and Carr, P. F. (1993) Tectonics of the northern New England Fold Belt. *In* Flood, P. G. and Aitchison, J. C. (eds) *New England Orogen, Eastern Australia*. Department of Geology and Geophysics, University of New England, Armidale, Australia, 505-513.

Hess, H. H. (1960) Stillwater Igneous Complex, Montana – a quantitative mineralogical study. *Geological Society of America*, Memoir 80, 230 pp.

Hess, P. C. (1989) Origins of igneous rocks. Harvard University Press, Massachusetts, 336 pp.

Hoefs, J. (1987) Stable Isotope Geochemistry, Springer-Verlag, Berlin, 241 pp.

Hoefs, J. (1997) *Stable Isotope Geochemistry*. 4th enlarged edition, 201 pp Berlin, Heidelberg, New York (Springer).

Holcombe, R. J. and Little, T. A. (1994) Blueschists of the North D'Aguilar Block: structural development of the Rocksberg Greenstone and associated units near Mt Mee, southeast Queensland, *Australian Journal of Earth Sciences* 41, 115-130.

Holcombe, R. J., Stephens, C. J., Fielding, C. R., Gust, D., Little, T. A., Sliwa, R. McPhie, J. and Ewart, A. (1997b) Tectonic evolution of the northern New England Fold Belt: Carboniferous to Early Permian transition from active accretion to extension. *In* Ashley, P. M. and Flood, P. G. (eds) *Tectonics and Metallogenesis of the New England Orogen.* Geological Society of Australia Special Publication 19, pp 66-79.

Holcombe, R. J., Stephens, C. J., Fielding, C. R., Gust, D., Little, T. A., Sliwa, R., Kassan, J., McPhie, J. and Ewart, A. (1997a) Tectonic evolution of the northern New England Fold Belt: the Permian-Triassic Hunter-Bowen event. *In* Ashley, P. M. and Flood, P. G. (eds) *Tectonics and Metallogenesis of the New England Orogen.* Geological Society of Australia Special Publication 19, 52-65.

Holm, P. M. and Munksgaard, N. C. (1982) Evidence for mantle metasomatism: and oxygen and strontium isotope study of the Vusinian District, Central Italy. *Earth and Planetary Science Letters* 60, 376-388.

Hoover, J. D. (1978) Petrologic features of the Skaergaard margianl border group. *Year Book, Carnegie Iustn. Wash.* 77, 732-739.

Hoover, J. D. (1989) Petrology of the Marginal Border Series of the Skaergaard Intrusion. *Journal of Petrology* 30, 399-439.

Horan, M. F., Morgan, J. W., Walker, R. J. and Copper, R. W. (2001) Re-Os isotopic constraints on magma mixing in the Peridotite Zone of the Stillwater Complex Montana, USA. *Contributions to Mineralogy and Petrology* 141, 446-457.

Huppert, H. E. and Sparks, R. S. J. (1985) Cooling and contamination of mafic and ultramafic magmas during ascent through continental crust. *Earth and Planetary Science Letters* 105, 134-148.

Huppert, H. E. and Sparks, R. S. J. (1988) The generation of granitic magmas by intrusion of basalt into continental crust. *Journal of Petrology* 29, 599-624.

Huppert, H. E., Sparks, R. S. J., Wilson, J. R. and Hallworth, M. A. (1986) Cooling and crystallization at an inclined plane. *Earth and Planetary Science Letters* 79, 319-328.

Irvine, T. N. (1970) Crystallization sequences in the Muskox intrusion and other layered intrusions. I. Olivine-Pyroxene-Plagioclase relations: *Geological Society of South Africa Special Publication* 1, 441-476.

Irvine, T. N. (1979) Rocks whose compositions are determined by crystal accumulation and sorting. *In* Yoder, H. S. Jr. (ed) *Evolution of the Igneous Rocks*, Fiftieth Anniversary Perspective, Princeton, Princeton University Press 245-306.

Irvine, T. N. (1980) Magmatic infiltration metasomatism, double-diffusive fractional crystallization, and adcumulus growth in the Muskox intrusion and other layered intrusions. *In* Hargraves, R. B. (ed), *Physics of Magmatic Processes*, Princeton University Press, Princeton, N. J. 325-385.

Irvine, T. N. (1982) Terminology for layered intrusions. *Journal of Petrology* 23, 127-162.

Irvine, T. N. (1987) Appendix I. Glossary of terms for layered intrusions. *In* Parsons, I. (ed) *Origins of Igneous Layering*. Dortrecht, Reidel, 641-647.

Irvine, T. N. and Baragar, W. R. A. (1971) A guide to the geochemical classification of the common volcanic rocks. *Canadian Journal of Earth Sciences* 8, 523-548.

Irvine, T. N. and Smith, C. H. (1967) The ultramafic rocks of the Muskox intrusion, Northwest Territories, Canada, 38-49. *In* Wilson, P. J. (ed). *Ultramafic and Related Rocks*. John Wiley and Sons, Inc., New York, 464 pp.

Irvine, T. N., Keith, D. W. and Todd, S. G. (1983) The J-M platinum-palladium Reef of the Stillwater Complex, Montana: II Origin by double-diffusive convective magma mixing and implications for the Bushveld Complex. *Economic Geology* 78, 1287-1334.

Irving, A. J. and Dungan, M. A., eds. (1980) The Jackson Volume: a special volume of the American Journal of Science in Memory of Everett Dale Jackson. *American Journal of Science* 280, 1925-1978.

Jackson, E. D. (1961) Primary textures and mineral associations in the ultramafic zone of Stillwater complex. *U.S. Geological Survey Professional Paper* 358, 106 pp.

Jackson, E. D. (1970) The cyclic unit in layered intrusion-a comparison of repetitive stratigraphy in the ultramafic parts of the Stillwater, Muskox, Great Dyke and Bushveld complexes. *Geological Society of South Africa Special Paper* 1, 391-424.

Jahn, B. M., Auvray, B., Shen, Q. H. and 7 others (1988) Archaean crustal evolution in China: the Taishan Complex, and evidence for juvenile crustal addition from long-term depleted mantle. *Precambrian Research* 38, 381-403.

Jang, Y. D., Naslund, H. R. and McBirney, A. R. (2001) The differentiation trend of the Skaergaard intrusion and the timing of magnetite crystallization: Iron enrichment revisited. *Earth and Planetary Science Letters* 189, 189-196.

Jaques, A. L. and Green, D. H. (1980) Anhydrous melting of peridotite at 0-15 kb pressure and the genesis of tholeiitic basalts. *Contributions to Mineralogy and Petrology* 73, 287-310.

Johnson, C. M. (1991) Large scale crust formation and lithosphere modification beneath middle to late Cenozoic calderas and Volcanic fields, Western North America, *Journal of Geophysical Research* 96, 13485-13507.

Johnson, C. M. and O'Neil, J. R. (1984) Triple junction magmatism: a geochemical study of Neogene volcanic rocks in Western California. *Earth and Planetary Science Letters* 71, 241-262.

Keskin, M. (2002) FC-Modeler: a Microsoft Excel spreadsheet program for modelling Rayleigh fractionation vectors in closed magmatic systems. *Computers and Geosciences* 28, 919-928.

Klewin, K. W. (1990) Petrology of the Proterozoic Potato River layered intrusion, northern Wisconsin, USA. *Journal of Petrology* 31, 1115-1139.

Korsch, R. J. (1984) Sandstone compositions from the New England Orogen, eastern Australia: Implications for tectonic setting. *Journal of Sedimentary Petrology* 54, 192-211.

Kuno, H. (1968) Differentiation of basaltic magmas. *In* Hess, H. H. and Poldervaart, A. (eds) *Basalts*, New York, Wiley-Interscience, 623-688.

Kyser, T. K. (1986) Stable isotope variations in the mantle. In Stable Isotopes in High Temperature Geological Processes (eds J. W., Valley, et al.), *Reviews in Mineralogy* 16, 141-164.

Lambert, D. D., Unrush, D. M. and Simmons, E. C. (1985) Isotopic investigations of the Stillwater Complex: a review. *In* Czamanske, G. K. and Zientek, M. L. (eds) *Stillwater Complex*. Mont. Bur Mines Geol. Spec. Publ. 92, 46-54.

Langmuir, C. H., Vocke, R. D., Hanson, G. N. and Hart, S. R. (1978) A general mixing equation with applications to Icelandic basalts. *Earth and Planetary Science Letters* 37, 380-392.

Le Bas, M. J. (1962) The role of aluminium in igneous pyroxenes with relation to their parentage: *American Journal of Science* 260, 267-288.

Le Bas, M. J., Le Maitre, R. W., Streckeisen, A. and Zanettin, B. (1986) A chemical classification of volcanic rocks based on the total alkali-silica diagram. *Journal of Petrology* 27, 745-750.

Le Maitre, R. W. (1976) The chemical variability of some common igneous rocks. *Journal of Petrology* 17, 589-637.

Le Maitre, R. W. (1989) A classification of igneous rocks and glossary of terms. *Blackwell Scientific Publications*, 193 pp.

Leitch, E. C. (1974) The Geological development of the southern part of the New England Fold Belt. *Journal of Geological Society of Australia* 21, 133-156.

Leitch, E. C. (1975) Plate tectonic interpretation of the Paleozoic history of the New England Fold Belt. *Geological Society of America Bulletin* 86, 141-144.

Leitch, E. C., Fergusson, C. L., Henderson, R. A. and Morand, V. J. (1994) Late Palaeozoic arc flank and fore-arc basin sequence of the New England Fold Belt in the Stanage Bay region, central Queensland. *Australian Journal of Earth Sciences* 41, 301-310.

Lindsley, D. H. and Frost, B. R. (1992) Equilibria among Fe-Ti oxides, pyroxenes, olivine and quartz: Part I. Theory. *American Mineralogist* 77, 987-1003.

Little, T. A., Holcombe, R. J., Gibson, G. M., Offler, R., Gans, P. B. and McWilliams, M. O. (1992) Exhumation of Late Palaeozoic blueschists in Queensland, Australia, by extensional faulting. *Geology* 20, 231-234.

Lorand, J. P. (1990) Are spinel lherzolite xenoliths representative of the sulphur content of the upper mantle? *Geochimica et Cosmochimica Acta* 54, 1487-1492.

Loucks, R. R. (1990) Discrimination of ophiolitic from nonophiolitic ultramafic-mafic allochthons in orogenic belts by the Al/Ti ratio in clinopyroxene. *Geology* 18, 346-349.

Ludwig, K. R. (1994) Isoplot – a plotting and regression program for radiogenic-isotope data, Version 2.75. *USGS Open-File Report* 91-445.

MacDonald, G. A. and Katsura, T. (1964) Chemical composition of Hawaiian lavas. *Journal of Petrology* 5, 82-133.

Marsh, B. D. (1989) On convective style and vigour in sheet-like magma chambers. *Journal of Petrology* 30, 479-530.

Marsh, B. D. and Maxey, M. R. (1985) On the distribution and separation of crystals in convecting magma. *Journal of Volcanology and Geothermal Research* 24, 95-150.

Mathison, C. I. (1967) The Somerset Dam layered basic intrusion, southeast Queensland. *Journal of the Geological Society of Australia* 14, 57-86.

Mathison, C. I. (1987) Cyclic units in the Somerset Dam layered gabbro intrusion, southeast Queensland, Australia. *Lithos* 20, 187-205.

Mattey, P., Lowry, D. and MacPherson, A. (1994) Oxygen isotope composition of mantle peridotite. *Earth and Planetary Science Letters* 128, 231-242.

McBirney, A. R. (1975) Differentiation of the Skaergaard intrusion. *Nature* 253, 691-694.

McBirney, A. R. (1980) Mixing and unmixing of magmas. *Journal of Volcanology and Geothermal Research* 7, 357-371.

McBirney, A. R. (1989) The Skaergaard Layered Series: I. Structure and average compositions. *Journal of Petrology* 30, 363-397.

McBirney, A. R. (1993) *Igneous Petrology*, 2nd Ed., Boston: Jones and Bartlett, 508 pp.

McBirney, A. R. (1995) Mechanisms of differentiation of layered intrusions: Evidence from the Skaergaard intrusion. *Journal of Geological Society, London* 152, 421-435.

McBirney, A. R. (1996) The Skaergaard intrusion. *In* Cawthorn, R. G. (ed) *Layered Intrusions*. Developments in Petrology 15. Elsevier, 147-180.

McBirney, A. R. and Nakamura, Y. (1973) Immiscibility in late-stage magmas of the Skaergaard intrusion. *Carnegie Institute of Washington Year Book* 72, 348-352.

McBirney, A. R. and Naslund, H. R. (1990) The differentiation of the Skaergaard intrusion. A discussion of Hunter and Sparks (Contributions to Mineralogy and Petrology 95, 451-461). *Contributions to Mineralogy and Petrology* 104, 235-240.

McBirney, A. R. and Noyes, R. M. (1979) Crystallization and layering of the Skaergaard intrusion. *Journal of Petrology* 20, 487-554.

McBirney, A. R., Baker, B. H. and Nilson, R. H. (1985) Liquid fractionation. Part I. Basic principles and experimental simulations. *Journal of Volcanology and Geothermal Research* 24, 1-24.

McCallum, I. S. (1996) The Stillwater Complex. *In* Cawthorn, R. G. (ed) *Layered intrusions*. Developments in Petrology 15. Elsevier, 441-484.

McCallum, I. S., Raedeke, L. D. and Mathez, E. A. (1980) Investigations of the Stillwater Complex: I. Stratigraphy and structure of the banded zone. *American Journal of Science 280A,* 59-87.

McDonough, W. F., Sun, S., Ringwood, A. E., Jagoutz, E. and Hofmann, A. W. (1992) K, Rb and Cs in the earth and moon and the evolution of the earth's mantle. *Geochimica et Cosmochimica Acta*, Ross Taylor Symposium Volume.

Middlemost, E. A. K. (1975) The basalt clan. *Earth Science Reviews* 11, 337-364.

Miyashiro, A. (1974) Volcanic rock series in island arc and active continental margins. *American Journal of Science* 274, 321-355.

Miyashiro, A. (1978) Nature of alkalic volcanic rock series. *Contributions to Mineralogy and Petrology* 66, 91-104.

Miyashiro, A. and Shido, F. (1975) Tholeiitic and calc-alkalic series in relation to the behaviours of titanium, vanadium, chromium and nickel. *American Journal of Science* 275, 265-277.

Morris, J. D. and Hart, S. R. (1983) Isotopic and incompatible element constraints on the genesis of island arc volcanics from Cold Bay and Amak Island, Aleutians, and implications for mantle structure, *Geochimica et Cosmochimica Acta* 47, 2015-2030.

Morse, A. A. (1990) The differentiation of the Skaergaard intrusion. A discussion of Hunter and Sparks (Contributions to Mineralogy and Petrology 95, 451-461). *Contributions to Mineralogy and Petrology* 104, 240-244.

Morse, S. A. (1983) Emplacement history of the Nain Complex. *Univ. Mass. Geol. Dept. Contr.* 40, 9-15.

Mortensen, J. K. (1993) U-Pb geochronology of the eastern Abitibi Subprovince. Part I: Chibougamau – Matagami – Joutel region. *Canadian Journal of Earth Sciences* 30, 11-28.

Murray, C. G. (1975) 1:250,000 Geological Series-Explanatory Notes. Rockhampton, Queensland. Australian Government Publishing Service.

Murray, C. G. (1986) Metallogeny and tectonic development of the Tasman Fold Belt system in Queensland. *Ore Geology Reviews* 1, 315-400.

Murray, C. G. (1987) Tectonic evolution and metallogenesis of the New England Fold Belt, eastern Australia. *In* Proceedings Pacific Rim Congress 87, 353-358. Australian Institute of Mining and Metallurgy, Melbourne.

Murray, C. G. (1997) From geosyncline to fold belt: a personal perspective on the development of ideas regarding the tectonic evolution of the New England Orogen. *In* Ashley, P. M. and Flood, P. G. (eds) Tectonics and metallogenesis of the New England Orogen. *Geological Society of Australia Special Publication* 19, 1-28.

Murray, C. G., Fergusson, C. L., Flood, P. G., Whitaker, W. G. and Korsch, R. J. (1987) Plate tectonic model for the Carboniferous evolution of the New England Fold Belt. *Australian Journal of Earth Sciences* 34, 213-236.

Myers, J. S. (1988) Oldest known terrestrial anorthosite at Mount Narryer, Western Australia. *Precambrian Research* 38, 309-323.

Nakamura, E., Campbell, I. H., McCulloch, M. T. and Sun, S. S. (1989) Geochemical geodynamics in a back arc region around the sea of Japan: implications for the genesis of alkaline basalts in Japan, Korea and China. *Journal of Geophysical Research* 94, 4634-4654.

Nakamura, N. (1974) Determination of REE, Ba, Fe, Mg, Na and K in Carbonaceous and ordinary chondrites. *Geochimica et Cosmochimica Acta* 38, 757-775.

Naldrett, A. J. (1981) Platinum group element deposits. *In* Platinum Group Elements: Mineralogy, Geology, Recovery (L.J. Cabri, ed.). *Can. Inst. Min. Metall., Spec. Vol.* 23, 197-231.

Naldrett, A. J. and Duke, J. M. (1980) Platinum metals in magmatic sulphide ores. *Science* 208, 1417-1424.

Naldrett, A. J. and Gruenewaldt, G. (1989) Association of PGE with chromitite in layered intrusions and ophiolite complexes. *Economic Geology* 84, 180-187.

Naldrett, A. J. and MacDonald, A. J. (1980) Tectonic settings of Ni-Cu sulphide ores: their importance in genesis and exploration. *In* Strangway, D. W. Continental Crust and its Mineral Deposits. *Geological Association of Canada, Special Paper* 20, 633-657.

Naldrett, A. J., Brugmann, G. E. and Wilson, A. H. (1990) Models for the concentration of PGE in layered intrusions. *The Canadian Mineralogist* 28, 389-408.

Naslund, H. R. (1976) Mineralogical variations in the upper part of the Skaergaard intrusion, East Greenland. *Year Book, Carnegie Instn. Wash.* 75, 640-644.

Naslund, H. R. (1983) The effect of oxygen fugacity on liquid immiscibility in iron-bearing silicate melts. *American Journal of Science* 280-A, 159-170.

Naslund, H. R. (1989) Petrology of the Basistoppen Sill, East Greenland: a calculated magma differentiation trend. *Journal of Petrology* 30, 299-319.

Naslund, H. R. and McBirney, A. R. (1996) Mechanisms of formation of igneous layering. *In* Cawthorn, R. G. (ed). *Layered Intrusions*. Developments in Petrology 15. Elsevier, 1-44.

Natland, J. H., Meyer, P. S., Dick, H. J. B. and Bloomer, S. H. (1991) Magmatic oxides and sulphides in gabbroic rocks from Hole 735B and the later development of the liquid line of decent. In *Proceedings of the Ocean Drilling Program, Scientific Results* 118, 75-112.

Nesbitt, R. W. (1970) Report on the Westwood Gabbro Complex. BHP Co. Report 912.

Neumann, E. R., Larsen, B. T. and Sundvoll, B. (1985) Compositional variations among gabbroic intrusions in the Oslo rift. *Lithos* 18, 35-59.

Nwe, Y. Y. (1975) Two different pyroxene crystallization trends in the trough bands of the Skaergaard intrusion, East Greenland. *Contributions to Mineralogy and Petrology* 49, 285-300.

Nielson, T. F. D. and Brooks, C. K. (1995) Precious metals in magmas of East Greenland: factors important to the mineralization in the Skaergaard intrusion. *Economic Geology* 90, 1911-1917.

Nier, A. O. (1940) A mass spectrometer for routine isotope abundance measurements. *Rev. Sci. Instrum.* 11, 212-216.

Nier, A. O. (1981) Some reminiscences of isotopes, geochronology and mass spectrometry. *Annu. Rev. Earth and Planet. Sci.* 9, 1-17.

Nisbet, E. G. and Pearce, J. A. (1977) Clinopyroxene compositions in mafic lavas from different tectonic settings. *Contributions to Mineralogy and Petrology* 63, 149-160.

Norrish, K. and Chappell, B. W. (1977) X-ray fluorescence spectrometry. *In* Zussman, J. (ed) *Physical Methods in Determinative Mineralogy*. Academic Press, London, 201-272.

Ohmoto, H. (1986) Stable isotope geochemistry of ore deposits. *In* Stable Isotopes in High Temperature Geological Processes (eds J. W. Valley et al.) *Reviews in Mineralogy* 16, 491-559.

Paces, J. B. and Miller, J. D. Jr., (1993) Precise U-Pb ages of Duluth Complex and related mafic intrusions, northeastern Minnesota: new insights for physical, petrogenetic, paleomagnetic and tectono-magmatic processes associated with 1.1 Ga Midcontinent rifting. *Journal of Geophysical Research* 98, 13997-14013.

Palacz, Z. A. (1984) Isotopic and geochemical evidence for the evolution of a cyclic unit in the Rhum intrusion, northwest Scotland, *Nature* 307, 618-620.

Peach, C. L., Mathez, E. A. and Keays, R. R. (1990) Sulphide melt-silicate melt distribution coefficients for the noble metals and other chalcophile metals as deduced from MORB: implications for partial melting. *Geochimica et Cosmochimica Acta* 54, 3379-3389.

Pearce, J. A. (1987) An expert system for the tectonic characterization of ancient volcanic rocks (ESCORT). *Journal of Volcanology and Geothermal Research* 32, 51-65.

Pearce, J. A., Bender, J. F., De Long, S. E., Kidd, W. S. F., Low, P. J., Guner, Y., Saroglu, F., Yilmaz, Y., Moorbath, S. and Mitchell, J. G. (1990) Genesis of collision volcanism in Eastern Anatolia, Turkey. *Journal of Volcanology and Geothermal Research* 44, 189-229.

Peck, D. C. and Keays, R. R. (1990) Insights into the behaviour of precious metals in primitive, S-undersaturated magmas: evidence from the Heazlewood River Complex, Tasmania. *Canadian Mineralogist* 28, 553-577.

Peng, Z. X., Mahoney, J. J., Hooper, P. R., MacDougall, J. D. and Krishnamurthy, P. (1998) Basalts from the northeastern Deccan Traps, India: Isotopic and elemental geochemistry and relation to southwestern Deccan stratigraphy. *Journal of Geophysical Research* 103, 29843-29865.

Perry, F. V., DePaolo, D. J. and Baldridge, W. S. (1993) Neodymium isotopic evidence for decreasing crustal contributions to Cenozoic ignimbrites of the western United States: implications for the thermal evolution of the Cordilleran crust, *Geological Society of America Bulletin* 105, 872-882.

Petrini, R., Joron, J. L., Ottonello, G., Bonatti, E. and Seyler, M. (1988) Basaltic dykes from Zabargad island, Red Sea: petrology and geochemistry. *Tectonophysics* 150, 229-248.

Philpotts, A. R. (1990) *Principles of Igneous and Metamorphic Petrology*. Prentice Hall, New Jersey, 498 pp.

Poulson, S. R. and Ohmoto, H. (1990) An evaluation of the solubility of sulphide sulphur in silicate melts from experimental data and natural samples. *Chemical Geology* 85, 57-75.

Pye, E. G., Naldrett, A. J. and Giblin, P. E. (Editors) (1984) Geology and ore deposits of the Sudbury structure. *Ontario Geological Survey, Special Volume* 1, 603 pp.

Raedeke, L. D. and McCallum, I. S. (1984) Investigations of Stillwater Complex: II. Petrology and petrogenesis of the ultramafic series. *Journal of Petrology* 25, 395-420.

Ragland, P. C. (1989) *Basic Analytical Petrology*. Oxford University Press, Oxford, 369 pp.

Reeves, S. J. and Keays, R. R. (1995) The platinum group element geochemistry of the Bucknalla layered Complex, central Queensland. *Australian Journal of Earth Sciences* 42, 187-201.

Ripley, E. M., Lambert, D. D. and Erick, L. R. (1999) Re-Os, Sm-Nd, and Pb isotopic constraints on mantle and crustal contributions to magmatic sulphide mineralization in the Duluth complex. *Geochimica et Cosmochimica Acta* 62, 3349-3365.

Roberts, J. and Engel, B. A. (1980) Carboniferous palaeography of the Yarrol and New England Orogens eastern Australia. *Journal of the Geological Society of Australia* 27, 167-186.

Robertson, A. D. (1971) Preliminary report – Wateranga reserve. Geological Survey of Queensland, unpublished Report, 8 pp.

Robins, B. Haukvik, L. and Jansen, S. (1987) The organization and internal structure of cyclic units in the Honningsvas intrusive suites, North Norway: implications for intrusive mechanisms, double-diffusive convection and pore-magma infiltration. *In* Parsons, I (ed), *Origins of Igneous Layering*, NATO ASI Series C, Boston, 287-312.

Rollinson, H. (1993) *Using Geochemical Data: Evaluation, Presentation and Interpretation*. Longman Group UK Limited. 352 pp.

Ramos, V. A. and Kay, S. M. (1992) Southern Patagonian plateau basalts and deformation: back arc testimony of ridge collisions. *In* Oliver, R. A., Vatin-Perignon, N. and Laubacher, G. (eds) Andean geodynamics. *Tectonophysics* 205, 261-282.

Sakuyama, M. (1981) Petrological study of the Myoko and Kurohime volcanoes, Japan: crystallization sequence and evidence for mixing. *Journal of Petrology* 22, 553-583.

Saunders, A. D., Storey, M., Kent, R. W. and Norry, M. J. (1992) Consequences of plume-lithosphere interactions. *In* Storey, B. C., Alabaster, T. and Pankhurst, R. J. (eds) Magmatism and the causes of continental break up. *Geological Society Special Publication* 68, 41-60.

Sharpe, M. R. (1985) Strontium isotopic evidence for preserved density stratification in the main zone of the Bushveld Complex, South Africa. *Nature* 316, 119-126.

Sivell, W. J. and McCulloch, M. T. (1997) Geochemistry and Sm-Nd isotope systematics of Early Permian basalts from Gympie Province and fault basins in southeast Queensland: implications for mantle sources in a backarc setting at the Gondwana rim. *In* Ashley, P. M. and Flood, P. G. (eds) *Tectonics and Metallogenesis of the New England Orogen.* Geological Society of Australia, Special Publication 19, 148-160.

Sivell, W. J. and McCulloch, M. T. (2001) Geochemical and Nd-isotopic systematics of the Permo-Triassic Gympie Group, southeast Queensland. *Australian Journal of Earth Sciences* 48, 377-393.

Sivell, W. J. and Waterhouse, J. B. (1987) Volcanic rocks of the Highbury Volcanics and Rammutt Formation – remnant portion of an Early Permian intra-oceanic arc. *In* Murrary, C. G. and Waterhouse, J. B. (eds) 1987 *Field Conference, Gympie District*. Geological Society of Australia, Queensland Division, 34-43.

Smith, T. E., Huang, C. E., Walawender, M. J., Cheung, P. and Wheeler, C. (1983) The gabbroic rocks of the Peninsular Ranges batholith, southern California: Cumulate rocks associated with salc-alkaline basalts and andesites. *Journal of Volcanology and Geothermal Research* 18, 249-278.

Sorensen, H. S. and Wilson, J. R. (1995) A strontium and neodymium isotopic investigation of the Fongen-Hyllingen layered intrusions. *Journal of Petrology* 36, 161-187.

Sparks, R. S. J. (1986) The role of crustal contamination in magma evolution through time. *Earth and Planetary Science Letters* 78, 211-223.

Spera, F. J., Yuen, D. A. and Kemp, D. V. (1984) Mass transfer rates along vertical walls in magma chambers and marginal upwelling. *Nature* 310, 764-767.

Spera, F. J., Yuen, D. A. and Kirschvink, S. J. (1982) Thermal boundary layer convection in silicic magma chambers: effects of temperature-dependent

rheology and implications for thermogravitational chemical fractionation. *Journal of Geophysical Research* 87, 8755-8767.

Spera, F. J., Yuen, D. A., Clark, S. and Hong, H. J. (1986) Double diffusive convection in magma chambers: single or double layers? *Geophysical Research Letters* 13, 153-156.

Spulber, S. D. and Rutherford, M. J. (1981) The origin of rhyolite and plagiogranite in oceanic crust: An experimental study. *Journal of Petrology* 24, 1-25.

Staudigel, H., Muehlenbachs, K., Richardson, S. H. and Hart, R. (1981) Agents of low temperature ocean crust alteration. *Contributions to Mineralogy and Petrology* 77, 150-157.

Stein, M., Navon, O. and Kessel, R. (1997) Chromatographic metasomatism of the Arabian-Nubian lithosphere. *Earth and Planetary Science Letters* 152, 75-91.

Stern, R. J. (1979) On the origin of andesite in the northern Mariana island arc: Implications from Agrigan. *Contributions to Mineralogy and Petrology* 68, 207-219.

Stewart, B. W. and DePaolo, D. J. (1990) Isotopic studies of processes in mafic magma chambers: II. The Skaergaard intrusion, east Greenland. *Contributions to Mineralogy and Petrology* 104, 125-141.

Streckeisen, A. (1976) To each plutonic rock its proper name: *Earth-Science Reviews* 12, 1-33.

Sun, S. S. (1980) Lead isotopic study of young volcanic rocks from mid-ocean ridges, ocean islands and island arcs. *Philosophical Transactions of Royal Society* A297, 409-445.

Sun, S. S. (1982) Chemical composition and origin of the earth's primitive mantle. *Geochimica et Cosmochimica Acta* 46, 179-192.

Sun, S. S. and McDonough, W. F. (1989) Chemical and isotopic systematics of oceanic basalts: implications for mantle compositions and processes. *In* Saunders, A. D. and Norry, M. J. (eds) *Magmatism in the Ocean Basins*. Geological Society, London, Special Publication 42, 313-345.

Talusani, R. V. R. (2002) Geochemistry of the late Pleistocene alkalic basalts, southeast Queensland, Australia. Geological Society of New Zealand, Annual Conference, Northland, 2-5 December 2002.

Talusani, R. V. R. and Sivell, W. J. (2002) Nd-Sr-O isotopic and trace element characteristics of the Wateranga mafic layered intrusion, southeast Queensland, Australia: Implications for open system magmatic processes in a post-collisional setting. *Geological Society of Australia.* 16th Australian Geological Convention, Abstracts 67, 94 p.

Talusani, R. V. R., Sivell, W. J. and Ashley, P. M. (2000) The Wateranga intrusion, southeast Queensland, Australia: A high-Al and low-K mafic tholeiitic layered intrusion. *Geological Society of Australia, Abstracts* 59, 490 p.

Taylor, H. P. Jr. (1980) The effects of assimilation of country rocks by magmas on $^{18}O/^{16}O$ and $^{87}Sr/^{86}Sr$ systematics of igneous rocks. *Earth and Planetary Science Letters* 47, 243-254.

Taylor, H. P. Jr. (1986) Igneous rocks: II. Isotopic case studies of circumpacific magmatism. *In* Stable Isotopes in High Temperature Geological Processes (eds J. W. Valley et al.) *Reviews in Mineralogy* 16, 272-317.

Taylor, H. P. Jr. and Sheppard, S. M. F. (1986) Igneous rocks: I. Processes of isotopic fractionation and isotopic systematics. *In* Stable Isotopes in High Temperature Geological Processes (eds J. W. Valley et al.) *Reviews in Mineralogy* 16, 227-271.

Taylor, H. P. Tr., Turi, B. and Cundari, A. (1984) $^{18}O/^{16}O$ and chemical relationships in K-rich volcanic rocks from Australia, East Africa, Antarctica and San Venanzo-Cupaello, Italy. *Earth and Planetary Science Letters* 69, 263-276.

Taylor, S. R. and McLennan, S. M. (1985) *The Continental Crust: its Composition and Evolution.* Blackwell, Oxford 41-51, 312 pp.

Tegner, C. (1997) Iron in plagioclase as a monitor of the differentiation of the Skaergaard intrusion. *Contributions to Mineralogy and Petrology* 128, 45-51.

Tegner, C., Robins, B., Reginiussen, H. and Grundvig, S. (1999) Assimilation of crustal xenoliths in a basaltic magma chamber: Sr and Nd isotopic constraints from the Hasvik layered intrusion, Norway. *Journal of Petrology* 40, 363-380.

Theriault, R. D., Barnes, S. J. and Severson, M. J. (2000) Origin of Cu-Ni-PGE sulphide mineralization in the Partrige River intrusion, Duluth Complex, Minnesota. *Economic Geology* 95, 929-943.

Thompson, R. N. (1982) British Tertiary volcanic province. *Scottish Journal of Geology* 18, 49-107.

Thompson, R. N., Morrison, M. A., Dickin, A. P. and Hendry, G. L. (1983) Continental flood basalts .... arachnids rule OK?. *In* Hawkesworth, C. J. and Norry, M. J. (eds) *Continental Basalts and Mantle Xenoliths*. Shiva Nantwitch 158-185.

Tilley, C. E., Yoder, H. T. and Schairer, J. F. (1967) Melting relations of igneous rock series. *Carnegie Institute of Washington, Yearbook* 66, 260-269.

Tribuzio, R., Tiepolo, M., Vannucci, R. and Bottazzi, P. (1998) Ti-rich amphibole of igneous origin in MOR type gabbroic rocks (Northern Apennine ophiolites, Italy): and ion microprobe study. *Mineralogical Magazine* 62A, 1537-1538.

Turner, J. S. (1980) A fluid-dynamical model of differentiation and layering in magma chambers. *Nature* 285, 213-215.

Upton, B. G. J. (1988) History of Tertiary igneous activity in the N Atlantic borderlands. *In* Morton, A. C. and Parson, L. M. (eds) *Early Tertiary Volcanism and the Opening of The NE Atlantic*. Special Publication Geological Society of London 39, 429-454.

Viljoen, M. J. (1994) A review of regional variations in facies and grade distribution of the Merensky Reef, Western Bushveld Complex, with some mining implications. *In*: Anhaeusser, C. R. (ed.) *Proc. XVth CMMI Congress*. S. Afr. Inst. Mining Metal., Johannesburg, 3, 183-194.

Vogel, D. C. and Keays, R. R. (1997) The petrogenesis and platinum-group element geochemistry of the Newer Volcanic Province, Victoria, Australia. *Chemical Geology* 136, 181-204.

Wager, L. R. and Brown, G. M. (1968) *Layered Igneous Rocks*. Edinburgh, Oliver and Boyd, 538 pp.

Wager, L. R. and Deer, W. A. (1939) The petrology of the Skaergaard intrusion, Kangerdlugssuaq, east Greenland. Meddel. Groen. 105, 352 pp.

Wager, L. R., Brown, G. M. and Wadworth, W. J. (1960) Types of igneous cumulates. *Journal of Petrology* 1, 73-85.

Walker, D. and DeLong, S. E. (1982) Soret separation of MORB magma. *Contributions to Mineralogy and Petrology* 79, 231-240.

Walker, R. J. Morgan, J. W., Naldrett, A. J., Li, Chusi and Fassett, J. (1991) Re-Os isotopic systematics of Ni-Cu sulphide ores Sudbury igneous Complex, Ontario: evidence for a major crustal component. *Earth and Planetary Science Letters* 105, 416-429.

Weiblen, P. W. and Morey, G. B. (1980) A summary of the stratigraphy, petrology and structure of the Duluth Complex. *American Journal of Science* 280A, 88-133.

Wellman, P. (1978) Potassium-argon ages of Cainozoic volcanic rocks from Bundaberg, Rockhampton and Clermont areas of eastern Queensland. Proc. R. Soc. Qld 89, 59-64.

Wendlandt, R. F. (1982) Sulphide saturation of basalt and andesite melts at high pressures and temperatures. *American Mineralogist* 67, 877-885.

Wiebe, R. A. (1988) Structural and magmatic evolution of a magma chamber: the Newark Island Layered Intrusion, Nain Labrador. *Journal of Petrology* 29, 383-411.

Willams, R. J. (1971) Reaction constants in the system Fe-MgO-SiO_2-O_2 intensive parameters in the Skaergaard intrusion, East Greenland. *American Journal of Science* 271, 132-146.

Wilson, A. H., Naldrett, A. J. and Tredoux, M. (1989) Distribution and controls of platinum-group element and base metal mineralisation in the Darwendale subchamber of the Great Dyke, Zimbabwe. *Geology* 17, 649-652.

Wilson, J. R., Menuge, J. F., Pedersen, S. and Engell-Sorensen, O. (1987) The southern part of the Fongen-Hyllingen layered mafic complex, Norway: emplacement and crystallization of compositionally stratified magma. *In* Parsons, I. (ed.) *Origin of Igneous Layering*. D. Reidel Publishing Co., Dordrecht, 145-184.

Wilson, M. (1989) *Igneous Petrogenesis*. Unwin Hyman, London, 472 pp.

Wilson, M. M. and Mathison, C. I. (1968) The Eulogie Park Gabbro, a layered basic intrusion from eastern Queensland. *Journal of the Geological Society of Australia* 15, 139-158.

Wood, B. J. and Fraser, D. G. (1976) *Elementary Thermodynamics for Geologists*. Oxford University Press, Oxford, 303 pp.

York (1969) Least squares fitting of a straight line with correlated errors. *Earth and Planetary Science Letters* 5, 320-324.

Zindler, A., Staudigel, H. and Batiza, R. (1984) Isotope and trace element geochemistry of young Pacific seamounts: implications for the scale of upper mantle heterogeneity. *Earth and Planetary Science Letters* 70, 175-195.

Appendices

Appendix 1. X-ray fluorescence analysis

Introduction

Although the technique of X-ray fluorescence (XRF) analysis is normally attributed to the work of Moseley in the second decade of the 20th century, it was not until the development of commercial instrumentation in the 1960s that the technique became widely adopted in many geochemical laboratories. XRF was arguably the first technique to provide rapid, high precision, high sensitivity analytical measurements of the major elements and a range of geochemically important trace elements (including Ba, Cr, Cu, Ga, Nb, Pb, Rb, Sr, Th, V, Y, Zn, Zr) in silicate rocks.

Analytical details

All geochemical analyses were performed on carefully selected fresh samples, based on petrographic observations. Powders for whole-rock analyses were prepared by crushing in a tungsten carbide mill. Whole-rock major and trace elements were analyzed by X-ray fluorescence spectrometry using a fully automated SRS 300 Siemens spectrometer at the University of New England. Major element oxides were determined using 1:6 lithium tetraborate/lithium carbonate/lanthanum oxide glass disks, following analytical procedures of Norrish and Chappell (1977). Trace elements were analysed using pressed powder pellets (5 gms of sample) following analytical procedures of Chappell (1991). All samples were run in duplicate. International standards G-2, W-1, AGV-1, BCG-1, DTS-1, BHVO-1, GSP-1 and PCC-1 were used for quality control. Precision and accuracy for major and trace element analyses are respectively better than 1% and 5%. All chemical analyses were carried out using uniform calibration conditions to ensure internal consistency in the database. Ignition loss (LOI) was determined by gravimetry at 1100°C for one hour and FeO was determined by titration with a known concentration of ammonium ceric sulphate.

In this study, seventy-two whole-rock samples were analysed for major and trace elements by XRF. Additionally, 22 unpublished XRF analyses (analysed in 1974-75 using Siemens spectrometer at the Macquarie University) were provided by P. M. Ashley and 22 unpublished analyses (analysed using SRS 300 Siemens spectrometer

at the University of New England) were taken from Evans (1992). In the following pages complete XRF analyses are presented in Tables 1-3.

Rock names for the abbreviations used in Table 1

Olivine gabbro	OG
Anorthosite	A
Norite	N
Granite	GR
Olivine gabbronorite	OGN
Troctolite	T
Noritic gabbro	NG
Ferro gabbro	FG
Olivine noritegabbro	ONG
Olivine norite	ON
Anorthositic norite	AN
Picrite	P
Apatite-oxide-olivine rich rock	AOOR
Orthopyroxenite	OP
Hornblende rich norite	HN

Rock names for the abbreviations used in Table 3

Olivine gabbro	OG
Olivine gabbronorite	OGN
Orthopyroxenite	OP
Hornblende bearing gabbronorite	HGN
Hornblendite	H
Hornblende gabbro	HG
Norite	N
Pyroxene-hornblende gabbbronorite	PHGN
Granophyre	GRA

Table 1. Whole-rock major oxide (wt%) and trace element (ppm) analyses and calculated CIPW norms of the Wateranga intrusion *(data obtained for this study)*

Rock Type	OG	OG	A	OG	OG	OG	N	GR[d]	OGN[c]	OGN	OGN	OGN
Sample	WG7	WG16	WG26	WG27	WG31	WG35	WG38	WG39	WG44	WG55	WG58	WG70
SiO_2	48.03	47.04	51.29	47.15	48.17	47.46	48.71	77.01	47.10	48.52	47.40	48.32
TiO_2	0.78	0.98	0.15	0.90	2.20	1.14	0.60	0.04	1.61	0.63	0.29	0.46
Al_2O_3	16.52	15.86	27.48	17.85	22.09	17.07	16.56	13.95	15.92	18.39	18.07	17.93
Fe_2O_3	1.56	1.77	0.46	1.30	1.88	1.26	1.47	0.11	1.47	1.82	0.87	1.62
FeO	7.13	6.87	1.29	6.74	5.35	7.25	7.16	0.05	9.71	5.87	5.53	5.84
MnO	0.17	0.16	0.03	0.14	0.11	0.16	0.18	0.01	0.21	0.15	0.11	0.14
MgO	9.38	11.49	1.36	10.79	5.31	9.08	9.32	0.12	8.53	8.84	12.01	9.30
CaO	12.06	12.18	11.11	10.82	9.63	11.92	12.03	0.25	11.15	11.20	10.86	11.64
Na_2O	3.06	2.07	4.38	2.69	3.69	2.43	2.43	6.08	2.65	2.78	3.07	3.57
K_2O	0.14	0.09	0.16	0.09	0.15	0.10	0.11	1.94	0.12	0.17	0.11	0.13
P_2O_5	0.02	0.02	0.03	0.06	0.03	0.02	0.03	0.02	0.03	0.12	0.02	0.02
S	0.14	0.04	0.02	0.10	0.06	0.14	0.12	0.01	0.16	0.07	0.08	0.10
LOI	1.03	1.40	1.91	0.98	0.67	1.13	1.18	0.30	0.80	0.93	1.18	0.93
Total	**100.02**	**99.97**	**99.69**	**99.62**	**99.33**	**99.15**	**99.89**	**99.88**	**99.45**	**99.49**	**99.58**	**99.99**
Mg#[a]	72.06	76.67	65.17	76.74	70.72	72.87	71.53	68.90	66.01	73.25	80.95	74.33
CIPW normative minerals[b]												
Q								33.48				
Or	0.83	0.53	0.95	0.53	0.89	0.59	0.65	11.47	0.71	1.00	0.65	0.77
Ab	20.03	17.52	36.91	21.65	31.22	20.56	20.56	51.45	22.42	23.52	19.11	20.51
An	30.93	33.72	54.85	36.36	43.27	35.37	33.95	1.11	31.19	37.20	35.20	32.51
Ne	3.18		0.08	0.60							3.72	5.25
Di	23.31	21.39	0.06	13.62	3.50	19.12	20.70		19.55	14.22	14.84	20.27
Hy		1.11			1.64	2.61	5.48	0.48	1.37	3.41		
Ol	17.38	20.67	4.19	22.38	12.40	15.80	14.39		18.02	16.14	23.01	17.27
Mt	1.64	1.62	0.33	1.52	1.35	1.61	1.63	0.03	2.11	1.44	1.21	1.40
Ilm	1.48	1.86	0.28	1.71	4.18	2.16	1.14	0.08	3.06	1.20	0.55	0.87
Ap	0.05	0.05	0.07	0.14	0.07	0.05	0.07	0.05	0.07	0.28	0.05	0.05
Trace elements (ppm)												
Nb	<1	<1	<1	1	<1	2	<1	4	<1	<1	<1	1
Zr	19	22	4	15	27	21	18	100	30	70	12	13
Y	11	12	<1	8	<1	11	11	13	14	12	5	8
Sr	259	248	479	259	383	266	263	80	268	283	240	269
Rb	1	<1	3	1	2	<1	<1	44	<1	<1	<1	<1
Th	<2	4	<2	<2	4	5	<2	27	4	<2	6	<2
Pb	<2	<2	<2	<2	<2	4	<2	22	4	<2	<2	<2
As	<1	<1	4	<1	<1	<1	<1	<1	<1	<1	<1	<1
U	<1	<1	<1	<1	<1	<1	<1	7	<1	<1	<1	<1
Ga	15	15	22	13	18	14	14	10	14	16	14	13
Zn	54	55	12	57	42	53	52	<1	72	50	37	46
Cu	54	10	34	61	18	63	40	<2	63	59	82	49
Ni	87	172	29	155	51	88	67	<1	84	75	249	81
Cr	300	649	29	219	75	309	263	<3	219	214	490	309
Ce	<5	<5	12	6	7	12	9	47	<5	<5	13	12
Nd	3	14	4	5	7	13	6	23	15	12	10	11
Ba	44	43	143	26	108	51	78	126	100	160	32	83
V	199	247	20	129	231	208	191	<2	309	133	76	134
La	18	15	7	<3	11	8	<3	18	12	9	4	4
Sc	31	41	3	24	9	39	33	<2	27	27	19	28

[a] Mg# = 100Mg/(Mg + Fe^{2+}), calculated assuming Fe_2O_3/FeO = 0.15. [c] Fine grained samples

[b] Norms calculated on an anhydrous basis with iron ratio normalized to 0.15, as above. [d] Granite

Table 1. (Contd.)

Rock Type	N	OGN	A	A	T	T	OGN	OG	ONG[c]	OG	NG
Sample	WG75	WG84	WG92	WG96	WG103	WG108	WG115	WG123	WG124	WG128	NS2/1
SiO_2	48.36	48.42	52.07	51.50	48.08	50.16	48.97	48.05	48.76	48.83	49.91
TiO_2	0.54	0.88	0.51	0.28	2.24	0.36	0.43	0.75	0.37	0.44	1.61
Al_2O_3	17.20	16.87	28.29	27.94	22.03	24.21	16.41	16.50	17.19	17.75	15.08
Fe_2O_3	1.26	2.08	0.56	0.35	1.48	0.71	0.97	0.84	0.93	1.07	1.51
FeO	6.41	6.12	0.87	0.94	5.90	4.45	7.34	7.36	6.62	5.37	10.45
MnO	0.14	0.15	0.02	0.02	0.11	0.08	0.17	0.15	0.15	0.12	0.34
MgO	9.64	9.67	0.66	0.58	5.43	5.14	10.28	10.78	10.50	10.80	6.66
CaO	11.89	12.02	10.96	10.96	9.66	9.98	11.66	11.25	11.47	12.20	9.56
Na_2O	2.90	2.48	4.79	4.92	3.82	3.91	2.60	2.76	2.71	2.48	2.71
K_2O	0.11	0.10	0.19	0.38	0.16	0.17	0.10	0.11	0.10	0.07	0.19
P_2O_5	0.01	0.02	0.02	0.03	0.02	0.02	0.03	0.02	0.02	0.02	0.38
S	0.10	0.06	0.02	0.06	0.06	0.06	0.10	0.09	0.08	0.08	0.11
LOI	1.11	1.05	0.69	1.66	0.70	0.67	1.02	0.86	0.80	0.71	1.13
Total	**99.71**	**99.92**	**99.65**	**99.63**	**99.69**	**99.93**	**100.08**	**99.52**	**99.69**	**99.93**	**99.65**
Mg#[a]	74.59	74.41	63.02	56.39	70.56	69.94	73.72	75.77	75.89	79.62	57.99
CIPW normative minerals[b]											
Q											0.46
Or	0.65	0.59	1.12	2.25	0.95	1.00	0.59	0.65	0.59	0.41	1.12
Ab	21.75	20.99	38.94	35.92	31.10	33.09	22.00	22.14	22.93	20.99	22.93
An	33.59	34.60	54.24	53.03	42.49	48.01	32.81	32.31	34.44	37.09	28.42
Ne	1.51		0.86	3.09	0.66			0.66			
Di	20.45	20.10		0.95	4.30	1.12	20.07	18.83	17.99	18.67	13.65
Hy		3.30				0.39	3.08		0.68	1.62	25.63
Ol	17.99	15.88	2.13	1.80	13.69	13.88	17.96	20.98	20.01	18.25	
Mt	1.45	1.53	0.26	0.24	1.39	0.98	1.57	1.56	1.43	1.21	2.26
Ilm	1.03	1.67	0.97	0.53	4.25	0.68	0.82	1.42	0.70	0.84	3.06
Ap	0.02	0.05	0.05	0.07	0.05	0.05	0.07	0.05	0.05	0.05	0.90
Trace elements (ppm)											
Nb	<1	1	<1	<1	2	<1	<1	<1	<1	<1	4
Zr	13	20	8	7	29	10	21	26	15	15	115
Y	8	9	1	<1	2	<1	8	8	7	8	21
Sr	245	240	431	446	376	377	257	244	239	203	256
Rb	<1	<1	2	6	<1	<1	<1	<1	<1	1	4
Th	4	3	2	<2	4	3	6	6	<2	3	4
Pb	5	2	<2	<2	5	<2	<2	<2	<2	3	<3
As	<1	<1	<1	14	<1	<1	<1	<1	<1	<1	<1
U	<1	<1	<1	<1	<1	<1	2	<1	<1	<1	2
Ga	14	12	21	19	18	17	13	15	13	11	17
Zn	47	47	12	8	43	35	44	45	40	38	96
Cu	44	49	39	76	23	30	45	52	129	83	39
Ni	92	88	19	42	51	45	99	146	158	179	48
Cr	277	353	10	11	90	18	275	629	561	569	283
Ce	6	15	<5	<5	12	19	7	10	14	18	16
Nd	14	14	8	5	6	14	11	12	12	14	17
Ba	61	65	163	141	70	110	134	138	143	36	317
V	146	183	51	35	240	38	182	153	135	107	320
La	11	7	<3	5	13	5	8	6	9	<3	16
Sc	24	24	5	5	14	3	31	31	29	28	53

(continuted)

Table 1. (Contd.)

Rock Type	N	OG	T	FG	OG	NG	GR[d]	OGN	N	ON	ON
Sample	NS2/2	NS2/3	NS2/4	NS2/5	NS2/8	NS2/9	NS2/10	NS2/11	NS2/14	NS2/17	NS2/18
SiO_2	49.67	46.62	44.04	39.62	43.15	45.12	71.70	48.17	50.85	47.35	47.91
TiO_2	1.31	1.13	2.91	4.31	3.40	3.10	0.03	1.48	1.01	1.24	1.62
Al_2O_3	15.89	16.44	17.11	11.13	14.28	5.88	13.05	15.63	18.32	17.13	14.94
Fe_2O_3	1.25	2.11	3.42	3.18	4.64	4.70	0.17	1.87	1.53	2.02	2.70
FeO	9.27	11.90	11.69	17.35	8.26	15.46	0.81	8.32	7.82	5.85	8.81
MnO	0.25	0.28	0.27	0.38	0.23	0.46	0.12	0.22	0.21	0.15	0.24
MgO	6.98	6.87	5.01	8.02	5.31	11.74	0.71	7.20	5.54	8.09	7.66
CaO	10.35	8.96	7.68	9.15	11.69	6.80	3.10	10.77	8.10	11.51	11.09
Na_2O	2.65	2.94	3.47	2.38	2.99	1.35	4.24	3.52	3.97	2.93	2.67
K_2O	0.21	0.25	0.23	0.19	0.20	0.17	2.38	0.20	0.24	0.19	0.15
P_2O_5	0.48	0.63	1.32	2.31	2.42	1.02	0.02	0.07	0.34	0.06	0.09
S	0.11	0.17	0.15	0.30	0.23	0.55	0.02	0.13	0.12	0.15	0.21
LOI	1.18	1.57	2.36	1.42	3.13	3.37	3.34	2.28	1.66	2.82	1.58
Total	**99.61**	**99.88**	**99.66**	**99.74**	**99.93**	**99.71**	**99.69**	**99.86**	**99.71**	**99.48**	**99.66**
Mg#[a]	62.03	53.59	47.71	52.15	56.15	60.17	58.83	64.35	59.01	72.99	63.00
CIPW normative minerals[b]											
Q							30.77				
Or	1.24	1.48	1.36	1.12	1.18	1.00	14.07	1.18	1.42	1.12	0.89
Ab	22.42	24.88	29.36	20.14	25.30	11.42	35.88	26.72	33.59	23.44	22.59
An	30.84	30.92	29.48	19.12	24.95	9.48	9.54	26.26	31.46	33.03	28.34
Ne								1.66		0.73	
Di	14.27	7.82		9.31	14.27	14.48	4.70	21.87	5.37	19.16	21.40
Hy	22.87	9.96	9.40	6.56	6.02	46.16	1.07		15.64		7.64
Ol	1.08	16.79	15.64	24.31	10.10	1.01		14.81	5.96	14.97	11.46
Mt	1.99	2.64	2.83	3.87	2.38	3.77	0.18	1.92	1.76	1.47	2.15
Ilm	2.49	2.15	5.53	8.18	6.46	5.89	0.06	2.81	1.92	2.35	3.08
Ap	1.13	1.49	3.11	5.45	5.71	2.41	0.05	0.17	0.80	0.14	0.21
Trace elements (ppm)											
Nb	3	3	6	9	5	7	9	4	3	2	3
Zr	152	125	137	207	170	312	62	112	106	69	81
Y	28	23	24	53	54	36	21	18	13	12	15
Sr	259	285	331	227	274	106	22	256	338	233	240
Rb	7	5	2	5	4	6	169	2	3	4	3
Th	<2	6	5	8	4	<3	19	<2	4	3	4
Pb	<2	4	6	4	4	<3	23	3	4	<2	<2
As	<1	<1	<1	<1	<1	2	<1	5	<1	<1	<1
U	<1	<1	<1	<2	<1	<2	10	<1	<1	<1	<1
Ga	15	18	21	14	15	8	11	12	17	16	14
Zn	85	92	91	127	93	165	14	74	79	63	74
Cu	31	43	31	95	50	178	<2	45	35	61	59
Ni	70	61	13	50	28	126	<1	77	39	118	74
Cr	453	212	23	104	55	282	<3	324	130	360	352
Ce	47	31	49	85	83	44	30	33	27	<5	17
Nd	24	24	43	63	63	33	14	15	20	5	15
Ba	350	350	407	302	331	115	57	284	392	107	205
V	236	170	180	430	454	436	7	246	196	194	334
La	20	27	29	54	37	29	8	7	18	9	6
Sc	34	26	14	39	50	62	2	50	22	32	54

(continuted)

Table 1. (Contd.)

Rock Type	ON	N	ON	OG	T	N	OG	N	AN	N
Sample	NS2/19	NS2/22	NS2/29	NS2/31	NS2/33	NS2/34	NS2/35	NS2/40	NS2/41	NS2/42
SiO_2	47.53	45.49	48.74	43.74	45.20	48.04	45.59	49.41	51.35	50.85
TiO_2	1.58	4.03	1.37	2.29	4.52	1.42	1.05	2.06	1.33	1.28
Al_2O_3	15.45	10.73	16.05	15.50	14.89	15.70	16.93	20.42	20.76	18.31
Fe_2O_3	3.43	3.36	2.40	1.62	3.45	3.13	5.51	2.07	1.22	1.90
FeO	7.36	11.48	6.85	15.64	10.57	7.02	6.43	5.11	5.26	6.94
MnO	0.22	0.32	0.20	0.28	0.29	0.21	0.21	0.14	0.15	0.20
MgO	7.42	8.86	7.63	8.47	6.55	7.51	5.69	4.31	4.51	6.46
CaO	11.07	11.38	11.48	6.78	8.24	10.32	8.88	9.36	9.08	8.04
Na_2O	2.82	2.09	2.77	3.15	3.20	2.78	3.82	4.35	4.06	3.60
K_2O	0.19	0.14	0.12	0.17	0.16	0.13	0.18	0.22	0.25	0.21
P_2O_5	0.14	0.11	0.14	0.42	0.33	0.03	0.65	0.20	0.20	0.15
S	0.18	0.24	0.21	0.28	0.18	0.05	0.44	0.04	0.08	0.10
LOI	2.11	1.72	1.62	1.32	2.33	3.36	4.26	1.98	1.38	1.75
Total	**99.50**	**99.94**	**99.57**	**99.66**	**99.91**	**99.70**	**99.64**	**99.66**	**99.60**	**99.79**
Mg#[a]	64.17	64.70	68.09	55.16	61.00	65.61	54.04	65.66	65.79	65.16
CIPW normative minerals[b]										
Q										
Or	1.12	0.83	0.71	1.00	0.95	0.77	1.06	1.30	1.48	1.24
Ab	23.86	17.68	23.44	26.65	27.08	23.52	29.83	36.62	34.35	30.46
An	28.94	19.48	31.01	27.65	25.79	29.98	28.52	35.54	37.68	33.18
Ne							1.35	0.10		
Di	20.53	29.67	20.39	2.69	10.64	17.19	9.38	7.84	4.95	4.68
Hy	4.32	9.02	8.51	1.25	9.91	11.41			12.69	20.50
Ol	12.91	10.47	8.92	30.28	10.91	8.60	18.72	10.42	2.77	3.36
Mt	2.00	2.78	1.73	3.28	2.62	1.88	2.18	1.34	1.22	1.66
Ilm	3.00	7.65	2.60	4.35	8.58	2.70	1.99	3.91	2.53	2.43
Ap	0.33	0.26	0.33	0.99	0.78	0.07	1.53	0.47	0.47	0.35
Trace elements (ppm)										
Nb	3	5	3	3	5	3	1	4	3	2
Zr	88	108	64	78	93	75	47	101	103	74
Y	17	19	19	8	9	17	16	11	11	10
Sr	237	180	264	294	264	246	304	364	390	335
Rb	4	2	2	<1	2	<1	2	2	3	3
Th	3	<3	<2	4	<3	5	7	3	5	4
Pb	<2	<3	<2	4	<3	3	4	<2	3	3
As	<1	<1	<1	<1	<1	<1	<1	<1	<1	1
U	<1	2	<1	<2	<1	<1	<1	<1	<1	<1
Ga	14	12	14	15	16	15	15	19	19	17
Zn	72	91	73	106	80	74	73	60	51	74
Cu	57	74	49	82	62	49	36	33	18	34
Ni	79	65	68	68	29	66	41	31	20	42
Cr	330	231	334	81	85	342	119	65	70	95
Ce	20	21	25	31	9	25	29	18	42	17
Nd	19	20	20	16	12	17	24	15	23	11
Ba	204	227	178	274	219	259	312	440	523	383
V	285	670	260	232	581	236	210	239	212	235
La	6	16	17	17	15	11	19	20	15	14
Sc	42	85	46	17	33	44	17	26	23	22

(continuted)

Table 1. (Contd.)

Rock Type	ON	ON	OGN	OG	ON	OG	ON	OG	N	ON	ON
Sample	NS2/48	NS2/53	NS2/54	NS2/57	NS2/59	NS2/61	NS2/63	NS2/65	NS3/2	NS3/4	NS3/7
SiO_2	49.19	48.62	48.62	48.30	48.02	47.18	47.47	46.10	46.07	47.85	47.22
TiO_2	0.70	0.93	0.80	0.86	0.77	1.23	1.12	2.39	2.81	2.24	2.38
Al_2O_3	17.27	17.55	17.78	16.95	16.44	17.82	18.30	15.84	14.89	16.19	15.40
Fe_2O_3	1.22	2.32	2.43	2.09	2.31	2.01	2.59	3.20	3.68	4.13	3.75
FeO	6.44	5.91	5.43	6.10	6.55	6.97	4.64	7.01	8.55	7.07	7.88
MnO	0.15	0.14	0.14	0.15	0.17	0.15	0.13	0.19	0.21	0.20	0.22
MgO	9.18	8.50	8.39	9.16	9.06	9.81	8.84	8.35	8.14	7.21	7.71
CaO	11.67	10.92	10.83	11.16	10.73	10.13	10.74	10.27	10.56	10.13	10.63
Na_2O	3.07	2.89	3.19	2.99	3.05	2.95	2.87	2.90	2.48	2.77	2.54
K_2O	0.11	0.14	0.17	0.11	0.20	0.14	0.14	0.12	0.11	0.14	0.11
P_2O_5	0.02	0.03	0.05	0.04	0.03	0.07	0.04	0.07	0.02	0.06	0.02
S	0.08	0.15	0.18	0.09	0.14	0.10	0.13	0.31	0.11	0.14	0.25
LOI	0.89	1.72	1.73	1.71	2.25	1.04	2.58	3.12	2.26	1.71	1.80
Total	**99.98**	**99.83**	**99.73**	**99.72**	**99.71**	**99.58**	**99.57**	**99.87**	**99.89**	**99.84**	**99.90**
Mg#[a]	74.11	72.05	72.47	73.34	71.09	73.64	76.46	70.70	66.13	64.58	65.22
CIPW normative minerals[b]											
Q											
Or	0.65	0.83	1.00	0.65	1.18	0.83	0.83	0.71	0.65	0.83	0.65
Ab	24.67	24.45	26.66	24.90	24.78	24.19	24.29	24.54	20.99	23.44	21.49
An	33.02	34.50	33.69	32.50	30.58	34.97	36.64	29.85	29.17	31.33	30.29
Ne	0.71		0.18	0.22	0.55	0.42					
Di	19.99	15.78	15.96	18.27	18.22	11.99	13.19	16.75	18.86	15.17	18.25
Hy		4.61					1.76	1.42	7.28	12.41	10.75
Ol	17.14	14.28	17.10	18.01	18.71	21.80	16.46	16.39	12.71	8.08	9.48
Mt	1.44	1.53	1.46	1.53	1.65	1.68	1.34	1.89	2.27	2.07	2.16
Ilm	1.33	1.77	1.52	1.63	1.46	2.34	2.13	4.54	5.34	4.25	4.52
Ap	0.05	0.07	0.12	0.09	0.07	0.17	0.09	0.17	0.05	0.14	0.05
Trace elements (ppm)											
Nb	<1	3	2	1	<1	2	<1	3	3	3	4
Zr	49	95	108	50	75	74	68	96	40	34	25
Y	17	14	20	16	15	11	14	19	15	14	11
Sr	203	190	184	184	211	241	230	246	234	285	258
Rb	3	3	2	3	3	4	2	2	<1	<1	<1
Th	6	2	<2	<2	6	3	3	4	<2	6	<2
Pb	<2	3	<2	4	3	<2	4	3	<3	3	4
As	<1	<1	<1	<1	<1	<1	<1	<1	<1	<1	<1
U	<1	<1	<1	<1	<1	<1	<1	<1	<1	2	3
Ga	14	15	15	15	14	15	16	16	17	17	15
Zn	58	64	65	66	71	63	61	75	94	86	84
Cu	49	57	74	51	80	72	80	41	56	45	55
Ni	96	108	115	102	124	196	237	80	90	29	51
Cr	407	263	280	402	350	298	446	296	423	144	152
Ce	19	23	26	8	18	19	18	16	13	17	14
Nd	10	17	8	15	13	8	8	3	13	14	13
Ba	128	124	134	118	113	123	118	201	84	117	117
V	140	146	151	157	146	162	156	326	482	324	465
La	7	7	12	18	13	13	5	9	8	8	10
Sc	37	29	32	31	30	28	28	48	39	37	47

(continuted)

Table 1. (Contd.)

Rock Type	N	T	OGN	N	N	OGN	AN	N	T	N	N
Sample	NS3/8	NS3/10	NS3/12	NS3/18	NS3/20	NS3/25	NS3/28	NS3/31	NS3/32	NS3/34	NS3/38
SiO_2	49.56	48.55	47.17	48.23	50.06	47.09	50.93	49.35	50.88	51.03	51.45
TiO_2	2.09	2.07	1.88	1.49	0.95	1.42	0.36	0.34	0.25	0.41	0.35
Al_2O_3	16.72	23.15	16.43	16.27	16.58	16.32	17.77	17.70	20.64	16.76	17.96
Fe_2O_3	2.40	1.80	3.44	2.58	2.05	1.45	1.67	2.49	1.57	1.23	1.86
FeO	7.12	4.83	6.40	6.97	6.10	8.38	4.80	4.38	3.48	4.66	2.93
MnO	0.19	0.10	0.18	0.17	0.16	0.17	0.15	0.15	0.12	0.14	0.12
MgO	7.53	3.70	7.68	8.24	8.20	9.31	8.86	9.58	7.35	9.66	9.21
CaO	9.72	9.49	11.15	10.82	10.39	11.12	10.18	10.55	11.35	11.65	11.81
Na_2O	2.91	3.95	2.58	2.39	2.60	2.64	2.71	2.53	2.90	2.46	2.75
K_2O	0.14	0.21	0.12	0.13	0.17	0.13	0.10	0.09	0.14	0.08	0.09
P_2O_5	0.02	0.02	0.02	0.02	0.01	0.02	0.01	0.01	0.01	0.01	0.02
S	0.13	0.08	0.19	0.17	0.06	0.13	0.05	0.03	0.06	0.08	0.05
LOI	1.00	1.88	2.02	1.88	2.53	1.22	1.73	2.79	0.95	1.31	1.04
Total	**99.53**	**99.85**	**99.26**	**99.35**	**99.86**	**99.39**	**99.33**	**99.99**	**99.67**	**99.49**	**99.63**
Mg#[a]	69.33	65.08	68.51	69.43	71.47	70.78	75.93	76.36	76.99	79.24	82.06
CIPW normative minerals[b]											
Q											
Or	0.83	1.24	0.71	0.77	1.00	0.77	0.59	0.53	0.83	0.47	0.53
Ab	24.62	33.42	21.83	20.22	22.00	22.34	22.93	21.41	24.54	20.82	23.27
An	32.15	44.82	32.90	33.28	33.07	32.30	36.03	36.67	42.89	34.45	36.40
Ne											
Di	12.96	1.75	18.14	16.48	14.93	18.45	11.61	12.56	10.74	18.67	17.62
Hy	18.14	1.79	7.04	14.81	19.97	0.42	21.05	14.52	12.57	17.46	13.68
Ol	3.79	9.54	10.77	6.96	2.85	19.16	3.33	9.38	5.59	4.27	5.33
Mt	1.78	1.24	1.82	1.78	1.52	1.86	1.21	1.27	0.94	1.10	0.88
Ilm	3.97	3.93	3.57	2.83	1.80	2.70	0.68	0.65	0.47	0.78	0.66
Ap	0.05	0.05	0.05	0.05	0.02	0.05	0.02	0.02	0.02	0.02	0.05
Trace elements (ppm)											
Nb	3	3	4	1	<1	2	<1	<1	<1	<1	<1
Zr	22	14	32	28	25	20	9	8	5	7	9
Y	9	<1	17	12	10	11	5	7	5	6	6
Sr	306	417	274	250	318	241	315	273	288	225	277
Rb	<1	<1	<1	<1	3	1	<1	1	<1	<1	1
Th	4	<2	<2	4	2	2	4	<2	2	4	5
Pb	<2	<2	<2	<2	<2	<2	2	<2	<2	<2	<2
As	<1	1	<1	28	3	3	<1	<1	<1	<1	<1
U	<1	<1	<1	<1	<1	<1	<1	<1	<1	<1	<1
Ga	17	21	18	16	16	15	15	14	14	12	13
Zn	66	43	76	74	66	67	48	44	36	39	30
Cu	50	22	49	55	39	47	31	40	18	34	30
Ni	31	31	80	77	59	97	68	74	51	60	43
Cr	131	34	194	184	204	246	246	251	178	329	267
Ce	16	<5	21	27	13	<5	17	<5	10	<5	7
Nd	12	6	13	11	5	7	12	7	5	5	8
Ba	104	142	106	74	162	63	82	22	98	30	33
V	274	208	289	308	213	210	145	139	121	167	129
La	9	<3	<3	5	<3	14	11	<3	<3	11	<3
Sc	34	14	36	39	44	27	30	28	29	34	38

(continuted)

Table 1. (Contd.)

Rock Type	A	P	N	AOOR	OP	HN
Sample	NS3/40	NS3/51	NS3/53	NS5/4	NS5/6	NS5/23
SiO_2	51.67	43.64	48.43	20.77	40.59	47.79
TiO_2	0.15	0.15	1.72	10.78	2.69	1.14
Al_2O_3	25.92	15.97	16.58	3.36	3.70	16.84
Fe_2O_3	0.41	2.07	2.50	9.22	5.70	1.29
FeO	1.58	7.60	7.08	25.22	23.65	6.71
MnO	0.04	0.14	0.20	0.63	0.66	0.15
MgO	2.67	16.56	9.39	4.60	7.98	9.72
CaO	10.49	7.23	8.87	12.04	9.06	10.95
Na_2O	4.43	1.71	2.64	2.25	1.23	2.81
K_2O	0.22	0.10	0.10	0.46	0.55	0.53
P_2O_5	0.02	0.02	0.02	8.57	1.53	0.14
S	0.07	0.12	0.19	0.70	0.04	0.06
LOI	2.14	4.91	2.05	1.38	2.09	1.95
Total	**99.82**	**100.22**	**99.78**	**99.99**	**99.47**	**100.06**
Mg#[a]	75.95	79.14	72.59	30.07	39.38	75.60
CIPW normative minerals[b]						
Q						
Or	1.30	0.59	0.59	2.72	3.25	3.13
Ab	37.49	14.47	22.34	2.27	10.41	21.81
An	50.19	35.60	33.09		2.95	31.77
Ne				6.74		1.06
Di	1.39	0.11	8.73	3.21	27.11	17.44
Hy	0.73	8.16	19.10		18.24	
Ol	5.79	34.03	8.46	33.83	21.03	18.83
Mt	0.37	1.81	1.79	4.52	5.51	1.51
Ilm	0.28	0.28	3.27	20.47	5.11	2.16
Ap	0.05	0.05	0.05	20.22	3.61	0.33
Trace elements (ppm)						
Nb	<1	<1	3	29	7	4
Zr	5	8	24	219	172	84
Y	1	2	7	177	86	22
Sr	431	144	246	104	38	218
Rb	4	2	<1	14	19	15
Th	2	3	<2	9	5	6
Pb	3	4	3	6	7	5
As	<1	<1	<1	<1	<1	<1
U	<1	<1	<1	4	2	<1
Ga	21	11	16	14	18	15
Zn	13	71	83	214	274	65
Cu	42	115	54	184	19	46
Ni	56	203	84	46	133	119
Cr	32	33	292	146	194	407
Ce	<5	14	11	174	96	9
Nd	5	8	<3	153	68	15
Ba	130	14	72	92	130	67
V	30	22	258	784	295	191
La	<3	13	22	75	55	9
Sc	13	6	35	51	109	29

Table 2. Whole-rock major oxide (wt%) and trace element (ppm) analyses and calculated CIPW norms of the Wateranga intrusion *(P. M. Ashley, unpublished data)*

Sample	A-WG1	A-WG2	A-WG3	A-WG4	A-WG5	A-WG6	A-WG7	A-WG8
SiO_2	48.48	53.14	51.11	49.99	48.98	50.19	49.91	48.94
TiO_2	0.54	0.64	0.78	0.30	0.30	0.52	1.08	0.40
Al_2O_3	16.89	24.20	18.37	17.80	20.39	15.42	16.98	17.11
Fe_2O_3	1.35	1.22	1.46	1.17	0.95	1.53	1.60	1.41
FeO	7.21	2.75	4.71	5.71	4.66	6.79	7.42	7.76
MnO	0.15	0.07	0.12	0.13	0.10	0.17	0.17	0.16
MgO	11.33	2.79	7.63	10.07	9.37	9.49	8.30	9.61
CaO	10.56	9.56	13.12	11.91	12.97	12.87	11.11	11.53
Na_2O	2.67	4.91	2.75	2.54	2.01	2.15	2.64	2.47
K_2O	0.06	0.22	0.12	0.08	0.10	0.09	0.09	0.07
P_2O_5	0.01	0.10	0.03	0.03	0.04	0.04	0.02	0.02
LOI	0.76	0.57	0.65	1.07	1.34	1.25	1.21	1.21
Total	**100.01**	**100.17**	**100.85**	**100.80**	**101.21**	**100.51**	**100.53**	**100.69**
Mg#[a]	75.40	65.18	75.69	76.81	79.29	72.51	69.54	70.35
CIPW normative minerals[b]								
Q								
Or	0.35	1.30	0.71	0.47	0.59	0.53	0.53	0.41
Ab	22.59	41.55	23.27	21.49	17.01	18.19	22.34	20.90
An	33.92	43.34	37.43	36.93	46.32	32.16	34.22	35.39
Ne								
Di	14.83	2.81	22.14	17.67	14.24	25.44	16.88	17.60
Hy	3.26	2.65	7.47	7.43	8.31	12.75	13.93	6.62
Ol	21.60	5.70	6.42	13.77	11.65	7.50	7.58	15.99
Mt	1.61	0.74	1.15	1.30	1.06	1.56	1.70	1.73
Ilm	1.03	1.22	1.48	0.57	0.57	0.99	2.05	0.76
Ap	0.02	0.24	0.07	0.07	0.09	0.09	0.05	0.05
Trace elements (ppm)								
Zr	22	108	67	34	59	63	25	20
Y	9	12	20	10	11	18	14	13
Sr	259	518	348	341	305	288	352	335
Rb	1.5	3	0.8	<0.5	0.6	2.5	0.5	1.4
Th	3.8	1.2	2.6	1.4	0.6	3.1	<0.5	3.2
Pb	7.2	3.2	3.2	1	2.4	5.5	5.4	5.9
U	1.6	0.9	<0.5	1.5	<0.5	1.2	<0.5	1.2
Ga	13	21	18	14	16	12	17	13
Zn	48	26	38	40	37	50	55	57
Cu	117	23	76	38	121	109	52	70
Ni	193	33	83	101	186	158	84	80
Cr	520	19	402	350	645	1159	215	300
V	106	55	166	101	73	165	201	116

[a] Mg# = 100Mg/(Mg + Fe^{2+}), calculated assuming Fe_2O_3/FeO = 0.15.

(continued)

[b] Norms calculated on an anhydrous basis with iron ratio normalized to 0.15, as above.

Table 2. (Contd.)

Sample	A-WG9	A-WG10	A-WG11	A-WG12	A-WG13	A-WG14	A-WG15	A-WG16
SiO_2	51.32	50.71	48.88	51.79	47.57	47.69	48.47	48.96
TiO_2	0.48	0.94	0.75	0.33	2.03	1.57	0.89	0.25
Al_2O_3	20.96	22.58	15.18	17.42	19.22	16.43	17.49	16.93
Fe_2O_3	1.95	1.83	1.56	0.98	0.87	1.76	1.89	3.39
FeO	5.18	4.98	7.09	4.19	12.49	7.60	6.17	5.54
MnO	0.13	0.10	0.15	0.12	0.21	0.16	0.14	0.14
MgO	7.33	5.53	12.59	8.74	3.14	8.67	9.52	11.04
CaO	9.27	9.74	10.97	12.30	8.40	12.28	11.99	10.65
Na_2O	3.28	3.70	2.42	2.25	3.83	2.28	2.18	2.67
K_2O	0.12	0.13	0.10	0.14	0.25	0.08	0.06	0.06
P_2O_5	0.03	0.03	0.08	0.03	1.01	0.03	0.03	0.03
LOI	0.70	0.71	0.82	0.92	1.79	1.22	1.22	1.27
Total	**100.75**	**100.98**	**100.59**	**99.21**	**100.81**	**99.77**	**100.05**	**100.93**
Mg#[a]	70.77	67.71	77.66	79.60	37.59	71.06	74.50	73.83
CIPW normative minerals[b]								
Q				0.67				
Or	0.71	0.77	0.59	0.83	1.48	0.47	0.35	0.35
Ab	27.75	31.31	20.48	19.04	32.41	19.29	18.45	22.59
An	42.11	44.62	30.26	37.02	34.51	34.36	37.76	34.03
Ne								
Di	2.99	2.86	19.00	19.08	0.48	21.39	17.38	15.03
Hy	17.07	8.08	5.75	19.96	12.07	5.99	9.93	4.80
Ol	7.00	9.42	20.41		9.43	12.18	11.61	20.43
Mt	1.33	1.27	1.63	0.97	2.54	1.76	1.51	1.65
Ilm	0.91	1.79	1.42	0.63	3.85	2.98	1.69	0.47
Ap	0.07	0.07	0.19	0.07	2.38	0.07	0.07	0.07
Trace elements (ppm)								
Zr	18	18	45	17	1356	36	20	12
Y	5	2	20	11	23	14	21	4
Sr	430	401	113	211	415	259	270	74
Rb	2	1.5	2.4	4.3	2.5	0.6	0.8	<0.5
Th	1.9	1.3	<0.5	<0.5	<0.5	<0.5	<0.5	0.8
Pb	2.7	3.1	<0.5	8.3	10.7	5.7	7.3	5.7
U	<0.5	1.1	<0.5	1.9	1	<0.5	2.2	<0.5
Ga	17	22	16	14	25	16	17	6
Zn	56	38	57	36	67	60	53	47
Cu	22	28	70	81	34	67	68	68
Ni	56	67	268	88	16	92	132	1102
Cr	32	55	802	1020	20	273	523	3179
V	54	94	147	173	148	179	207	51

(continued)

Table 2. (Contd.)

Sample	A-WG17	A-WG18	A-WG19	A-WG22	A-WG23	A-WG24
SiO_2	48.07	53.22	44.94	46.18	47.78	24.79
TiO_2	0.71	0.18	1.39	2.89	1.36	8.28
Al_2O_3	19.84	28.39	8.76	15.52	15.75	3.45
Fe_2O_3	1.29	0.16	1.49	2.74	1.60	22.34
FeO	4.73	0.61	10.66	11.94	8.00	21.37
MnO	0.10	0.01	0.19	0.38	0.16	0.50
MgO	10.25	0.36	22.12	4.12	5.10	4.75
CaO	12.00	11.55	7.51	10.05	14.74	9.52
Na_2O	2.23	4.53	0.23	2.79	2.73	0.44
K_2O	0.01	0.33	0.04	0.69	0.29	0.19
P_2O_5	0.03	0.03	0.24	0.52	0.15	1.85
LOI	1.14	1.28	1.47	1.39	2.24	1.66
Total	**100.40**	**100.65**	**99.04**	**99.21**	**99.90**	**99.14**
Mg#[a]	80.94	57.84	81.75	43.29	57.59	23.78
CIPW normative minerals[b]						
Q		0.22				
Or	0.06	1.95	0.24	4.08	1.71	
Ab	18.87	38.33	1.95	23.61	17.85	
An	44.10	56.16	22.75	27.79	29.86	6.88
Ne					2.85	2.02
Di	12.19	0.78	10.34	15.74	34.94	10.18
Hy	5.80	1.37	32.72	8.52		
Ol	15.65		24.09	8.56	5.67	42.77
Mt	1.13	0.14	2.30	2.76	1.81	7.95
Ilm	1.35	0.34	2.64	5.49	2.58	15.72
Ap	0.07	0.07	0.57	1.23	0.35	4.36
Trace elements (ppm)						
Zr	20	6	114	345	94	7668
Y	12	1	23	71	37	180
Sr	142	459	13	314	219	41
Rb	<0.5	5.1	<0.5	11.2	8.7	1.8
Th	0.7	<0.5	0.6	0.7	<0.5	6.7
Pb	5.2	3.3	7.9	10.7	6.8	15.5
U	<0.5	0.8	0.9	<0.5	0.5	8.5
Ga	15	22	12	30	22	23
Zn	40	7	93	130	86	415
Cu	66	10	61	49	57	44
Ni	283	15	947	46	110	9
Cr	228	5	1509	21	305	80
V	104	21	166	183	237	337

Table 3. Whole-rock major oxide (wt%) and trace element (ppm) analyses of the Wateranga intrusion *(Evans (1992), unpublished data)*

Rock Type	OG	OGN	OGN	OGN	OGN	OG	OGN	OGN	OP
Sample	E-NS2/1	E-NS2/4	E-NS2/9	E-NS2/17	E-NS2/29	E-NS3/3	E-NS5/1	E-NS5/2	E-NS5/3
SiO_2	49.38	39.21	50.47	41.39	48.90	47.15	42.20	46.77	36.04
TiO_2	1.46	5.24	1.11	2.20	0.88	2.77	3.16	2.82	5.28
Al_2O_3	14.43	13.29	18.53	9.21	19.24	15.25	12.01	12.48	4.50
Fe_2O_3	2.02	3.81	2.06	8.45	1.02	2.71	23.57	19.62	7.77
FeO	9.84	15.15	7.53	16.48	7.35	9.75	-	-	24.75
MnO	0.28	0.32	0.21	0.41	0.14	0.20	0.45	0.39	0.58
MgO	6.92	6.01	4.96	11.39	8.34	7.10	3.53	3.14	5.88
CaO	10.51	9.28	8.61	3.83	10.25	10.95	8.89	9.75	10.30
Na_2O	2.62	3.16	3.90	1.53	3.37	2.63	2.72	3.05	0.95
K_2O	0.20	0.24	0.24	0.11	0.10	0.13	0.49	0.49	0.15
P_2O_5	0.25	2.71	0.34	0.26	0.03	0.01	2.28	1.52	3.13
S	0.17	0.23	0.19	1.10	0.10	0.20	0.25	0.24	0.04
LOI	2.30	2.19	1.04	2.13	0.92	1.69	0.40	0.24	1.66
Total	**100.38**	**100.84**	**99.19**	**98.49**	**100.64**	**100.54**	**99.95**	**100.51**	**101.03**
Mg#[a]	59.07	49.62	56.08	52.70	70.76	62.09	29.50	31.16	32.35
CIPW normative minerals[b]									
Q									
Or	1.18	1.42	1.42	0.65	0.59	0.77	2.90	2.90	0.89
Ab	22.17	25.42	33.00	12.95	27.90	22.25	23.02	25.81	8.04
An	27.02	21.37	32.35	17.30	37.08	29.42	19.11	18.91	7.57
Ne		0.71			0.34				
Di	19.37	5.82	6.75		11.02	20.40	8.66	16.72	19.73
Hy	20.22		13.93	32.57		7.77	16.56	20.92	22.87
Ol	2.31	23.75	5.74	21.64	19.38	10.31	11.62	0.78	16.51
Mt	2.23	3.56	1.80	4.61	1.58	2.34	4.06	3.38	6.08
Ilm	2.77	9.95	2.11	4.18	1.67	5.26	6.00	5.35	10.03
Ap	0.59	6.39	0.80	0.61	0.07	0.02	5.38	3.59	7.38
Trace elements (ppm)									
Nb	6	14	4	5	2	5	12	17	11
Zr	130	231	152	87	37	30	99	90	193
Y	26	61	13	9	8	13	67	83	108
Sr	234	280	352	151	210	266	254	262	83
Rb	8	6	5	4	3	3	7	10	3
Th	2	2	2	2	1	2	3	4	5
Pb	5	5	5	6	4	2	7	9	7
As	2	<1	4	<1	<1	<1	3	3	<1
U	2	2	<2	<2	2	3	2	3	5
Ga	16	16	20	11	17	15	18	21	19
Zn	107	120	75	172	61	89	170	151	276
Cu	56	78	57	180	69	57	78	88	31
Ni	231	94	70	144	143	59	13	11	89
Cr	289	32	124	94	175	115	24	23	85
Ce	27	84	20	18	9	8	49	51	95
Nd	21	77	18	9	6	6	44	53	92
Ba	315	375	407	203	145	135	189	212	86
V	279	447	192	268	111	411	136	206	183
La	14	38	14	10	5	4	25	24	47
Sc	52	32	22	25	20	51	60	79	114

[a] Mg# = 100Mg/(Mg + Fe^{2+}), calculated assuming Fe_2O_3/FeO = 0.15.

(continued)

[b] Norms calculated on an anhydrous basis with iron ratio normalized to 0.15, as above.

Table 3. (Contd.)

Rock Type	HGN	H	HG	N	PHGN	PHGN	PHGN	HG	HG
Sample	E-NS5/4	E-NS5/5	E-NS5/6	E-NS5/7	E-NS5/8	E-NS5/9	E-NS5/10	E-NS5/11	E-NS5/12
SiO_2	47.30	36.82	45.96	48.77	45.11	48.27	48.63	48.44	47.59
TiO_2	2.03	4.19	2.01	1.73	1.73	1.59	0.99	1.52	2.16
Al_2O_3	18.29	9.50	14.37	18.71	13.74	15.67	17.52	17.17	15.98
Fe_2O_3	15.74	26.01	13.51	9.76	14.72	10.12	7.71	9.88	13.81
FeO	-	-	-	-	-	-	-	-	-
MnO	0.25	0.40	0.24	0.16	0.25	0.16	0.13	0.15	0.38
MgO	2.87	7.03	8.16	2.54	8.16	9.08	9.10	6.70	5.80
CaO	7.72	9.18	9.70	7.75	10.06	9.86	10.61	9.47	4.84
Na_2O	4.03	1.45	2.71	4.09	2.53	2.79	2.91	3.17	3.51
K_2O	0.63	0.69	0.91	0.50	0.81	0.84	0.63	0.75	1.57
P_2O_5	0.49	1.32	0.18	0.57	0.34	0.19	0.13	0.19	0.49
S	0.04	0.13	0.08	0.17	0.07	0.08	0.06	0.06	0.03
LOI	0.58	2.71	1.41	4.94	0.04	0.75	1.14	2.14	3.66
Total	**99.97**	**99.43**	**99.24**	**99.69**	**97.56**	**99.40**	**99.56**	**99.64**	**99.82**
Mg#[a]	33.70	44.13	63.33	43.75	60.29	72.26	76.65	66.23	54.44
CIPW normative minerals[b]									
Q				0.17					
Or	3.72	4.08	5.38	2.96	4.79	4.96	3.72	4.43	9.28
Ab	34.10	12.27	21.34	34.61	19.65	23.61	24.62	26.82	29.70
An	29.96	17.37	24.36	31.22	23.74	27.75	32.88	30.40	20.81
Ne			0.86		0.95				
Di	4.39	16.45	18.52	2.95	19.72	16.13	15.22	12.52	
Hy	2.00	0.13		15.53		3.70	0.41	5.50	16.17
Ol	16.09	28.49	19.54		20.69	16.31	17.31	11.85	10.45
Mt	2.71	4.48	2.33	1.68	2.54	1.74	1.33	1.70	2.38
Ilm	3.85	7.96	3.82	3.29	3.29	3.02	1.88	2.89	4.10
Ap	1.16	3.11	0.42	1.34	0.80	0.45	0.31	0.45	1.16
Trace elements (ppm)									
Nb	9	35	5	20	14	7	5	6	18
Zr	193	2422	123	920	285	127	98	115	270
Y	46	219	35	40	84	31	23	29	41
Sr	378	83	219	380	198	237	240	280	289
Rb	8	11	16	9	16	23	15	13	56
Th	6	5	4	3	4	4	2	4	3
Pb	7	7	5	9	5	5	4	6	8
As	3	5	9	20	11	2	3	1	3
U	4	6	2	2	4	2	1	2	2
Ga	27	22	17	21	17	15	14	15	19
Zn	168	259	136	138	154	75	59	79	149
Cu	33	121	99	104	58	62	85	51	38
Ni	37	97	134	29	170	175	181	66	169
Cr	45	110	352	35	484	515	468	177	321
Ce	34	107	21	42	40	22	22	18	34
Nd	32	131	21	34	46	22	17	21	33
Ba	257	156	208	253	267	155	95	175	740
V	245	409	319	84	256	241	158	245	232
La	19	38	9	19	19	12	7	12	16
Sc	32	169	38	15	58	40	34	34	39

All iron as Fe_2O_3 - in samples E-NS5/1, E-NS5/2 and E-NS5/4 to E-NS5/16. (continued)

Table 3. (Contd.)

Rock Type	PHGN	GRA	GRA	GRA
Sample	E-NS5/13	E-NS5/14	E-NS5/15	E-NS5/16
SiO_2	48.92	52.56	52.54	51.82
TiO_2	1.72	1.52	1.58	1.70
Al_2O_3	13.85	18.57	18.13	17.83
Fe_2O_3	10.91	10.75	11.08	11.84
FeO	-	-	-	-
MnO	0.28	0.21	0.22	0.24
MgO	6.52	2.27	2.31	2.39
CaO	9.14	7.17	6.89	6.53
Na_2O	3.37	5.15	5.05	4.85
K_2O	1.05	0.62	0.65	0.74
P_2O_5	0.09	0.49	0.52	0.51
S	0.07	0.06	0.05	0.05
LOI	3.65	0.65	0.89	1.53
Total	**99.57**	**100.02**	**99.91**	**100.03**
Mg#[a]	63.08	37.33	37.06	36.33
CIPW normative minerals[b]				
Q				
Or	6.21	3.66	3.84	4.37
Ab	28.52	43.58	42.73	41.04
An	19.56	25.72	24.88	24.69
Ne				
Di	20.66	5.65	5.02	3.72
Hy	3.67	9.74	13.50	15.20
Ol	10.92	4.14	1.91	1.93
Mt	1.88	1.85	1.91	2.04
Ilm	3.27	2.89	3.00	3.23
Ap	0.21	1.16	1.23	1.20
Trace elements (ppm)				
Nb	7	17	18	18
Zr	164	346	395	478
Y	45	73	71	73
Sr	221	346	339	332
Rb	24	6	8	12
Th	3	3	5	5
Pb	10	8	11	8
As	1	3	2	3
U	3	1	1	3
Ga	18	26	26	24
Zn	88	151	152	167
Cu	66	36	36	28
Ni	96	8	9	9
Cr	260	14	14	15
Ce	23	54	55	54
Nd	24	51	49	50
Ba	340	374	378	380
V	278	109	98	118
La	16	19	24	25
Sc	33	27	31	26

Table 4 Correlation matrix (r values) for major oxides and trace elements of the Wateranga intrusion

	SiO_2	TiO_2	Al_2O_3	Fe_2O_3	FeO	MnO	MgO	CaO	Na_2O	K_2O	P_2O_5	S	Nb	Zr	Y	Sr	Rb	Th	Pb	As	U	Ga	Zn	Cu	Ni	Cr	Ce	Nd	Ba	V	La	Sc
SiO_2	1.00																															
TiO_2	-0.59	1.00																														
Al_2O_3	0.82	-0.61	1.00																													
Fe_2O_3	-0.46	0.67	-0.55	1.00																												
FeO	-0.58	0.72	-0.74	0.73	1.00																											
MnO	-0.54	0.73	-0.75	0.71	0.96	1.00																										
MgO	-0.09	0.02	-0.28	0.08	0.60	0.45	1.00																									
CaO	0.09	-0.33	0.17	-0.46	-0.34	-0.35	0.13	1.00																								
Na_2O	0.51	-0.23	0.72	-0.20	-0.49	-0.42	-0.51	0.00	1.00																							
K_2O	-0.14	0.37	-0.13	0.55	0.07	0.23	-0.47	-0.39	0.30	1.00																						
P_2O_5	-0.55	0.68	-0.57	0.61	0.56	0.62	-0.22	-0.47	-0.16	0.57	1.00																					
S	-0.45	0.46	-0.40	0.21	0.65	0.49	0.29	-0.16	-0.28	-0.16	0.32	1.00																				
Nb	-0.42	0.79	-0.49	0.79	0.65	0.65	-0.21	-0.49	-0.08	0.68	0.78	0.28	1.00																			
Zr	-0.46	0.73	-0.53	0.67	0.67	0.65	-0.06	-0.42	-0.22	0.55	0.81	0.28	0.84	1.00																		
Y	-0.48	0.65	-0.65	0.73	0.74	0.78	0.19	-0.17	-0.34	0.40	0.69	0.29	0.74	0.80	1.00																	
Sr	0.55	-0.27	0.76	-0.31	-0.48	-0.45	-0.45	0.08	0.87	0.15	-0.27	-0.25	-0.25	-0.30	-0.42	1.00																
Rb	-0.18	0.34	-0.23	0.49	0.13	0.26	-0.36	-0.36	0.17	0.82	0.62	0.00	0.65	0.57	0.47	-0.01	1.00															
Th	-0.28	0.26	-0.25	0.38	0.24	0.34	0.06	-0.23	0.03	0.29	0.26	-0.01	0.20	0.23	0.22	-0.03	0.20	1.00														
Pb	-0.29	0.34	-0.31	0.48	0.33	0.35	-0.14	-0.36	-0.17	0.36	0.49	0.13	0.66	0.53	0.51	-0.20	0.41	0.09	1.00													
As	0.08	0.09	0.04	0.39	-0.22	-0.02	-0.40	-0.24	0.17	0.57	0.22	-0.10	0.36	0.32	0.20	0.11	0.44	-0.01	0.27	1.00												
U	-0.45	0.45	-0.51	0.59	0.35	0.43	-0.13	-0.27	-0.24	0.45	0.49	0.09	0.69	0.50	0.51	-0.26	0.47	0.28	0.48	0.36	1.00											
Ga	0.02	0.25	0.16	0.16	-0.21	-0.08	-0.66	-0.19	0.33	0.52	0.31	-0.38	0.37	0.35	0.13	0.36	0.37	-0.01	0.28	0.36	0.22	1.00										
Zn	-0.58	0.79	-0.74	0.84	0.94	0.93	0.27	-0.46	-0.41	0.38	0.69	0.40	0.79	0.78	0.83	-0.48	0.39	0.34	0.47	0.18	0.54	0.10	1.00									
Cu	-0.31	0.13	-0.30	0.23	0.35	0.29	0.35	-0.03	-0.27	-0.07	0.14	0.58	0.23	0.19	0.30	-0.30	0.11	-0.03	0.16	0.17	0.16	-0.40	0.26	1.00								
Ni	0.04	-0.26	-0.09	-0.17	0.16	0.02	0.69	0.22	-0.41	-0.40	-0.32	0.06	-0.29	-0.23	-0.05	-0.46	-0.20	-0.19	-0.13	-0.15	-0.19	-0.64	-0.07	0.39	1.00							
Cr	0.02	-0.13	-0.18	-0.05	0.31	0.21	0.80	0.38	-0.42	-0.40	-0.31	0.09	-0.26	-0.13	0.15	-0.42	-0.27	-0.07	-0.19	-0.25	-0.14	-0.67	0.05	0.33	0.78	1.00						
Ce	-0.47	0.56	-0.54	0.62	0.58	0.64	-0.05	-0.37	-0.18	0.46	0.75	0.28	0.71	0.73	0.69	-0.36	0.50	0.37	0.57	0.21	0.49	0.17	0.71	0.22	-0.18	-0.16	1.00					
Nd	-0.52	0.58	-0.58	0.65	0.57	0.63	-0.15	-0.28	-0.19	0.57	0.82	0.15	0.72	0.74	0.75	-0.37	0.54	0.45	0.61	0.23	0.59	0.24	0.69	0.17	-0.24	-0.22	0.79	1.00				
Ba	0.03	0.45	-0.01	0.35	0.22	0.30	-0.41	-0.46	0.38	0.55	0.60	0.13	0.57	0.65	0.37	0.23	0.51	0.14	0.39	0.25	0.31	0.48	0.36	-0.06	-0.40	-0.31	0.51	0.47	1.00			
V	-0.43	0.81	-0.54	0.50	0.74	0.74	0.38	-0.06	-0.29	0.13	0.37	0.49	0.48	0.48	0.58	-0.26	0.12	0.23	0.08	-0.11	0.31	-0.10	0.65	0.19	0.01	0.32	0.33	0.34	0.27	1.00		
La	-0.47	0.60	-0.54	0.50	0.61	0.63	-0.04	-0.36	-0.19	0.41	0.74	0.29	0.61	0.69	0.61	-0.36	0.44	0.37	0.55	0.10	0.44	0.17	0.66	0.15	-0.16	-0.14	0.61	0.66	0.44	0.38	1.00	
Sc	-0.34	0.57	-0.66	0.55	0.63	0.75	0.43	0.08	-0.58	0.14	0.35	0.29	0.48	0.51	0.78	-0.60	0.21	0.15	0.22	0.02	0.45	-0.17	0.67	0.17	0.17	0.46	0.40	0.43	0.11	0.73	0.33	1.00

Note: For Nb, As, Ce, Nd, Ba, La and Sc (N = 92); For all other trace elements and major oxides (N = 114); Correlation matrix is calculated from the log values of the major and trace elements

Appendix 2. Electron microprobe analysis

Introduction

The electron microprobe analysis concept was developed by Casting in the early 1950s, and electron microprobes become widely available in the 1970s. During the past three decades this technique has greatly improved and characterization of materials allowing routine non-destructive chemical analyses of minerals in situ.

Electron microprobe performs quantitative X-ray spectrometric analyses, but its main function is quantitative analysis of very small volumes of materials. Under electron bombardment the sample's constituent atoms emit X-rays. The wavelengths of the X-rays are identified and their intensities measured by X-ray spectrometers (wavelength or energy-dispersive) and detectors. Comparison of the sample's characteristic X-ray intensities with those of a standard, after correction for matrix effects, leads to quantitative analysis.

Methods of analyses

More than 400 mineral analyses were performed using a JEOL JSM-5800LV Scanning Electron Microscope fitted with an Oxford Link ISIS EDS system at the University of New England. Analytical conditions were 20 kV accelerating voltage, 20 nA beam current and 100 seconds counting time. A variety of synthetic and natural mineral standards were used. Final results were processed by a ZAF correction program. In addition, about 130 unpublished mineral analyses were provided by P. M. Ashley.

In the following pages (Tables 1-8) the compositions of plagioclase, clinopyroxene, orthopyroxene, olivine, ilmenite, magnetite, amphibole and biotite which were determined by the author, are listed.

Notes

(a) Plagioclase

An = cationic ratio of Ca / (Ca + Na + K)

Ab = cationic ratio of Na / (Ca + Na + K)

Or = cationic ratio of K / (Ca + Na + K)

(b) Clino- and orthopyroxenes

En = cationic ratio of Mg / (Mg + Fe + Ca)

Fs = cationic ratio of Fe / (Mg + Fe + Ca)

Wo = cationic ratio of Ca / (Mg + Fe + Ca)

Mg# = cationic ratio of Mg / (Mg + Fe)

(c) Olivine

Fo = cationic ratio of Mg / (Mg + Fe)

Fa = cationic ratio of Fe / (Mg + Fe)

Mg# = cationic ratio of Mg / (Mg + Fe)

(d) Trivalent iron contents and haematite and ulvospinel contents of ilmenite and magnetite respectively have been calculated using QUILF95 program (Andersen et al., 1993).

(e) Two independent geothermometers were applied: two-pyroxene and magnetite-ilmenite thermometry using QUILF95 program (Andersen et al., 1993).

Table 1. Plagioclase mineral compositions of the Wateranga intrusion

Sample	NS-2/1	NS-2/1	NS-2/1	NS-2/1	NS-2/1	NS-2/1	NS-2/2	NS-2/2	NS-2/2	NS-2/4	NS-2/4	NS-2/4
Oxide (wt%)												
SiO_2	54.67	55.21	55.66	53.76	54.21	54.86	55.22	54.92	54.32	56.45	55.75	57.51
TiO_2	0.10	0.07	<0.05	<0.05	0.06	0.18	<0.05	<0.05	<0.05	<0.05	0.17	<0.05
Al_2O_3	29.02	27.81	27.99	28.62	29.06	28.16	27.78	28.84	28.18	27.68	28.04	25.33
FeO*	0.33	0.21	0.18	0.28	0.22	0.05	0.05	0.17	0.19	0.13	0.05	0.13
MnO	<0.05	0.08	0.05	0.05	0.06	<0.05	0.06	<0.05	0.09	0.06	<0.05	<0.05
MgO	0.06	0.10	0.08	0.11	0.07	0.12	0.11	<0.05	0.05	<0.05	<0.05	0.33
CaO	10.17	9.63	9.74	10.87	10.65	9.52	9.85	9.97	10.35	8.57	9.55	8.06
Na_2O	5.58	6.06	6.02	5.35	5.38	6.09	5.87	5.48	5.71	6.57	6.16	7.15
K_2O	0.25	0.30	0.33	0.29	0.31	0.32	0.35	0.42	0.37	0.46	0.13	0.31
BaO	<0.05	0.15	<0.05	0.11	0.06	<0.05	0.27	0.26	<0.05	0.11	0.34	0.45
Sum	100.18	99.62	100.05	99.44	100.08	99.30	99.56	100.06	99.26	100.03	100.19	99.27
Cations per 8 oxygens												
Si	2.48	2.50	2.52	2.46	2.46	2.49	2.51	2.48	2.48	2.53	2.50	2.60
Ti	0.00	0.00	0.00	0.00	0.00	0.01	0.00	0.00	0.00	0.00	0.01	0.00
Al	1.54	1.49	1.47	1.53	1.54	1.49	1.48	1.53	1.51	1.46	1.48	1.38
Fe	0.01	0.01	0.01	0.01	0.01	0.00	0.00	0.01	0.01	0.01	0.00	0.00
Mn	0.00	0.00	0.00	0.00	0.00	0.00	0.00	0.00	0.00	0.00	0.00	0.00
Mg	0.00	0.00	0.00	0.00	0.00	0.00	0.00	0.00	0.00	0.00	0.00	0.02
Ca	0.48	0.45	0.46	0.53	0.51	0.45	0.48	0.48	0.49	0.41	0.46	0.39
Na	0.48	0.53	0.52	0.46	0.46	0.53	0.51	0.48	0.49	0.56	0.53	0.59
K	0.01	0.02	0.02	0.02	0.02	0.02	0.02	0.02	0.02	0.03	0.01	0.02
Ba	0.00	0.00	0.00	0.00	0.00	0.00	0.00	0.00	0.00	0.00	0.01	0.01
Sum	5.00	5.00	5.00	5.01	5.00	4.99	5.00	5.00	5.00	5.00	5.00	5.01
End members (mole%)												
An	49.5	45.0	46.0	52.5	51.5	45.0	47.5	49.0	49.0	41.0	46.0	39.0
Ab	49.5	53.0	52.0	45.5	46.5	53.0	50.5	49.0	49.0	56.0	53.0	59.0
Or	1.0	2.0	2.0	2.0	2.0	2.0	2.0	2.0	2.0	3.0	1.0	2.0

* Total iron as FeO. Lower detection limit for all elements is 0.05 wt%.

Table 1. (Contd.)

Sample	NS-2/4	NS-2/4	NS-2/11	NS-2/14	NS-2/14	NS-2/14	NS-2/14	NS-2/19	NS-2/19	NS-2/19	NS-2/19	NS-2/19
Oxide (wt%)												
SiO_2	56.40	57.34	53.73	55.13	55.86	56.37	56.29	54.75	53.73	52.63	49.20	54.49
TiO_2	0.18	<0.05	0.06	0.05	0.05	<0.05	0.05	<0.05	0.06	<0.05	0.05	0.12
Al_2O_3	26.60	25.86	29.08	27.66	27.65	27.97	28.20	28.28	28.30	30.80	32.87	28.18
FeO*	0.05	<0.05	0.23	0.34	0.23	0.16	0.19	0.17	0.23	0.13	0.10	0.27
MnO	0.11	0.08	0.06	<0.05	0.06	<0.05	<0.05	0.13	0.05	0.06	0.05	<0.05
MgO	<0.05	<0.05	0.12	0.10	<0.05	<0.05	<0.05	<0.05	<0.05	<0.05	<0.05	<0.05
CaO	8.42	7.17	10.43	9.33	9.15	9.19	8.88	9.57	9.78	11.89	14.28	9.89
Na_2O	6.57	7.79	5.46	6.16	6.25	6.28	6.54	5.81	5.69	4.56	3.14	5.84
K_2O	0.37	0.40	0.21	0.34	0.33	0.28	0.19	0.21	0.31	0.18	0.15	0.29
BaO	<0.05	0.59	0.10	0.06	0.09	0.12	0.06	0.12	<0.05	0.11	<0.05	<0.05
Sum	98.70	99.23	99.48	99.17	99.67	100.37	100.40	99.04	98.15	100.36	99.84	99.08
Cations per 8 oxygens												
Si	2.55	2.59	2.44	2.50	2.53	2.51	2.50	2.49	2.46	2.37	2.25	2.48
Ti	0.01	0.00	0.00	0.00	0.00	0.00	0.00	0.00	0.00	0.00	0.00	0.00
Al	1.44	1.39	1.55	1.48	1.47	1.47	1.48	1.51	1.53	1.63	1.76	1.52
Fe	0.00	0.00	0.01	0.01	0.01	0.01	0.01	0.01	0.01	0.01	0.00	0.01
Mn	0.00	0.00	0.00	0.00	0.00	0.00	0.00	0.01	0.00	0.00	0.00	0.00
Mg	0.00	0.00	0.00	0.00	0.00	0.00	0.00	0.00	0.00	0.00	0.00	0.00
Ca	0.40	0.35	0.50	0.45	0.44	0.44	0.43	0.47	0.48	0.58	0.70	0.47
Na	0.57	0.65	0.48	0.54	0.54	0.55	0.57	0.51	0.51	0.40	0.28	0.49
K	0.02	0.02	0.01	0.02	0.02	0.02	0.01	0.01	0.02	0.01	0.01	0.02
Ba	0.00	0.01	0.00	0.00	0.00	0.00	0.00	0.00	0.00	0.00	0.00	0.00
Sum	4.99	5.01	4.99	5.00	5.01	5.00	5.00	5.01	5.01	5.00	5.00	4.99
End members (mole%)												
An	40.4	34.3	50.5	44.6	44.0	43.6	42.6	47.5	47.5	58.6	70.7	48.0
Ab	57.6	63.7	48.5	53.5	54.0	54.5	56.4	51.5	50.5	40.4	28.3	50.0
Or	2.0	2.0	1.0	2.0	2.0	2.0	1.0	1.0	2.0	1.0	1.0	2.0

* Total iron as FeO

Table 1. (Contd.)

Sample	NS-2/22	NS-2/22	NS-2/31	NS-2/31	NS-2/35	NS-2/35	NS-2/41	NS-2/48	NS-2/48	NS-2/48	NS-2/54	NS-2/57
Oxide (wt%)												
SiO_2	54.87	54.02	53.61	55.82	56.67	53.74	56.15	51.78	51.65	51.02	54.05	54.60
TiO_2	0.17	0.07	<0.05	0.17	<0.05	0.16	<0.05	0.08	0.05	<0.05	<0.05	0.08
Al_2O_3	28.37	28.17	29.44	27.23	27.55	28.69	28.21	30.43	30.71	31.01	26.94	27.82
FeO*	0.23	0.22	0.18	0.27	0.37	0.05	0.11	0.20	0.29	0.36	0.37	0.36
MnO	<0.05	<0.05	0.05	0.09	0.06	<0.05	<0.05	0.05	0.06	<0.05	0.05	<0.05
MgO	<0.05	<0.05	<0.05	<0.05	<0.05	<0.05	<0.05	<0.05	<0.05	<0.05	0.44	0.30
CaO	10.27	10.48	9.57	9.15	8.69	10.68	9.36	12.38	12.87	13.17	10.57	11.19
Na_2O	5.82	5.63	5.93	6.39	6.14	5.49	6.20	4.65	4.18	3.96	5.14	5.30
K_2O	0.27	0.31	0.10	0.33	0.44	0.27	0.24	0.09	0.22	0.12	0.23	0.07
BaO	0.10	0.08	0.11	<0.05	0.14	<0.05	0.13	<0.05	0.20	0.08	0.34	<0.05
Sum	100.10	98.98	98.99	99.45	100.06	99.08	100.40	99.66	100.23	99.72	98.13	99.72
Cations per 8 oxygens												
Si	2.47	2.46	2.49	2.53	2.55	2.44	2.52	2.35	2.34	2.33	2.50	2.48
Ti	0.01	0.00	0.00	0.01	0.00	0.01	0.00	0.00	0.00	0.00	0.00	0.00
Al	1.50	1.52	1.51	1.45	1.46	1.54	1.49	1.63	1.64	1.66	1.47	1.49
Fe	0.01	0.01	0.01	0.01	0.01	0.00	0.00	0.01	0.01	0.01	0.01	0.01
Mn	0.00	0.00	0.00	0.00	0.00	0.00	0.00	0.00	0.00	0.00	0.00	0.00
Mg	0.00	0.00	0.00	0.00	0.00	0.00	0.00	0.00	0.00	0.00	0.03	0.02
Ca	0.49	0.51	0.46	0.43	0.42	0.52	0.45	0.59	0.63	0.64	0.52	0.54
Na	0.50	0.48	0.52	0.55	0.54	0.48	0.54	0.40	0.37	0.35	0.45	0.46
K	0.02	0.02	0.01	0.02	0.03	0.02	0.01	0.01	0.01	0.01	0.01	0.00
Ba	0.00	0.00	0.00	0.00	0.00	0.00	0.00	0.00	0.00	0.00	0.01	0.00
Sum	5.00	5.00	5.00	5.00	5.01	5.01	5.01	4.99	5.00	5.00	5.00	5.00
End members (mole%)												
An	48.5	50.5	46.5	43.0	42.4	51.0	45.0	59.0	62.4	64.0	53.1	54.0
Ab	49.5	47.5	52.5	55.0	54.5	47.1	54.0	40.0	36.6	35.0	45.9	46.0
Or	2.0	2.0	1.0	2.0	3.0	2.0	1.0	1.0	1.0	1.0	1.0	0.0

* Total iron as FeO

Table 1. (Contd.)

Sample	NS-2/57	NS-2/57	NS-2/57	NS-2/59	NS-2/59	NS-2/61	NS-2/61	NS-2/61	NS-2/63	NS-2/63	NS-2/63	NS-3/2
Oxide (wt%)												
SiO_2	54.36	52.86	49.69	54.30	51.49	53.45	53.73	51.60	52.61	50.27	47.55	54.57
TiO_2	<0.05	<0.05	0.05	0.08	0.05	0.12	0.12	<0.05	0.16	0.12	0.15	<0.05
Al_2O_3	28.42	28.75	29.70	27.40	29.97	28.01	28.67	28.81	27.69	30.34	28.40	28.20
FeO*	0.58	0.35	0.50	0.48	0.06	0.08	0.14	0.10	0.20	0.35	0.14	0.16
MnO	0.06	<0.05	<0.05	0.05	<0.05	<0.05	<0.05	<0.05	0.05	<0.05	<0.05	<0.05
MgO	0.40	0.22	0.59	0.44	0.26	0.49	0.50	0.37	0.45	0.27	<0.05	<0.05
CaO	10.84	12.73	14.52	11.45	14.33	12.71	12.44	12.84	13.64	14.66	20.20	12.16
Na_2O	5.20	4.35	3.69	5.35	3.78	4.91	4.56	4.38	4.29	3.84	3.25	4.70
K_2O	0.06	0.12	0.09	<0.05	<0.05	0.06	0.12	0.21	0.19	0.06	0.07	0.06
BaO	0.14	<0.05	0.25	0.09	0.28	0.20	0.21	0.42	<0.05	<0.05	<0.05	0.29
Sum	100.06	99.38	99.08	99.64	100.22	100.03	100.49	98.73	99.28	99.91	99.76	100.14
Cations per 8 oxygens												
Si	2.44	2.42	2.31	2.48	2.38	2.44	2.45	2.39	2.40	2.35	2.30	2.47
Ti	0.00	0.00	0.00	0.00	0.00	0.00	0.00	0.00	0.01	0.00	0.01	0.00
Al	1.51	1.55	1.62	1.48	1.62	1.54	1.55	1.58	1.56	1.64	1.59	1.52
Fe	0.02	0.01	0.02	0.02	0.00	0.00	0.01	0.00	0.01	0.01	0.01	0.01
Mn	0.00	0.00	0.00	0.00	0.00	0.00	0.00	0.00	0.00	0.00	0.00	0.00
Mg	0.03	0.02	0.04	0.03	0.02	0.03	0.03	0.02	0.03	0.02	0.00	0.00
Ca	0.53	0.62	0.69	0.54	0.68	0.62	0.60	0.62	0.64	0.68	0.84	0.57
Na	0.46	0.38	0.32	0.45	0.31	0.38	0.36	0.37	0.34	0.30	0.25	0.41
K	0.00	0.01	0.01	0.00	0.00	0.00	0.01	0.01	0.01	0.00	0.00	0.00
Ba	0.00	0.00	0.00	0.00	0.00	0.00	0.00	0.01	0.00	0.00	0.00	0.01
Sum	4.99	5.01	5.01	5.00	5.01	5.01	5.01	5.00	5.00	5.00	5.00	4.99
End members (mole%)												
An	53.5	61.4	67.6	54.5	68.7	62.0	61.9	62.0	64.6	69.4	77.1	58.2
Ab	46.5	37.6	31.4	45.5	31.3	38.0	37.1	37.0	34.3	30.6	22.9	41.8
Or	0.0	1.0	1.0	0.0	0.0	0.0	1.0	1.0	1.0	0.0	0.0	0.0

* Total iron as FeO

Table 1. (Contd.)

Sample	NS-3/7	NS-3/8	NS-3/12	NS-3/12	NS-3/25	NS-3/25	NS-3/25	NS-3/34	NS-3/53	NS-5/12	NS-5/15	WG-7
Oxide (wt%)												
SiO_2	53.93	54.17	51.03	52.10	53.37	53.83	53.96	51.94	53.44	55.38	54.90	52.33
TiO_2	<0.05	0.16	0.11	0.05	0.06	0.18	0.06	0.09	0.13	<0.05	<0.05	0.19
Al_2O_3	27.53	27.83	29.13	29.19	28.03	28.27	28.02	29.03	28.72	27.45	27.82	28.90
FeO*	0.32	0.28	0.61	<0.05	0.56	0.28	0.27	0.39	0.60	0.12	0.18	0.30
MnO	0.09	<0.05	<0.05	<0.05	<0.05	<0.05	<0.05	<0.05	0.08	<0.05	<0.05	0.14
MgO	0.48	0.36	0.16	0.55	0.53	0.31	0.19	0.44	0.51	0.14	0.11	0.40
CaO	12.37	11.75	14.56	12.71	12.81	12.78	11.77	13.47	12.28	10.46	11.23	13.03
Na_2O	4.66	5.01	3.91	4.47	4.66	4.82	5.03	4.16	4.55	5.82	5.74	4.57
K_2O	0.17	0.21	<0.05	0.27	0.21	0.05	0.09	0.05	<0.05	0.22	<0.05	0.13
BaO	0.36	<0.05	<0.05	0.28	<0.05	<0.05	0.17	<0.05	<0.05	0.14	0.30	0.05
Sum	99.91	99.77	99.51	99.62	100.23	100.52	99.56	99.57	100.31	99.73	100.28	100.04
Cations per 8 oxygens												
Si	2.46	2.46	2.39	2.40	2.45	2.45	2.46	2.37	2.44	2.50	2.48	2.40
Ti	0.00	0.01	0.00	0.00	0.00	0.01	0.00	0.00	0.00	0.00	0.00	0.01
Al	1.50	1.50	1.60	1.59	1.55	1.56	1.55	1.61	1.55	1.48	1.48	1.55
Fe	0.01	0.01	0.02	0.00	0.02	0.01	0.01	0.01	0.02	0.00	0.01	0.01
Mn	0.00	0.00	0.00	0.00	0.00	0.00	0.00	0.00	0.00	0.00	0.00	0.01
Mg	0.03	0.02	0.01	0.04	0.04	0.02	0.01	0.03	0.03	0.01	0.01	0.03
Ca	0.58	0.55	0.65	0.55	0.56	0.57	0.54	0.63	0.58	0.50	0.53	0.62
Na	0.41	0.44	0.33	0.38	0.37	0.38	0.43	0.35	0.38	0.50	0.48	0.34
K	0.01	0.01	0.00	0.02	0.01	0.00	0.01	0.00	0.00	0.01	0.00	0.01
Ba	0.01	0.00	0.00	0.01	0.00	0.00	0.00	0.00	0.00	0.00	0.01	0.00
Sum	5.01	5.00	5.00	4.99	5.00	5.00	5.01	5.00	5.00	5.00	5.00	4.98
End members (mole%)												
An	58.0	55.0	66.3	57.9	59.6	60.0	55.1	64.3	60.4	49.5	52.5	63.9
Ab	41.0	44.0	33.7	40.0	39.4	40.0	43.9	35.7	39.6	49.5	47.5	35.1
Or	1.0	1.0	0.0	2.1	1.1	0.0	1.0	0.0	0.0	1.0	0.0	1.0

* Total iron as FeO

Table 1. (Contd.)

Sample	WG-27	WG-27	WG-27	WG-31	WG-35	WG-44	WG-84	WG-84	WG-92	WG-107	WG-124
Oxide (wt%)											
SiO_2	52.91	49.20	52.16	51.88	52.55	53.57	52.86	53.03	53.19	52.45	53.52
TiO_2	<0.05	0.15	0.05	0.09	0.12	<0.05	0.15	<0.05	0.09	<0.05	0.06
Al_2O_3	29.39	30.81	28.95	28.61	28.63	28.66	28.52	28.33	28.48	29.11	28.50
FeO*	0.29	<0.05	0.10	0.22	0.17	0.31	0.48	0.29	0.28	0.37	0.27
MnO	<0.05	0.12	<0.05	0.05	0.10	<0.05	0.12	<0.05	0.06	<0.05	<0.05
MgO	0.06	0.21	0.15	0.20	0.06	0.21	<0.05	0.18	0.07	0.24	0.06
CaO	12.70	15.13	13.67	12.39	13.58	12.36	12.63	12.38	12.71	12.89	12.79
Na_2O	4.64	3.56	4.64	4.69	3.63	4.74	4.43	4.95	5.05	4.44	4.65
K_2O	0.06	0.08	0.10	0.09	0.22	0.08	0.24	0.09	0.14	0.06	0.07
BaO	<0.05	<0.05	0.26	0.24	<0.05	0.35	<0.05	0.18	<0.05	0.40	0.15
Sum	100.05	99.26	100.08	98.46	99.06	100.28	99.43	99.43	100.07	99.96	100.07
Cations per 8 oxygens											
Si	2.40	2.32	2.42	2.41	2.42	2.43	2.42	2.42	2.42	2.38	2.43
Ti	0.00	0.01	0.00	0.00	0.00	0.00	0.01	0.00	0.00	0.00	0.00
Al	1.57	1.66	1.55	1.56	1.55	1.53	1.53	1.54	1.52	1.56	1.53
Fe	0.01	0.00	0.00	0.01	0.01	0.01	0.03	0.01	0.01	0.01	0.01
Mn	0.00	0.00	0.00	0.00	0.00	0.00	0.00	0.00	0.00	0.00	0.00
Mg	0.00	0.01	0.01	0.01	0.00	0.01	0.00	0.01	0.00	0.02	0.00
Ca	0.62	0.70	0.65	0.62	0.68	0.60	0.62	0.60	0.62	0.63	0.62
Na	0.41	0.29	0.36	0.39	0.33	0.42	0.38	0.40	0.42	0.39	0.41
K	0.00	0.00	0.01	0.01	0.01	0.00	0.01	0.01	0.01	0.00	0.00
Ba	0.00	0.00	0.00	0.00	0.00	0.01	0.00	0.00	0.00	0.01	0.00
Sum	5.01	4.99	5.00	5.01	5.00	5.01	5.00	4.99	5.00	5.00	5.00
End members (mole%)											
An	60.2	70.7	63.7	60.8	66.7	58.8	61.4	59.4	59.0	61.8	60.2
Ab	39.8	29.3	35.3	38.2	32.4	41.2	37.6	39.6	40.0	38.2	39.8
Or	0.0	0.0	1.0	1.0	1.0	0.0	1.0	1.0	1.0	0.0	0.0

* Total iron as FeO

Table 2. Clinopyroxene mineral compositions of the Wateranga intrusion

Sample	NS-2/1	NS-2/1	NS-2/11	NS-2/11	NS-2/11	NS-2/11	NS-2/11	NS-2/11	NS-2/11	NS-2/11	NS-2/11	NS-2/11	NS-2/11
Oxide (wt%)													
SiO_2	52.35	53.08	52.95	52.39	51.72	50.02	51.46	51.53	51.14	51.43	52.65	51.66	51.22
TiO_2	0.64	0.34	0.30	0.31	0.18	0.31	0.37	0.35	0.37	0.37	0.12	0.22	0.34
Al_2O_3	1.86	1.49	1.14	1.38	1.25	1.51	1.59	1.77	1.27	1.41	0.95	0.91	1.29
FeO*	12.60	11.80	10.55	10.83	10.88	12.34	10.87	11.32	12.65	11.38	11.29	12.65	11.71
MnO	0.46	0.46	0.74	0.45	0.23	0.56	0.34	0.58	0.47	0.43	0.57	0.59	0.58
MgO	11.37	12.01	13.16	13.64	13.13	13.08	13.03	13.29	13.85	12.87	13.62	13.53	13.48
CaO	20.14	20.39	20.92	21.12	21.00	20.94	21.13	20.23	19.77	21.66	20.59	19.85	20.31
Na_2O	0.12	0.10	0.16	0.16	0.16	0.16	0.16	0.17	0.17	0.16	0.16	0.16	0.16
K_2O	0.08	0.17	<0.05	<0.05	0.06	0.07	0.06	0.06	<0.05	<0.05	0.07	0.05	0.09
Cr_2O_3	<0.05	0.13	0.19	0.05	0.32	0.22	0.30	0.34	0.25	0.17	<0.05	0.14	0.12
NiO	<0.05	0.05	<0.05	<0.05	<0.05	0.05	<0.05	<0.05	<0.05	0.13	<0.05	0.11	<0.05
Sum	99.62	100.02	100.11	100.33	98.93	99.26	99.31	99.64	99.94	100.01	100.02	99.87	99.30
Cations per 6 oxygens													
Si	2.00	2.00	1.99	1.96	1.98	1.92	1.96	1.95	1.92	1.93	1.98	1.94	1.95
Ti	0.02	0.01	0.01	0.01	0.01	0.01	0.01	0.01	0.01	0.01	0.00	0.01	0.01
Al	0.08	0.07	0.05	0.06	0.06	0.07	0.07	0.08	0.06	0.06	0.04	0.04	0.06
Fe	0.40	0.37	0.33	0.34	0.34	0.39	0.34	0.36	0.40	0.36	0.35	0.40	0.37
Mn	0.01	0.01	0.02	0.01	0.01	0.02	0.01	0.02	0.02	0.01	0.02	0.02	0.02
Mg	0.66	0.69	0.73	0.76	0.73	0.74	0.73	0.75	0.78	0.73	0.76	0.77	0.76
Ca	0.83	0.84	0.84	0.85	0.86	0.83	0.86	0.82	0.79	0.88	0.83	0.81	0.83
Na	0.00	0.00	0.01	0.01	0.01	0.01	0.01	0.01	0.01	0.01	0.01	0.01	0.01
K	0.00	0.01	0.00	0.00	0.00	0.00	0.00	0.00	0.00	0.00	0.00	0.00	0.00
Cr	0.00	0.00	0.01	0.00	0.01	0.01	0.01	0.01	0.01	0.01	0.00	0.00	0.00
Ni	0.00	0.00	0.00	0.00	0.00	0.00	0.00	0.00	0.00	0.00	0.00	0.00	0.00
Sum	4.00	4.00	3.99	4.00	4.01	4.00	4.00	4.01	4.00	4.00	3.99	4.00	4.01
End members (mole%)													
En	34.9	36.3	38.4	39.0	37.8	37.8	37.8	38.9	39.6	37.1	39.2	38.9	38.8
Fs	21.2	19.5	17.4	17.4	17.6	19.9	17.6	18.7	20.3	18.3	18.0	20.2	18.9
Wo	43.9	44.2	44.2	43.6	44.6	42.3	44.6	42.5	40.1	44.7	42.8	40.9	42.3
mg#	62.3	65.1	68.9	69.1	68.2	65.5	68.2	67.6	66.1	67.0	68.5	65.8	67.3

* Total iron as FeO. Lower detection limit for all elements is 0.05 wt%.

Table 2. (Contd.)

Sample	NS-2/11	NS-2/11	NS-2/11	NS-2/14	NS-2/14	NS-2/14	NS-2/14	NS-2/19	NS-2/19	NS-2/19	NS-2/19	NS-2/19	NS-2/22
Oxide (wt%)													
SiO_2	52.21	52.14	52.17	51.67	51.40	51.74	51.90	51.46	52.00	50.94	50.89	51.09	52.18
TiO_2	0.39	0.20	0.37	0.36	0.28	0.28	0.33	0.24	0.48	0.44	0.58	0.52	0.36
Al_2O_3	1.66	1.20	1.66	1.44	1.20	1.38	1.28	1.23	1.55	1.64	1.67	1.76	1.37
FeO*	11.35	12.32	10.56	11.23	13.03	11.56	11.33	10.15	10.24	10.17	10.75	9.97	10.26
MnO	0.42	0.34	0.49	0.35	0.59	0.45	0.36	0.51	0.28	0.48	0.21	0.40	0.52
MgO	13.57	14.13	13.25	13.34	13.04	12.78	13.02	13.64	13.84	13.76	13.48	13.87	13.99
CaO	20.37	18.94	21.20	20.07	18.90	20.86	21.10	20.93	21.40	21.55	21.50	21.04	20.90
Na_2O	0.16	0.16	0.16	0.17	0.15	0.16	0.16	0.18	0.18	0.17	0.16	0.16	0.16
K_2O	0.11	<0.05	0.05	0.08	0.06	<0.05	0.09	0.05	0.06	0.06	0.05	0.09	0.05
Cr_2O_3	<0.05	0.05	0.17	0.05	0.23	0.13	0.14	<0.05	0.13	0.06	0.21	0.06	<0.05
NiO	<0.05	0.18	<0.05	<0.05	0.05	<0.05	0.29	<0.05	<0.05	0.05	<0.05	0.06	0.20
Sum	100.24	99.66	100.08	98.76	98.93	99.34	100.00	98.39	100.16	99.32	99.50	99.02	99.99
Cations per 6 oxygens													
Si	1.95	1.97	1.96	1.97	1.97	1.97	1.96	1.96	1.95	1.91	1.93	1.92	1.96
Ti	0.01	0.01	0.01	0.01	0.01	0.01	0.01	0.01	0.01	0.01	0.02	0.01	0.01
Al	0.07	0.05	0.07	0.06	0.05	0.06	0.06	0.06	0.07	0.07	0.07	0.08	0.06
Fe	0.36	0.39	0.33	0.36	0.42	0.37	0.36	0.32	0.32	0.32	0.33	0.32	0.32
Mn	0.01	0.01	0.02	0.01	0.02	0.01	0.01	0.02	0.01	0.02	0.01	0.01	0.02
Mg	0.76	0.79	0.74	0.75	0.74	0.72	0.73	0.78	0.77	0.78	0.76	0.78	0.78
Ca	0.82	0.76	0.85	0.83	0.78	0.85	0.85	0.86	0.86	0.88	0.87	0.85	0.84
Na	0.01	0.01	0.01	0.01	0.01	0.01	0.01	0.01	0.01	0.01	0.01	0.01	0.01
K	0.01	0.00	0.00	0.00	0.00	0.00	0.00	0.00	0.00	0.00	0.00	0.00	0.00
Cr	0.00	0.00	0.00	0.00	0.01	0.00	0.00	0.00	0.00	0.00	0.01	0.00	0.00
Ni	0.00	0.01	0.00	0.00	0.00	0.00	0.01	0.00	0.00	0.00	0.00	0.00	0.01
Sum	4.00	4.00	3.99	4.00	4.01	4.00	4.00	4.02	4.00	4.00	4.01	3.98	4.01
End members (mole%)													
En	39.2	40.7	38.5	38.7	38.1	37.1	37.6	39.8	39.5	39.4	38.7	40.0	40.2
Fs	18.6	20.1	17.2	18.6	21.6	19.1	18.6	16.3	16.4	16.2	17.0	16.4	16.5
Wo	42.3	39.2	44.3	42.8	40.2	43.8	43.8	43.9	44.1	44.4	44.3	43.6	43.3
mg#	67.9	66.9	69.2	67.6	63.8	66.1	67.0	70.9	70.6	70.9	69.5	70.9	70.9

* Total iron as FeO

Table 2. (Contd.)

Sample	NS-2/29	NS-2/29	NS-2/31	NS-2/41	NS-2/54	NS-2/54	NS-2/57	NS-2/57	NS-2/57	NS-2/59	NS-2/61	NS-2/63	NS-3/2
Oxide (wt%)													
SiO_2	51.67	51.83	51.68	51.19	52.50	51.96	51.45	51.92	51.30	46.28	50.89	52.58	50.53
TiO_2	0.42	0.51	0.35	0.34	0.39	0.20	0.64	0.59	0.55	2.21	0.65	0.45	0.43
Al_2O_3	1.61	1.83	1.33	1.07	1.53	1.31	2.04	1.85	2.16	8.35	1.94	2.40	1.63
FeO*	8.99	10.69	11.54	11.57	8.27	8.35	8.54	9.24	7.52	14.92	8.05	6.73	11.79
MnO	0.21	0.41	0.48	0.33	0.28	0.12	0.20	0.37	0.16	0.28	0.20	0.35	0.35
MgO	14.64	15.31	13.61	13.68	15.05	16.04	15.58	15.99	15.81	14.48	14.98	14.40	14.44
CaO	21.20	19.02	20.20	21.14	21.00	20.13	21.08	19.87	21.18	12.16	22.22	22.29	19.34
Na_2O	0.15	0.16	0.15	0.16	0.16	0.16	0.16	0.14	0.17	0.16	0.16	0.16	0.18
K_2O	<0.05	0.05	0.05	<0.05	<0.05	<0.05	0.07	0.06	0.07	0.86	0.09	0.05	0.05
Cr_2O_3	0.22	0.26	0.06	0.17	0.13	0.17	0.18	0.06	0.21	<0.05	0.40	0.71	0.05
NiO	0.21	<0.05	<0.05	0.33	0.25	0.06	0.06	0.21	0.17	0.09	0.06	<0.05	<0.05
Sum	99.32	100.07	99.45	99.98	99.56	98.50	100.00	100.30	99.30	99.79	99.64	100.12	98.79
Cations per 6 oxygens													
Si	1.94	1.94	1.96	1.90	1.96	1.96	1.90	1.91	1.93	1.73	1.89	1.97	1.93
Ti	0.01	0.01	0.01	0.01	0.01	0.01	0.02	0.02	0.02	0.06	0.02	0.01	0.01
Al	0.07	0.08	0.06	0.05	0.07	0.06	0.09	0.08	0.09	0.37	0.09	0.10	0.07
Fe	0.28	0.33	0.36	0.37	0.26	0.26	0.27	0.29	0.23	0.47	0.25	0.21	0.37
Mn	0.01	0.01	0.02	0.01	0.01	0.00	0.01	0.01	0.00	0.01	0.01	0.01	0.01
Mg	0.81	0.85	0.76	0.77	0.84	0.90	0.86	0.88	0.87	0.81	0.84	0.79	0.81
Ca	0.86	0.76	0.82	0.86	0.84	0.81	0.83	0.78	0.84	0.50	0.89	0.88	0.79
Na	0.01	0.01	0.01	0.01	0.01	0.01	0.01	0.01	0.01	0.01	0.01	0.01	0.01
K	0.00	0.00	0.00	0.00	0.00	0.00	0.00	0.00	0.00	0.04	0.00	0.00	0.00
Cr	0.01	0.01	0.00	0.01	0.00	0.01	0.01	0.00	0.01	0.00	0.01	0.02	0.00
Ni	0.01	0.00	0.00	0.01	0.00	0.00	0.00	0.01	0.00	0.00	0.00	0.00	0.00
Sum	4.01	4.00	4.00	4.00	4.00	4.02	4.00	3.99	4.00	4.00	4.01	4.00	4.00
End members (mole%)													
En	41.5	43.8	39.2	38.5	43.3	45.7	43.9	45.1	44.8	45.5	42.4	42.0	41.1
Fs	14.4	17.0	18.6	18.5	13.4	13.2	13.8	14.9	11.9	26.4	12.6	11.2	18.8
Wo	44.1	39.2	42.3	43.0	43.3	41.1	42.3	40.0	43.3	28.1	44.9	46.8	40.1
mg#	74.3	72.0	67.9	67.5	76.4	77.6	76.1	75.2	79.1	63.3	77.1	79.0	68.6

* Total iron as FeO

Table 2. (Contd.)

Sample	NS-3/2	NS-3/2	NS-3/7	NS-3/7	NS-3/8	NS-3/12	NS-3/12	NS-3/25	NS-3/34	NS-3/53	NS-5/12	WG-7	WG-7
Oxide (wt%)													
SiO_2	51.11	52.22	50.38	51.13	50.28	51.82	51.99	52.02	52.34	51.82	48.69	52.92	51.56
TiO_2	0.55	0.33	0.43	0.32	0.33	0.27	0.48	0.30	0.33	0.55	0.11	0.45	0.42
Al_2O_3	1.58	0.94	1.62	1.43	1.43	1.35	1.79	1.54	1.63	1.88	0.57	1.87	1.98
FeO*	11.62	9.69	10.41	10.05	11.13	14.38	8.86	12.55	7.00	8.53	20.71	8.89	9.37
MnO	0.58	0.13	0.24	0.45	0.50	0.52	0.63	0.24	0.37	0.58	1.34	0.16	0.42
MgO	14.13	14.12	13.89	13.40	14.37	17.53	15.80	14.77	15.56	14.82	7.48	15.51	15.37
CaO	20.22	22.47	21.89	22.15	20.42	13.68	19.95	17.78	22.87	22.00	19.25	19.88	19.78
Na_2O	0.16	0.16	0.15	0.14	0.16	0.16	0.16	0.16	0.16	0.16	0.19	0.14	0.16
K_2O	0.06	<0.05	<0.05	0.13	<0.05	<0.05	0.05	0.06	<0.05	<0.05	<0.05	<0.05	0.05
Cr_2O_3	<0.05	0.06	<0.05	<0.05	0.06	<0.05	0.15	<0.05	0.14	<0.05	0.06	0.06	0.05
NiO	0.08	<0.05	0.16	<0.05	0.43	0.41	0.15	<0.05	<0.05	<0.05	0.44	0.08	0.09
Sum	100.09	100.12	99.17	99.20	99.11	100.12	100.01	99.42	100.40	100.34	98.84	99.96	99.25
Cations per 6 oxygens													
Si	1.90	1.96	1.89	1.92	1.89	1.93	1.92	1.96	1.91	1.90	1.97	1.94	1.92
Ti	0.02	0.01	0.01	0.01	0.01	0.01	0.01	0.01	0.01	0.02	0.00	0.01	0.01
Al	0.07	0.04	0.07	0.06	0.06	0.06	0.08	0.07	0.07	0.08	0.03	0.08	0.09
Fe	0.37	0.30	0.33	0.32	0.35	0.45	0.28	0.39	0.22	0.27	0.69	0.28	0.29
Mn	0.02	0.00	0.01	0.01	0.02	0.02	0.02	0.01	0.01	0.02	0.04	0.01	0.01
Mg	0.79	0.79	0.79	0.76	0.81	0.97	0.88	0.83	0.86	0.82	0.44	0.88	0.85
Ca	0.81	0.90	0.89	0.90	0.84	0.55	0.80	0.73	0.91	0.88	0.82	0.79	0.80
Na	0.01	0.01	0.01	0.01	0.01	0.00	0.01	0.01	0.01	0.01	0.01	0.01	0.01
K	0.00	0.00	0.00	0.01	0.00	0.00	0.00	0.00	0.00	0.00	0.00	0.00	0.00
Cr	0.00	0.00	0.00	0.00	0.00	0.00	0.00	0.00	0.00	0.00	0.00	0.00	0.00
Ni	0.00	0.00	0.00	0.00	0.01	0.00	0.00	0.00	0.00	0.00	0.01	0.00	0.01
Sum	3.99	4.01	4.00	4.00	4.00	3.99	4.00	4.01	4.00	4.00	4.01	4.00	3.99
End members (mole%)													
En	40.1	39.7	39.3	38.4	40.5	49.2	44.9	42.6	43.2	41.6	22.6	45.1	43.8
Fs	18.8	15.1	16.4	16.2	17.5	22.8	14.3	20.0	11.1	13.7	35.4	14.4	14.9
Wo	41.1	45.2	44.3	45.5	42.0	27.9	40.8	37.4	45.7	44.7	42.1	40.5	41.2
mg#	68.1	72.5	70.5	70.4	69.8	68.3	75.9	68.0	79.6	75.2	38.9	75.9	74.6

* Total iron as FeO

Table 2. (Contd.)

Sample	WG-7	WG-7	WG-27	WG-31	WG-31	WG-31	WG-35	WG-35	WG-35	WG-44	WG-84	WG-92	WG-107	WG-124
Oxide (wt%)														
SiO_2	52.98	51.14	52.69	52.12	52.29	51.39	50.48	50.61	51.66	51.90	53.01	51.92	52.33	51.52
TiO_2	0.31	0.51	0.39	0.60	0.34	0.56	0.48	0.41	0.21	0.52	0.30	0.27	0.41	0.68
Al_2O_3	2.02	1.99	2.23	1.88	1.94	1.78	1.91	1.95	1.26	1.62	1.49	1.39	1.77	1.98
FeO*	8.09	8.22	6.01	8.60	9.19	10.93	8.21	9.45	9.06	11.40	12.81	9.33	7.21	7.79
MnO	0.21	0.29	0.23	0.34	0.16	0.52	0.63	0.45	0.17	0.58	0.41	0.54	0.26	0.23
MgO	15.09	14.44	15.74	15.48	15.71	16.09	14.53	14.77	15.33	15.32	19.01	14.39	15.64	15.43
CaO	20.27	21.44	21.26	20.75	19.92	17.63	22.36	21.16	20.76	17.88	12.49	21.34	21.59	21.94
Na_2O	0.15	0.16	0.16	0.16	0.16	0.16	0.16	0.18	0.18	0.16	0.15	0.16	0.16	0.16
K_2O	0.05	0.18	0.12	<0.05	0.07	<0.05	0.05	<0.05	0.07	<0.05	0.06	0.06	0.05	0.05
Cr_2O_3	0.44	0.30	0.85	0.16	<0.05	0.08	0.11	0.47	0.12	<0.05	0.19	<0.05	0.18	0.11
NiO	<0.05	0.15	0.31	0.05	0.23	0.37	0.13	0.27	0.52	<0.05	<0.05	0.10	0.45	0.13
Sum	99.61	98.82	99.99	100.14	100.01	99.51	99.05	99.72	99.34	99.38	99.92	99.50	100.05	100.02
Cations per 6 oxygens														
Si	1.96	1.93	1.94	1.93	1.92	1.92	1.90	1.89	1.93	1.95	1.95	1.94	1.93	1.89
Ti	0.01	0.01	0.01	0.02	0.01	0.02	0.01	0.01	0.01	0.01	0.01	0.01	0.01	0.02
Al	0.09	0.09	0.10	0.08	0.09	0.08	0.08	0.09	0.06	0.07	0.06	0.06	0.08	0.09
Fe	0.26	0.26	0.19	0.27	0.29	0.34	0.26	0.30	0.28	0.36	0.40	0.29	0.22	0.24
Mn	0.01	0.01	0.01	0.01	0.01	0.02	0.02	0.01	0.01	0.02	0.01	0.02	0.01	0.01
Mg	0.84	0.81	0.86	0.85	0.87	0.89	0.81	0.82	0.85	0.86	1.05	0.81	0.86	0.86
Ca	0.81	0.87	0.84	0.83	0.79	0.71	0.91	0.85	0.84	0.73	0.50	0.86	0.86	0.88
Na	0.01	0.01	0.01	0.01	0.01	0.01	0.01	0.01	0.01	0.01	0.01	0.01	0.01	0.01
K	0.00	0.01	0.01	0.00	0.00	0.00	0.00	0.00	0.00	0.00	0.00	0.00	0.00	0.00
Cr	0.01	0.01	0.02	0.00	0.00	0.00	0.00	0.01	0.00	0.00	0.01	0.00	0.01	0.00
Ni	0.00	0.00	0.01	0.00	0.01	0.01	0.00	0.01	0.02	0.00	0.00	0.00	0.01	0.00
Sum	4.00	4.01	4.00	4.00	4.00	4.00	4.00	4.00	4.01	4.01	4.00	4.00	4.00	4.00
End members (mole%)														
En	44.0	41.8	45.5	43.6	44.6	45.9	40.9	41.6	43.1	44.1	53.8	41.3	44.3	43.4
Fs	13.6	13.4	10.1	13.8	14.9	17.5	13.1	15.2	14.2	18.5	20.5	14.8	11.3	12.1
Wo	42.4	44.8	44.4	42.6	40.5	36.6	46.0	43.1	42.6	37.4	25.6	43.9	44.3	44.4
mg#	76.4	75.7	81.9	75.9	75.0	72.4	75.7	73.2	75.2	70.5	72.4	73.6	79.6	78.2

* Total iron as FeO

Table 3. Orthopyroxene mineral compositions of the Wateranga intrusion

Sample	NS-2/1	NS-2/1	NS-2/1	NS-2/2	NS-2/2	NS-2/2	NS-2/2	NS-2/11	NS-2/11	NS-2/14	NS-2/14	NS-2/14	NS-2/19
Oxide (wt%)													
SiO_2	52.52	52.23	52.14	53.14	52.43	52.62	51.48	52.12	51.44	52.03	51.94	51.60	51.34
TiO_2	0.06	0.17	0.30	0.13	0.31	0.40	0.56	0.20	0.15	0.14	0.18	0.25	0.20
Al_2O_3	1.13	0.88	0.66	0.91	0.69	1.28	1.12	0.62	0.64	0.59	0.67	0.67	0.66
FeO*	28.17	27.36	27.68	24.44	25.89	24.94	25.74	25.42	24.77	26.14	24.23	26.17	23.70
MnO	0.86	0.97	0.92	0.86	0.51	0.56	0.45	0.63	0.76	0.83	0.82	0.71	0.91
MgO	16.34	16.83	16.76	18.22	18.40	17.45	18.17	18.85	20.22	18.92	19.01	18.96	20.52
CaO	0.88	1.14	1.13	1.71	1.53	2.70	1.82	1.99	1.43	1.04	2.24	1.34	1.54
Na_2O	0.13	0.11	0.14	0.12	0.12	0.11	0.09	0.16	0.16	0.18	0.18	0.16	0.17
K_2O	0.06	0.11	0.06	<0.05	0.11	<0.05	0.07	<0.05	0.06	<0.05	0.10	0.05	0.06
Cr_2O_3	0.09	0.10	<0.05	0.14	0.11	<0.05	0.06	<0.05	0.06	0.14	0.06	<0.05	<0.05
NiO	<0.05	0.06	0.10	0.06	<0.05	0.06	<0.05	0.25	0.05	0.06	<0.05	0.13	<0.05
Sum	100.24	99.96	99.89	99.73	100.10	100.12	99.56	100.24	99.74	100.07	99.43	100.04	99.10
Cations per 6 oxygens													
Si	1.99	2.00	1.99	2.00	2.00	1.99	1.98	1.97	1.95	1.98	1.96	1.97	1.94
Ti	0.00	0.00	0.01	0.00	0.01	0.01	0.02	0.01	0.00	0.00	0.01	0.01	0.01
Al	0.05	0.04	0.03	0.04	0.03	0.06	0.05	0.03	0.03	0.03	0.03	0.03	0.03
Fe	0.91	0.88	0.89	0.80	0.82	0.79	0.83	0.81	0.79	0.83	0.78	0.84	0.76
Mn	0.03	0.03	0.03	0.03	0.02	0.02	0.01	0.02	0.02	0.03	0.03	0.02	0.03
Mg	0.98	0.99	1.00	1.06	1.04	1.02	1.03	1.06	1.15	1.07	1.08	1.08	1.16
Ca	0.04	0.05	0.05	0.07	0.06	0.11	0.07	0.08	0.06	0.04	0.09	0.05	0.06
Na	0.00	0.00	0.00	0.00	0.00	0.00	0.00	0.01	0.01	0.01	0.01	0.01	0.01
K	0.00	0.01	0.00	0.00	0.01	0.00	0.00	0.00	0.00	0.00	0.01	0.00	0.00
Cr	0.00	0.00	0.00	0.00	0.00	0.00	0.00	0.00	0.00	0.00	0.00	0.00	0.00
Ni	0.00	0.00	0.00	0.00	0.00	0.00	0.00	0.01	0.00	0.00	0.00	0.00	0.00
Sum	4.00	4.00	4.00	4.00	3.99	4.00	3.99	4.00	4.01	3.99	4.00	4.01	4.00
End members (mole%)													
En	50.8	51.6	51.5	54.9	54.2	53.1	53.4	54.4	57.5	55.2	55.4	54.8	58.6
Fs	47.2	45.8	45.9	41.5	42.7	41.1	43.0	41.5	39.5	42.8	40.0	42.6	38.4
Wo	2.1	2.6	2.6	3.6	3.1	5.7	3.6	4.1	3.0	2.1	4.6	2.5	3.0
mg#	51.9	52.9	52.9	57.0	55.9	56.4	55.4	56.7	59.3	56.3	58.1	56.3	60.4

* Total iron as FeO. Lower detection limit for all elements is 0.05 wt%.

Table 3. (Contd.)

Sample	NS-2/19	NS-2/19	NS-2/22	NS-2/22	NS-2/22	NS-2/22	NS-2/29	NS-2/29	NS-2/35	NS-2/41	NS-2/54	NS-2/59	NS-2/59
Oxide (wt%)													
SiO_2	52.18	52.60	52.48	51.17	51.60	51.85	52.48	52.32	51.70	51.09	53.63	53.00	51.96
TiO_2	0.12	0.22	0.20	0.22	0.26	0.16	0.20	0.25	0.10	0.14	0.14	<0.05	0.07
Al_2O_3	0.77	0.87	0.71	0.76	0.63	0.57	0.68	0.71	0.61	0.62	0.64	0.16	0.64
FeO*	21.40	21.30	23.71	23.57	25.04	24.86	20.32	20.62	24.79	24.83	18.42	20.48	20.03
MnO	0.64	0.67	0.77	0.94	0.69	0.71	0.51	0.59	1.03	0.76	0.58	0.75	0.69
MgO	21.52	22.11	20.51	19.68	20.24	20.50	23.29	22.56	19.65	19.08	25.17	24.14	24.08
CaO	1.96	1.91	1.67	2.37	1.41	1.02	1.51	1.99	1.30	2.15	1.39	0.71	1.24
Na_2O	0.17	0.16	0.16	0.16	0.16	0.16	0.14	0.16	0.19	0.20	0.16	0.16	0.20
K_2O	0.05	0.06	0.06	0.06	0.06	0.06	<0.05	<0.05	<0.05	0.06	0.07	0.06	<0.05
Cr_2O_3	<0.05	<0.05	0.07	<0.05	<0.05	0.12	0.05	<0.05	<0.05	<0.05	<0.05	0.06	0.20
NiO	<0.05	0.12	<0.05	<0.05	<0.05	0.06	<0.05	<0.05	<0.05	<0.05	<0.05	0.05	0.05
Sum	98.81	100.02	100.34	98.93	100.09	100.07	99.18	99.20	99.37	98.93	100.20	99.57	99.16
Cations per 6 oxygens													
Si	1.98	1.96	1.96	1.95	1.93	1.95	1.94	1.95	1.98	1.97	1.96	1.96	1.91
Ti	0.00	0.01	0.01	0.01	0.01	0.00	0.01	0.01	0.00	0.00	0.00	0.00	0.00
Al	0.03	0.04	0.03	0.03	0.03	0.03	0.03	0.03	0.03	0.03	0.03	0.03	0.03
Fe	0.68	0.66	0.75	0.76	0.79	0.79	0.64	0.65	0.79	0.79	0.57	0.63	0.63
Mn	0.02	0.02	0.02	0.03	0.02	0.02	0.02	0.02	0.03	0.02	0.02	0.02	0.02
Mg	1.22	1.23	1.15	1.12	1.15	1.16	1.29	1.25	1.12	1.10	1.36	1.33	1.33
Ca	0.08	0.08	0.07	0.10	0.06	0.04	0.06	0.08	0.05	0.09	0.05	0.03	0.05
Na	0.01	0.01	0.01	0.01	0.01	0.01	0.01	0.01	0.01	0.01	0.01	0.01	0.01
K	0.00	0.00	0.00	0.00	0.00	0.00	0.00	0.00	0.00	0.00	0.00	0.00	0.00
Cr	0.00	0.00	0.00	0.00	0.00	0.00	0.00	0.00	0.00	0.00	0.00	0.00	0.01
Ni	0.00	0.00	0.00	0.00	0.00	0.00	0.00	0.00	0.00	0.00	0.00	0.00	0.00
Sum	4.02	4.01	4.00	4.01	4.00	4.00	4.00	4.00	4.01	4.01	4.00	4.01	3.99
End members (mole%)													
En	61.6	62.4	58.4	56.6	57.5	58.3	64.8	63.1	57.1	55.6	68.7	66.8	66.2
Fs	34.3	33.5	38.1	38.4	39.5	39.7	32.2	32.8	40.3	39.9	28.8	31.7	31.3
Wo	4.0	4.1	3.6	5.1	3.0	2.0	3.0	4.0	2.6	4.5	2.5	1.5	2.5
mg#	64.2	65.1	60.5	59.6	59.3	59.5	66.8	65.8	58.6	58.2	70.5	67.9	67.9

* Total iron as FeO

Table 3. (Contd.)

Sample	NS-2/61	NS-3/7	NS-3/8	NS-3/12	NS-3/25	NS-3/34	NS-3/53	NS-5/6	NS-5/6	NS-5/15	WG-44	WG-44	WG-107	WG-107
Oxide (wt%)														
SiO_2	52.22	51.97	52.79	56.80	52.22	53.52	53.08	49.42	48.93	53.18	52.64	52.15	53.43	53.98
TiO_2	0.10	0.07	0.30	0.17	0.27	0.26	0.22	0.07	0.13	0.25	0.22	0.20	0.26	0.26
Al_2O_3	1.08	0.72	0.67	0.26	0.86	0.86	0.80	0.25	0.66	0.24	0.75	0.87	1.06	0.94
FeO*	18.16	23.32	21.85	8.60	20.60	16.08	18.51	34.85	32.13	21.07	21.01	20.43	17.18	16.70
MnO	0.70	0.35	0.76	0.23	0.74	0.38	0.48	1.58	1.36	0.51	0.67	0.30	0.42	0.58
MgO	25.62	21.88	21.52	32.56	21.88	26.88	24.20	12.27	13.83	22.84	23.39	22.72	25.89	25.89
CaO	1.26	1.57	1.86	0.43	1.46	0.96	1.66	1.31	1.49	0.66	1.23	1.67	1.18	1.42
Na_2O	0.16	0.16	0.16	0.16	0.15	0.15	0.17	0.17	0.16	0.16	0.16	0.15	0.16	0.16
K_2O	0.05	0.06	0.14	0.05	0.11	0.06	<0.05	<0.05	<0.05	0.11	<0.05	0.09	0.05	0.06
Cr_2O_3	0.08	0.05	<0.05	<0.05	0.18	0.16	0.06	<0.05	0.09	0.10	0.26	0.06	0.09	<0.05
NiO	0.09	<0.05	<0.05	0.39	0.29	0.42	0.41	<0.05	0.35	0.29	<0.05	0.31	<0.05	0.07
Sum	99.52	100.15	100.05	99.65	98.76	99.73	99.59	99.92	99.13	99.41	100.33	98.95	99.72	100.06
Cations per 6 oxygens														
Si	1.91	1.93	1.97	1.99	1.97	1.93	1.96	1.97	1.95	1.98	1.93	1.92	1.94	1.95
Ti	0.00	0.00	0.01	0.00	0.01	0.01	0.01	0.00	0.00	0.01	0.01	0.01	0.01	0.01
Al	0.05	0.03	0.03	0.01	0.04	0.04	0.03	0.01	0.03	0.01	0.03	0.04	0.05	0.04
Fe	0.56	0.73	0.68	0.25	0.65	0.49	0.57	1.17	1.07	0.66	0.65	0.64	0.53	0.51
Mn	0.02	0.01	0.02	0.01	0.02	0.01	0.01	0.05	0.05	0.02	0.02	0.01	0.01	0.02
Mg	1.39	1.23	1.20	1.70	1.23	1.46	1.34	0.73	0.82	1.26	1.29	1.27	1.40	1.40
Ca	0.05	0.06	0.07	0.02	0.06	0.04	0.07	0.06	0.06	0.03	0.05	0.07	0.05	0.06
Na	0.01	0.01	0.01	0.01	0.01	0.01	0.01	0.01	0.01	0.01	0.01	0.01	0.01	0.01
K	0.00	0.00	0.01	0.00	0.01	0.01	0.00	0.00	0.00	0.01	0.00	0.00	0.00	0.00
Cr	0.00	0.00	0.00	0.00	0.01	0.00	0.00	0.00	0.00	0.00	0.01	0.00	0.00	0.00
Ni	0.00	0.00	0.00	0.01	0.01	0.00	0.01	0.00	0.01	0.01	0.00	0.01	0.00	0.00
Sum	3.99	4.00	4.00	4.00	4.02	4.00	4.01	4.00	4.00	4.00	4.00	3.98	4.00	4.00
End members (mole%)														
En	69.5	60.9	61.5	86.3	63.4	73.4	67.7	37.2	42.1	64.6	64.8	64.1	70.7	71.1
Fs	28.0	36.1	34.9	12.7	33.5	24.6	28.8	59.7	54.9	33.8	32.7	32.3	26.8	25.9
Wo	2.5	3.0	3.6	1.0	3.1	2.0	3.5	3.1	3.1	1.5	2.5	3.5	2.5	3.0
mg#	71.3	62.8	63.8	87.2	65.4	74.9	70.2	38.4	43.4	65.6	66.5	66.5	72.5	73.3

* Total iron as FeO

Table 4. Olivine mineral compositions of the Wateranga intrusion

Sample	NS-2/4	NS-2/4	NS-2/4	NS-2/19	NS-2/29	NS-2/29	NS-2/29	NS-2/29	NS-2/31	NS-2/31	NS-2/31	NS-2/35
Oxide (wt%)												
SiO_2	35.45	34.47	34.64	34.83	35.50	35.60	36.15	35.58	34.57	34.17	34.16	34.75
FeO*	44.58	45.95	44.74	40.84	36.77	36.60	35.98	35.44	41.96	43.01	42.44	42.28
MnO	0.87	0.75	0.96	0.74	0.75	0.57	0.66	0.64	0.79	0.70	0.94	0.73
MgO	18.57	18.98	17.87	23.72	26.74	26.61	27.07	27.29	21.98	21.79	22.16	21.56
CaO	<0.05	<0.05	0.05	<0.05	0.06	<0.05	0.06	<0.05	<0.05	0.16	0.08	0.07
NiO	0.16	0.12	<0.05	0.05	<0.05	0.13	0.16	<0.05	0.08	0.06	0.06	0.12
Sum	99.63	100.27	98.26	100.18	99.82	99.51	100.08	98.95	99.38	99.89	99.84	99.51
Cations per 4 oxygens												
Si	1.05	1.02	1.04	1.00	1.00	1.01	1.02	1.00	1.01	0.99	0.99	1.01
Fe	1.10	1.13	1.12	0.97	0.86	0.86	0.84	0.84	1.01	1.04	1.03	1.03
Mn	0.02	0.02	0.03	0.02	0.02	0.01	0.02	0.02	0.02	0.02	0.02	0.02
Mg	0.82	0.83	0.80	1.01	1.12	1.12	1.12	1.15	0.95	0.94	0.96	0.94
Ca	0.00	0.00	0.00	0.00	0.00	0.00	0.00	0.00	0.00	0.01	0.00	0.00
Ni	0.00	0.00	0.00	0.00	0.00	0.00	0.00	0.00	0.00	0.00	0.00	0.00
Sum	2.99	3.00	2.99	3.00	3.00	3.00	3.00	3.01	2.99	3.00	3.00	3.00
End members (mole%)												
Fo	42.7	42.3	41.7	51.0	56.6	56.6	57.1	57.8	48.5	47.5	48.2	47.7
Fa	57.3	57.7	58.3	49.0	43.4	43.4	42.9	42.2	51.5	52.5	51.8	52.3

* Total iron as FeO. Lower detection limit for all elements is 0.05 wt%.

Table 4. (Contd.)

Sample	NS-2/48	NS-2/54	NS-2/54	NS-2/57	NS-2/59	NS-2/59	NS-2/59	NS-2/59	NS-2/61	NS-2/63	NS-2/63	NS-3/12
Oxide (wt%)												
SiO_2	37.14	37.01	36.07	36.05	35.65	35.20	36.31	36.11	36.60	36.49	36.31	34.90
FeO*	29.50	30.81	29.82	32.59	34.90	35.12	33.86	33.15	30.29	26.40	27.04	33.75
MnO	0.57	0.71	0.25	0.59	0.78	0.52	0.42	0.16	0.29	0.33	0.47	0.23
MgO	32.29	31.21	32.18	29.79	28.04	28.63	29.70	30.31	32.07	35.99	35.01	29.95
CaO	0.06	<0.05	<0.05	0.12	<0.05	0.25	0.06	0.07	<0.05	<0.05	<0.05	0.13
NiO	0.05	<0.05	0.12	0.17	<0.05	0.18	<0.05	<0.05	<0.05	<0.05	0.31	0.06
Sum	99.61	99.74	98.44	99.31	99.37	99.90	100.35	99.80	99.25	99.21	99.14	99.02
Cations per 4 oxygens												
Si	1.01	1.01	0.99	1.00	1.00	0.98	1.00	0.99	1.00	0.99	0.98	0.96
Fe	0.67	0.70	0.69	0.75	0.82	0.82	0.78	0.76	0.70	0.59	0.61	0.79
Mn	0.01	0.02	0.01	0.01	0.02	0.01	0.01	0.01	0.01	0.01	0.00	0.01
Mg	1.31	1.27	1.32	1.24	1.16	1.18	1.22	1.24	1.29	1.41	1.41	1.24
Ca	0.00	0.00	0.00	0.00	0.00	0.01	0.00	0.00	0.00	0.00	0.00	0.00
Ni	0.00	0.00	0.00	0.00	0.00	0.00	0.00	0.00	0.00	0.00	0.01	0.00
Sum	3.00	3.00	3.01	3.00	3.00	3.00	3.01	3.00	3.00	3.00	3.01	3.00
End members (mole%)												
Fo	66.2	64.5	65.7	62.3	58.6	59.0	61.0	62.0	64.8	70.5	69.8	61.1
Fa	33.8	35.5	34.3	37.7	41.4	41.0	39.0	38.0	35.2	29.5	30.2	38.9

* Total iron as FeO

Table 4. (Contd.)

Sample	NS-3/12	NS-3/25	NS-3/25	NS-5/12	NS-5/12	WG-27	WG-27	WG-27	WG-31	WG-35	WG-44	WG-84	WG-107	WG-124
Oxide (wt%)														
SiO_2	36.33	35.72	35.54	30.25	29.82	37.66	39.15	38.50	36.68	36.03	35.93	37.08	36.50	36.30
FeO*	32.59	35.68	36.32	62.53	62.49	24.72	23.27	24.84	32.22	31.30	36.49	27.91	30.76	29.32
MnO	0.65	0.83	0.80	2.19	1.95	0.41	0.26	0.59	0.50	0.40	0.64	0.33	0.53	0.60
MgO	29.90	27.73	27.46	4.65	4.18	36.76	36.44	35.74	30.81	31.11	26.24	34.09	31.98	33.05
CaO	<0.05	0.19	0.15	0.05	0.15	<0.05	0.06	<0.05	0.13	<0.05	0.14	0.06	<0.05	<0.05
NiO	0.08	<0.05	<0.05	0.07	<0.05	0.30	0.06	0.13	<0.05	0.28	0.18	0.12	0.12	<0.05
Sum	99.55	100.15	100.27	99.74	98.59	99.85	99.24	99.80	100.34	99.12	99.62	99.59	99.89	99.27
Cations per 4 oxygens														
Si	1.00	1.00	0.99	0.99	1.00	0.99	1.03	1.02	1.00	0.99	1.01	1.00	0.99	0.99
Fe	0.75	0.83	0.85	1.72	1.74	0.55	0.51	0.55	0.74	0.72	0.85	0.63	0.70	0.67
Mn	0.02	0.02	0.02	0.06	0.05	0.01	0.01	0.02	0.01	0.01	0.02	0.01	0.01	0.01
Mg	1.23	1.14	1.14	0.23	0.20	1.44	1.44	1.41	1.25	1.27	1.11	1.36	1.30	1.33
Ca	0.00	0.01	0.00	0.00	0.01	0.00	0.00	0.00	0.00	0.00	0.00	0.00	0.00	0.00
Ni	0.00	0.00	0.00	0.00	0.00	0.01	0.00	0.00	0.00	0.01	0.00	0.00	0.00	0.00
Sum	3.00	3.00	3.00	3.00	3.00	3.00	2.99	3.00	3.00	3.00	2.99	3.00	3.00	3.00
End members (mole%)														
Fo	62.1	57.9	57.3	11.8	10.3	72.4	73.8	71.9	62.8	63.8	56.6	68.3	65.0	66.5
Fa	37.9	42.1	42.7	88.2	89.7	27.6	26.2	28.1	37.2	36.2	43.4	31.7	35.0	33.5

* Total iron as FeO

Table 5. Ilmenite mineral compositions of the Wateranga intrusion

Sample	NS-2/1	NS-2/2	NS-2/2	NS-2/11	NS-2/19	NS-2/19	NS-2/22	NS-2/22	NS-2/22	NS-2/22	NS-2/22
Oxide (wt%)											
TiO_2	52.46	52.02	51.80	52.35	51.55	46.91	50.96	50.09	49.98	50.40	51.32
Al_2O_3	0.05	0.11	0.22	0.19	0.11	1.68	0.16	0.15	0.07	0.16	0.09
FeO(t)	44.95	43.40	45.49	45.48	44.52	44.52	46.60	46.60	47.66	47.25	46.35
MnO	2.31	0.53	0.80	0.75	0.52	3.19	0.85	0.87	0.92	0.79	0.67
MgO	0.05	0.96	0.18	1.24	2.06	3.00	0.51	1.10	0.06	0.81	1.39
Cr_2O_3	0.13	0.22	<0.05	0.14	0.14	0.05	0.05	0.07	<0.05	0.24	0.18
ZnO	0.09	0.50	0.38	<0.05	0.06	0.20	<0.05	<0.05	0.05	<0.05	<0.05
Sum	100.04	97.74	98.87	100.15	98.96	99.54	99.13	98.88	98.74	99.65	100.00
Cations per 3 oxygens											
Ti	1.00	1.00	0.98	0.98	0.98	0.86	0.97	0.95	0.97	0.96	0.97
Al	0.00	0.00	0.01	0.01	0.00	0.05	0.00	0.00	0.00	0.00	0.00
Fe^{3+}	0.01	0.00	0.00	0.02	0.05	0.22	0.06	0.09	0.08	0.09	0.07
Fe^{2+}	0.94	0.93	0.96	0.92	0.89	0.69	0.93	0.90	0.93	0.90	0.90
Mn	0.05	0.01	0.02	0.02	0.01	0.07	0.02	0.02	0.02	0.02	0.01
Mg	0.00	0.04	0.01	0.05	0.08	0.11	0.02	0.04	0.00	0.03	0.05
Cr	0.00	0.00	0.00	0.00	0.00	0.00	0.00	0.00	0.00	0.00	0.00
Zn	0.00	0.01	0.01	0.00	0.00	0.00	0.00	0.00	0.00	0.00	0.00
Sum	2.00	1.99	1.99	2.00	2.01	2.00	2.00	2.00	2.00	2.00	2.00
He %	0.1	0.0	0.0	1.5	2.7	13.6	2.8	4.9	4.1	4.6	3.8

He % = hematite % in ilmenite. Lower detection limit for all elements is 0.05 wt%.

Table 5. (Contd.)

Sample	NS-2/31	NS-2/31	NS-2/31	NS-2/59	NS-2/59	NS-2/59	NS-3/2	NS-3/7	NS-3/7	NS-3/8	NS-3/25	NS-3/53
Oxide (wt%)												
TiO_2	51.30	41.41	52.20	51.10	52.80	50.44	50.17	50.42	49.30	51.96	51.35	52.07
Al_2O_3	0.22	4.45	0.20	0.12	0.19	0.22	0.39	0.45	0.33	<0.05	<0.05	<0.05
FeO(t)	45.19	48.48	44.50	45.03	44.18	45.85	46.23	45.77	47.55	45.82	45.60	46.28
MnO	0.72	0.88	0.67	0.67	0.38	0.59	0.88	1.34	0.92	0.68	0.52	1.15
MgO	1.28	4.23	1.15	1.76	1.47	1.58	0.60	0.60	0.22	1.22	1.79	<0.05
Cr_2O_3	0.20	<0.05	0.13	0.07	<0.05	0.05	0.05	0.51	<0.05	0.12	<0.05	0.12
ZnO	0.41	0.06	0.32	<0.05	<0.05	<0.05	0.12	<0.05	<0.05	0.10	<0.05	0.28
Sum	99.32	99.52	99.17	98.75	99.02	98.73	98.44	99.09	98.32	99.90	99.26	99.90
Cations per 3 oxygens												
Ti	0.97	0.74	0.99	0.98	1.00	0.96	0.96	0.97	0.95	0.98	0.97	1.00
Al	0.01	0.12	0.01	0.00	0.01	0.01	0.01	0.01	0.01	0.00	0.00	0.00
Fe^{3+}	0.04	0.39	0.01	0.06	0.00	0.08	0.07	0.06	0.10	0.04	0.06	0.01
Fe^{2+}	0.90	0.58	0.93	0.88	0.93	0.88	0.92	0.90	0.91	0.92	0.89	0.97
Mn	0.02	0.02	0.01	0.01	0.01	0.01	0.02	0.03	0.02	0.01	0.01	0.02
Mg	0.05	0.15	0.04	0.07	0.05	0.06	0.02	0.02	0.01	0.05	0.07	0.00
Cr	0.00	0.00	0.00	0.00	0.00	0.00	0.00	0.01	0.00	0.00	0.00	0.00
Zn	0.01	0.00	0.00	0.00	0.00	0.00	0.00	0.00	0.00	0.00	0.00	0.00
Sum	2.00	2.00	1.99	2.00	2.00	2.00	2.00	2.00	2.00	2.00	2.00	2.00
He %	2.3	24.0	0.3	3.3	0.0	4.4	3.4	3.2	5.0	2.2	3.6	0.7

He % = hematite % in ilmenite

Table 5. (Contd.)

Sample	NS-3/53	NS-5/6	NS-5/6	NS-5/6	NS-5/12	WG-27	WG-27	WG-27	WG-31	WG-31	WG-44	WG-84	WG-107	WG-107	WG-124
Oxide (wt%)															
TiO_2	48.98	50.55	50.34	52.15	51.61	51.49	50.72	49.52	50.30	51.30	51.07	50.78	52.89	51.65	50.81
Al_2O_3	0.37	<0.05	0.34	0.38	<0.05	0.47	<0.05	2.09	0.47	0.44	0.12	0.17	0.14	0.29	0.21
FeO(t)	47.64	47.30	44.61	45.28	46.77	42.10	45.30	41.71	43.70	43.22	47.10	45.29	42.12	41.20	44.35
MnO	0.19	1.06	1.25	1.02	1.19	0.68	0.32	0.73	0.79	0.47	0.49	0.64	0.40	0.78	0.58
MgO	0.76	<0.05	0.26	0.37	0.32	4.51	3.78	5.26	3.08	3.21	1.62	1.80	3.73	3.61	3.42
Cr_2O_3	0.53	0.06	<0.05	<0.05	0.23	<0.05	<0.05	0.18	0.08	0.15	<0.05	0.44	0.19	0.20	0.19
ZnO	0.50	<0.05	0.54	<0.05	<0.05	<0.05	<0.05	<0.05	0.46	0.32	<0.05	<0.05	<0.05	0.10	0.05
Sum	98.97	98.97	97.34	99.20	100.12	99.25	100.12	99.50	98.88	99.11	100.40	99.12	99.47	97.83	99.61
Cations per 3 oxygens															
Ti	0.93	0.98	0.98	1.00	0.98	0.95	0.92	0.90	0.95	0.96	0.95	0.96	0.98	0.97	0.94
Al	0.01	0.00	0.01	0.01	0.00	0.01	0.00	0.06	0.01	0.01	0.00	0.00	0.00	0.01	0.01
Fe^{3+}	0.11	0.06	0.02	0.00	0.04	0.09	0.14	0.15	0.09	0.07	0.10	0.07	0.03	0.04	0.11
Fe^{2+}	0.90	0.94	0.94	0.95	0.94	0.77	0.79	0.69	0.81	0.83	0.88	0.88	0.84	0.82	0.80
Mn	0.00	0.02	0.03	0.02	0.03	0.01	0.01	0.01	0.02	0.01	0.01	0.01	0.01	0.02	0.01
Mg	0.03	0.00	0.01	0.01	0.01	0.17	0.14	0.19	0.11	0.12	0.06	0.07	0.14	0.14	0.13
Cr	0.01	0.00	0.00	0.00	0.00	0.00	0.00	0.00	0.00	0.00	0.00	0.01	0.00	0.00	0.00
Zn	0.01	0.00	0.01	0.00	0.00	0.00	0.00	0.00	0.01	0.01	0.00	0.00	0.00	0.00	0.00
Sum	2.00	2.00	2.00	1.99	2.00	2.00	2.00	2.00	2.00	2.01	2.00	2.00	2.00	2.00	2.00
He %	5.7	3.2	1.2	0.0	2.3	5.6	8.1	9.2	5.7	3.9	5.1	4.0	2.0	2.5	6.4

He % = hematite % in ilmenite

Table 6. Magnetite mineral compositions of the Wateranga intrusion

Sample	NS-2/31	NS-2/35	NS-2/48	NS-2/59	NS-2/59	NS-2/59	NS-2/59	NS-2/59	NS-3/7
Oxide (wt%)									
TiO_2	2.92	0.05	0.10	4.05	12.93	2.32	5.02	2.49	1.37
Al_2O_3	2.65	0.08	0.30	0.70	1.78	0.76	1.17	0.87	1.48
FeO(t)	85.86	98.96	99.11	93.16	81.16	95.52	91.92	96.43	95.10
MnO	0.14	0.06	0.10	0.11	0.51	<0.05	0.16	<0.05	0.24
MgO	0.06	0.08	0.05	0.05	2.88	0.23	0.37	<0.05	0.21
Cr_2O_3	5.57	0.11	0.07	0.15	0.18	0.11	0.16	0.35	1.12
ZnO	0.50	0.44	0.28	0.17	0.06	0.05	<0.05	<0.05	<0.05
Sum	97.70	99.78	100.01	98.39	99.50	98.99	98.80	100.14	99.52
Cations per 4 oxygens									
Ti	0.08	0.00	0.00	0.12	0.35	0.06	0.14	0.07	0.04
Al	0.11	0.00	0.02	0.03	0.07	0.03	0.05	0.04	0.06
Fe^{3+}	1.60	1.98	1.97	1.73	1.23	1.84	1.68	1.82	1.84
Fe^{2+}	1.01	1.00	1.01	1.11	1.18	1.05	1.11	1.06	0.99
Mn	0.01	0.00	0.00	0.00	0.02	0.00	0.00	0.00	0.01
Mg	0.00	0.01	0.00	0.00	0.15	0.02	0.02	0.00	0.01
Cr	0.16	0.00	0.00	0.01	0.01	0.00	0.01	0.01	0.03
Zn	0.02	0.01	0.01	0.01	0.00	0.00	0.00	0.00	0.00
Sum	2.99	3.00	3.00	3.00	3.00	3.00	3.00	3.00	2.98
Usp %	8.8	0.0	0.1	11.2	35.4	6.4	13.8	6.9	3.5

Usp = ulvospinel % in magnetite. Lower detection limit for all elements is 0.05 wt%.

Table 6. (Contd.)

Sample	NS-3/25	NS-5/12	NS-5/12	WG-27	WG-31	WG-107	WG-107
Oxide (wt%)							
TiO_2	2.28	1.33	0.93	13.72	0.44	0.88	2.10
Al_2O_3	0.60	1.24	0.92	1.07	0.87	1.03	0.89
FeO(t)	92.01	97.18	96.10	82.12	96.98	94.13	92.28
MnO	0.09	<0.05	0.20	0.06	0.09	<0.05	0.09
MgO	<0.05	<0.05	0.14	0.49	<0.05	0.32	0.23
Cr_2O_3	2.80	<0.05	0.10	0.57	1.62	2.79	2.89
ZnO	<0.05	0.57	0.34	0.21	<0.05	<0.05	0.14
Sum	97.78	100.32	98.73	98.24	100.00	99.15	98.62
Cations per 4 oxygens							
Ti	0.06	0.04	0.02	0.38	0.02	0.02	0.06
Al	0.02	0.05	0.04	0.04	0.04	0.05	0.04
Fe^{3+}	1.80	1.86	1.91	1.18	1.90	1.85	1.80
Fe^{2+}	1.03	1.03	1.01	1.35	1.00	0.97	1.00
Mn	0.00	0.00	0.01	0.00	0.00	0.00	0.00
Mg	0.00	0.00	0.01	0.03	0.00	0.02	0.02
Cr	0.09	0.00	0.00	0.02	0.05	0.08	0.08
Zn	0.00	0.02	0.01	0.01	0.00	0.00	0.00
Sum	3.00	3.00	3.00	3.00	3.00	2.98	2.99
Usp %	6.4	3.7	2.2	39.1	1.1	2.5	5.9

Usp = ulvospinel % in magnetite

Table 7. Amphibole mineral compositions of the Wateranga intrusion

Sample	NS-2/1	NS-2/1	NS-2/4	NS-2/11	NS-2/14	NS-2/22	NS-2/22	NS-2/31	NS-2/41
Oxide (wt%)									
SiO_2	52.03	52.06	54.27	46.06	45.56	44.67	44.72	45.10	45.66
TiO_2	0.06	0.06	<0.05	2.39	2.65	3.32	3.26	3.53	3.88
Al_2O_3	0.58	0.56	1.75	9.85	9.29	10.54	10.36	10.72	10.08
FeO*	11.44	10.95	20.89	14.52	15.06	14.03	14.15	14.44	14.32
MnO	0.47	0.53	0.95	0.22	0.11	0.25	0.09	0.24	0.21
MgO	11.54	12.07	16.18	10.48	10.25	10.29	10.33	10.40	9.84
CaO	20.50	19.86	2.34	9.67	9.71	10.07	9.82	10.16	10.30
Na_2O	0.18	0.18	0.29	2.05	1.76	2.07	2.21	2.15	1.71
K_2O	0.10	0.10	0.08	0.68	0.93	0.93	0.81	0.77	0.71
Cr_2O_3	0.16	0.06	0.06	<0.05	0.30	0.06	0.08	0.08	0.10
Sum	97.05	96.43	96.81	95.92	95.61	96.21	95.84	97.59	96.81
Cations per 23 oxygens									
Si	7.74	7.76	7.98	6.90	6.87	6.68	6.71	6.66	6.77
Ti	0.00	0.00	0.00	0.27	0.30	0.37	0.37	0.39	0.43
Al^{iv}	0.26	0.24	0.02	1.10	1.13	1.32	1.29	1.34	1.23
Al^{vi}	0.16	0.14	0.28	0.64	0.52	0.54	0.54	0.53	0.53
Fe	1.42	1.36	2.59	1.82	1.90	1.76	1.78	1.78	1.78
Mn	0.06	0.07	0.12	0.03	0.01	0.03	0.01	0.03	0.03
Mg	2.56	2.68	3.59	2.34	2.30	2.30	2.31	2.29	2.18
Ca	3.27	3.17	0.43	1.55	1.57	1.62	1.58	1.61	1.64
Na	0.05	0.05	0.08	0.60	0.51	0.60	0.65	0.61	0.49
K	0.02	0.02	0.01	0.13	0.18	0.18	0.16	0.15	0.13
Cr	0.02	0.00	0.00	0.00	0.03	0.00	0.01	0.01	0.01
Sum	15.56	15.49	15.10	15.38	15.32	15.40	15.41	15.40	15.22
mg#	64.3	66.3	58.1	56.3	54.8	56.7	56.5	56.3	55.1

* Total iron as FeO. Lower detection limit for all elements is 0.05 wt%.

Table 7. (Contd.)

Sample	NS-2/59	NS-2/59	NS-2/61	NS-2/63	NS-5/6	WG-84	WG-107
Oxide (wt%)							
SiO_2	45.50	44.09	45.05	45.57	45.26	42.55	50.42
TiO_2	0.61	3.18	3.86	3.63	2.36	0.11	0.16
Al_2O_3	12.08	11.14	11.20	10.89	8.94	13.34	5.62
FeO*	12.30	12.65	11.31	10.20	19.90	15.51	21.32
MnO	0.08	0.13	0.15	0.11	0.43	0.19	0.35
MgO	12.77	11.06	13.09	13.27	6.98	14.45	15.62
CaO	10.21	10.10	9.50	10.55	9.46	8.98	1.16
Na_2O	2.35	2.09	2.23	2.34	2.04	0.47	0.56
K_2O	0.44	0.55	0.64	0.42	0.92	0.14	0.76
Cr_2O_3	0.06	0.17	0.09	0.21	0.37	0.06	0.05
Sum	96.39	95.17	97.11	97.19	96.64	95.80	96.02
Cations per 23 oxygens							
Si	6.70	6.62	6.57	6.62	6.92	6.37	7.49
Ti	0.07	0.36	0.42	0.40	0.27	0.01	0.02
Al^{iv}	1.30	1.38	1.43	1.38	1.08	1.63	0.51
Al^{vi}	0.80	0.59	0.49	0.48	0.53	0.72	0.47
Fe	1.51	1.59	1.38	1.24	2.55	1.94	2.65
Mn	0.01	0.02	0.02	0.01	0.05	0.02	0.04
Mg	2.80	2.47	2.85	2.87	1.59	3.22	3.46
Ca	1.61	1.62	1.49	1.64	1.55	1.44	0.18
Na	0.67	0.61	0.63	0.66	0.60	0.14	0.16
K	0.08	0.11	0.12	0.08	0.18	0.03	0.14
Cr	0.00	0.02	0.01	0.02	0.04	0.00	0.01
Sum	15.55	15.39	15.41	15.40	15.36	15.52	15.13
mg#	65.0	60.8	67.4	69.8	38.4	62.4	56.6

* Total iron as FeO

Table 8. Biotite mineral compositions of the Wateranga intrusion

Sample	NS-2/4	NS-2/4	NS-5/6	NS-5/15
Oxide (wt%)				
SiO_2	35.78	39.01	36.73	40.59
TiO_2	3.79	2.33	5.93	4.57
Al_2O_3	15.62	16.60	8.39	9.36
FeO	17.53	11.78	25.85	13.69
MnO	0.07	0.11	0.32	<0.05
MgO	12.00	16.41	7.74	16.94
CaO	<0.05	<0.05	<0.05	<0.05
Na_2O	0.45	0.15	0.86	0.95
K_2O	8.63	9.72	9.96	9.45
Cr_2O_3	0.05	0.29	<0.05	0.25
BaO	1.60	0.32	0.13	0.48
Sum	95.52	96.72	95.92	96.28
Cations per 22 oxygens				
Si	5.47	5.65	5.86	6.02
Ti	0.44	0.25	0.71	0.51
Al^{iv}	2.53	2.35	2.14	1.98
Al^{vi}	0.28	0.48	0.56	0.34
Fe	2.24	1.43	3.45	1.70
Mn	0.01	0.01	0.04	0.00
Mg	2.74	3.54	1.84	3.75
Ca	0.00	0.00	0.00	0.00
Na	0.13	0.04	0.27	0.27
K	1.68	1.80	2.03	1.79
Cr	0.00	0.03	0.00	0.03
Ba	0.10	0.02	0.01	0.03
Sum	15.62	15.60	16.91	16.42
mg#	55.0	71.2	34.8	68.8

* Total iron as FeO. Lower detection limit for all elements is 0.05 wt%.

Appendix 3. Inductively coupled plasma mass spectrometry (ICP-MS)

Introduction

ICP-MS is a technique for analyzing elements using mass spectrometry of ions generated by an inductively coupled plasma. Analytical benefits of ICP-MS are detection limits at part per trillion levels for most elements, inherent spectral simplicity, rapid multi-element analysis, applicability to more than 75 elements, and isotope ratio analysis with a precision to the 0.1-2% range.

Analytical details

Rare earth element (REE) abundances of 20 whole-rock samples and platinum-group element and Au concentration of 10 whole-rock samples were measured by ICP-MS analysis at Australian Laboratory Services, Brisbane. Analyses are presented in Tables 4.5 and 4.6 (Chapter 4).

REE: Samples were digested using a proprietary near-total mixed acid digest incorporating perchloric, hydrofluoric, nitric and hydrochloric acids. Resulting solutions were analyzed by ICP-MS. In-house standards were also digested and analyzed with each batch of samples to check the accuracy of the method. Estimated precision and accuracy are better than 5%.

PGE and Au: Samples were fused by a classical gold fire assay using a silver containing lead oxide flux with the gold, platinum and palladium being collected together with the excess silver. The precious metals were then dissolved in aqua regia and the resulting solutions were analyzed by ICP-MS. In-house standards were used to check the accuracy of the method. Analytical precision and accuracy are generally better than 5%.

Appendix 4. Isotope analysis

A. Introduction

Revolution in geochemistry occurred with the invention of mass spectrometers (Nier, 1940, 1981). These instruments measure not only the concentrations of elements but also the ratios of their isotopes. Today there are many kinds of mass spectrometers used to measure different elements and their isotopes. The main difference in all the modern mass spectrometers is in how they ionize the sample.

B. Thermal ionization mass spectrometers

Thermal ionization mass spectrometers are used for the heavier elements and require the sample as a salt or metal which is then ionized on a filament. These are the instrument of choice for analyzing the isotopic composition of Rb, Sr, Sm, Nd, U, Th, Pb, Re, Os. Thermal ionization mass spectrometers have made a powerful impact on all fields of geology, particularly by their capability of routinely measuring the isotopes of U-Pb, Sm-Nd and Rb-Sr. Data from these isotopic systems have had a profound effect in whole Earth and planetary studies.

C. Isotope dilution

Isotope dilution is a chemical technique used for more precise measurements in thermal ionization mass spectrometry. It is based on adding a standard with a different isotopic composition to that of the unknown, and measuring the resulting isotopic composition is the recognized accepted technique with the lowest analytical uncertainties, which are better than 1% routinely.

D. Gas source mass spectrometers

Gas source mass spectrometers are used to measure the isotopic compositions of C, S, N, O, Cl, H and rare gases. Mass spectrometers with gas inlet can measure the isotopes of C, O, N, S and Ar and the other rare gases, which have had a strong impact in the fields of geochronology ($^{40}Ar/^{39}Ar$), atmospheric evolution (rare gases in general, but particularly He), economic geology and geohydrology (isotopes of C, O, S and Cl).

E. Analytical details

In this study, ten whole-rock samples were analyzed for Sr and O isotopes, and eight whole-rock samples were analyzed for Nd isotopes in the CSIRO isotope laboratories at North Ryde, Sydney, Australia. Analyses are presented in Tables 5.1 and 5.2 (Chapter 5). Analytical details are given below.

(i) Methodology for radiogenic isotope analyses (Sr, Nd, Sm)

Sample preparation: 2ml HF and 10 drops HNO_3 is added to approximately 0.1g of crushed sample and allowed to react for several hours or overnight to obtain maximum dissolution. The sample is then taken to incipient dryness and another 2ml HF added. The sample was then placed in a Teflon pressure vessel at 190°C for 2 days. The HF was again evaporated to incipient dryness. A few drops of $HClO_4$ is added to aid removal of fluorides and taken to dryness. The sample is then converted to a chloride form using 6M HCl and finally brought up in 2.5M HCl an appropriate acid for separation by cation exchange chromatography.

Column separations: Sr is separated on Dowex AG50W – X8 cation exchange resin. The rare earth elements are collected from this separation if Nd/Sm is required. The Nd and Sm are then separated further on HDEHP coated Bio-Beads.

Mass spectrometry: Sr is loaded onto single tantalum filaments, Nd and Sm are loaded onto triple rhenium filaments and analysed by **VG Sector 354** thermal ionisation mass spectrometer. The measured $^{87}Sr/^{86}Sr$ ratios were normalized to $^{86}Sr/^{88}Sr = 0.1194$, $^{143}Nd/^{144}Nd$ ratios to $^{146}Nd/^{144}Nd = 0.7219$ for mass fraction correction. During the collection of isotopic data for this study, repeated analyses of the NBS 987 (Sr standard) yielded an average value of $^{87}Sr/^{86}Sr = 0.710247 \pm 17$ (2σ; n = 11) and O'Nions (Nd standard) gave an average value of $^{143}Nd/^{144}Nd = 0.5811114 \pm 12$ (2σ; n = 15). Measurement of precisions for individual runs of $^{87}Sr/^{86}Sr$ and $^{143}Nd/^{144}Nd$ were better than ± 0.000011 and ± 0.000008 respectively.

(ii) Methodology for stable isotope analyses (O)

The function of the stable isotope laboratory is to convert solid or liquid materials to gaseous forms and then to analyze them on the mass spectrometer. The absolute

value of the isotopic ratio of a sample is not determined. Instead, the relative value is determined.

All prepared gases are analysed on a **Finnigan 252** mass spectrometer in dual inlet mode. Samples are analysed against a laboratory reference gas prepared using similar procedures for solid or liquid material. These laboratory standards have been calibrated against international reference materials. International reference standards and other laboratory standards are run on a regular basis to test instrument reference gas and extraction procedures. Oxygen extraction follows a method described by Clayton and Mayeda (1963). O_2 is separated using the standard BrF_5 method and converted to CO_2 by reaction with carbon. CO_2 is trapped by selective freezing techniques and analysed on mass spectrometer. The error for this method is 0.2 per mil.

Appendix 5. Rock catalogue

Sample Number	UNE Number	Stratigraphic depth (m)	Rock type
Reddy V.R. Talusani collection			
Surface samples			
WG-7	R80571	111	Olivine gabbro
WG-16	R80572	80	Olivine gabbro
WG-26	R80573	106	Anorthosite
WG-27	R80574	122	Olivine gabbro
WG-31	R80575	130	Olivine gabbro
WG-35	R80576	10	Olivine gabbro
WG-38	R80577	18	Norite
WG-39	R80578	23	Granite
WG-44	R80579	125	Olivine gabbronorite
WG-55	R80580	138	Olivine gabbronorite
WG-58	R80581	140	Olivine gabbronorite
WG-70	R80582	95	Olivine gabbronorite
WG-75	R80583	100	Norite
WG-84	R80584	85	Olivine gabbronorite
WG-92	R80585	63	Anorthosite
WG-96	R80586	56	Anorthosite
WG-103	R80587	78	Troctolite
WG-107	R80588		
WG-108	R80589	117	Troctolite
WG-115	R80590	111	Olivine gabbronorite
WG-123	R80591	128	Olivine gabbro
WG-124	R80592	120	Olivine gabbronorite
WG-128	R80593	139	Olivine gabbro
Drill hole samples			
NS-2/1	R80594	149.75	Noritic gabbro
NS-2/2	R80595	154.02	Norite
NS-2/3	R80596	157.68	Olivine gabbro
NS-2/4	R80597	160.42	Troctolite
NS-2/5	R80598	162.25	Ferro gabbro
NS-2/8	R80599	167.43	Olivine gabbro
NS-2/9	R80600	177.49	Noritic gabbro
NS-2/10	R80601	181.15	Granite
NS-2/11	R80602	188.77	Olivine gabbronorite
NS-2/14	R80603	199.74	Norite
NS-2/17	R80604	219.86	Olivine norite
NS-2/18	R80605	225.04	Olivine norite
NS-2/19	R80606	225.65	Olivine norite
NS-2/22	R80607	231.44	Norite
NS-2/29	R80608	250.95	Olivine norite
NS-2/31	R80609	270.45	Olivine gabbro
NS-2/33	R80610	277.46	Troctolite
NS-2/34	R80611	282.95	Norite
NS-2/35	R80612	286.30	Olivine gabbro
NS-2/40	R80613	296.67	Norite
NS-2/41	R80614	303.07	Anorthositic norite

Sample Number	UNE Number	Stratigraphic depth (m)	Rock type
NS-2/42	R80615	307.34	Norite
NS-2/48	R80616	386.89	Olivine norite
NS-2/53	R80617	405.79	Olivine norite
NS-2/54	R80618	411.27	Olivine gabbronorite
NS-2/57	R80619	419.20	Olivine gabbro
NS-2/59	R80620	432.61	Olivine norite
NS-2/61	R80621	464.00	Olivine gabbro
NS-2/63	R80622	472.84	Olivine norite
NS-2/65	R80623	488.08	Olivine gabbro
NS-3/2	R80624	163.77	Norite
NS-3/4	R80625	177.19	Olivine norite
NS-3/7	R80626	186.02	Olivine norite
NS-3/8	R80627	195.47	Norite
NS-3/10	R80628	198.52	Troctolite
NS-3/12	R80629	202.18	Olivine gabbronorite
NS-3/18	R80630	222.91	Norite
NS-3/20	R80631	233.27	Norite
NS-3/25	R80632	270.45	Olivine gabbronorite
NS-3/28	R80633	306.42	Anorthositic norite
NS-3/31	R80634	319.83	Norite
NS-3/32	R80635	329.89	Troctolite
NS-3/34	R80636	344.83	Norite
NS-3/38	R80637	369.21	Norite
NS-3/40	R80638	372.87	Anorthosite
NS-3/51	R80639	460.53	Picrite
NS-3/52	R80640	462.50	Norite
NS-3/53	R80641	466.75	Norite
NS-5/4	R80642	182.06	Apatite-oxide-olivine rich rock
NS-5/6	R80643	199.44	Orthopyroxenite
NS-5/12	R80644		
NS-5/15	R80645		
NS-5/23	R80646	262.83	Hornblende rich norite
P.M. Ashley collections			
A-WG1		122	
A-WG2		119	
A-WG3		136	
A-WG4		137	
A-WG5		134	
A-WG6		132	
A-WG7		117	
A-WG8		33	
A-WG9		20	
A-WG10		57	
A-WG11		140	
A-WG12		138	
A-WG13		125	
A-WG14		115	
A-WG15		112	
A-WG16		104	
A-WG17		90	

Sample Number	UNE Number	Stratigraphic depth (m)	Rock type
A-WG18		85	
A-WG19		121	
A-WG22		123	
A-WG23		124	
A-WG24		126	
W. J. Evans collection			
E-NS2/1	R70804	150.58	Olivine gabbro
E-NS2/4	R70805	164.38	Olivine gabbronorite
E-NS2/9	R70806	190.74	Olivine gabbronorite
E-NS2/17	R70807	271.06	Olivine gabbronorite
E-NS2/29	R70808	412.80	Olivine gabbronorite
E-NS3/3	R70809	179.62	Olivine gabbro
E-NS5/1	R70812	162.25	Olivine gabbronorite
E-NS5/2	R70813	162.56	Olivine gabbronorite
E-NS5/3	R70810	193.64	Orthopyroxenite
E-NS5/4	R70814	207.36	Hornblende bearing gabbronorite
E-NS5/5	R70815	210.71	Hornblendite
E-NS5/6	R70816	215.59	Hornblende gabbro
E-NS5/7	R70817	223.52	Norite
E-NS5/8	R70818	224.73	Pyroxene-hornblende gabbronorite
E-NS5/9	R70819	232.05	Pyroxene-hornblende gabbronorite
E-NS5/10	R70820	237.84	Pyroxene-hornblende gabbronorite
E-NS5/11	R70821	261.92	Hornblende gabbro
E-NS5/12	R70822	271.68	Hornblende gabbro
E-NS5/13	R70823	279.60	Pyroxene-hornblende gabbronorite
E-NS5/14	R70824	285.69	Granophyre
E-NS5/15	R70825	289.05	Granophyre
E-NS5/16	R70826	292.60	Granophyre

Appendix 6. Recent publications

Journal articles

Talusani R.V.R., Sivell W.J. and Ashley P.M. (2003) Mineral chemistry and petrogenesis of the Wateranga layered intrusion, southeast Queensland, Australia – submitted to *Mineralogy and Petrology*.

Talusani R.V.R. (2003) Bimodal tholeiitic and alkalic basalts from Bhir area, Central Deccan Volcanic Province, India: Geochemistry and petrogenesis – submitted to *Bulletin of Volcanology*.

Talusani R.V.R. (2001) Possible Carlin-type disseminated gold mineralization in the Mahakoshal fold belt, central India. *Ore Geology Reviews* **17,** 241-247.

Talusani R.V.R. (2001) A newly reported alkali basalt flow near Bhir, Deccan Volcanic Province, India. *Journal of Asian Earth Sciences* **19,** 501-506.

Talusani R.V.R., Sivell W.J. and Ashley P.M. (in prep) Nd-Sr-O isotopic and geochemical studies of the Wateranga layered intrusion, Australia – to be submitted to *Journal of Petrology*

Conference publications

Talusani R.V.R. and Sivell W.J. (2002) Nd-Sr-O isotopic and trace element characteristics of the Wateranga mafic layered intrusion, southeast Queensland, Australia: implications for open system magmatic processes in a post-collisional setting. *16th Australian Geological Convention,* Adelaide, July 1-5, 2002. Geological Society of Australia, Abstracts 67, p.94.

Talusani R.V.R. (2002) Chemistry of late-Archaean komatiites from the Mahakoshal greenstone belt, central India. *16th Australian Geological Convention,* Adelaide, July 1-5, 2002. Geological Society of Australia, Abstracts 67, p.53.

Talusani R.V.R. (2002) Geochemistry of the late pleistocene alkali basalts, southeast Queensland, Australia. Geological Society of New Zealand, Annual Conference, Northland, 2-5 December 2002.

Talusani R.V.R. (2002) Origin of low-Ti-P-K basalts from the Mahakoshal Greenstone belt, central India. Geological Society of New Zealand, Annual Conference, Northland, 2-5 December 2002.

Talusani R.V.R. (2001) Felsic volcanism from the Mahakoshal Greenstone Belt near Barhi, Madhya Pradesh, India. *4th International Archaean Symposium,* Perth, Australia, Sept. 24-28, 2001. AGSO – Geoscience Australia Record 2001/37, p.202-204.

Talusani R.V.R. (2000) Geology and geochemistry of the sediment-hosted gold mineralization at Barhi and Jhal, Madhya Pradesh, India. *15th Australian Geological*

Convention, Sydney, July 3-7, 2000. Geological Society of Australia, Abstracts 59, p.489.

Talusani R.V.R., Sivell W.J. and Ashley P.M. (2000) The Wateranga intrusion, southeast Queensland, Australia: a high-Al and low-K mafic, tholeiitic layered intrusion. *15th Australian Geological Convention,* Sydney, July 3-7, 2000. Geological Society of Australia, Abstracts 59, p.490.

Talusani R.V.R. (2000) Geochemistry of the Deccan Trap lava flows around Bhir, India: Contemporaneous tholeiitic and alkalic Lavas. *31st International Geological Congress*, Brazil, Aug. 6-17, 2000, Abstracts Volume.

Reports

Talusani R.V.R. (1994) Ground evaluation of AEM anomalies and the occurrence of gold mineralization within the Mahakoshal rocks of central India. Geological Survey of India, *Open File Report*, 24 pp.

Several full papers, targeted to publish in international journals, on the papers presented at conferences (e.g. rhyolites, komatiites and basalts) are in preparation.

Research interests

I am interested in a wide variety of igneous processes, with my greatest enthusiasm being in the study of basic and ultrabasic rocks from mantle domains.

Projects undertaken

I am currently working on the magmatic rocks of the Late Archaean Mahakoshal greenstone belt in central India. Four projects compose this broad research area. They are: (1) basalts, (2) komatiites, (3) alkaline rocks and (4) rhyolites. The work I am doing in these areas incorporates field mapping, petrology, mineral chemistry, whole rock geochemistry, and radiogenic and stable isotope studies. The igneous rocks of the Mahakoshal greenstone belt record different stages of magmatic history and provide an excellent opportunity to study the tectonomagmatic evolution of Late Archaean crust and mantle.

Parallel to these studies, I am also working on geochemistry and petrogenesis of Deccan Trap basalts from central and northeastern portions of the Deccan Volcanic Province.